

Copyright Statement

This copy of the thesis has been supplied on condition that anyone who consults it is understood to recognise that its copyright rests with its author and due acknowledgement must always be made of the use of any material contained in, or derived from, this thesis.

A condition based approach to the tribology of
RNLI marine systems

MAYANK ANAND

Thesis submitted in partial fulfilment of the requirement of
Bournemouth University for the degree of
Doctor of Philosophy

January 2015

Faculty of Science and Technology
Bournemouth University
In collaboration with
Royal National Lifeboat Institution

Abstract

A condition based approach to the tribology of RNLI marine systems

Mayank Anand

Lubricant degradation mechanisms in the 4-stroke heavy duty diesel engines of RNLI lifeboats were investigated. These mechanisms lead to the increased wear of main engine components, such as cylinder liners. The lifeboat application is distinct from the other marine applications from an engine lubrication perspective, since it involves infrequent engine running conditions and is often subjected to either under or over engine maintenance due to the unpredictable usage of lifeboats. This research has demonstrated the key lubricant properties which were affected by the lifeboat operations. Analysis of used lubricants was conducted such as Wear Debris Analysis (Analytical Ferrography) to identify the wear mechanism of affected tribological contacts and Nuclear Magnetic Resonance (NMR) analysis to analyse the trend in reduced effectiveness of antiwear additives. Other standard lubricant analysis technique were also performed to supplement the information about the lubricant condition.

The experimental test rig involved the modification of a high frequency reciprocating tribometer (Plint TE77) to simulate piston ring and cylinder liner configuration. Boundary lubrication conditions that exist near the top dead centre region of cylinder liner were simulated in order to evaluate the tribological performance of lubricant additives. Also real-time condition monitoring of engine lubricant samples was carried out using a commercially available on-line sensing system. The obtained results from oil sensor were sufficiently promising to conduct engine level tests in lifeboat to monitor lubricant performance in real-time and build the system as part of the planned maintenance strategies of the RNLI.

The work also involved recovering the tribological performance of used engine lubricants for further use at the end of their service life. Ionic Liquids (ILs) were tested as performance improving additives in used engine lubricants at engine start and

running conditions using the modified Plint TE77 experimental test setup. Additional tests were conducted with different fully-formulated and mineral base oils with ILs as additives. Post-test surface analysis for wear mechanism and surface chemistry analysis of boundary antiwear films were performed to relate the chemical composition of films with its tribological performance. Obtained results demonstrated significant improvement in tribological performance of used engine lubricants. Also interference between Phosphonium ILs and existing additives in engine oils was noted. ILs effectively contributed to the boundary film formation when already present additives (such as ZDDP) are substantially depleted as seen in the case of used engine oil. The extension of service life of used engine oils can be achieved and has potential of significant savings in terms of fuel economy, engine reliability and by reduced oil consumption and drainage into the environment.

Publications resulting from this thesis

Journal Publications

1. **M. Anand**, M. Hadfield, J.L. Viesca, B. Thomas, A. Hernández Battez, S. Austen. "Ionic Liquids as tribological performance improving additive for in-service and used fully-formulated diesel engine lubricants". *Wear* (Submitted)

International Conferences

1. **M. Anand**, M. Hadfield, J.L. Viesca, B. Thomas, A. Hernández Battez, S. Austen. "Ionic Liquids as tribological performance improving additive for in-service and used fully-formulated diesel engine lubricants". *Wear of Materials 2015*, 12-16 Apr 2015, Toronto, Canada (Abstract Accepted)
2. **M. Anand**, M. Hadfield, B. Thomas, R. Cantrill, S. Austen, J. Viesca, N. Garland. "Experimental analysis of anti-wear performance of marine engine lubricants". *World Tribology Congress 2013*, 8-13 Sep 2013, Torino, Italy
3. **M. Anand**, M. Hadfield, S. Austen. "A tribological approach to condition monitoring of lubricants used in marine diesel engines". *STLE 68th Annual Meeting & Exhibition*, 5-9 May 2013, Detroit, USA

Poster Conferences

1. **M. Anand**, M. Hadfield, B. Thomas, S. Austen, R. Cantrill. "Lubricant Condition Monitoring for RNLI Lifeboats In-Service". *SET for Britain*, 18 Mar 2013, House of Commons, Parliament, UK
2. **M. Anand**, M. Hadfield, B. Thomas, S. Austen, R. Cantrill. "Lubricant Condition Monitoring for RNLI Lifeboats In-Service". *6th Annual Bournemouth University Postgraduate Research Conference*, 22 May 2013
3. **M. Anand**, M. Hadfield, B. Thomas, S. Austen. "Condition Monitoring of Royal National Lifeboat Institution's Marine Systems". *5th Annual Bournemouth University Postgraduate Research Conference*, 23 May 2012

Industrial Presentations

1. **M. Anand.** "A Condition Based Approach to the Tribology of RNLI Marine Systems". BP Technology Centre, Pangbourne, UK, 22 Feb 2012
2. **M. Anand.** "A Condition Based Approach to the Tribology of RNLI Marine Systems". Royal National Lifeboat Institution, Head Quarter, UK, 19 Jun 2012
3. **M. Anand.** "A condition based approach to the tribology of RNLI lifeboat engine lubricants". Royal National Lifeboat Institution, Head Quarter, UK, 16 Oct 2012
4. **M. Anand.** "A condition based approach to the tribology of RNLI lifeboat engine lubricants". Royal National Lifeboat Institution, Head Quarter, UK, 4 Mar 2013
5. **M. Anand.** "A tribological approach to condition monitoring of lubricants used in marine diesel engines". BP Marine Limited, Sunbury-on-Thames, UK, 21 May 2013
6. **M. Anand.** "Additive depletion in used lubricants from RNLI lifeboat engines". Bournemouth University, UK, 30 Aug 2013
7. **M. Anand.** "A condition based approach to tribology of RNLI marine systems". BP Technology Centre, Pangbourne, UK, 28 May 2014
8. **M. Anand.** "A condition based approach to tribology of RNLI marine systems". Royal National Lifeboat Institution, Head Quarter, UK, 4 Jul 2014

Awards and Honours

1. Santander Scholarship worth £2,500 covering international travel and experimental research at University of Oviedo, Spain. Research visit involved performing surface analysis of boundary films formed by lubricants and Ionic Liquids using state-of-the-art equipment such as XPS and SEM – EDX
2. Post-Graduate Research Development funding worth £1,200 for presenting research paper at World Tribology Congress, 8-13 Sep 2013, Italy
3. PhD project supported by Tobias Ellwood MP and highlighted on Member of Parliament website
www.tobiasellwood.com/news/phd-student-bu-presented-his-research-mps-house-commons-london

Table of content

Copyright Statement	i
Abstract	III
Publications resulting from this thesis	V
Journal Publications	V
List of Figure	X
List of Tables	XVI
Acknowledgements	XVIII
Author’s Declaration	XIX
Chapter 1 Introduction	1
1.1. Background of the project.....	1
1.2. Research aims.....	5
1.3. Research questions.....	5
1.4. State of the art.....	6
1.5. Outline of this thesis	6
Chapter 2 Literature Review	8
2.1. Engine tribology.....	8
2.2. Engine lubricants and additives	9
2.3. Lubricant test methods	12
2.3.1. Chemical testing of lubricants.....	14
2.3.2. Lubricant condition monitoring.....	14
2.3.3. Tribological testing of lubricants.....	14
2.3.4. Simulating piston ring/cylinder liner contact in tribometers.....	16
2.4. Ionic liquids as lubricant and additive.....	20
2.4.1. Limitations for ionic liquids in diesel engines application.....	22
2.4.2. Phosponium ionic liquids	23

2.4.3.	Mechanism and structure of tribo-film formed by ionic liquids	25
2.4.4.	Interaction between ionic liquids and conventional anti-wear additive	28
2.4.5.	Experimental techniques to evaluate boundary film formation of ionic liquids	29
Chapter 3	Experimental Methodology	30
3.1.	Lubricant samples collection	30
3.2.	Pre-test Stage (Lubricant Analysis).....	32
3.2.1.	Viscosity measurement (IP71/ASTM D445).....	32
3.2.2.	Gas Chromatography (Diesel Fuel Dilution).....	33
3.2.3.	ICP Spectroscopy (ASTM D4951/D5185).....	33
3.2.4.	Nuclear Magnetic Resonance (NMR)	35
3.2.5.	Analytical Ferrography	36
3.3.	Test Stage (Lubricant Tribological Analysis and Condition Monitoring)	37
3.3.1.	Test rig setup to simulate engine lubricant conditions	37
3.3.2.	Test materials.....	41
3.3.3.	Test parameters	53
3.3.4.	Test procedure	54
3.4.	Post-test Stage (Surface analysis).....	56
3.4.1.	3D White Light Interferometer.....	57
3.4.2.	Sample preparation for SEM, EDX and XPS analyses.....	58
3.4.3.	Scanning Electron Microscopy (SEM).....	59
3.4.4.	Energy Dispersive X-ray Microanalysis (EDX)	60
3.4.5.	X-ray Photoelectron Spectroscopy (XPS)	61
Chapter 4	Results of Lubricant Analysis.....	64
4.1.	Viscosity Measurements.....	64
4.2.	Gas Chromatography (Diesel Fuel Dilution).....	65
4.3.	Elemental concentration of wear debris and additives by ICP	65

4.4.	Nuclear Magnetic Resonance (NMR).....	67
4.5.	Oil Condition Monitoring by Oil Sensor	69
4.6.	Analytical Ferrography.....	72
4.7.	Wear analysis of actual cylinder liner from RNLI marine engines.....	74
4.8.	Stability of lubricant and ionic liquid mixtures	77
Chapter 5 Results of Tribological Analysis.....		85
5.1.	Friction and ECR results.....	86
5.2.	Wear results	96
5.2.1.	Wear volume results at 100°C	97
5.2.2.	Wear volume results at 25°C	101
5.2.3.	Wear rate results	104
5.3.	Wear mechanisms.....	105
5.4.	Surface Chemistry (EDX and XPS analysis)	115
5.4.1.	Mineral base oil with/without IL1 and IL2 (at 100°C)	117
5.4.2.	New Oil with/without IL1 and IL2 (at 100°C).....	123
5.4.3.	In-service oil (135h) with/without IL1 and IL2 (at 100°C).....	130
5.4.4.	Used Oil (315h) with/without IL1 and IL2 (at 100°C)	136
5.4.5.	New Oil with/without IL1 and IL2 (at 25°C).....	142
5.4.6.	Used Oil with/without IL1 and IL2 (at 25°C)	149
5.5.	Validation of tribological experimental results	156
Chapter 6 Conclusions and recommendations for future work		161
References		163
Appendix A:	Contact Pressure Calculation.....	174
Appendix B:	Theoretical Lubrication Regime.....	175
Appendix C:	MAN Engine Test Report.....	178

List of Figure

Figure 1: Wear element concentration measured by ICP spectroscopy for Trent Class lifeboat engine ON1253-P	4
Figure 2: Wear element concentration measured by ICP spectroscopy for Trent Class lifeboat engine ON1253-S.....	4
Figure 3: Three levels of testing of engine lubricants and materials [16]	13
Figure 4: Trihexyltetradecyl phosphonium bis(2,4,4-tri-methylpentyl) phosphinate [28]	24
Figure 5: Trihexyltetradecyl phosphonium bis(2-ethylhexyl) phosphate [28].....	24
Figure 6: Monolayer formed by IL on metal surface. Image source: [39]	26
Figure 7: (a) Used oil samples collected from Trent Class Lifeboat at different service intervals; (b) and (c) New lubricating oil (SAE 15W40) from two different manufacturers; (d) Mineral base oil.....	31
Figure 8: AVANCE III HD NMR Spectrometer at BP Lubricants (Pangbourne, UK). Image source: Bruker website.....	35
Figure 9: Process of making a ferrogram by separating particles from the oil [76].....	36
Figure 10: Schematic of modified High Frequency Friction tribometer TE77	37
Figure 11: Fluid properties oil sensor system	38
Figure 12: (a) Centrifugal micro oil pump; (b) Manifold for mounting oil sensor	38
Figure 13: Modified TE77 test rig including real time on-line lubricant condition monitoring system.....	39
Figure 14: Piston ring cutting procedure.....	41
Figure 15: Dremel rotary cutting tool (Model 398) along with fiber glass reinforced cut-off wheel	42
Figure 16: Typical flat plate and cylindrical pin samples used in experiments	42
Figure 17: Preparation for EDX analysis of piston ring coating.....	43
Figure 18: EDX analysis of piston ring cross-section shown in Figure 17(d); (a) coating thickness shown between green lines; (b) EDX spectrum of coating; (c) EDX spectrum of base material of piston ring	44

Figure 19: Typical surface roughness map of unworn piston ring running face along with roughness distribution scale	47
Figure 20: Typical surface roughness map of unworn flat plate specimen used as cylinder liner along with roughness distribution scale	47
Figure 21: Trihexyltetradecyl phosphonium bis(2,4,4-tri-methylpentyl) phosphinate (Sigma-Aldrich) and Trihexyltetradecyl phosphonium bis(2-ethylhexyl) phosphate (lolitec).....	49
Figure 22: Mixing of different lubricating oil and IL using sonicator; (a) New engine oil; (b) Used (315h) engine oil; (c) Sonicator.....	51
Figure 23: Stability analysis of mixtures of new and used engine lubricants with different ILs using Turbiscan Lab	52
Figure 24: Specimen stored in desiccator	56
Figure 25: 3D White Light Interferometer	57
Figure 26: Bench top cut-off machine (Struers Accutom-5) shown in (a); and flat specimen during cutting process shown in (b)	58
Figure 27: Samples installation on the sample mount is shown in (a); SEM equipment used for analysis of worn surfaces is shown in(b)	59
Figure 28: Samples installation in load chamber of XPS equipment is shown in (a); XPS equipment is shown in (b)	62
Figure 29: 31-P NMR spectra for different lubricant samples	67
Figure 30: Dynamic viscosity measurements obtained by Oil Sensor	69
Figure 31: Density measurements obtained by Oil Sensor.....	69
Figure 32: Dielectric constant measurements obtained by Oil Sensor.....	70
Figure 33: Ferrography Micrographs of three used oil samples.....	72
Figure 34: Actual cylinder liner used for wear analysis of bore surface in (a); sample preparation in (b); samples used for surface analysis in (c)	75
Figure 35: Surface profile of three sections cut from an actual cylinder at TDC, MID stroke and BDC locations	76
Figure 36: Stability analysis spectra for 6% volume IL1 in New 15W40 engine oil at 30°C using Turbiscan Lab Expert. The horizontal axis corresponds to height of oil	

sample bottle. The colour of different profiles corresponds to time scale on vertical axis on right.	81
Figure 37: Stability analysis spectra for 6% volume IL2 in New 15W40 engine oil at 30°C using Turbiscan Lab Expert. The horizontal axis corresponds to height of oil sample bottle. The colour of different profiles corresponds to time scale on vertical axis on right	82
Figure 38: Stability analysis spectra for 6% volume IL1 in Used 15W40 engine oil at 30°C using Turbiscan Lab Expert. The horizontal axis corresponds to height of oil sample bottle. The colour of different profiles corresponds to time scale on vertical axis on right	83
Figure 39: Stability analysis spectra for 6% volume IL2 in Used 15W40 engine oil at 30°C using Turbiscan Lab Expert. The horizontal axis corresponds to height of oil sample bottle. The colour of different profiles corresponds to time scale on vertical axis on right	84
Figure 40: Mean Friction coefficient and Electrical Contact Resistance behaviour for different lubricants and lubricant-IL mixtures during 3h sliding testing at 100°C	90
Figure 41: Mean Friction coefficient and Electrical Contact Resistance behaviour for different lubricants and lubricant-IL mixtures during 3 h sliding testing at 25°C	94
Figure 42: Wear Volume results of cast iron specimens after 3h sliding at 100°C. Repeatability (relative standard deviation) of results is within 15%.....	100
Figure 43: Wear Volume results of cast iron specimens after 3h sliding at 25°C. Repeatability (relative standard deviation) of results is within 15%.....	103
Figure 44: SEM images of worn flat specimen in Mineral Base Oil w/o 6% ILs after 3h sliding at 100°C; (a) Magnification of images is 200x; (b) Magnification of images is 1500x.....	108
Figure 45: SEM images of worn flat specimen in New 15W40 Oil w/o 6% ILs after 3h sliding at 100°C; (a) Magnification of images is 200x; (b) Magnification of images is 1500x.....	109
Figure 46: SEM images of worn flat specimen in Inservice 15W40 Oil (135h) w/o 6% ILs after 3h sliding at 100°C; (a) Magnification of images is 200x; (b) Magnification of images is 1500x.....	110

Figure 47: SEM images of worn flat specimen in Inservice 15W40 Oil (196h) w/o 6% ILs after 3h sliding at 100 ⁰ C; (a) Magnification of images is 200x; (b) Magnification of images is 1500x.....	111
Figure 48: SEM images of worn flat specimen in Used 15W40 Oil (315h) w/o 6% ILs after 3h sliding at 100 ⁰ C; (a) Magnification of images is 200x; (b) Magnification of images is 1500x.....	112
Figure 49:SEM images of worn flat specimen in New 15W40 Oil w/o 6% ILs after 3h sliding at 25 ⁰ C; (a) Magnification of images is 200x; (b) Magnification of images is 1500x.....	113
Figure 50:SEM images of worn flat specimen in Used 15W40 Oil (315h) w/o 6% ILs after 3h sliding at 25 ⁰ C; (a) Magnification of images is 200x; (b) Magnification of images is 1500x.....	114
Figure 52: High resolution Fe 2p _{3/2} XPS spectra of the worn surface on cast iron flat samples lubricated with (a) Mineral Base Oil (b) Outside wear scar – Mineral Base Oil (c) Mineral Base Oil + 6% IL1 (d) Mineral Base Oil + 6% IL2	119
Figure 53: High resolution O1s XPS spectra of the worn surface on cast iron flat samples lubricated with (a) Mineral Base Oil (b) Outside wear scar – Mineral Base Oil (c) Mineral Base Oil + 6% IL1 (d) Mineral Base Oil + 6% IL2	120
Figure 54: High resolution P2p XPS spectra of the worn surface on cast iron flat samples lubricated with (a) Mineral Base Oil (b) Outside wear scar – Mineral Base Oil (c) Mineral Base Oil + 6% IL1 (d) Mineral Base Oil + 6% IL2	122
Figure 56: High resolution Fe 2p _{3/2} XPS spectra of the worn surface on cast iron flat samples lubricated with (a) New Oil (b) New Oil + 6% IL1 (c) New Oil + 6% IL2	126
Figure 57: High resolution O1s XPS spectra of the worn surface on cast iron flat samples lubricated with (a) New Oil (b) New Oil + 6% IL1 (c) New Oil + 6% IL2	127
Figure 58: High resolution Ca 2p XPS spectra of the worn surface on cast iron flat samples lubricated with (a) New Oil (b) New Oil + 6% IL1 (c) New Oil + 6% IL2	128
Figure 59: High resolution P 2p XPS spectra of the worn surface on cast iron flat samples lubricated with (a) New Oil (b) New Oil + 6% IL1 (c) New Oil + 6% IL2	129
Figure 61: High resolution Fe 2p _{3/2} XPS spectra of the worn surface on cast iron flat samples lubricated with (a) Inservice Oil (135h); (b) Inservice Oil (135h) + 6% IL1; (c) Inservice Oil (135h) + 6% IL2.....	132

Figure 62: High resolution O1s XPS spectra of the worn surface on cast iron flat samples lubricated with (a) In-service Oil (135h); (b) In-service Oil (135h) + 6% IL1; (c) In-service Oil (135h) + 6% IL2	133
Figure 63: High resolution Ca2p XPS spectra of the worn surface on cast iron flat samples lubricated with (a) In-service Oil (135h); (b) In-service Oil (135h) + 6% IL1; (c) In-service Oil (135h) + 6% IL2	134
Figure 64: High resolution P2p XPS spectra of the worn surface on cast iron flat samples lubricated with (a) In-service Oil (135h); (b) In-service Oil (135h) + 6% IL1; (c) In-service Oil (135h) + 6% IL2	135
Figure 66: High resolution Fe 2p _{3/2} XPS spectra of the worn surface on cast iron flat samples lubricated with (a) Used Oil (135h); (b) Used Oil (135h) + 6% IL1;(c) Used Oil (135h) + 6% IL2	138
Figure 67: High resolution O1s XPS spectra of the worn surface on cast iron flat samples lubricated with (a) Used Oil (135h); (b) Used Oil (135h) + 6% IL1; (c) Used Oil (135h) + 6% IL2.....	139
Figure 68: High resolution Ca 2p XPS spectra of the worn surface on cast iron flat samples lubricated with (a) Used Oil (135h); (b) Used Oil (135h) + 6% IL1; (c) Used Oil (135h) + 6% IL2.....	140
Figure 69: High resolution P 2p XPS spectra of the worn surface on cast iron flat samples lubricated with (a) Used Oil (315h); (b) Used Oil (315h) + 6% IL1; (c) Used Oil (315h) + 6% IL2.....	141
Figure 71: High resolution Fe 2p _{3/2} XPS spectra of the worn surface on cast iron flat samples lubricated with (a) New Oil (b) New Oil + 6% IL1 (c) New Oil + 6% IL2	144
Figure 72: High resolution Ca 2p XPS spectra of the worn surface on cast iron flat samples lubricated with (a) New Oil (b) New Oil + 6% IL1 (c) New Oil + 6% IL2	145
Figure 73: High resolution P2p XPS spectra of the worn surface on cast iron flat samples lubricated with (a) New Oil (b) New Oil + 6% IL1 (c) New Oil + 6% IL2	146
Figure 74: High resolution Zn 2p XPS spectra of the worn surface on cast iron flat samples lubricated with (a) New Oil (b) New Oil + 6% IL1 (c) New Oil + 6% IL2	147
Figure 75: High resolution S 2p XPS spectra of the worn surface on cast iron flat samples lubricated with (a) New Oil (b) New Oil + 6% IL1 (c) New Oil + 6% IL2	148

Figure 77: High resolution Fe 2p _{3/2} XPS spectra of the worn surface on cast iron flat samples lubricated with (a) Used Oil (315h); (b) Used Oil (315h) + 6% IL1; (c) Used Oil (315h) + 6% IL2.....	151
Figure 78: High resolution Ca 2p XPS spectra of the worn surface on cast iron flat samples lubricated with (a) Used Oil (315h); (b) Used Oil (315h) + 6% IL1; (c) Used Oil (315h) + 6% IL2.....	152
Figure 79: High resolution P2p XPS spectra of the worn surface on cast iron flat samples lubricated with (a) Used Oil (315h); (b) Used Oil (315h) + 6% IL1; (c) Used Oil (315h) + 6% IL2.....	153
Figure 80: High resolution Zn 2p XPS spectra of the worn surface on cast iron flat samples lubricated with (a) Used Oil (315h); (b) Used Oil (315h) + 6% IL1; (c) Used Oil (315h) + 6% IL2.....	154
Figure 81: High resolution S 2p XPS spectra of the worn surface on cast iron flat samples lubricated with (a) Used Oil (315h); (b) Used Oil (315h) + 6% IL1; (c) Used Oil (315h) + 6% IL2.....	155
Figure 76: SEM images of actual cylinder liners near top dead centre; (a) unworn surface of new liner; (b) worn surface of used liner at end of its service life	157
Figure 83: SEM images of cast iron test specimens; (a) unworn surface before test; (b) worn surface after test at 100°C; (c) worn surface after test at 25°C.....	158

List of Tables

Table 1: Details of RNLI fleet of lifeboats with engine and lubricant description	1
Table 2: Details of serviceable life and reasons for changing lubricants.....	3
Table 3: Examples of bench test parameters used for simulating reciprocating piston ring – cylinder liner contact near TDC	19
Table 4: Material description of test specimens.....	46
Table 5: Surface roughness values in root mean square (Rrms).....	48
Table 6: Kinematic viscosities of oils and ILs at standard temperatures	50
Table 7: Kinematic viscosities different lubricants in this study.....	64
Table 8: Diesel fuel dilution in different lubricants samples	65
Table 9: Elemental concentration in part per million (ppm).....	66
Table 10: Comparison of specific wear rate	104
Table 11: Elemental concentration inside worn surface obtained by EDX analysis	118
Table 12: XPS results – binding energy shifts – worn surface on cast iron flat samples	118
Table 13: Elemental concentration inside worn surface obtained by EDX analysis	124
Table 14: XPS results – binding energy shifts – inside worn surface on cast iron flat samples	124
Table 15: Elemental concentration inside worn surface obtained by EDX analysis	131
Table 16: XPS results – binding energy shifts – inside worn surface on cast iron flat samples	131
Table 17: Elemental concentration inside worn surface obtained by EDX analysis	137
Table 18: XPS results – binding energy shifts – inside worn surface on cast iron flat samples	137
Table 19: Elemental concentration inside worn surface obtained by EDX analysis	143
Table 20: XPS results – binding energy shifts – inside worn surface on cast iron flat samples	143
Table 21: Elemental concentration inside worn surface obtained by EDX analysis	150

Table 22: XPS results – binding energy shifts – inside worn surface on cast iron flat samples	150
Table 23: Known parameters of piston ring segment-on-flat contact	174
Table 24: Known data for minimum lubricant film thickness	176

Acknowledgements

This project has been a great opportunity for me to gain expertise within the field of research, and I am thankful to Bournemouth University and the Royal National Lifeboat Institution (RNLI) to provide me with this opportunity.

I would like to pay my gratitude to Professor Mark Hadfield for his continuous guidance and endless efforts to provide every possible contribution as a supervisor from the beginning till the end of my PhD. His suggestions during the project meetings have always made life much easier to proceed to the next stage. Also I am thankful to him to provide me with the opportunities to get involve in various research activities for my professional and personal development.

I would like to thank Dr Ben Thomas for his support in the experimental work and also providing feedbacks during the project meetings. Professor Josė Luis Viesca, University of Oviedo, Spain for his invaluable suggestions and tired less support in helping with experimental work on Ionic Liquids. Professor Viesca and his tribology group's expertise in lubricant science have been very useful and have helped in achieving major milestones of the project.

I am thankful to Steve Austen, Head of Engineering, RNLI for providing me the opportunity to spend time with the Engineering department at RNLI Headquarters in UK. This stay was very useful to learn technical aspects of the research project. Rob Cantrill, Principal Mechanical Engineer, RNLI for his valuable technical support and patient help with arranging the resources needed for the experimental work involved in this project.

I would like to thank Dawn Rivers and Simon Edwards from BP Technology Centre, Pangbourne, along with many other research staff for their in-kind technical support and valuable suggestions. LH (Part of the Wabtec Group) and Pilkington Marine Engineering Ltd for providing engine components required for the experimental work.

My appreciation also goes to Dr Alfonso Fernandez Gonzalez for University of Oviedo, Spain for help with XPS analysis. Dr Nigel Garland for his support at the initial stages of the project. I also thank the laboratory staff of Bournemouth University for their technical support. I thank my co-researchers and the director (Dr Zulfiqar Khan) from Sustainable Design Research Centre for their support and encouragement.

Finally, I would like to dedicate this PhD thesis to my parents for their love and belief.

Author's Declaration

This thesis contains the original work of the author except otherwise indicated.

Chapter 1 Introduction

1.1. Background of the project

The current research project is conducted in collaboration between the Royal National Lifeboat Institution (RNLI) and Bournemouth University (BU). The RNLI is a charitable organisation which rescues life at sea and comprises of a fleet of various sizes and classes of lifeboat. These lifeboats are needed depending on geographical features, such as sea, river, estuary, or muddy areas, and also the kind of rescue work. The Trent Class Lifeboat is one of the highly used primary All-Weather afloat Lifeboats used in the RNLI fleet (others include the Tamar, Severn and Mersey class). There are over 350 lifeboats which operate across the coasts of UK and Ireland from 238 lifeboat stations. These lifeboats function in severe and high impact rough sea environments to perform rescue operations with the priority to reach the rescue destination as quickly as possible. The lifeboat application is distinct from the other marine applications from an engine lubrication perspective, since it involves extreme engine running conditions at varied intervals and often subjected to either under or over engine maintenance due to unpredictable usage of lifeboats. The details of each class of lifeboats in terms of marine engine description and the type of lubricant used in the respective engines are mentioned in Table 1.

Table 1: Details of RNLI fleet of lifeboats with engine and lubricant description

Lifeboat Fleet	Marine Engines in Lifeboats			Lubricant Oil
	Engine Model	Power Output	Cylinders	
Trent Class	MAN D2840LE	850hp @2300rpm	10	SAE 15W40
Tamar Class	Caterpillar C-18	1001hp @2300rpm	6	SAE 15W40
Severn Class	Caterpillar 3412T	1250hp @2300rpm	12	SAE 15W40
Mersey Class	Caterpillar 3208T	280hp @2800rpm	8	SAE 15W40

In addition the current RNLI maintenance system for the engine lubricants is based on set intervals between inspections. The engine lubricant condition is analysed on quarterly basis by following a standard oil sampling procedure. The lubricant samples collected from the marine engines of lifeboats are analysed using different laboratory based standard tests including measurement of the kinematic viscosity of the lubricants at 40°C by capillary tube viscometer; wear and contaminant debris elements concentration by Inductively Coupled Plasma (ICP) - atomic emission spectroscopy; and soot content by Fourier Transform Infra-Red (FTIR) spectrometry. The collective report from these results provides information about the lubricant condition.

The time based maintenance approach followed by the RNLI is expensive considering the size of lifeboat fleet which influences the costs of each lubricant analysis performed; labour hours involved in extracting lubricant samples from each engine and the cost of logistics involved. In addition, the lubricant maintenance system is also time consuming as it has a high turn-around-time on getting the final analysis results and to plan the required maintenance work.

Survey of lubricant degradation in lifeboats operation

An investigative survey of the lubricant degradation in the marine engines of RNLI lifeboats fleet (details mentioned in Table 1) was undertaken. The oil parameters such as kinematic viscosity, elemental concentration of wear and contaminant debris, and soot content, were analysed as part of an oil analysis report. Over 4000 reports were studied which were maintained by the RNLI as a record of oil analysis carried out between the time period of 2009 and 2012. The study involved evaluating the average serviceable life of lubricants in marine engines between two consecutive lubricant changes. Also the primary reasons for lubricant changes in their respective serviceable engines were also analysed.

From the oil analysis data studied, it was noted that generally engine lubricants are changed after their serviceable life is completed usually due to the presence of high concentration of wear or contaminant debris and occasionally due to drastic drop in

lubricant viscosity owing to fuel or coolant leakage in the lubricant. The serviceable life of lubricants in different class of lifeboats was averaged from the available data by reviewing the complete history of lubricant changes carried out on different engines along with the engine maintenance records to eliminate any error in recorded data. For the ease of analysis purpose, the average of serviceable life of lubricants in marine engine was considered and the details are as shown in Table 2.

Table 2: Details of serviceable life and reasons for changing lubricants

Lifeboats Fleet	Average service-life of lubricants	Reasons for lubricant change in lifeboats
Trent Class	300 Hours	High concentration of iron
Tamar Class	300 Hours	High concentration of iron
Severn Class	300 Hours	High concentration of iron
Mersey Class	300 Hours	High iron/high viscosity

It was noted that contamination of lubricant by high concentration of iron element which resulted from the wear debris at around 300 hours of lubricant serviceable life in engines often resulted in lubricant changes. This phenomenon was noted for Trent, Severn and Tamar Classes of Lifeboat fleet. The reason for lubricant changes in Mersey Class lifeboats was also noted to be mainly high concentration of iron element but in conjunction with high viscosity of lubricant.

For detailed investigation, a trend analysis of changes in wear element concentration against the complete serviceable life of lubricant in the MAN manufactured engines of a Trent Class Lifeboat was carried out. Clearly, it was observed from Figure 1 and 2 that iron is the major constituent of wear metals debris generated during the engine operation. The main source of iron wear debris found in degraded lubricants was identified as the cylinder liner which has a material composition of around 92% of iron and each engine has 10 cylinders installed. It has also been mentioned in the literature that although the iron in lubricant can come from any ferrous engine component, the cylinder liners represent, by far, the greatest surface area [1].

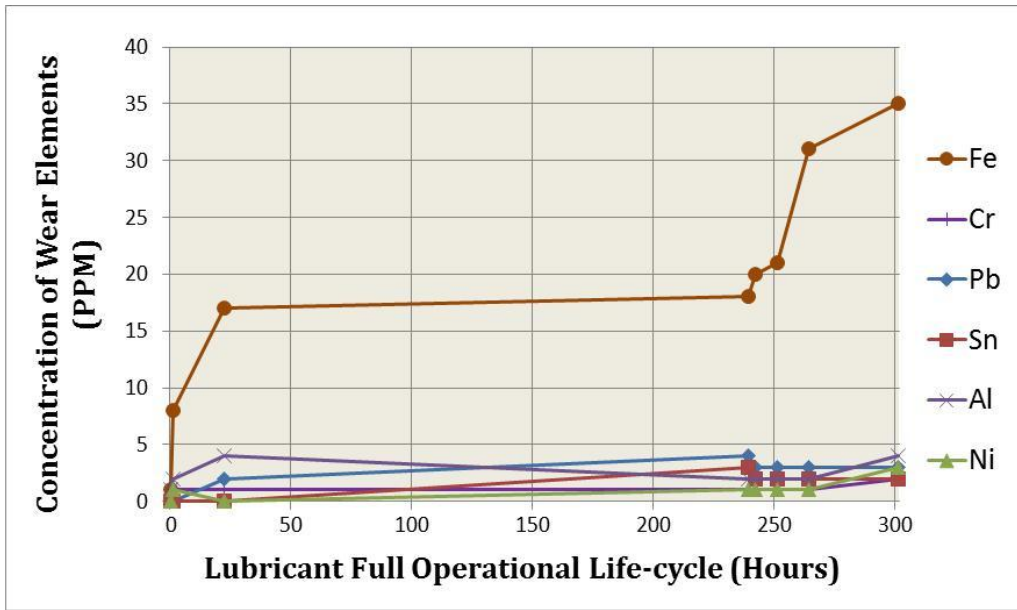


Figure 1: Wear element concentration measured by ICP spectroscopy for Trent Class lifeboat engine ON1253-P

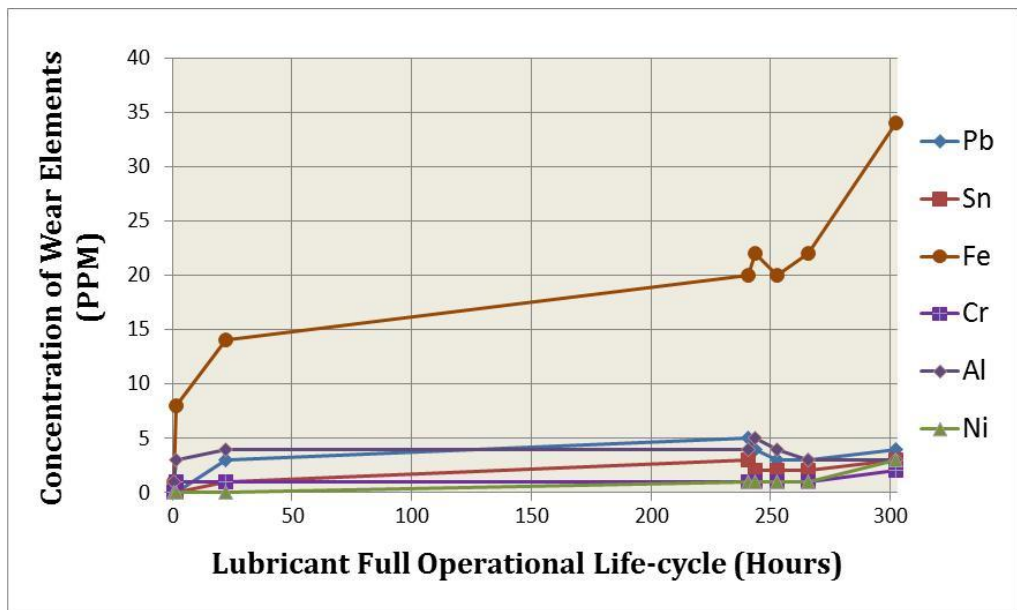


Figure 2: Wear element concentration measured by ICP spectroscopy for Trent Class lifeboat engine ON1253-S

It is known that about 50% of the total frictional losses taking place in internal combustion engine accounts to the power cylinder unit [2]. Although, the larger part of the cylinder liner – piston ring interaction area in the actual engine during each piston

stroke experiences hydrodynamic lubrication [3], but at Top Dead Centre (TDC) near the top piston ring reversal point boundary lubrication is prevalent. Therefore, significant amount of wear takes place in this region due to extremely high friction forces which are directly proportional to excessive combustion gas pressure, and furthermore, relatively slow piston speed prevents the hydrodynamic lubricant film to build up. Therefore it was found to be essential to conduct experimental research based on evaluating the tribological performance and effective serviceable life-cycle of lubricant in RNLI marine engines by simulating the piston ring and cylinder liner contact near TDC operating conditions.

1.2. Research aims

The primary aim of current research is to understand the key degradation mechanisms of diesel engine lubricants and affected engine components in lifeboat operations. The secondary aim is to provide a way to monitor real time lubricant degradation and investigate whether the tribological performance of diesel engine lubricants can be improved near the end of their service-life for wear reduction of main engine components. This will help reduce the maintenance costs and increase reliability of lifeboat engines.

1.3. Research questions

The research questions based on above aims are as follow:

- Understand the lubricant degradation mechanisms and the critical lubricated surface components subject to wear in diesel engines of RNLI lifeboats.
- Design laboratory based experiments that can accurately simulate engine testing environment, thence facilitating the real-time lubricant degradation monitoring using the on-line oil sensor system.
- Investigate and understand future improvements in the tribological performance of diesel engine lubricants near the end of their service-life.

1.4. State of the art

Based on the survey of the current state-of-the-art research on lubricant degradation mechanisms and wear mechanisms that cause severe wear of engine components, the detailed analysis of lubricant condition in diesel engines of lifeboats using some specific lubricant testing methods was carried out. These laboratory based lubricant tests helped identifying the depletion of ZDDP anti-wear additives as a function of lubricant duty-cycle in lifeboat engines.

Further the literature survey showed the use of Ionic Liquids (ILs) as additive in mineral based engine lubricant during product development stages. Thence indicating that IL could also possibly be employed as additive to the lubricant already in service in engine, thus reducing the effect of lubricant degradation on wear of engine components. Limitations to the use of ILs in diesel engine application were also studied. Therefore, in current research the novel idea of mixing phosphonium-based ILs as additive to engine-aged (in-service and used) lubricants was investigated with the hypothesis that the resulting mixture would reduce wear of such components.

The reciprocating bench testing rig was modified to accurately simulate the tribo-system of top piston ring and cylinder liner contact near top dead centre region. The above tribo-system was simulated for two primary reasons; firstly the cylinder liners installed in diesel engines used in lifeboat operation are the majorly affected components due to lubricant degradation resulting from ZDDP anti-wear additive depletion. Secondly, reproducing the boundary lubrication regime as experienced by piston ring-liner contact at TDC region facilitates the evaluation of anti-wear tribofilm formation behaviour of IL additives in aged lubricants. This involved the novel modification of an existing experimental test rig including a commercially available lubricant condition monitoring sensing system.

1.5. Outline of this thesis

Chapter 1 presents the background of the research project, research aims and questions which are addressed through the state of the art work carried in this research. This chapter also outlines the structure of the thesis.

Chapter 2 describes the comprehensive literature review of research topics related with this project, including engine tribology, engine lubricants and additives, different lubricant testing methods, condition monitoring of lubricants and ILs as lubricants and additives.

Chapter 3 outlines the different experimental techniques employed in current research for lubricant analysis along with their detailed procedures. It includes information about the materials preparation for tribological experiments. The test rig design and details about tribological analysis of different lubricants and their mixtures with ILs as performance improving additive are discussed. Different surface analysis techniques such as XPS, SEM-EDX and 3D white light interferometry which are either used for characterisation of boundary films or topographical changes on worn surfaces, are discussed. Finally this chapter also provides information about the stability analysis of lubricant and IL mixtures carried out using Turbiscan Lab Expert.

Chapter 4 describes the results obtained from the various lubricant analysis techniques. The condition monitoring results for in-service lubricant samples are also mentioned. These results explain the degradation mechanism of lubricant in RNLI lifeboat engines. Also the surface characterisation of actual cylinder liner from a MAN engine of a Trent Class Lifeboat is presented.

Chapter 5 describes the friction and wear analysis of different lubricant samples under boundary lubrication condition simulated using the modified tribometer. The comparison of friction and wear results with those obtained after addition of two different phosphonium ILs is made. Worn surface of flat plate samples was further employed for evaluating changes in the topography of surface and chemistry of boundary film. Results obtained in the form of XPS and EDX spectra for different elemental composition of boundary film are presented. Finally this chapter also includes the results for stability analysis of lubricant and IL mixtures.

Chapter 6 presents the discussion of results, conclusions and suggestions for the future research work.

References and appendices are presented at the end of this thesis.

Chapter 2 Literature Review

A comprehensive survey of published findings in the field of internal combustion diesel engines and performance of lubricants used in these engines was carried out. The objective was to explore the areas where there are openings for further research contributions whilst achieving the solution to the given industrial problem. The survey acts as a guiding path to frame the correct methodologies to accomplish the aims of the intended research with minimum diversions and also develops the breadth of understanding of the state-of-the-art.

2.1. Engine tribology

Lowering emission rates and improved fuel efficiency of IC engines has always been a challenge for the automotive industry due to stringent government regulation. This leads to demand for higher energy-conserving engine oils to reduce friction and conserve natural resource. There are many tribological contacts in IC Engines that need effective lubrication to avoid energy losses; these include piston assembly, bearings, transmissions, gears and drive train components [4].

Frictional losses alone accounts for 48 % of the total energy consumption in an engine [5]. Piston skirt, piston rings and bearings are responsible for approximately 66% of total friction loss and rest is covered by the valve train, crankshaft, transmission and gears [4, 6]. The major contributor of frictional losses in IC engine of 2-stroke and 4-stroke type, diesel or petrol based is due to the sliding contact of piston rings and piston skirt against the interfacing cylinder liner.

The top compression piston ring experiences the most complicated tribological contact against liner walls due to complex variations of load, speed, temperature and presence of lubricant. Although, the larger part of the ring-liner interaction area in the engine during each piston stroke experiences hydrodynamic lubrication [3], but at Top Dead Centre (TDC) near the top piston ring reversal point boundary lubrication is prevalent. High wear takes place in this region due to extremely high friction forces which are directly proportional to excessive combustion gas pressure and relatively

slow piston speed which prevent the hydrodynamic lubricant film building up. On the other hand, the piston itself also suffers from the transverse secondary movements towards the liner surface and tilting about the gudgeon pin. Such dynamics of pistons in cylinder blocks can result in piston slap which is the impact of the piston against the cylinder wall near top dead centre and may result in audible noise, increased sliding friction, and scoring of the running surfaces [7].

In addition to the effects of operational cycles of running engine, occurrence of regular start-stop conditions (as seen in lifeboat operations) results in disruptive EHL film formation in the mid-stroke region and potentially lead to a significant degree of asperity contact and possibly higher frictional energy loss and wear damage of the surfaces [8].

Major factors responsible for disrupting the oil film thickness are cylinder bore distortion mainly due to wear, piston speed, lubricant viscosity, top ring face profile, ring flexibility, boundary conditions and surface roughness characteristics [9]

2.2. Engine lubricants and additives

The prime functions of engine lubricants are to minimise wear and reduce energy losses due to friction. To reduce wear, lubricant forms a thick film separating two surfaces in relative motion with each other and taking the entire applied load. In high load and slow speed applications where thick fluid cannot be developed, lubricant provides wear protection by forming a thin chemical film on the surface. It also eliminates the risk against corrosion of components by neutralising the acids formed due to reaction of partially burned fuel during combustion with lubricant [4].

Engine lubricants contain a variety of chemical additives which are used to either enhance any pre-existing lubricant property or to impart a new desirable property. The chemical additives typically used to formulate engine lubricants are dispersants, detergents, oxidation inhibitors, film-forming agents (anti-wear/extreme pressure agents and rust/corrosion inhibitors) and polymeric additives (viscosity modifiers, pour point depressants, demulsifiers, foam inhibitors) [10]. Physical properties of finished lubricants are influenced by the structure and properties of lubricant base oil because

they make up the bulk of the lubricants. Chemical properties are attributed to the additives which added to the base oil. Commercial lubricating oils contain a number of multifunctional additives, either purchased as packages or formulated specifically to obtain a particular set of properties for any application [11]. The concentration of additives is typically around 10% w/w of a fully-formulated oil but can vary depending upon the nature of application [12].

In the 4-stroke heavy duty diesel engine, a complex environment including thermal, chemical and mechanical processes all taking place near TDC, results in insufficient availability of lubricant to form a thick film. The wear protection to liner and piston assembly surfaces is mainly provided by the chemical film formed by anti-wear additives present in lubricant. Scrapping and degradation of lubricant film results in accelerated wear losses. The prolonged use of lubricants in engine environments causes depleting additives levels and degradation of the lubricant physical and chemical properties [4].

Anti-wear additives

Anti-wear additives provide wear protection in boundary or mixed lubrication regimes which exhibit such conditions as low surface speed, high contact pressure and rough surfaces. Under extremely high operating load and high temperature, similar wear protection is provided by Extreme-Pressure additive or EP additives, such additives require higher activation temperature and load conditions than anti-wear additives. Both anti-wear and EP additives decompose by several known mechanisms to produce surface-active compounds which form a thin film in contact zone[13].

ZDDP (Zinc dialkyl dithiophosphate) is a multifunctional additive widely known for its anti-wear, antioxidant and corrosion inhibition properties. The ZDDP complexes are manufactured by reaction of alcohols, phosphorus pentasulphide and zinc salts [12]. ZDDPs break down to form a very thin (about 100–200 nm) amorphous polyphosphate film with varying chain lengths, this film known as tribo-film, anti-wear film or boundary film [14]. The pad-like tribo-film acts as a less stiff solid barrier which separates the contacting surfaces and accommodates the opposing asperities within

the soft substrate layers. It is also responsible for further reducing wear rate by digesting the abrasive oxide particle [15].

The mechanism of this tribo-film formation using different types of sophisticated instrumentation and laboratory based analyses has been investigated by various researchers in the past as mentioned in a review on ZDDP by Barnes et al. [12]. Also mentioned was the complexes which arise from the interaction between ZDDP and other co-additives present in lubricant during film formation.

Despite the useful anti-wear behaviour of ZDDP additives, the level of its use in automotive lubricants has reduced over years and will eventually be replaced by novel anti-wear additives that do not contain Phosphorus, Sulphur and any metal components[15]. Both governmental agencies and engine manufacturers are urging lubricant manufacturers to reduce the amount of ZDDP in the engine lubricants since phosphorus contaminant in the exhaust gas originated from the ZDDP gets deposited on the catalytic converter elements and reduces its serviceable life. Furthermore the US Environmental Protection Agency (EPA) has been regularly increasing the mandatory warranty periods for the catalytic converter, thus reducing the profit margin for engine manufacturers[14]. Sulphur is known to reduce the conversion efficiency of such exhaust gas components as CO, NO_x and un-burned hydrocarbons. Metallic ash produced by the burning of ZDDP additives affect the functioning of diesel particulate filter which increases the risk of contaminants emission [15].

Detergent additives

Detergents are an important class of automotive lubricant additive when used in crankcase engine oil. Ewa A. Bardasz and Gordon D. Lamb [13] described that in IC engines, combustion gases come in contact with crankcase oil due to blow-by processes during engine operation and since these gases contain sulphur oxides derived from the sulfur content of fuels (particularly in diesel engines), these interact with the base oil to produce sulfuric and organic acids. Therefore one of the primary functions of the detergent additives is to neutralize these in-organic acidic combustion by-products and also the organic acidic products formed by oil degradation processes. The second key function of detergents is to prevent the formation and build-up of varnishes on engine component surfaces that are operating at high-temperature such

as piston and piston rings. Furthermore these additives can also contribute to additional functionality like oxidation prevention of lubrications under the high speed and high load engine conditions. Studies have also shown in the past that Calcium based detergents and dispersants (phenates, sulfonates, salicylates) get absorbed on to the metal surfaces in competition to ZDDP, thus limiting ZDDP's effectiveness during engine operation.

Viscosity modifiers (or viscosity improvers)

Viscosity is another significant engine lubricant characteristic responsible for efficiently separating the contact surfaces in hydrodynamic regime. Low viscosity lubricants are needed for engine start-up, especially in cold climates. Also the tendency of lubricant viscosity to reduce with increase in temperature can result in excessive thinning of lubricants at normal engine operating conditions. Therefore engine lubricants are added with organic polymers based viscosity modifiers that change the solubility strength with differing temperatures. The solubility of the polymer improves as the temperature increases and the lubricant viscosity increases to its optimum value [14].

2.3. Lubricant test methods

Standard tests are used to evaluate the engine lubricant properties and performance to ensure the lubricant performs the way it should. These tests are performed at either engine dynamometer test beds or using bench test rigs. The tests include physical and chemical characterisation of lubricant, examining wear protection provided by additives and examining remaining effectiveness of the lubricant's additive package [4].

Figure 3 shows the three level sequence of lubricant testing followed by lubricant manufacturers when developing a new lubricant. Bench tests are accelerated tests which are performed to closely simulate the operational conditions which engine lubricants are subjected to in actual service. These tests are quick and very cost effective compared to full scale engine tests [11].

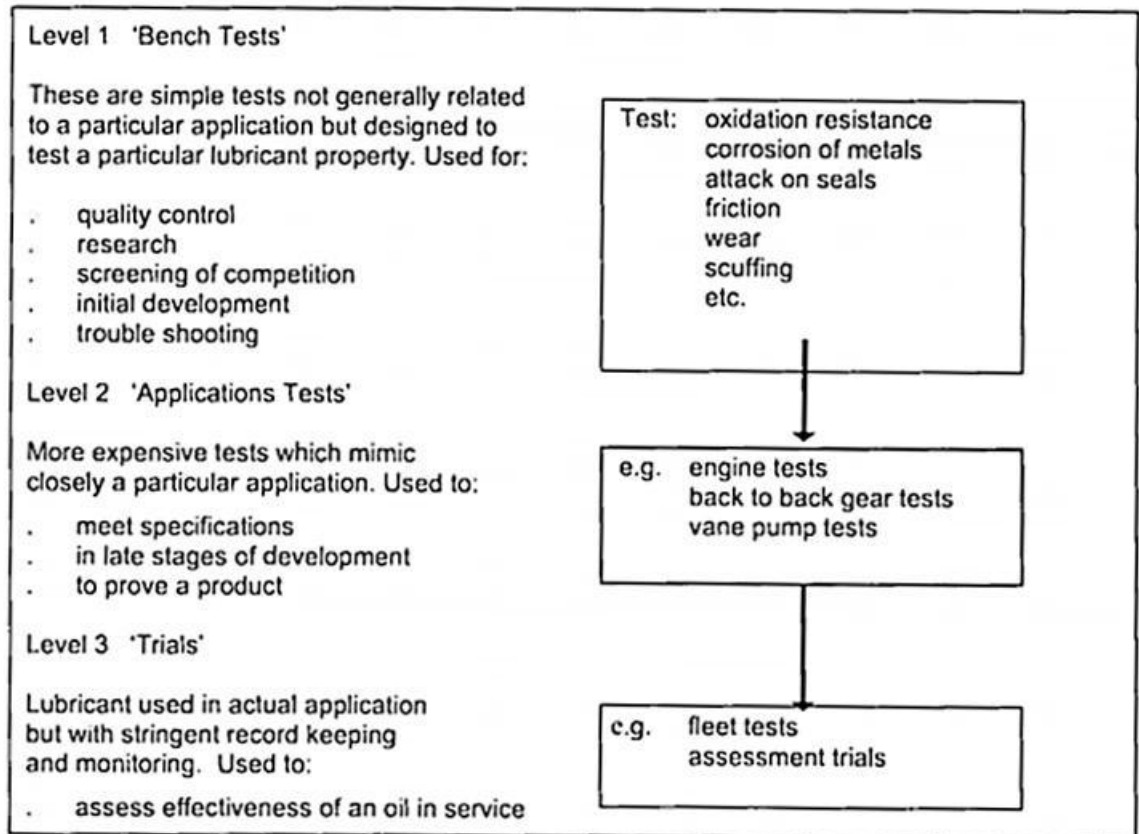


Figure 3: Three levels of testing of engine lubricants and materials [16]

Physical, chemical and mechanical (tribological) tests can be used to measure the composition and properties of a lubricant, the changes that occur as the lubricant ages, and the characteristics of any contaminants or wear debris that may have entered the lubricant.

Lubricant viscosity is measured at 40°C and 100°C, at atmospheric pressure and low-shear rates using viscometers. Capillary tube viscometers are used to measure kinematic viscosity which depends upon the force of gravity to drive set quantity of lubricant through the vertical capillary tube. Rotational-type Brookfield viscometers are also used to measure the absolute viscosity of lubricant for low temperature applications. Polymeric viscosity modifiers added to the lubricant are susceptible to shearing and result in viscosity drop with lubricant ageing depending upon magnitude and duration of shear forces [11].

2.3.1. Chemical testing of lubricants

Chemical tests involve a variety of elemental analysis techniques which are used for detecting concentration of wear metal and contaminant elements in used lubricants. Such techniques include atomic absorption spectroscopy (AAS), atomic emission spectroscopy (AES) and X-ray fluorescence (XRF). Inductively couple plasma (ICP) is an atomic emission technique most commonly used due to its cost effectiveness, speed and that it can detect several elements at same time. The elements detected can originate from the wear metal debris and also be a constituent of additives. Comparison with elemental composition of new oil is used to differentiate between the elements [11].

2.3.2. Lubricant condition monitoring

Lubricant condition monitoring can be done while it is in-service, by either collecting periodic lubricant samples for testing or using a real-time lubricant condition sensing system. The former is commonly known as oil-analysis or lubricant analysis of used oil, incorporating assessment of key lubricant condition parameters such as physical appearance, viscosity, wear metal or contaminant content and rate of lubricant degradation by reaction with combustion by-products in engine. The problems identified can be corrected by either adding the consumed additives or replacing the complete used lubricant [11].

2.3.3. Tribological testing of lubricants

Tribological tests are performed to assess the lubricant's performance in the laboratory. The outcomes of tribological tests depend upon the complete tribo-system involved namely, tribotester, operating conditions (surface load, speed, temperature), material type and condition of contacting surfaces, nature of contact, moisture, contaminants, and quality of base oil and additives [11]. These tests measure the effects of load and temperature on the film-forming capabilities of the lubricant, in terms of friction and wear outcomes. The results for new lubricants can be used for comparison with those for used lubricants to measure the relative effectiveness. In boundary lubrication regime applications, the friction and wear losses depend

primarily on the chemical composition of the tribo-film i.e. the additive package, and the rheological properties of the lubricant, i.e. viscosity, are of secondary importance. Since the formation of the tribo-film is a dynamic process which involves film formation and removal at the contacting surfaces [17], the chemical characteristics of tribo-film can be analyzed using energy dispersive X-ray analysis (EDX) and X-ray Photoelectron Spectroscopy (XPS) techniques.

According to Woydt et al. [18] the main objective behind conducting bench test (or tribometer test) should not be replacing engine test but seeking enough knowledge about friction coefficients, wear mechanisms and influence of process parameters which are difficult to obtain at engine level, considering both cost and time limitations. Similar argument was made by Morina et al. [19] mentioning about the difficulty in obtaining any meaningful and statistically significant correlations between the testing parameters and tribological performance from engine testing. The updated cost of engine testing has been mentioned to be between € 30,000 and € 400,000 (as published in early 2011 by Morina et al. [19]) depending on the equipment, instrumentation, engine size and test duration. Thus bench testing is cost effective alternative which allows a check before much expensive engine test that whether a tribo-couple or new lubricant would reach to reasonable engine performance level; thence reducing the large matrix of engine tests to a reasonable number.

Further, analysing the lubricant performance in a full scale engine test is complicated due to complex engine environment which involves interactions among the piston, piston rings, cylinder bore, lubricant, and chemical environment, with conditions varying from cold start to full power output. Therefore bench tribometer testing is a well-established alternative to engine testing. Obviously, it cannot fully simulate actual engine conditions such as mechanically applied load (instead of cyclic load variations), speeds are much lower, stroke is shorter (5-25mm compared to over 100mm), and the real motion of the piston ring (dynamic twists in piston groove) is not possible. But the advantage of bench testing is that it allows for better monitoring and control of the different operating parameters [20].

2.3.4. Simulating piston ring/cylinder liner contact in tribometers

Both mechanical and material parameters of tribo-system are important while designing a tribometer testing, so that similar wear mechanisms to those observed in the engine can be achieved [19]. Also, Lee et al. [21] in their review of test parameters for ring-liner contact in tribometer testing, demonstrated that it is not possible to simulate complete engine strokes at bench level, since the stroke is much shorter and also that varying the load throughout this short stroke length is extremely difficult in a tribometer. Hence only one position can be simulated i.e., TDC, BDC or mid-stroke. In the current research project, tribo-system of top piston ring and liner contact near TDC region is simulated for two primary reasons. One is that cylinder liners installed in diesel engines used in lifeboat operations are the main affected components due to lubricant degradation resulting from ZDDP anti-wear additive depletion. The second reason is that reproducing boundary lubrication regime as experienced by piston ring-liner contact at TDC region facilitates the evaluation of anti-wear tribofilm formation behaviour of IL additives in aged lubricants.

Previous research studies have simulated top piston ring and liner contact near TDC region using different operating conditions and test setups. Woydt et al. [18] in his review mentioned that there is no general consensus in testing community whether to use oscillating or continuous sliding motion which can simulate ring-liner contact and produce transferrable results, since both methods can operate under boundary/mixed lubrication conditions, as seen near TDC region of cylinder liner.

Test parameters– These must be set as close to actual applications (Woydt et al. [18]; Blau and Tung [16]) in contrast to that defined by standardised tests procedures like ASTM, DIN, and ISO etc. [18]. Blau and Tung [16] stated, simulating all aspects is not necessary but the key contact conditions of applications must be simulated, thence filtering out the more suitable candidate materials for further engine or field testing. For instance a simple unidirectional pin-on-disc sliding test under room temperature cannot be used for evaluating piston ring coating material.

Test configurations– The more commonly employed configurations include unidirectional sliding block-on-ring [22], reciprocating sliding piston ring segment-on-

liner section (conformal contact [19, 20, 23-29] and non-conformal contact [1, 30, 31]), reciprocating cylinder-on-flat [32], piston ring segment-on-rotary disc [18].

Reciprocating High-frequency friction and wear tester or tribometer, such as Plint TE77 (previously known as Cameron-Plint TE77), PCS HFR2, etc, has been used more often for simulating piston/cylinder bore dynamics. The main advantage of this configuration is that real engine components can be used hence preserving the metallurgy, geometry and surface finish effects; and the relative back and forth motion among the ring and liner specimens is similar to as seen in actual engine operation, which is otherwise not possible in unidirectional sliding block-on-ring setup [16, 33, 34].

Table 3 shows some examples of published work by other researchers using similar bench test parameters to simulate piston ring and cylinder liner contact near TDC region

Transferability of tribo-testing results - A qualitative wear ranking of tribo-couples as worst or best candidates can be done using tribo-testing; however there is no quantitative comparison possible with the engine testing [18]. Further it is mentioned that the worn surface morphology of bench test specimens to that of actual running engine components must be compared to look for same basic wear mechanism taking place [16, 18, 19].

For instance, Truhan et al. [1] simulated piston ring-on-cast iron flat under lubricated conditions at bench level and found wear rate of both liner and ring specimens was much higher than that in operating engine; but the actual basic wear mechanism was still same as seen in engine. They mentioned that the higher wear rate at bench level helps in conducting accelerated wear test so that results may be obtained in a reasonable test time.

Also as demonstrated by Noorman et al. [34] in their review of friction testing techniques at bench level that bench-measured friction coefficient results can be correlated with ultimate fuel economy results obtained from engine testing or vehicle testing. Also, the effect of different variables, exemplifying viscosities and additive

concentrations of different formulated lubricants, can also be correlated to Engine Fuel Efficiency data; thence depicting the highest contributing variable to the fuel economy.

Table 3: Examples of bench test parameters used for simulating reciprocating piston ring – cylinder liner contact near TDC

Source	Load	Stroke	Sliding frequency	Lubrication regime
Galligan et al. [20]	80N	5mm	4.4 Hz	Boundary regime
Truhan et al. [31]	240N	10mm	10Hz	Boundary regime
Truhan et al. [1]	240N	10mm	10Hz	Boundary regime
Qu et al. [30]	240N	10mm	10Hz	Boundary regime
Johansson et al.[26]	320N	8mm	10 Hz	Boundary/Mixed regime
Olander et al. [35]	15–150 N	40mm	5 Hz	Boundary regime

2.4. Ionic liquids as lubricant and additive

Ionic Liquids (ILs) are salts with melting point below 100°C. These ILs can be used in variety of applications, exemplifying as catalyst, liquid crystals, green solvent in organic synthesis, and in separations, electrochemistry for use as electrolytes in batteries or for metal electro deposition, photochemistry, CO₂ storage devices, etc. [36, 37]. They are also experimentally proven to possess superior inherent properties such as high thermal stability, very low volatility, and non-flammability and low melting point. Such properties makes them ideal candidate for use as lubricant in many tribological applications. The pioneer work by Liu et al. [37, 38] demonstrated the above argument by evaluating imidazolium based ILs for various material pairs such as steel/steel, steel/aluminium, steel/ceramics, etc. which proved the suitability of ILs as lubricant. The idea of Liu's group in above the work was to introduce ILs as a versatile lubricant which can be used irrespective of the application due to its inherent multipurpose properties.

Despite the useful anti-wear behaviour of ZDDP additive, the level of its use in automotive lubricants has reduced over years and would eventually be replaced by novel anti-wear additives that do not contain Phosphorus, Sulphur and any metal components [15]. Both governmental agencies and engine manufacturers are urging lubricant manufacturers to reduce the amount of ZDDP in the engine lubricants since phosphorus contaminant in the exhaust gas originated from the ZDDP is deposited on the catalytic converter elements and reduce its serviceable life. Furthermore the US Environmental Protection Agency (EPA) has been regularly increasing the mandatory warranty periods for the catalytic converter, thus reducing the profit margin for engine manufacturers [14]. Sulphur is known to reduce the conversion efficiency of such exhaust gas components as CO, NO_x and un-burned hydrocarbons. Metallic ash produced by the burning of ZDDP additives affect the functioning of the diesel particulate filter which increases the risk of contaminants emission [15].

Another reason for developing more effective novel anti-wear additives is to be used with low viscosity grade lubricants for internal combustion engines. This would provide wear protection in BL regions alongside the balance with lower viscosity would help reducing the shear resistance in EHL regions, hence less frictional losses [29, 39].

Both fundamental research which leads to development of components materials and lubricants, and real application based research which focuses mainly on product evaluation and failure analysis [40], can contribute significantly to the automotive industry. Bo Yu et al. [28] explained that the recent development into the IL research is mainly taking place in three areas: tailoring the molecular structure of cation and anion moieties of ILs to attain better lubricating performance; understanding the tribochemical interaction between the contacting material and IL; and modifying the surface of nanostructured materials using ILs to obtain synergistic effects.

Bermúdez et al. and Minami [41, 42] in their review papers explained that a lot of research has been carried out since 2001 investigating the behaviour of ILs for its potential use either as a lubricant in neat form or additive. However, the first investigation of use of IL as lubricant was carried out by Liu et al. [37] and their research outputs proved ILs possessing outstanding anti-wear and reduced friction behaviour.

Following to this initial investigation, many researchers have tried evaluating different combinations of cationic and anionic moieties to achieve superior tribological performance. These studies [43-50] showed common cations used are imidazolium, ammonium, pyridinium and phosphonium based with counterpart anions as BF_4^- , PF_6^- and $(\text{CF}_3\text{SO}_2)_2\text{N}^-$ and phosphate-derived.

The evolution in the understanding of various characteristics of anion and cation has led to some useful conclusions. For instance, hydrophobic anions $(\text{CF}_3\text{SO}_2)_2\text{N}^-$ possess less friction and wear than hydrophobic ones e.g. BF_4^- [51-53]. Tetra-alkylphosphonium and tetra-ammonium cations are known to exhibit better thermal stability than two-dimensional alkylimidazolium cations [53].

XuQing Liu et al. [36] in their experiments demonstrated the superior tribological performance of asymmetrical tetra-Phosphonium ILs compared to a most excellent alkyl-imidazolium lubricant (1-ethyl-3-hexylimidazolium hexafluorophosphate) for

Al/steel sliding contact. Similar performance of asymmetrical tetra-phosphonium ILs was seen for steel/steel contact compared to imidazolium ILs as demonstrated by Li Jun Weng [54]. Latter study stated that may be due to the presence of active element phosphorus (P) which reacts with the fresh metal surface to form a lower shear strength reaction film, the phenomenon seemed much effective at higher temperatures (100°C) compared to room temperature (20°C).

Ichiro Minami et al. [53] reported the effect of chemical structure of ILs on their tribological behaviour mainly focusing on salts of tetra-alkyl phosphonium cations. Their study demonstrated that combinations of tetra-alkyl phosphonium cations with phosphate, thiophosphate or $(CF_3SO_2)_2N^-$ anions possess better tribological properties over 1,3-alkylimidazolium bis(trifluoromethanesulfonyl) amide. The performance sequence of ILs of tetra-alkyl phosphonium cations with different anions noted as thiophosphate > phosphate > $(CF_3SO_2)_2N^-$. The reasoning mentioned to be based upon the formation of protective phosphate tribo-film in the first two cases than fluoride tribo-film in the last case. These iron-fluoride films are also known to cause rusting of iron surfaces and degradation of the lubricants through hydrolysis. In addition to above, the length of alkyl chains in the phosphonium cations also found to levy some positive effect on the tribological properties.

Some work has also been done to further improve the performance of IL by adding additives, similar in a way used for conventional base lubricants. Liu et al. [37] mentioned wear reducing capability of small quantity of water (ca. 5 wt.%) in ILs for major tribological pairs such as steel/steel, steel/aluminium and steel/ceramic, but with no change in frictional response. Although, later researches stated the corrosion related issue with alkyimidazolium or fluorine containing ILs when used against metal [36, 53, 55].

2.4.1. Limitations for ionic liquids in diesel engines application

In case of diesel engine applications, ammonium and imidazolium based ILs with $[(CF_3SO_2)_2N]^-$ anion moiety has been investigated for potential use both in lubricant form and lubricant's additive. Since these ILs are hydrophobic and chemically stable

when exposed to water, unlike other ILs containing BF_4^- and PF_6^- which react with water through hydrolysis to produce corrosive HF [30, 56, 57]. Other engine favourable properties of these ILs mentioned as high thermal stability, non-flammability, superior tribo-film forming capability and can prevent corrosion due its solvent nature which provides detergent behaviour [30]. However, they also mentioned the problem of low solubility of these ILs in mineral base oil when used as additives.

More recently (2013), low-viscosity imidazolium based IL was presented as neat lubricant for engine application [39]. The study concluded that less change in viscosity of IL at high contact pressure (due to inherent low pressure-viscosity coefficient for low and high temperatures) under ML and EHL regimes could results in lower shear traction compared to hydrocarbon based oils. This conclusion was attributed to the layered structure of the tribo-film formed by the ILs, discussed in detail later. In addition to superior tribological performance the IL also possessed non-corrosive nature to metals essential for diesel engine application. But at present using IL as additive, than neat lubricant, for engine application seems to be an economical option due to higher costs of IL. However, multiple-recycling of ILs after use could bring down the overall cost of employing ILs [58] in real applications.

Some experimental studies [28, 29] have addressed the issue of limited miscibility (<1%) of all ILs with non-polar hydrocarbon oils, both mineral and synthetic based. Such IL-oil blends are mentioned as unstable emulsions which can only accommodate very small quantity of ILs. Although, miscibility is not an issue when ILs are used in neat form or as additive in polar oils such as ester and poly (ethylene glycol) [28], but in real applications where large quantity of lubricating oil is needed, this option becomes less feasible from an economical point of view.

2.4.2. Phosponium ionic liquids

However, the development of two new Phosponium ILs [28, 29] Trihexyltetradecyl phosphonium bis(2,4,4-tri-methylpentyl) phosphinate and Trihexyltetradecyl phosphonium bis(2-ethylhexyl) phosphate which are fully miscible with both polar and non-polar oils seem to be a key to the miscibility problem. The molecular structure of these two newly developed phosphonium ILs is shown in Figure 4 and Figure 5.

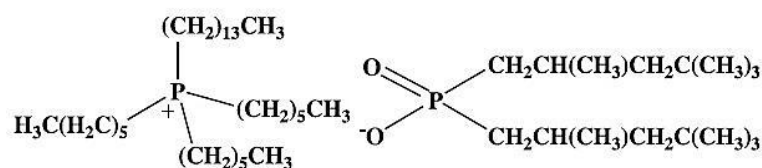


Figure 4: Trihexyltetradecyl phosphonium bis(2,4,4-trimethylpentyl) phosphinate [28]

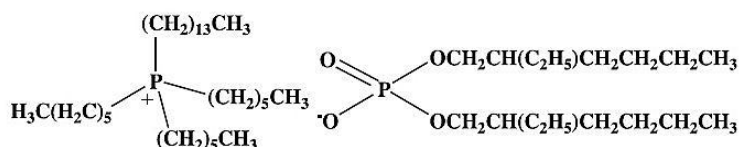


Figure 5: Trihexyltetradecyl phosphonium bis(2-ethylhexyl) phosphate [28]

The reasons behind better miscibility of such ILs with neutral or non-polar oil molecules are hypothesised as Three-dimensional quaternary structures with at least one alkyl with four carbons or more for both the cation and the anion to make the charge on ions diluted. Formation of hydrogen bonding between cation and anion moieties results in a quasi neutral molecule.

Other ILs either contain two-dimensional cation or the anion part is too small thus the polarity of ionic molecule is not diluted. The good examples given are imidazolium cation and bis(trifluoromethylsulfonyl)imide (Tf2N) anion [29]. It has also been emphasised that the role of both anion and cation structure is significant in wear reducing lubricating properties [30]. This research contribution by Bo Yu et al. [28] and Jun Yu et al [29] in the development of these new ILs has an incredible benefit to the lubrication industry since it proposes the above key areas to consider when tailoring the molecular structure of ILs to make them oil miscible. But the above hypothesis still needs to be further investigated. The research group also proved the 100% compatibility argument of above phosphonium ILs by mixing them in different proportions between 1% to 95% w/w of both base oils and fully formulated engine oils derived from petroleum (mineral oils) and synthetic sources (all these oils utilised in the experiments were fresh or new oils). The visual inspection of oil and IL mixtures were found stable with no cloud formation or phase separation at both low (-18^oC) and high (175^oC) temperatures, thus depicting stable 100% miscibility. Further

validation of miscibility was obtained by comparison of experimental viscosity values of different oil-IL blends with that of theoretical values obtained by using Refutas equation for single-phase multiple component liquid mixtures, Refutas equation is as mentioned below [28, 29].

Another experimentally proven benefit of these two phosphonium ionic-liquids is that they cause no corrosive attack to metal surfaces both at ambient and elevated (135^oC) temperatures owing to the hydrophobic nature. Research by both groups [28, 29] demonstrated that cast grey iron and cast aluminium showed no traces of pitting (indicative of corrosion) when left dipped for 7 days in phosphonium ILs at 135^oC, whereas a common imidazolium IL 1-benzyl-3-methylimidazolium bis(trifluoromethyl-sulfonyl)imide ([Bzmim][NTf₂]) showed pitting just after 2 days even at ambient conditions.

Further the superior tribological performance of quaternary structured phosphonium based ILs compared to imidazolium based IL was also proven by studies [36, 54]. They also mentioned about the corrosion associated problems with pyridine and imidazolium based IL when used as lubricants. The use of organic phosphorus is emphasised by mentioning its better compatibility with other lubricant additives.

2.4.3. Mechanism and structure of tribo-film formed by ionic liquids

Due to the still fairly new topic of research usage of IL as lubricant or additives, there is very limited information available which explains the tribo-film forming mechanism and its structure. So far it has been hypothesised that the tribo-chemical reactions between the metal surface and ILs results in the formation of tribo-film which prevent friction and wear losses [29, 36, 40, 54]. Both thermal and mechanical stresses play an important role in forming such a protective film [40] which is otherwise not present in lubricated non-contact zones.

Both XuQing Liu et al. [36] and LiJun Weng et al. [54] in their work explained the physical and chemical adsorption of IL on metal surfaces takes place because of the electronegative components in IL and the positive polarity on metal surfaces. They

explained that metal surfaces are known to be naturally positively charged and further their relative sliding motion creates active positively charged sites onto worn surfaces due to emission of low-energy electrons [59] from the colliding asperities. The negatively charged anion part of IL molecule may get adsorbed onto the positive sites thus forming a protective layer on metal surface. Liu [36] introduced the idea of layered structure of IL produced tribo-film which retains reduced friction and wear losses owing to its low shearing strength.

Later, Gregory Mordukhovich et al. [39] also mentioned about the film forming mechanism by further explaining the absorption process in terms of coulombic forces which creates the first mono-layer of ILs on the worn surface, as shown in figure 3. The subsequent layers on top of the mono-layer are formed by the coulombic attraction or weak hydrogen bonding between the cation part of thus formed mono-layer and the anion part of other molecules of IL, and so on. Therefore a multi-layered structure possessing low shear strength reduces the effect of tangential friction forces by slip conditions and also prevents wear by avoiding the direct contact between interfacing metallic asperities.

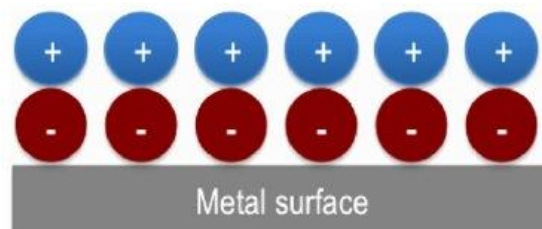


Figure 6: Monolayer formed by IL on metal surface. Image source: [39]

The tribo-film formation and removal from the metal surface is described as a continuous process and in steady-state conditions equilibrium in these two processes is deemed to be reached which prevents wear [39]. The tribo-film formation process is attributed to the reason described earlier but removal process could be because of degradation of film due to continuous sliding which eventually leads to film removal from the surfaces whereas the components of IL responsible for film formation are ineffective or consumed by being transferred into degradation by-products.

Ichiro Minami et al. [53] in their study of tribo-chemistry of several combinations of phosphonium cations with different anions showed severe reactivity of anionic moieties with metal substrate than cationic ones. However the reactivity of anionic moieties was demonstrated as a function of applied load and also influenced by the cationic moieties under certain conditions. Therefore, depicting the necessity of sufficient activation energy for the reaction of active elements in the anion part with the metal surface whereas at lower load applications mere adsorption of anion elements was noted. In the latter case, the cation moieties are noted to have some influence on the reaction of anionic moieties with metal surface leading to reduced reactivity of anion with metal. For instance, the reaction of (thio) phosphate anions produced a phosphate-containing tribo-film and amide anions produced fluoride-containing tribo-film. Whereas, at low load conditions, ILs made of phosphor based cation and fluorine based anion (amide anion) produced tribo-film that contained both phosphate and fluoride parts along with an adsorbed amide on top-surface of film. But at relatively higher load conditions for same IL, only fluoride-containing tribo-film has formed with no phosphorus in it. Hence, the study depicted the effect of load on the reactivity of anion moieties and also the involvement of cation moieties at lower load conditions.

Jun Qu and Miaofang Chi et al.[40] described the material dependent behaviour of IL towards tribo-film formation process and various characteristics such as film thickness, nanostructure and chemical composition. They demonstrated the distinct level of interaction of ammonium based IL with steel, grey cast iron (Fe) and Aluminium (Al) as substrate materials. The steel substrate showed tribo-film of 60 nm, Al of 200nm whereas in case of Fe 300nm thick film along with another 10-30nm thin interlayer between tribo-film and substrate was noted. Like steel, the nanostructure of tribo-film formed on Fe substrate was a fine dispersion of nano-crystals (size few nm) embedded in an amorphous matrix of IL material but also included an interlayer containing mixture amorphous IL material and deformed metallic particles generated from initial wear-in process. In case of Al substrate, the tribo-film was composed mainly of large metallic nano-particles (size up to 30nm) which are deemed to be generated during the initial wear-in process due to soft nature of Al. The chemical composition of the tribo-film, in all cases, portrayed as high in concentration with lubricant elements and oxides on film top surface gradually reducing to zero at the metal substrate. Altogether, tribo-film formation is explained as a gradual process

involving tribo-chemical reaction of ILs with metallic substrate until all metallic sites are consumed.

Jun Qu and Dinesh G. Bansal et al. [29] demonstrated similar behaviour of ILs towards tribo-film formation. They used phosphonium-based IL as additives in synthetic base oil and fully-formulated synthetic engine oil (already containing commercial ZDDP anti-wear additive), against grey cast iron surface. Their results showed good synergy between phosphonium IL and ZDDP additive which lead to formation of much thicker film (250-350 nm), unlike when added to synthetic base oil (film thickness 120-180 nm). Both mixtures outperformed when benchmarked against fully-formulated synthetic engine oil in which case thickness was 40-60 nm. Again the nanostructure of film in all cases composed mainly of amorphous matrix of nano-sized fine crystals [29].

2.4.4. Interaction between ionic liquids and conventional anti-wear additives

Very limited literature is available to study the interaction between ILs and conventional anti-wear additives (like ZDDP). Investigation by Jun Yu et al. [29] involving addition of phosphonium-based IL Trihexyltetradecyl phosphonium bis(2-ethylhexyl) phosphate as additive (5% w/w) to fully formulated synthetic engine oil (5W30) revealed good synergism with already present commercial additives (including ZDDP anti-wear additive) resulting in lower wear rate than neat 5W30 for cast grey iron. Zinc (Zn), sulphur (S) and phosphorus (P) were the major constituent elements of tribo-film noted on the worn cast iron surface in case of 5W30+IL (5% w/w) blend compared to neat synthetic 5W30 oil where little P but mainly Zn and S were noted.

In case of mineral-based fully-formulated 15W40 engine oil investigated by Jun Yu et al. [30], mainly Zn, P and Calcium (Ca) were found on the worn surface of grey cast iron. The source of Zn and P were mentioned to be ZDDP anti-wear additive whereas Ca from Calcium Sulphonate detergent additive.

2.4.5. Experimental techniques to evaluate boundary film formation of ionic liquids

Many researchers have tried to understand the different characteristics of tribo-films making use of various technologies available today. Chemical composition and the structure of chemical compounds present in the tribo-film by energy-dispersive x-ray spectroscopy (EDS) and X-ray photoelectron spectroscopy (XPS). The limitation with EDX is the difficulty to distinguish between the sources of different elements detected, therefore in such cases XPS could prove useful. XPS detects change in binding energy of active elements primarily present in lubricant (and/or additives) [30] or substrate material, depicting the chemical reactions taken place during the friction testing.

In the past, only 2-dimensional analysis of tribo-film from the top of worn surfaces could be performed, but recent advances in technology have enabled complete 3-dimensional characterization of tribo-films, including topographical and chemical analyses of top surface, cross-section and different layers of tribo-film on metallic substrate. The process involves preparation of the near-surface zones using Focused-Ion Beam (FIB) equipment which extracts a thin cross-section from the worn surface without disturbing the tribo-film surface structure. Scanning electron microscopy (SEM) and Transmission electron microscopy (TEM) can then be used for examination of film thickness and film physical composition (visualization of nano-particles embedded in IL composite material). EDX and XPS techniques can be employed to evaluate the film chemical composition and change in chemical composition from film surface to metal substrate [40]. Electron diffraction pattern has been used to study the nano-composition of tribo-film to confirm the presence of nano-crystals from lubricant and/or metallic nano-particles within the tribo-film which are produced during the initial wear-in process and get embedded into tribo-film.

Depth-composition profiles produced through ion-sputtering of worn surface by XPS analysis can be used to study the variation in chemical composition of tribo-film and indirectly also indicating the film thickness.

Chapter 3 Experimental Methodology

The experimental work was conducted in three stages, namely Pre-test Stage, Test Stage and Post-test Stage.

Pre-test Stage involved measuring the physical and chemical properties of different engine-aged lubricant samples collected from the marine diesel engines of the RNLI lifeboats. New 15W40 engine oil has also been tested in this stage for comparison with bench-marked performance level.

Test Stage involved evaluating the tribological performance of different lubricant samples with and without ILs as tribological performance improving additives using the high frequency reciprocating tribometer under the boundary lubricant conditions representative of those experienced by the ring-liner contact near the top ring reversal point of TDC in IC engines. Experiments at two different temperature conditions, i.e. 100°C and room temperature, representing engine running and cold start lubricant temperature were performed. In this test stage, real-time lubricant condition monitoring was also performed for different lubricants samples collected in situ with tribo-testing. Lubricant properties such as viscosity, density, dielectric constant were analysed in real-time using the Fluid Properties oil sensor.

Post-test Stage involved mainly the surface analysis of worn surfaces of test samples used in tribo-testing (Test Stage) to evaluate the effect of addition of ILs to different lubricant samples in terms of wear mechanisms and chemical composition of boundary film. This stage also involved surface analysis of actual cylinder liners from the marine engines of RNLI lifeboats to evaluate the wear mechanisms.

3.1. Lubricant samples collection

The lubricant tested in the experiment is commercially available mineral-based SAE 15W-40 engine oil typically used in heavy duty diesel engines. The same lubricating oil is used by RNLI in almost every diesel engine installed in RNLI Lifeboats.



Figure 7: (a) Used oil samples collected from Trent Class Lifeboat at different service intervals; (b) and (c) New lubricating oil (SAE 15W40) from two different manufacturers; (d) Mineral base oil

The lubricating oil samples were collected directly from the engine sump of MAN D2840LE401 diesel engines installed in Trent Class RNLI lifeboats. The samples were collected using the oil-suction pump into oil sampling bottles following the RNLI Oil Sampling Guidelines. These oil samples, as shown in Figure 7 (a), were collected at different service intervals such as 135h and 196h which represent the in-service condition of lubricating oil. Whereas the oil samples collected at 315h from the engine represents the completely used condition since its standard oil analysis report showed it unsuitable for further service. Furthermore, these oil samples were collected from oil

sump after running engine for at least half-an-hour. This was done to allow heating and thorough mixing of oil by circulation in engine prior to its sampling so that a uniform mixture of oil could be collected as a representative of whole engine sump oil.

New (or fresh) engine oil and mineral base oil also employed in experiments for performance comparison. Both the new 15W40 engine oil and mineral base oil were supplied in sealed container form, as shown in Figure 7 (b) to (d). These oils were supplied as an in-kind support from RNLI (UK) and Repsol S.A. (Spain).

3.2. Pre-test Stage (Lubricant Analysis)

A comprehensive lubricant analysis was performed on the new (fresh) lubricant and the engine-aged lubricant samples collected from actual marine engines of Trent Class Lifeboats at different hours of their service. The standard laboratory based tests were conducted on these samples to evaluate the physical and chemical properties of the lubricant before using them for reciprocating tribo-tests. The brief description of procedure used in each of the above lubricant analysis tests is mentioned below.

3.2.1. Viscosity measurement (IP71/ASTM D445)

Kinematic viscosity of the lubricant is tested to assess its resistance capability when flowing against gravity through the oil galleries in internal combustion engine environment. The lubricant was tested at 100°C as it corresponds to the average oil temperature in actual running marine engine. Also, 100°C reduces the rise of measurement interference for engine oil soot contamination [71].

The Capillary Tube Viscometer Test Method was used to determine the viscosity of lubricant. In the test, a measured quantity of lubricant is placed into a glass capillary U-tube held vertically in a chamber maintained at 100°C (or 40°C) and the time it takes for the lubricant to flow between the two marked points on the tube is noted. The lubricant flow-rate is calculated in mm²/s, and this defines the resistance of the oil flowing under gravity through the capillary tube. The detailed description of the procedure can be found in the test standard ASTM D445 [72].

3.2.2. Gas Chromatography (Diesel Fuel Dilution)

Fuel contaminants in engine lubricants leads to degradation of lubricating oil and can also lower its viscosity to a point where it loses its optimum functionality. Gas Chromatography (GC) test is often carried out on engine lubricants samples which shows significant drop in the trend of their viscosity. Again the GC results can also be trended for failure analysis but this process is little time consuming.

The procedure of the GC test involves separating of components of mixed substances, such that process involves mainly 3 steps; injection, separation and detection. In this test a small oil sample is injected into a flowing stream of inert gas which acts as a mobile phase and is made to vaporise. The separation of the oil components takes place onto the analytical column. The column consists of an inert solid (fused silica) containing a liquid stationary phase bonded to the surface of the fused silica. The separation of oil components depends upon a number of factors including the type of stationary phase in the column, boiling temperature of the components, flow rate of the mobile phase and temperature. The newly separated components of the mixture interact with the mobile and the stationary phases. The components with a high affinity to the mobile phase pass through the column first, while components with a higher affinity to the stationary phase are retained on the column for longer time. Flame ionization detector is used as a detector. The separated components are then made to pass through the detector which ionizes them by a small hydrogen flame. The charged ions thus produced then conduct electricity which is measured in mA by the collector electrode. The area under the graph obtained for time vs. mV is used for quantitative analysis [73].

3.2.3. ICP Spectroscopy (ASTM D4951/D5185)

This test determines the elemental concentration of wear metals and contaminants present in lubricants by ICP – atomic emission spectrometry. The detection time period takes only few minutes and results are obtained in part-per-million (ppm) or mg/kg. The analytical results obtained are particle (debris) size dependent, and low results are obtained for particles larger than a few microns. Therefore only particles smaller than 10µm in size are detectable by this technique. The knowledge of concentration of wear metals can be indicative of excessive wear by comparing the

data with base line concentration obtained from testing new lubricant. Similarly increase in concentration of elements like Boron, Sodium or potassium is indicative of contamination due to coolant leak in lubricant.

A lubricant sample is homogenised by placing in the ultrasonic bath, to obtain a test sample that is representative of entire quantity. A weighed portion of thoroughly homogenised sample is then mixed with a suitable dilution solvent until its concentration is 10 mass %. The solution is introduced into the ICP spectrometer by free aspiration or using peristaltic pump with the pumping speed in the range of 0.5 to 3 mL/min. Lastly, ICP employs the ultraviolet light and visible spectrometry to image the plasma at specific wavelength of the ionic excitation of elements of interest. The emissions intensities of elements thus obtained are compared with those measured with the standards, the difference in two thus provide the concentration of elements in the lubricant sample used. The detailed description of the procedure can be found in the test standard ASTM D5185 [74].

3.2.4. Nuclear Magnetic Resonance (NMR)



Figure 8: AVANCE III HD NMR Spectrometer at BP Lubricants (Pangbourne, UK).
Image source: Bruker website

Additive depletion effects engine oil losing its optimum functionality and can eventually leads to tribological and corrosive distress of main engine components if not diagnosed in time for the corrective measures. It is well known that as the lubricant enters into service in engines, the ZDDP additives molecules start to degrade. NMR technique can be used to detect the ZDDP additive depletion in the engine lubricants [75]. Lubricant sample of around 3ml (without solvent) along with benzene for field locking was added to a 10 mm tube and the P-31 spectra were recorded using the AVANCE III HD NMR Spectrometer, as shown in Figure 8. Each lubricant samples considered in the current research was tested for 8 hours and the obtained results are discussed in later in this thesis.

3.2.5. Analytical Ferrography

Analytical Ferrography can be used to identify the wear mode of lubricated components by examining the particles present in engine lubricant due to wear or contamination. A ferrogram is prepared with a glass microscope slide and has magnetic particles (such as iron) deposited on its surface. The ferrogram prepared is then examined under the optical microscope to distinguish particle size, concentration, composition, morphology and surface condition of the ferrous and non-ferrous wear particles. To prepare a ferrogram the lubricate sample is first diluted for improved particle precipitation and adhesion. The diluted sample flows down ferrogram which rests on a magnetic cylinder and attracts ferrous particles, separating them from the oil, as shown in Figure 9.

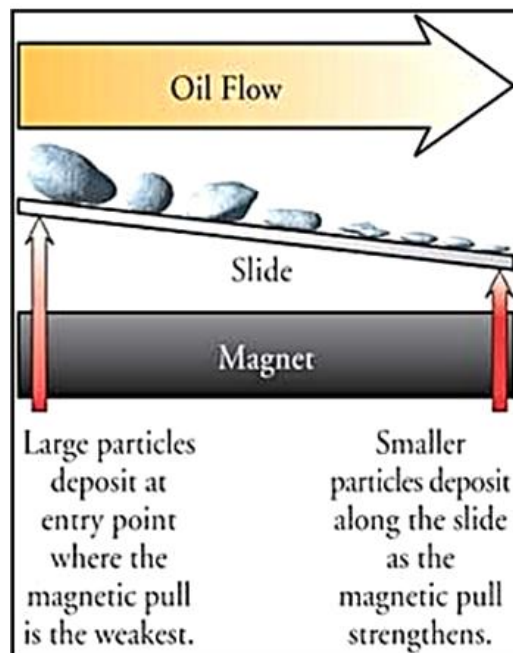


Figure 9: Process of making a ferrogram by separating particles from the oil [76]

The varying intensity of magnetic field obtained by keeping one end of slide at an angle helps with the alignment of ferrous particles. These particles become deposited along the length of the slide with the largest particles being deposited at the entry point, as shown in Figure 9. The non-ferrous particles are unaffected by the magnetic field and travel slide downstream and become deposited across the length of the slide. The ferrogram is then used for the examination under the microscope [76]. The detailed description of the procedure can be found in the test standard ASTM D7690 [77].

3.3. Test Stage (Lubricant Tribological Analysis and Condition Monitoring)

3.3.1. Test rig setup to simulate engine lubricant conditions

Schematic of the test rig setup designed and commissioned in this research is shown in Figure 10. High Frequency Friction tribometer TE77 (manufactured by Phoenix Tribology Limited) was modified to simulate engine lubricant conditions and perform a real time on-line lubricant condition monitoring.

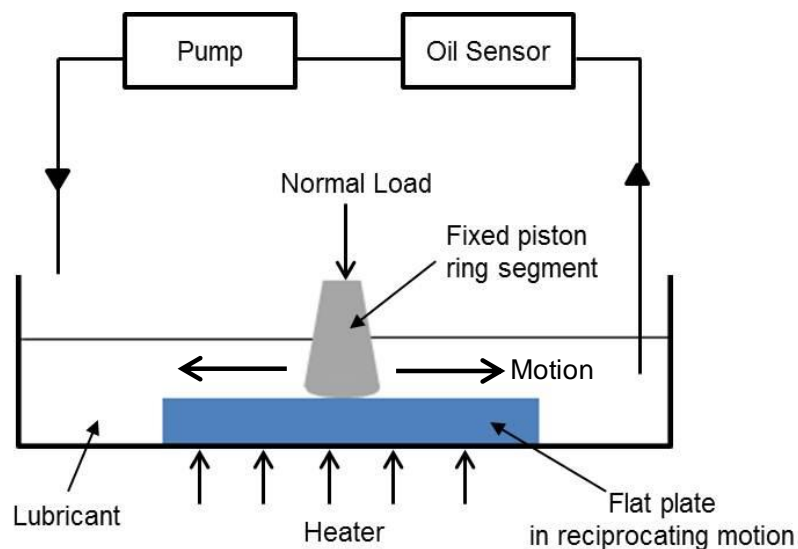


Figure 10: Schematic of modified High Frequency Friction tribometer TE77

Piston ring specimens were prepared by cutting a new compression piston ring into a number of small segments. Details of its material specification are mentioned in section 3.3.2. Piston ring segment was fitted into a holder which provides the optimal contact between piston ring running face and counter-facing flat plate used as cylinder liner bore surface. The normal load was applied to the piston ring specimen through the lever arm arrangement connected to a spring loading system, thus maintaining the required contact pressure at the piston ring and cylinder liner interface. Both specimens were contained within a test chamber filled with lubricant to be examined, such that the contact surface was completely immersed in lubricant. The level of lubricant was maintained constant for complete test duration while the lubricant was

circulated out of the chamber to the on-line condition monitoring sensor unit and fed back in to the chamber by a centrifugal micro oil pump; as illustrated in Figure 10.



Figure 11: Fluid properties oil sensor system

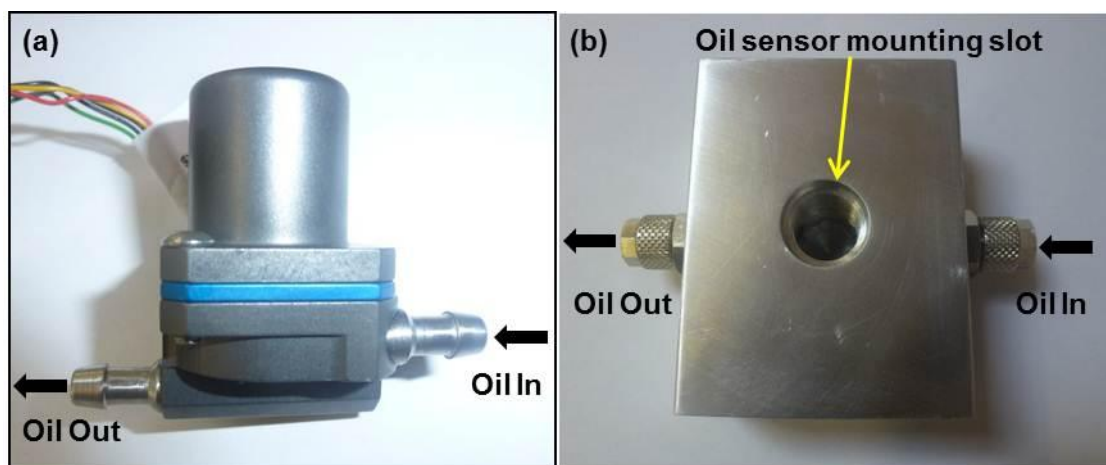


Figure 12: (a) Centrifugal micro oil pump; (b) Manifold for mounting oil sensor

Commercially available Fluid Properties sensor unit supplied by StrainSense Ltd (UK) was used to measure the required lubricant parameters. A high speed data logging system called Rebel Lt logger (part of sensor unit) records the lubricant data in real time and a dedicated software Dialog Version 4.4.0 displays the data as a function of time on computer screen and also archives data in a memory disk for future analysis.

A manifold was designed and manufactured to mount the sensor as shown in Figure 12(b). A steady and consistent fluid-flow across the sensing element was maintained at the rate of 0.2m/s to ensure rapid fluid exchange for attaining optimum sensor performance, as mentioned in the sensor installation guide [78] supplied along with sensor unit. The oil flow was maintained through a centrifugal micro oil pump which can operate at higher temperature range, which was also a requirement for conducting experiments at 100°C. Figure 12(a) shows the centrifugal micro oil pump. Tygoprene Pump tubing was used as oil galleries for its higher temperature range and excellent chemical resistance to engine lubricants. Figure 13 shows the final assembly of different components used to modify the TE77 test rig to simulate engine lubricant conditions and perform a real time on-line lubricant condition monitoring.

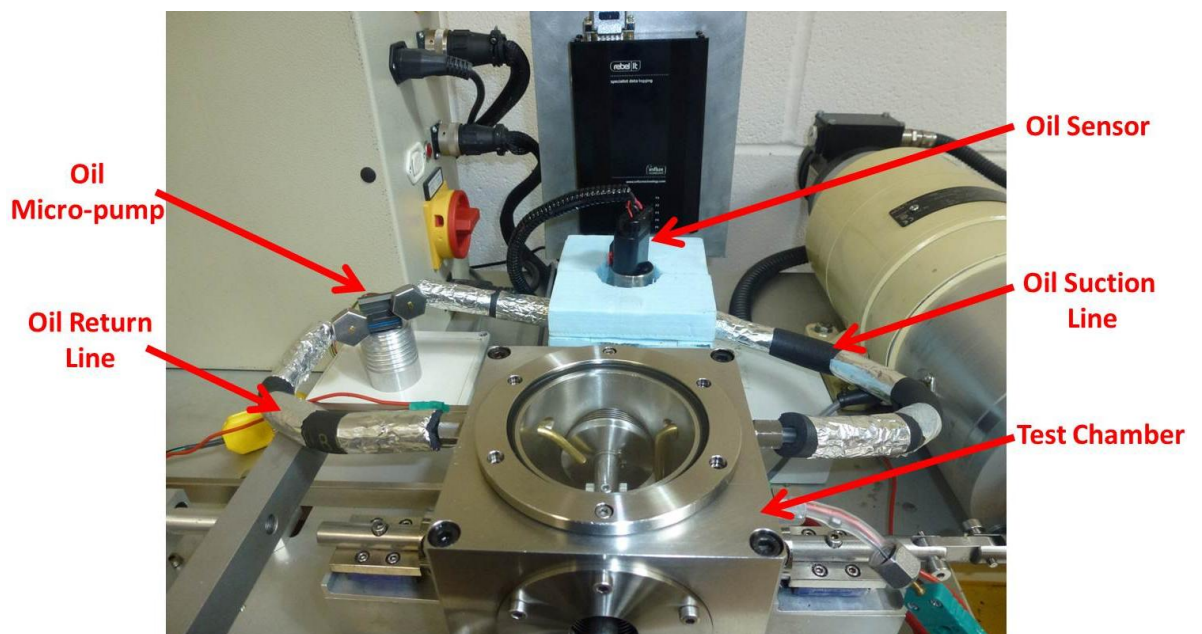


Figure 13: Modified TE77 test rig including real time on-line lubricant condition monitoring system

The temperature of the lubricant was maintained by the heater installed underneath the test chamber and controlled by a thermo-couple attached to it. The friction force was measured by a Kistler Type 9203 piezo-electric force transducer which generate charge proportional to frictional with a sensitivity as low as 45.7pC/N. The Kistler Type 5011 charge amplifier connected to force transducer converts this charge generated into proportional electrical voltage signal. Therefore by multiplying the acquired voltage signal with a scaling factor (such as N/V) gives a tangential friction force at the contact interface. Friction coefficients are then derived from measured friction force by dividing it with normal load applied manually [79]. The nature and extent of wear was analysed using the post-test surface analysis techniques, details of which are mentioned later in the section 3.4.

An Electrical Contact Resistance (ECR) method was used to analyse the boundary film formation between the two contacting surfaces. The insulating lubricant film formed during the sliding motion between the interfacing surfaces act as the resistance. The measure of this resistance through an electrical circuit gives the estimation of boundary film formation. The voltage of approximately 50mV is applied across the contact by connecting the positive end of circuit to one sample and the negative end to another, one of which is completely electrically insulated from rest of the metallic surfaces by using a non-conducting shim underneath. The presence of lubricant film in between interfacing surfaces act as a resistance and any change in its value results in corresponding voltage drop across the contact. Measure of such instantaneous change in voltage signals provides a qualitative way for analysing the boundary film formation capabilities of any lubricant [79]. Nylon 6.6 made mounting screws were used to hold the flat sample onto the reciprocating rod along with plastic shim underneath the flat sample to provide complete electrical insulation from surrounding metallic surfaces.

The ECR data was recorded continuously at set intervals and is presented in this thesis using following relation. This equation of representing ECR results have been used in past by other researchers [46, 51]

$$\text{Electrical Contact Resistance (\%)} = \frac{\text{Measured contact voltage}}{\text{Applied contact voltage}} \times 100$$

The data acquisition was executed by a control unit incorporating a SUPERSLIM Serial Link Interface Module, connected to a host computer system installed with the COMPEND 2000 software.

3.3.2. Test materials

3.3.2.1 Test samples preparation

The piston rings employed in the experiments are used in the MAN D2840LE401 diesel engines installed in Trent Class RNLI lifeboats. Piston ring specimens were prepared by machining new top compression piston rings (uncompressed outer diameter of 133.5mm) into several small segments of inner arc length 21mm. The new piston rings were purchased from Pilkington Marine Engineering (UK). The machining process was done by using a Dremel rotary cutting tool (Model 398) using fiber glass reinforced cut-off wheels. The process of cutting various piston rings into segments is shown in sequence from (a) to (d) in Figure 14, and the Dremel tool used is shown in Figure 15.

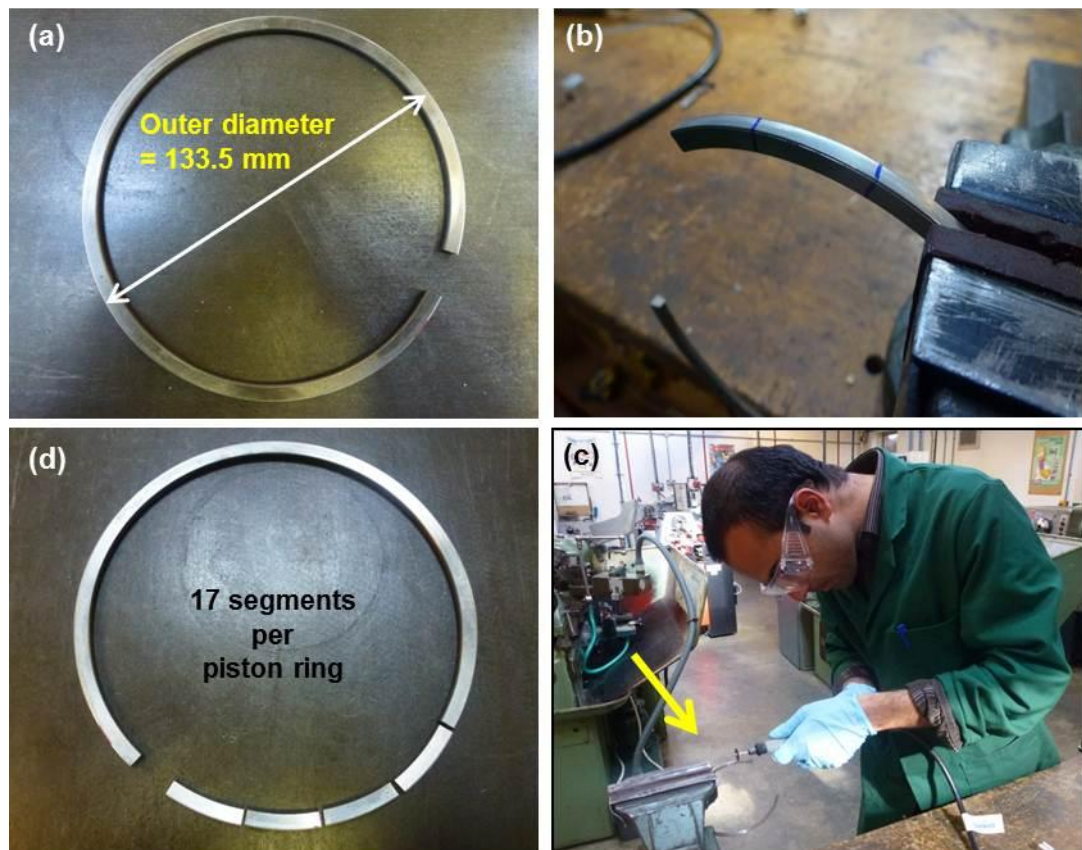


Figure 14: Piston ring cutting procedure



Figure 15: Dremel rotary cutting tool (Model 398) along with fiber glass reinforced cut-off wheel

After cutting, ring segments were carefully cleaned ultra-sonically in acetone for 30 minutes to remove debris generated during the cutting process.

The flat plate specimens of size 10mm x 33mm to use as replica of cylinder liner were purchase from Phoenix Tribology Limited (UK). Figure 16 shows the typical flat sample used in the experimental work.



Figure 16: Typical flat plate sample used in experiments

3.3.2.2 Material Specification of test samples

The piston ring was found to be coated on its running face which interfaces with the cylinder liner surface during sliding; therefore it was thought useful to evaluate the chemical composition of coating material. EDX technique was employed for this purpose. A segment of length 10mm from actual piston ring was cut and embedded in Bakelite resin holder, such that the cross-section of ring could be analysed for its material composition by EDX. The procedure of preparing a piston ring segment for the EDX analysis is shown in sequence from (a) to (d) in Figure 17.

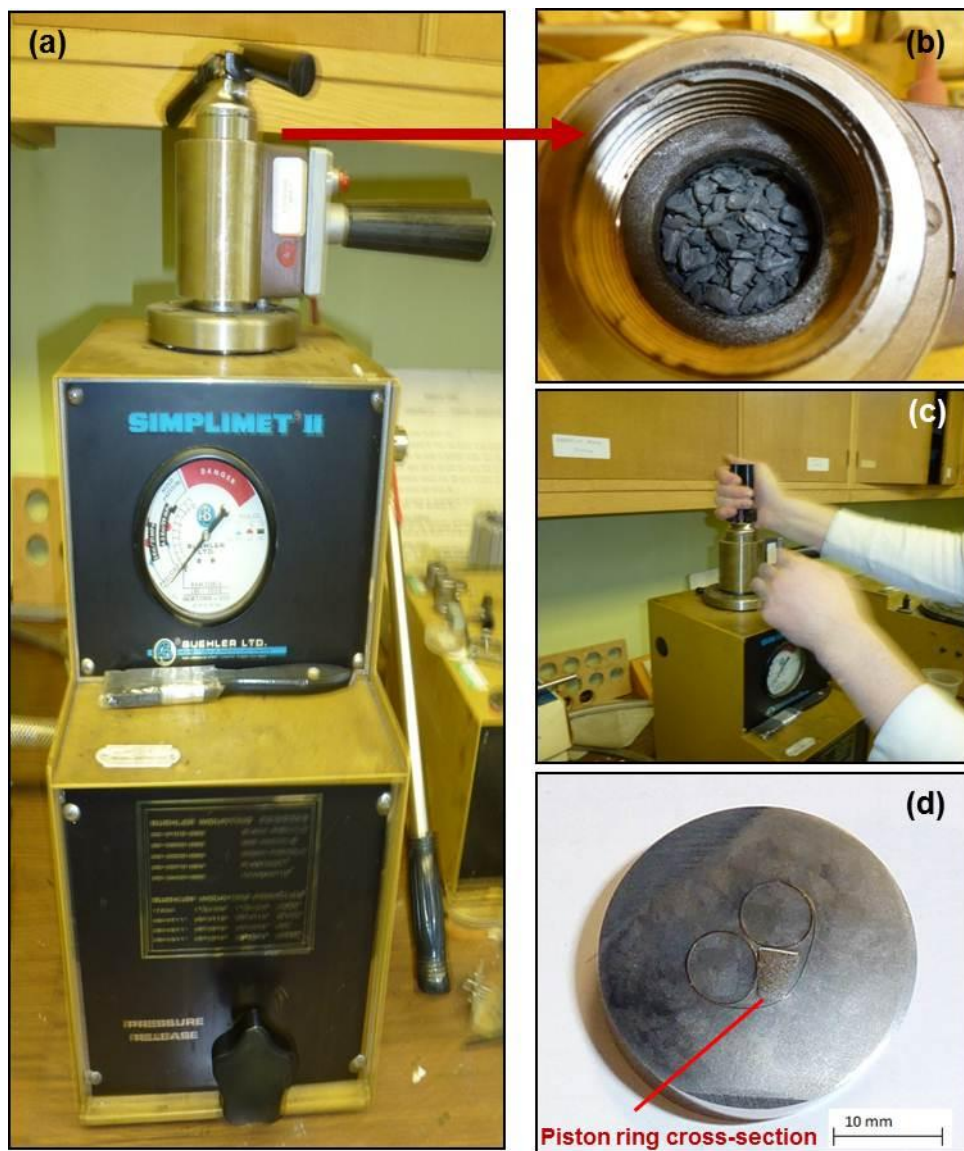


Figure 17: Preparation for EDX analysis of piston ring coating

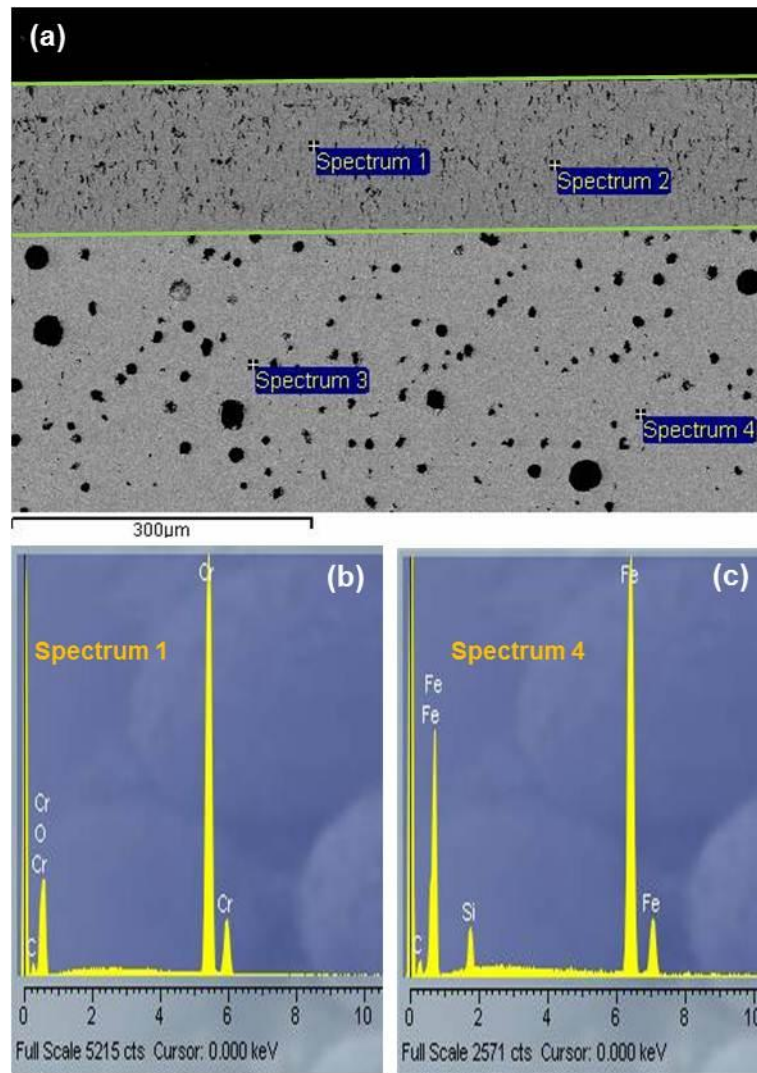


Figure 18: EDX analysis of piston ring cross-section shown in Figure 17(d); (a) coating thickness shown between green lines; (b) EDX spectrum of coating; (c) EDX spectrum of base material of piston ring

EDX analysis of piston ring cross-section showed that piston ring's running face is covered with chromium coating of thickness approximately 152 μm, whereas the base (substrate) material has composition of that of cast iron. Figure 18(a) shows the cross-sectional view of piston ring illustrating the chromium coating thickness, shown between green lines. This finding was a useful input during the post-test surface analysis of wear scars for examining the nature of tribofilms and any material transfer taken place due to adhesion.

On the other hand, the material specification of flat specimens, as supplied by its supplier, was found very similar to those of actual cylinder liner used in MAN

D2840LE401 diesel engines installed in Trent Class RNLI lifeboats. The information about material specifications of cylinder liner was kindly supplied by the cylinder liner manufacturer, MAHLE International GmbH (Germany). The detailed description of material composition of different test specimens used in the experiments is given in Table 4.

Table 4: Material description of test specimens

Specimen type	Material	Fe (%)	C (%)	Si (%)	Mn (%)	P (%)	S (%)	Cr (%)	O (%)
Flat plate specimen	Grey Cast Iron (BS1452)	Balance	3.0-3.3	2.4-2.6	0.7-1.0	0.4-1.1	0.1-1.1	-	-
Piston ring running face (Coating)	Chrome Coating	-	4.92	-	-	-	-	93.53	1.55

3.3.2.3 Surface Characterisation of test samples

The surface roughness of all the test specimens was measured prior to each experiment using 3D Optical Interferometer (ZYGO). The typical surface maps of unworn piston ring running face and flat plate are shown in Figure 19 and Figure 20, respectively.

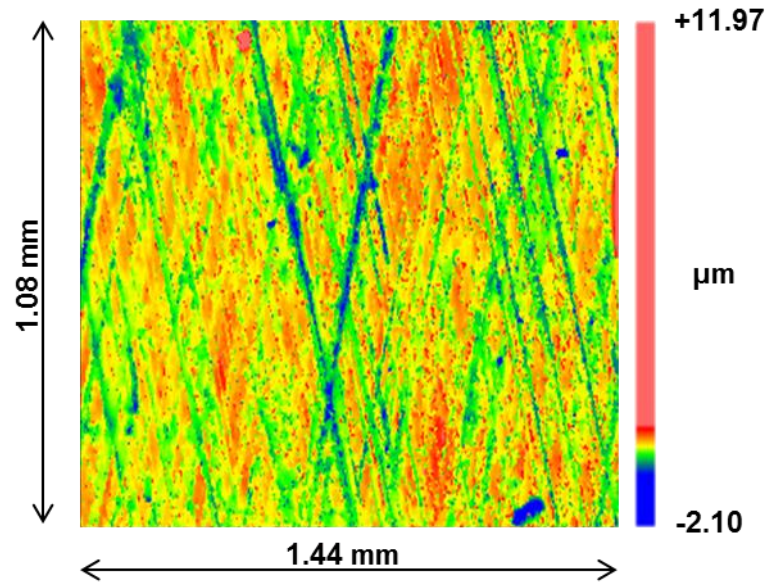


Figure 19: Typical surface roughness map of unworn piston ring running face along with roughness distribution scale

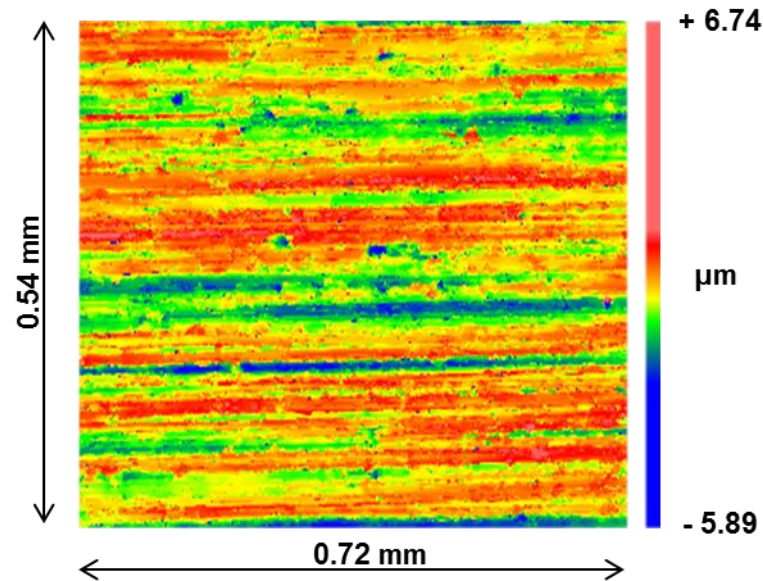


Figure 20: Typical surface roughness map of unworn flat plate specimen used as cylinder liner along with roughness distribution scale

For theoretical calculation of lubrication regime using oil film thickness and combined roughness of mating surfaces, the root mean square (R_{rms}) roughness values of above shown surface maps are used. Table 5 shows the respective R_{rms} values measured along the direction of measurement for the typical test samples of piston ring segment and flat plate.

Table 5: Surface roughness values in root mean square (Rrms)

	Piston Ring (running face)	Flat sample
Surface roughness (μm)	0.372	0.647
Direction of measurement	Parallel to piston ring sliding motion	Parallel to piston ring sliding motion

3.3.2.4 Lubricating oil and ionic liquids

Details of lubricating oil samples have previously been mentioned in section 3.1

Two commercially available phosphonium-based ILs, referred here as IL1 and IL2, used in the current research are Trihexyltetradecyl phosphonium bis(2,4,4-trimethylpentyl) phosphinate (purchased from Sigma-Aldrich) and Trihexyltetradecyl phosphonium bis(2-ethylhexyl) phosphate (purchased from Iolitec), respectively. Figure 21 shows these ILs as supplied by their manufacturers. The convention of ILs used in this research as mentioned above will be followed in this thesis for convenience.



Figure 21: Trihexyltetradecyl phosphonium bis(2,4,4-trimethylpentyl) phosphinate (Sigma-Aldrich) and Trihexyltetradecyl phosphonium bis(2-ethylhexyl) phosphate (Iolitec)

Both ILs were used as additives to improve anti-wear performance of in-service and used engine lubricating oil. These ILs were also used as additive in base oil and new engine lubricating oil for comparison purpose. The ILs were mixed in 6 volume % proportions in lubricating oil samples collected from the MAN diesel engines as mentioned above. The procedure and results of mixing oil and ILs are discussed in next section. Table 6 shows the kinematic viscosities of the oil and ILs at standard temperatures (40°C and 100°C) used to define the viscosity index of any lubricating oil.

Table 6: Kinematic viscosities of oils and ILs at standard temperatures

Lubricant	Viscosity at 40°C (cSt)	Viscosity at 100°C (cSt)
IL1	388.8†	35.4†
IL2	429.0†	49.5†

†source of information [28]

3.3.2.5 Mixing of lubricating oil and ionic liquid

Both IL1 and IL2 were mixed in 6 volume % proportions in base oil, new oil, in-service (135h and 196h) oils and used (315h) lubricating oil samples using an ultrasonic probe (Sonic Systems P100) as shown in Figure 22.

The mixing of lubricating oil and IL was carried out at room conditions for 5 minutes. In cases where both ILs were mixed with the new fully-formulated oil (15W40) and also with the mineral base oil, the visual inspection depicted no cloud formation (or phase separation between oil and IL due to slightly different densities) even after a month of storage in tightly sealed bottle.

Due to dark (blackish) colour of in-service and used lubricating oil, the phase separation could not be detected. Therefore, the stability of all the mixtures was further assessed experimentally by performing Stability Test. The procedure and analysis results of Stability Test as discussed in section 3.3.2.6 and 4.8, respectively.



Figure 22: Mixing of different lubricating oil and IL using sonicator; (a) New engine oil; (b) Used (315h) engine oil; (c) Sonicator

3.3.2.6 Stability analysis for lubricant and ionic liquid mixtures

The visual inspection of the mixtures of used oil (315h) and ILs was not possible due to their opaque appearance, The same problem was encountered in case of the in-service oils (135h and 196h) but the mixtures of ILs with new oil were clearly inspected with no phase separation (or cloud formation) even after a month of storage in tightly sealed bottle. In addition, although the visual inspection is quicker among the other analytical methods for oil stability analysis but it is rather subjective dependent upon the inspector's observation, and may possess some error.



Figure 23: Stability analysis of mixtures of new and used engine lubricants with different ILs using Turbiscan Lab

Turbiscan Lab Expert (manufactured by Formulacion, France), as shown in Figure 23 (c), based on the optical scanning technique provides an accurate evaluation of oil stability with the repeatability of $\pm 0.05\%$. Therefore, it was employed in case of mixtures of both new and used oil with the two phosphonium based ILs. Turbiscan Lab consists of a reading head which includes a pulsed near infrared light source (that emits light at wavelength of 880 nm) and two synchronous detectors, namely a transmission detector (that measures the light flux transmitted through the oil bottle) and a backscattering detector (that measures the light scattered back by the oil). The oil bottle is scanned vertically at different points and transmission/backscattering data is recorded using the software Turbisoft-AGS version 1.1. The same procedure is

repeated for a set number of times and any change in transmission of light through the oil as function of time defines the stability of the oil sample. No change in transmission of light is indicative of higher stability of the oil (or mixture of oil and IL in this case).

Figure 23 (a) shows a typical mixing of used oil and IL using ultrasonic probe prior to its stability analysis for about 10mins to achieve homogeneity. Around 22ml of the mixture was then transferred to a flat bottomed glass bottle (outer diameter of 27.5 mm and height of 70 mm), as shown in Figure 23 (b), and sealed with a modified polycarbonate screwed top cap and butyl/teflon sealing ring, as supplied.

The sample bottle was then placed in the chamber and analysis was performed for 11 days (once each day). The temperature was controlled at about 30°C for the complete duration of the analysis since temperature has an appreciable effect on the transmission of light and the results would not be comparable.

3.3.3. Test parameters

The test parameters were chosen to simulate boundary lubrication conditions as experienced by the top compression ring just below the top dead centre on the power stroke where the lubricant film thickness is thinnest, and combustion gas pressure and temperature are highest. Such conditions would enable assessing the anti-wear behaviour and tribofilm formation capabilities of IL as additive mixed in different engine lubricants.

The simplified non-conformal geometries of test samples were used instead of conformal mating surfaces of actual ring and liner. This was done to achieve proper alignment of samples in the test rig otherwise if a segment of piston ring is used against a curved specimen cut from actual liner, it would tend ring segment to have a larger curvature and rest on the edges of liner specimen unless the ring is pressed enough to achieve the same radius of curvature as liner surface [80]. Therefore to avoid this difficult mechanical alignment, samples having simplified geometry were used.

Therefore the tribo-testing was carried out at constant normal load of 50N (producing contact pressure of 284.9 MPa, as calculated by Hertz theory of non-conformal contacts see Appendix A), stroke length of 5mm, reciprocating frequency of 4.4Hz and constant uniform bulk oil temperature of 100°C and 25°C. The test time was set for 3h and measurements for friction force and ECR were made every 1s. Each test was replicated three times and average value of friction coefficient and wear volume was considered.

Lubrication regime modelling was done by calculating oil-film thickness ratio (or λ -ratio) which incorporates the minimum oil film thickness (MOFT) and combined rms roughness of unworn mating surfaces. MOFT was calculated using Hamrock and Dowson formula and the value of λ less than unity ensured boundary lubrication regime at the mid-stroke region of sliding test (see Appendix B for details on theoretical lubrication regime modelling). Due to continuous oscillatory motion between the sliding surfaces, the oil film thickness is expected to be thinner near the either ends of stroke (than the mid-stroke) where the sliding speed seemingly approaches to zero, as described by Truhan et al. [1], therefore boundary lubrication regime was prevalent throughout the stroke length during the tribo-testing.

3.3.4. Test procedure

The test procedure for piston ring and cylinder liner contact in lubricated conditions was performed as mentioned in ASTM G181 [80].

Sample preparation: Test specimens were cleaned ultrasonically in acetone for 10m to remove any traces of contaminant without disturbing the main surfaces. The fittings and all fixing screws which come in contact with the lubricant during testing were also cleaned in the same way prior to the test.

Surface roughness analyses: 3D White Light Interferometer was used to measure the surface roughness of both test specimens mating surfaces at three different locations.

Samples installation & alignment in test rig: Flat specimen was fitted onto the reciprocating arm of the rig and connected to the positive terminal of the contact resistance circuit. The base of the plate sample was insulated completely using plastic shims to complete the electrical contact resistance circuit. The negative terminal of the contact resistance circuit was connected to the piston ring holder. The contact area plane was aligned perpendicular to the applied load direction to achieve the uniform contact pressure distribution.

Lubricant Addition: The engine-aged lubricant collected from lifeboat engine (or mixture of lubricant and 6 volume % IL) was added to the test chamber such that the contact region of the mating samples get completely immersed.

Lubricant Heating Process: Lubricant was heated to 100°C by the heater of 800W of heat dissipation rate, installed underneath the test chamber. The heat conduction process takes around 1h to reach 100°C which is an average lubricant temperature in running engine, as can be seen from MAN diesel engine test report supplied by RNLI (Appendix C). The test chamber was top sealed by the toughened glass lid to maintain the lubricant temperature during full test duration. The lubricant temperature is recorded using the K-type thermocouple fitted in the chamber with its tip submerged completely inside the lubricant. The above heating procedure was not followed for tests conducted at room temperature. However test chamber was top sealed by the toughened glass lid to avoid foreign contamination entering the oil.

Test Parameters Set-up: All the test condition parameters such as load, stroke length, frequency and temperature were pre-defined in the test sequence file used by the software COMPEND that runs the test. The output results from the test were saved in the data file for the analyses purpose.

Results Data Display: Graphical display of the test parameters/results such as friction force, friction coefficient, electrical contact resistance and temperature of lubricant as a function of time was used on the computer screen as soon as the test begins.

Specimen storage for post-test analysis: After reciprocating bench test was completed and oil temperature has fallen down to room temperature, test samples were carefully removed from the test rig without disturbing their worn surfaces. The sample were rinsed under the acetone bath for removal of dust and excessive lubricant so their worn surface area can be examined with better visibility for both surface and chemical analyses.

All specimens were stored in stainless steel desiccators with a glass door using a 500g pack of silica gel (desiccant) as shown in Figure 24 to avoid any damage from the moisture in environment.



Figure 24: Specimen stored in desiccator

3.4. Post-test Stage (Surface analysis)

Different surface analyses techniques were employed to measure any change in the characteristics of worn surfaces. The measurements such as wear scar dimensions, wear volume, basic wear mechanisms and chemical nature of tribofilms formed on worn surfaces were carried out. The advanced surface analysis techniques employed

to perform the above required analyses included 3D White Light Interferometer, SEM, EDX and XPS. Each of these techniques is explained in detail below.

3.4.1. 3D White Light Interferometer

3D White Light Interferometer manufactured by ZYGO Corporation, as shown in Figure 25, was used to perform a quantitative surface characterisation of test samples used in reciprocating bench tests. The 3-dimensional surface mapping facilitated the comparison of surface roughness and surface profile of test samples before and after the bench tests.



Figure 25: 3D White Light Interferometer

Changes in surface profile clearly depicted material loss and the wear volume measurements of complete wear scar were made on cast iron flat specimens at 1x magnification. The low magnification helped in mapping the complete wear scar area without the need of additional editing of images or stitching of multiple images. This is a non-destructive method of surface characterisation with no need for sample preparation. The proper alignment of sample is required along with setting of focal length, light intensity, and dark and bright fringes to facilitate optimum scanning of the subjected surface area. Results were displayed over the computer screen and analysed using the software Metropro version 8.3.3. For detailed examination of worn

surface topography to investigate wear mechanisms taken place during tribo-testing, a higher magnification beyond the limits of optical source was needed and SEM was employed for this purpose as discussed in later sections.

3.4.2. Sample preparation for SEM, EDX and XPS analyses

Chemical analysis was performed on the worn surfaces of test specimens to extract information about the tribofilm formation process and tribofilm composition. Different surface analysis techniques such as EDX and XPS were employed for the above purpose. SEM was employed to extract information about the wear mechanisms taken place during the tribo-sliding process.

Due to the compact design of specimen holder and test chamber of equipment used for the above analysis techniques, all flat plate specimens inspected were needed to cut to the size of 10mm x 10mm. The cutting of flat specimens was carried out in a bench top cut-off machine (Struers Accutom-5), as shown in Figure 26 (a).

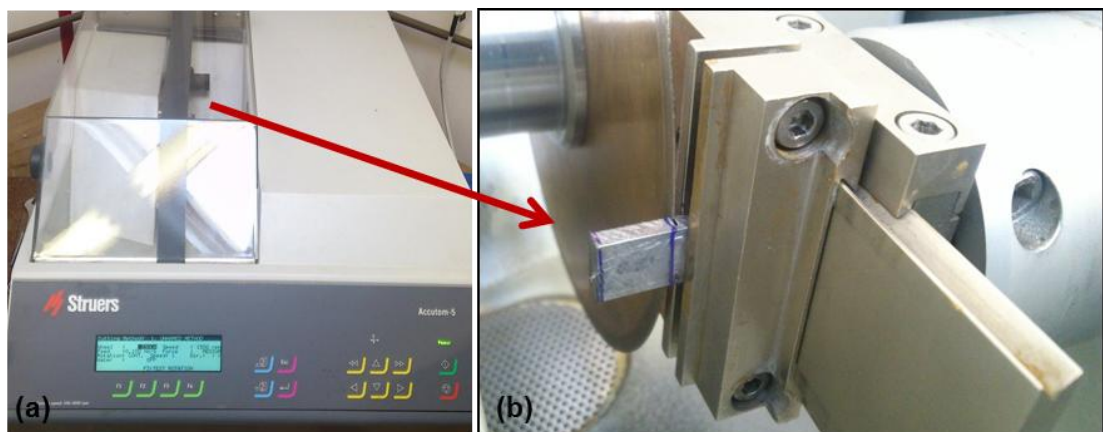


Figure 26: Bench top cut-off machine (Struers Accutom-5) shown in (a); and flat specimen during cutting process shown in (b)

This machine supports precision cutting of various material types (such as metals, ceramics, composites etc.) at low feed rate and cut-off wheel speed which reduces the chances of damaging the specimen due to frictional heating effects. The specimens were wrapped in multiple folds of cling film prior to cutting to avoid debris

generated during the cutting process to come in contact with the wear scar, since it may alter the results during analysis process. Thence, the specimens were held in holder as shown in Figure 26 (b). The cutting was carried out at cut-off wheel speed of 1500 rpm, feed rate of 0.01 mm/s and medium force.

3.4.3. Scanning Electron Microscopy (SEM)

To understand the nature of wear mechanism taken place during the tribo-testing process, it was decided to use the SEM technique for high magnification observation of the topography of worn surfaces. The equipment used for the SEM analysis was JEOL JSM-6610LV, as shown in Figure 27. The intensity of incident electron beam used was 20KV.

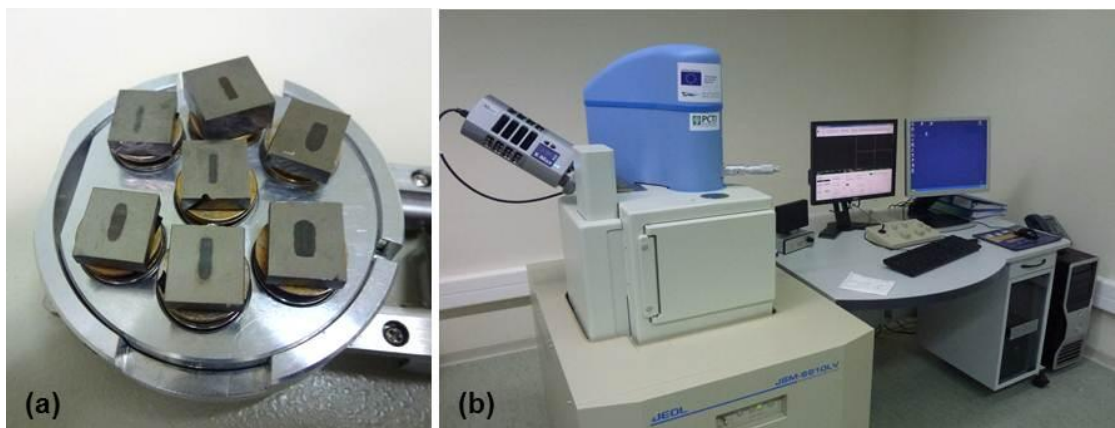


Figure 27: Samples installation on the sample mount is shown in (a); SEM equipment used for analysis of worn surfaces is shown in(b)

As the sample surface was metallic, no special preparation was needed; nevertheless due to compact design of the test chamber, each specimen was needed to be cut to the dimensions in range of approximately 10 mm x 10mm, using procedure mentioned earlier in section 3.4.2. The samples were carefully fixed onto the sample mount using adhesive tape (without disturbing the worn surfaces),as shown in Figure 27 (a), and thence the mount was installed on the sample movement stage inside the test chamber. The test chamber is then evacuated from air for a few minutes to maintain low pressure. The equipment was now ready for analysis of wear scar region using

the PC monitor and control knobs on working stage to make adjustments to the options such as focus, magnification, contrast, brightness, etc.

The initial examination of worn surfaces was done at low magnification 30x and 200x to identify the areas of interest and then the magnification was increased to 1500x for close inspection and imaging. The complete analysis was carried out using the secondary electrons mode. This mode helps in identifying the frequent occurring characteristic patterns of wear. As it is not practical to perform comprehensive examination of whole of the worn area, [81], only selected areas near the edges and middle of the worn scar were analysed.

3.4.4. Energy Dispersive X-ray Microanalysis (EDX)

Chemical analysis of the worn surfaces of test specimens was performed to evaluate the chemical composition of boundary film (tribo-film) using EDX microanalysis functionality of the SEM equipment. The working principle of this technique is based on the excitation of characteristic x-rays caused by the incident primary electrons. The energy intensity of emitted x-rays is then obtained in a spectrum format by the X-ray detector and Multi-Channel Analyzer. The equipment employed in this research was JEOL JSM-6610LV, as shown in Figure 27, and the electron beam intensity used for the analysis was 20KeV. EDX analysis was performed at the magnification of 30x covering the scanning area of approximately 2mm x 1mm at the centre of wear scar.

The change in chemical composition of tribofilm could be analysed to evaluate the additive depletion and/or presence of IL on surface. Secondly, EDX helped in analysing the wear mechanisms taken place during the tribo-testing, by comparing the chemical composition of the metallic particles embossed onto the worn surfaces with the known composition of test specimens. To check if these has been the case of material transfer (adhesion) between the mating surfaces, or are the foreign particles.

3.4.5. X-ray Photoelectron Spectroscopy (XPS)

The worn surfaces of test specimens were also subjected to XPS surface analysis technique which provides information about the chemical composition of the first nanometric layers mainly 1–5 nm. The working principle of XPS analysis is based on photoelectric effect in which the binding energies of the core electrons is determined by the difference between the known energy of photons incident onto surface and the measured energy of the ejected core electrons from the surface. The binding energy is the indicator of the type of atom and the flux of ejected electrons is proportional to the number of atoms in the analysed surface area. The change (or shift) in the binding energies of core electrons can be used to identify the change in chemical state of the atoms. These energy changes are in the range of 0.1 to 10 eV [82].

XPS equipment employed in this research is as shown in Figure 28. It incorporates a non-monochromatic $K\alpha$ (Mg) x-ray source (energy 1253.6 eV) and a flood electron gun when necessary to compensate electrical charge on specimen surface. The detector (SPECS Phoibos MCD 5) set-up included the use of a medium magnification electromagnetic lens and an entrance slit (diameter 3mm) in order to select either the inner part or the outer part of the wear scar. The background pressure in the analysis chamber was maintained below 5×10^{-9} mbar during data acquisition.

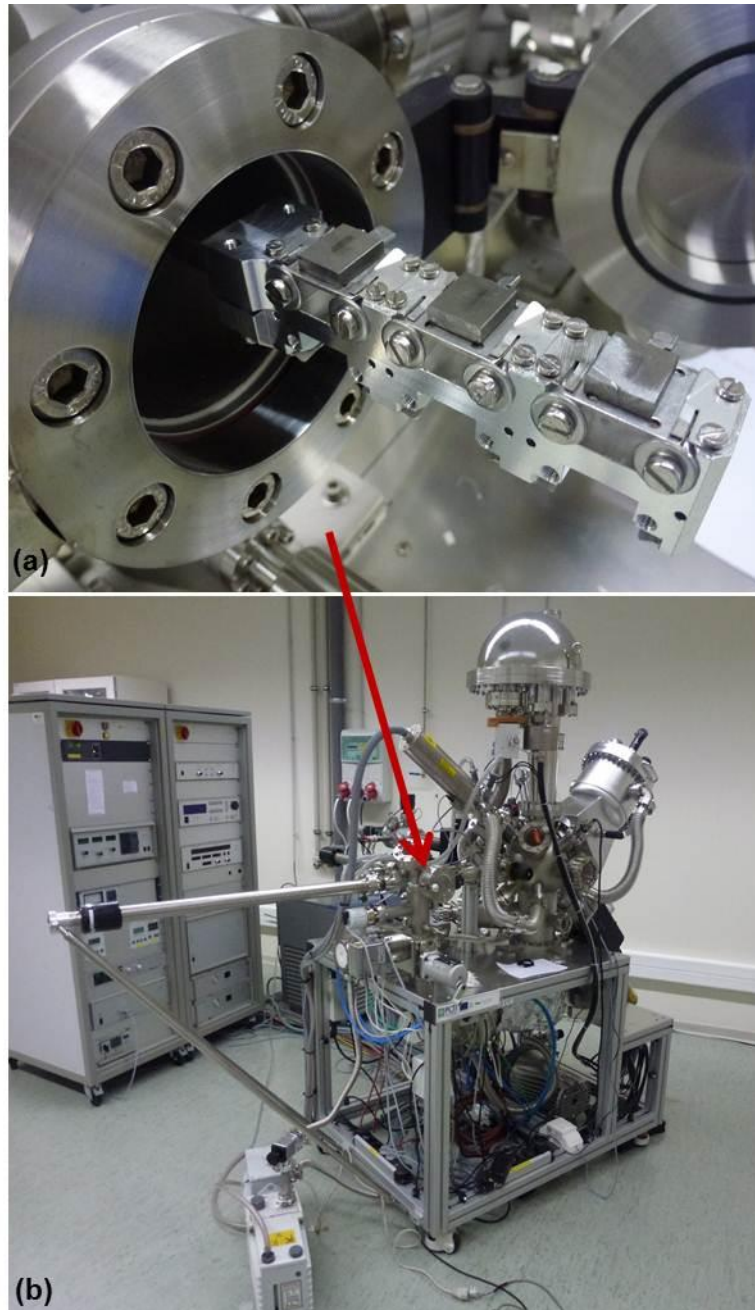


Figure 28: Samples installation in load chamber of XPS equipment is shown in (a); XPS equipment is shown in (b)

Each specimen was needed to be cut to the dimensions in range of approximately 10 mm x 10mm, using procedure mentioned earlier in section 3.4.2. For precision XPS analysis, each specimen was then washed with ethanol and cleaned by a soft paper to avoid contaminant entering into wear scar area before installing them into the XPS load chamber as shown in Figure 28 (a).

After samples installation, the pressure as low as 1×10^{-6} mbar was maintained in the load chamber, which is situated on left side of XPS equipment shown by arrow in Figure 28 (b), using a scroll pump and turbo molecular pump combination. This low pressure vacuum was restored in around $\frac{1}{2}$ hour. Each sample was then transferred to the main (analysis) chamber, situated on the right side of XPS equipment, where the pressure was even lower around 5×10^{-9} mbar. Correct positioning of the specimen in main chamber was done with the help of a laser beam.

The spectra were processed using Casa XPS software. Initially low resolution survey spectra inside and outside the wear scar was taken for every specimen to identify all key elements present in the surface. The elements with high intensity peaks are then considered for detailed analysis at high resolution. In current research, the high-resolution repeated spectra were taken for the different elements including Mn, Cr, C, O, Fe, Si, P, Zn, S and Ca. These elements are constituents of specimen material, lubricant, and ILs employed in current research. The high resolution spectrum helped to analyse these specific elements for shift in any their binding energy. This shift is representative of change in the oxidation state due to formation of new bonding with other elements or new compounds. For better results, high resolution spectrum for each element was repeated multiple times (10 - 20 times) and the average of counts per seconds, i.e. electrons received by HC analyser, is taken against binding energy.

It is worth mentioning that low intensity peaks formed due to binding energy of Auger electron are considered as noise (or error) and were neglected. Auger electron peaks were confirmed by changing the x-ray source from Mg $K\alpha$ to Al $K\alpha$, such that the kinetic energy of core electrons changes but for auger electrons remains unchanged. Hence the auger peaks were identified in spectrum.

Chapter 4 Results of Lubricant Analysis

4.1. Viscosity Measurements

Kinematic viscosity of the lubricant is tested to assess its resistance capability when flowing against gravity through the oil galleries in internal combustion engine environment. Therefore the lubricant analysis was performed on several different lubricant samples before using them for sliding tribo-testing. The details of the kinematic viscosities of lubricants at 40°C and 100°C are mentioned in Table 7. These two temperatures are commonly used for the viscosity index measurement and also 100°C is the average running engine temperature [31].

The lubricant flow-rate is measured in centistokes, i.e. cSt (or mm²/s), and this defines the resistance of the oil flowing under gravity through the capillary tube. Clearly it can be seen that the viscosity of the oil has reduced over its use in the marine diesel engines of RNLI lifeboat as a function of duty cycle in terms of hours of service (or usage). A significant drop in the viscosity of Used Oil (315 h) is noted at about 91.56 cSt which is 14% lower than the New Oil. The reason for this drop in viscosity was verified by performing Gas Chromatography test which examines the diesel fuel dilution of the engine lubricants. The details of the results of this test are discussed later in this chapter.

Table 7: Kinematic viscosities different lubricants in this study

Lubricant	Viscosity (cSt) at 40°C	Viscosity (cSt) at 100°C	Viscosity Index
Mineral base oil	43.4 ^a	6.4 ^a	-
New Oil	106.10	14.34	138
In-service Oil (135 h)	100.30	13.66	137
In-service Oil (196 h)	102.30	13.80	136
Used Oil (315 h)	91.56	12.74	136

Source of information: ^a Supplier; rest were measured experimentally as mentioned above

4.2. Gas Chromatography (Diesel Fuel Dilution)

It is expected to see some diesel fuel into the engine lubricant during the engine operation due to not complete combustion of fuel or difference in fuel injection timing. However the presence of fuel which has lower viscosity than engine oil reduces the viscosity of engine oil. In case of excessive fuel dilution the lubricating performance of engine oil could be affected. Therefore it is deemed important to measure to Gas Chromatography (GC) test to analyse the level of diesel fuel dilution in engine oil samples at regular intervals of engine operations.

Table 8: Diesel fuel dilution in different lubricants samples

Lubricant	%
Mineral base oil	-
New Oil	-
In-service Oil (135 h)	2.1
In-service Oil (196 h)	2.3
Used Oil (315 h)	3.0

Table 8 shows the results obtained from the GC test for the three engine-aged lubricant samples. Clearly the amount of diesel fuel has increased over the usage of oil within the diesel marine engines of RNLI. The high fuel dilution of Used Oil is also a possible reason for its lower viscosity as discussed earlier in this chapter.

4.3. Elemental concentration of wear debris and additives by ICP

The analytical results obtained from the ICP technique are particle (debris) size dependent, and low results are obtained for particles larger than a few microns. Therefore only particles smaller than 10µm in size are detectable by this technique. The knowledge of concentration of wear metals are indicative of excessive wear by comparing the data with base line concentration obtained from testing new lubricant.

Similarly increase in concentration of elements like Boron, Sodium or potassium is indicative of contamination due to coolant leak in lubricant.

Table 9: Elemental concentration in part per million (ppm)

Elements	New Oil	In-service Oil (135 h)	In-service Oil (196 h)	Used Oil (315 h)
Calcium	3071	2863	3063	2675
Magnesium	7	7	23	13
Phosphorus	1086	1153	1117	1413
Sulphur	<i>ni</i>	8621	8342	8100
Zinc	1281	1244	1322	1186
Aluminium	0	5	7	5
Boron	0	<5	7	10
Barium	0	<1	<1	<1
Cadmium	0	<1	<1	<1
Chromium	0	1	2	2
Copper	0	9	11	18
Iron	1	27	40	66
Manganese	1	<1	1	1
Molybdenum	1	<1	<1	10
Nickel	0	<2	<2	<2
Lead	0	3	5	5
Silicon	2	3	3	12
Tin	0	<1	1	3
Titanium	0	<1	<1	<1
Vanadium	0	<10	<1	<1
Sodium	3	<1	<10	10

ni – no information

The results of analyses along with the detail of tests performed are mentioned in Table 9. It can clearly be seen from the results that mainly Iron increases consistently to a higher value which is wear metal and other elements are in smaller quantity which constitute wear and contaminant debris. Also the concentration of in Used Oil sample is highest than the other lubricant samples. It was confirmed from the lubricant

manufacturer that Calcium, Phosphorous and Zinc are the additive elements and part of the lubricant, not generated from wear and contamination; hence their concentration is high in all the lubricant samples.

4.4. Nuclear Magnetic Resonance (NMR)

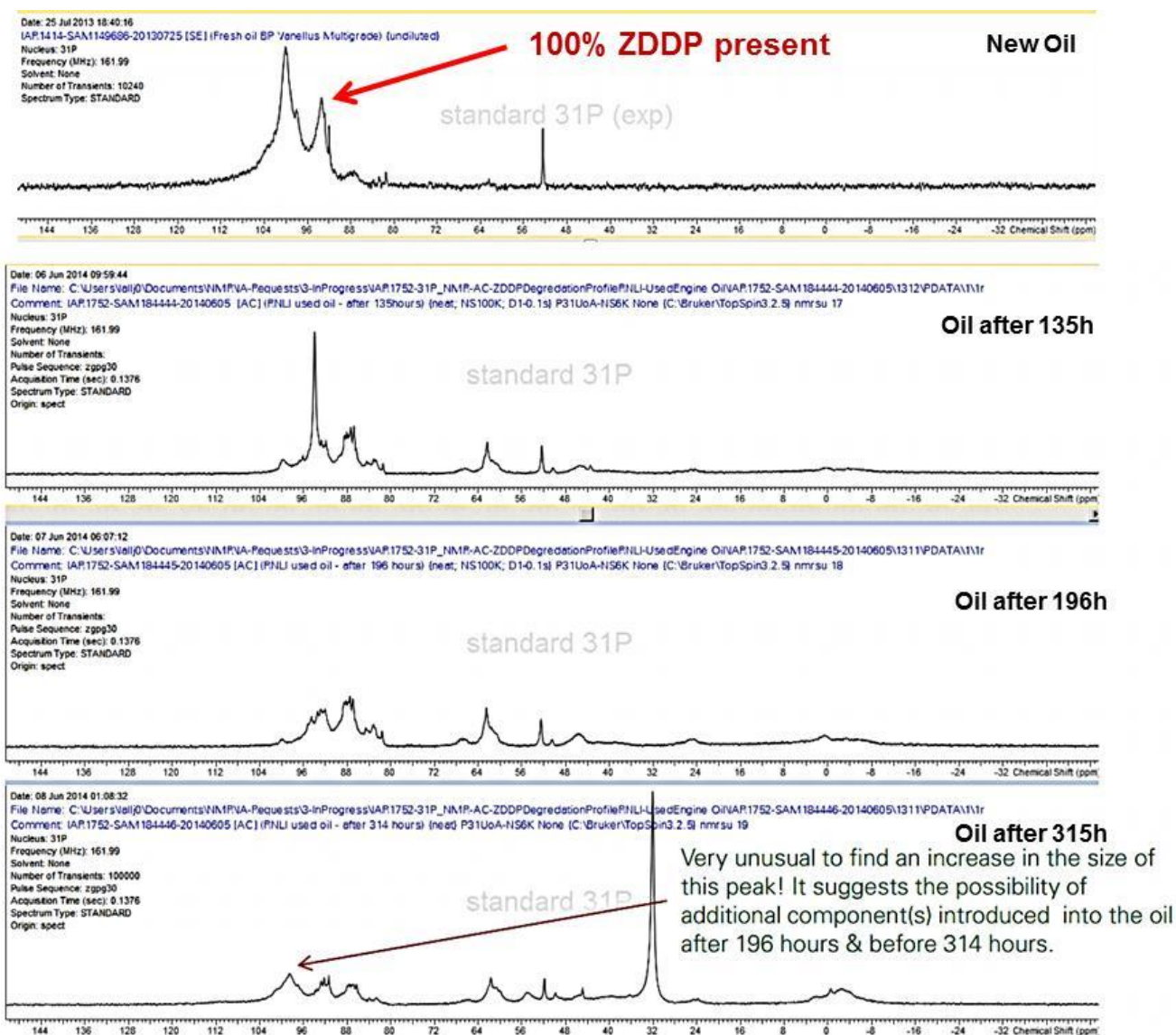


Figure 29: 31-P NMR spectra for different lubricant samples

Figure 29 shows the ^{31}P NMR spectra of four different lubricant samples including New Oil, In-service Oil (135 h), In-service Oil (196 h) and Used Oil (315 h). Each lubricant sample tested contains ZDDP anti-wear additive. New Oil contains the highest concentration of ZDDP in its most effective form which can provide maximum protection against wear of engine components. Whereas, Used Oil (315 h) contains the least concentration of effective ZDDP due its degradation within the marine engine over several duty cycles in past 315 h. The other two oil samples In-service (135 h) and In-service (196 h) contain intermediate level of ZDDP between New Oil and Used Oil (315 h). The peak height noted between 80 and 100 ppm (as mentioned along the horizontal axis) in New Oil case depicts the presence of effective ZDDP in its new form. However, with lubricant usage within the engine ZDDP is known to degrade and thus its chemistry also changes, which is clearly reflective from the reduction in the peak height and formation of new peaks on the right hand side, on comparison with spectra shown for New Oil. The presence of multiple peaks along the x-axis of the ^{31}P NMR spectrum indicates that phosphorus is present in several different chemical environments [75].

Under normal engine running conditions, ZDDP in engine oil decomposes due to oxidation. This process converts P-S compounds into P-O compounds such that a shift in the chemical state is noted on the x-axis of the spectra [75]. This change in chemical nature of P containing ZDDP anti-wear additive is not reflected by the ICP spectroscopy. ICP results in Table 9 shows a non-consistent increase in phosphorus, which could be due to the fresh oil top-ups to the engine oil before collecting the oil sample. Therefore the NMR spectroscopy is a useful tool in capturing the chemical state of the ZDDP additives and its depletion.

4.5. Oil Condition Monitoring by Oil Sensor

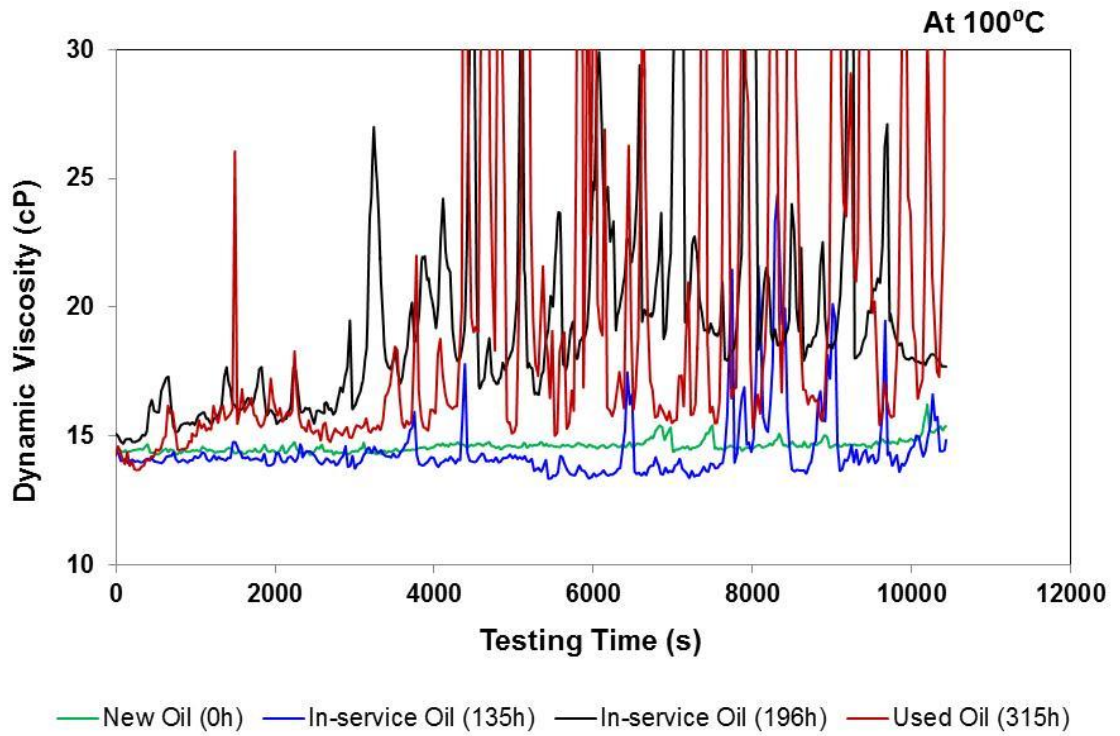


Figure 30: Dynamic viscosity measurements obtained by Oil Sensor

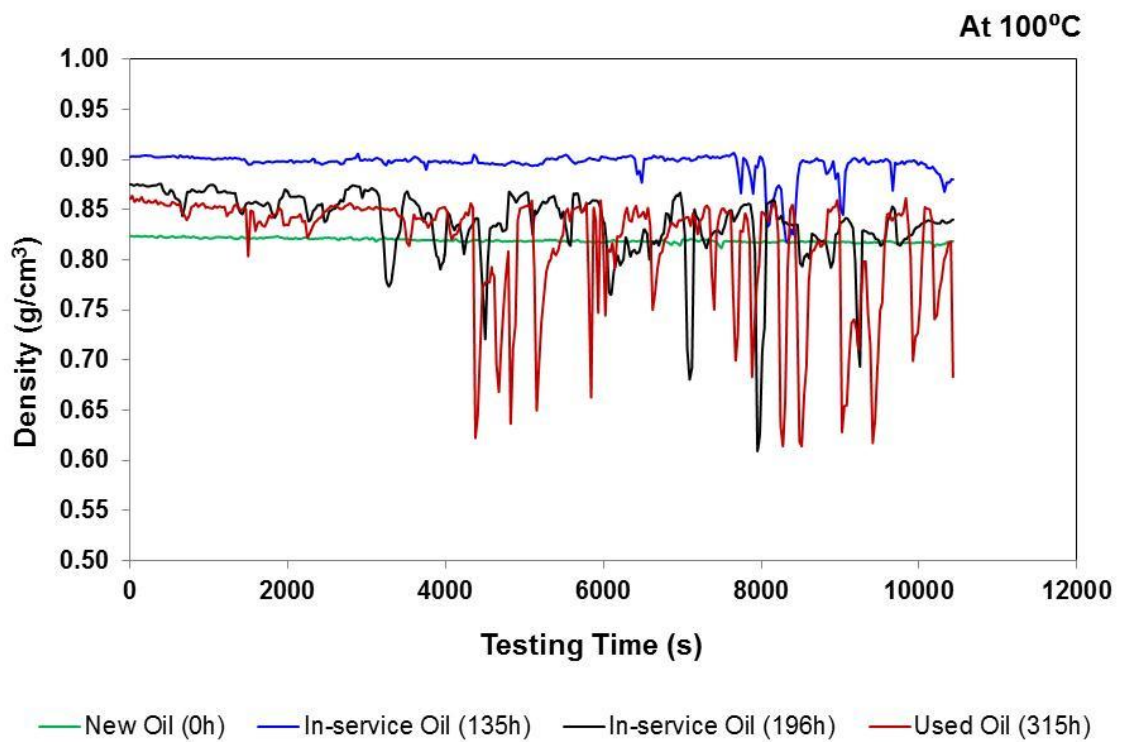


Figure 31: Density measurements obtained by Oil Sensor

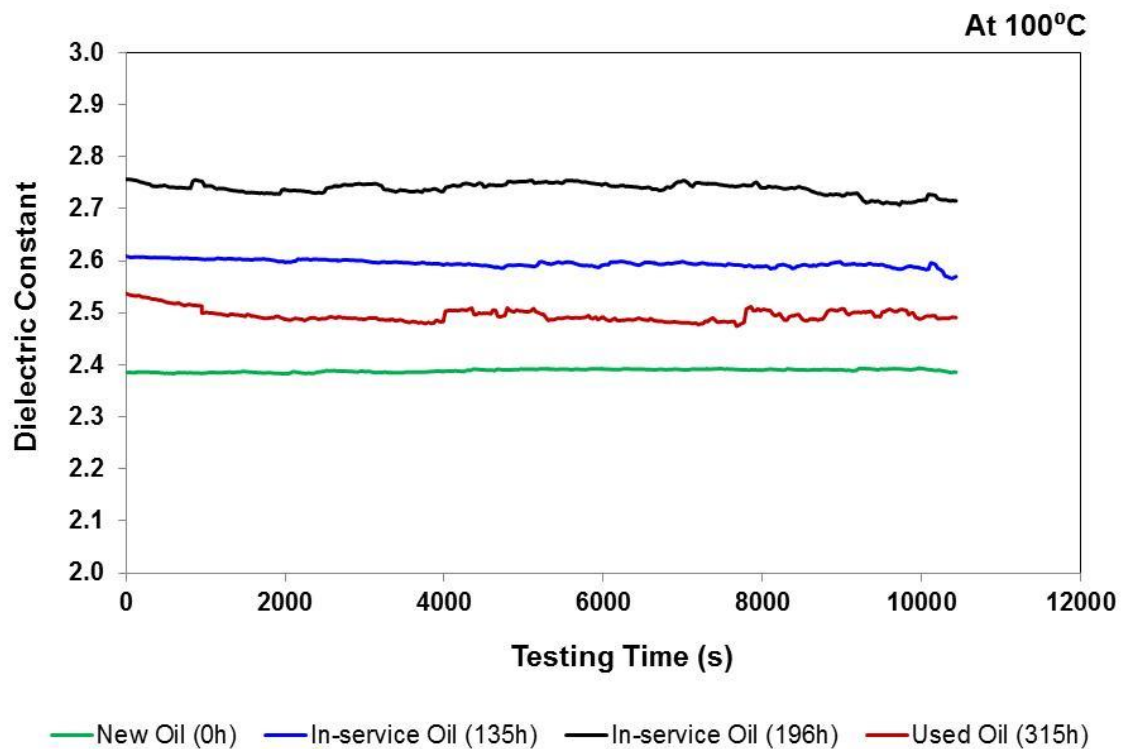


Figure 32: Dielectric constant measurements obtained by Oil Sensor

The fluid properties oil sensor was employed to measure the condition of oil in real-time. The oil sensor used is capable of measuring oil properties such as viscosity, density, dielectric constant and bulk temperature of the oil. The data is recorded by the oil sensor every 30 seconds for the complete test duration. Therefore for the benefit of detailed analysis the data was interpolated to obtain a value for every 1s interval for the complete test duration of 3 hrs.

Figure 30, Figure 31 and Figure 32 show the results obtained for the oil properties and since oil temperature was kept constant at 100°C, its values obtained by the oil sensor were not considered for analysis. Also the viscosity of oil at room temperature was considerably higher; therefore a flow rate of 0.2m/s was difficult to obtain which is necessary for the optimum measurements by the oil sensor. Therefore the measurements of oil properties in real-time by oil sensor were only made at 100°C which is also the average engine running temperature and in real application for oil sensor, it is expected that the measurements will be made at this high temperature in lifeboat engines.

Clearly it can be seen from the results of viscosity and density shown in Figure 30 and Figure 31 that with increase in wear or contaminant debris present within the oil, the error in the results of these two parameters also increases. It is envisaged that these errors (or high spikes) in the results are due to the increased interaction of wear debris with the sensor thus resulting in sudden high value of these parameters. On the other hand, Figure 32 shows a better representation of oil condition in terms of dielectric constant of the oil. It can be seen that with increasing number of duty cycles of the oil within the engine the dielectric constant value has also increased. The disturbance in the results is negligible in comparison to the data recorded for the other two oil parameters. The drop in the dielectric constant value of the Used Oil was unexpected since it should have the highest value in the range of lubricant samples tested. However, the possible explanation to this unique behaviour of this particular oil sample could be the addition of new (or fresh) oil into the engine before the sample was extracted for the experiment. This is a common practise in lifeboat applications to top-up the engine with fresh oil whenever the oil level is noted below its minimum. Therefore the dielectric constant of oil could be used as an indicator of change in oil quality in real-time oil condition monitoring system.

4.6. Analytical Ferrography

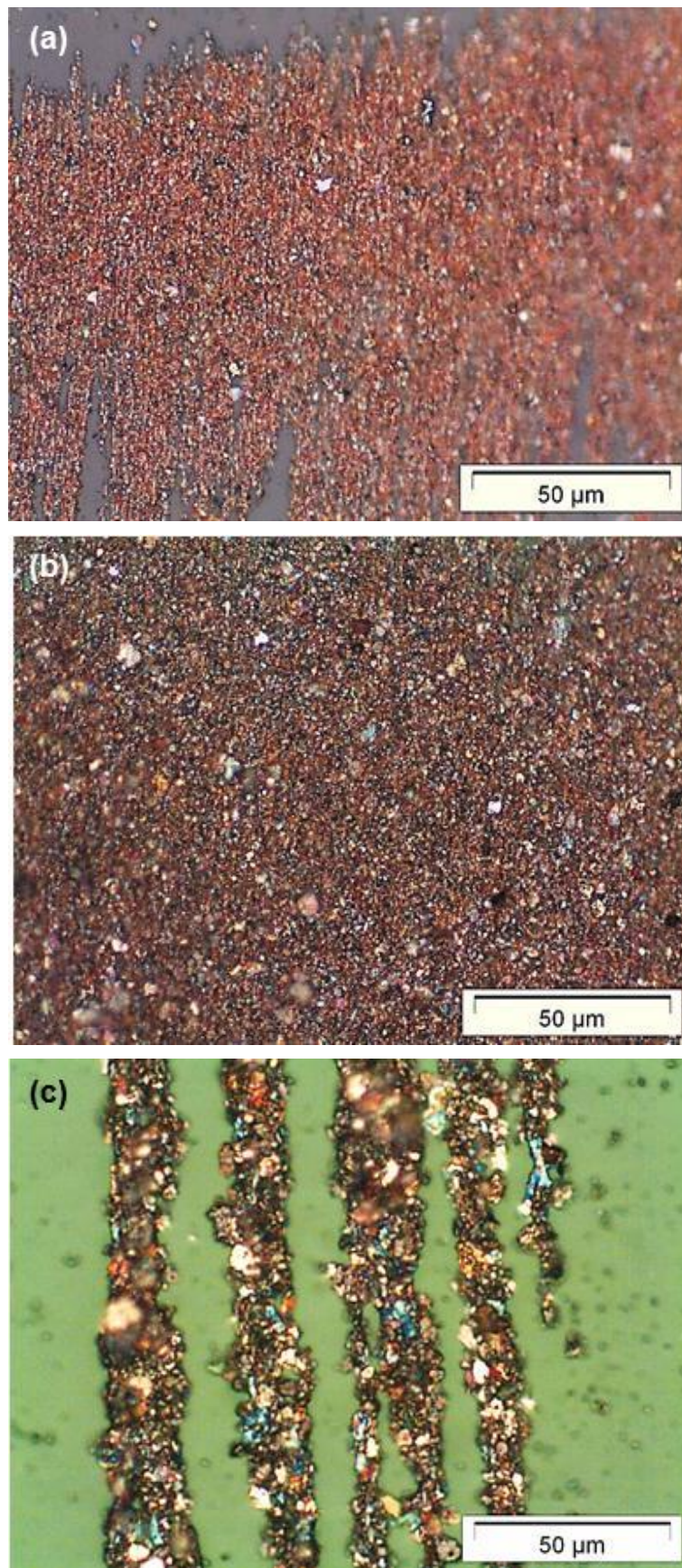


Figure 33: Ferrography Micrographs of three used oil samples

The analytical ferrography was performed on three engine lubricant samples each of which were near the end of their service life. The Figure 33 (a) shows the micrograph of lubricant sample collected from the MAN manufactured marine diesel engine of RNLI lifeboat after service for 270 h. Similarly, Figure 33 (b) and (c) are the results obtained from lubricant samples collected after 280 and 300 h. The microscopic analysis revealed that vast amounts of ferrous rubbing wear particles, mostly smaller than 5 μm are present in the oil samples. A wide variety of different types of ferrous wear particles, including severe sliding, abrasive wear, fatigue chunks and flakes with maximum diameters of respectively 15, 10, 15 and 20 μm , are also present. Heat treatment at the temperature range of 330°C showed a 60/40 ratio in medium/low alloy steel composition in lubricant sample shown in Figure 33 (c). A high level of dark ferrous oxides, less rust was noticed along with traces of oxidised non-ferrous rubbing wear. Also contamination particles include primordially fine crystalline and carbonaceous material are also observed.

4.7. Wear analysis of actual cylinder liner from RNLI marine engines

Piston ring reversal points both at top dead centre (TDC) and bottom dead centre (BDC) suffers from intense wear. Here momentary cessation of lubricant entrainment in ring-liner contact results in asperities interaction since lubricant is retained in the contact zone either due to squeeze film action or entrapment in the rough contiguous surfaces[83, 84]. In case of TDC near top ring reversal point, this effect is even much severe due to excessive combustion gas pressure and primary regime of lubrication is boundary. High wear also takes place in this region due to reversed tractions experienced by the contacting surfaces near the point of change in direction of reciprocating sliding motion[16]. Both sliding surfaces rely on the formation of protective tribo-film in the contact zone by the anti-wear additives present in engine lubricant to reduce the effect of thermal and mechanical stresses which lead to wear. Wear in TDC region of liner has been mentioned as a limiting factor to the lifetime of the engine. Such wear phenomena long since overcome in automobiles, still cause problems in the marine diesel engines. [85]

Therefore to better understand the extent of wear of cylinder liners installed in MAN engines of Trent Class of the RNLI Lifeboats, a typical cylinder liner was obtained from the actual engine that was undergoing the extensive overhaul. Figure 34 (a) shows the actual cylinder being obtained from the RNLI for wear analysis of bore surface. Three sections were cut at TDC, BDC and mid-stroke (MID) locations, as shown in Figure 34 (b), using a band saw cutting machine. Figure 34 (c) shows the bore surfaces of the three sections cut from the cylinder liner at TDC, MID and BDC region. These sections were then analysed for wear mapping under the 3D White Light Interferometer.

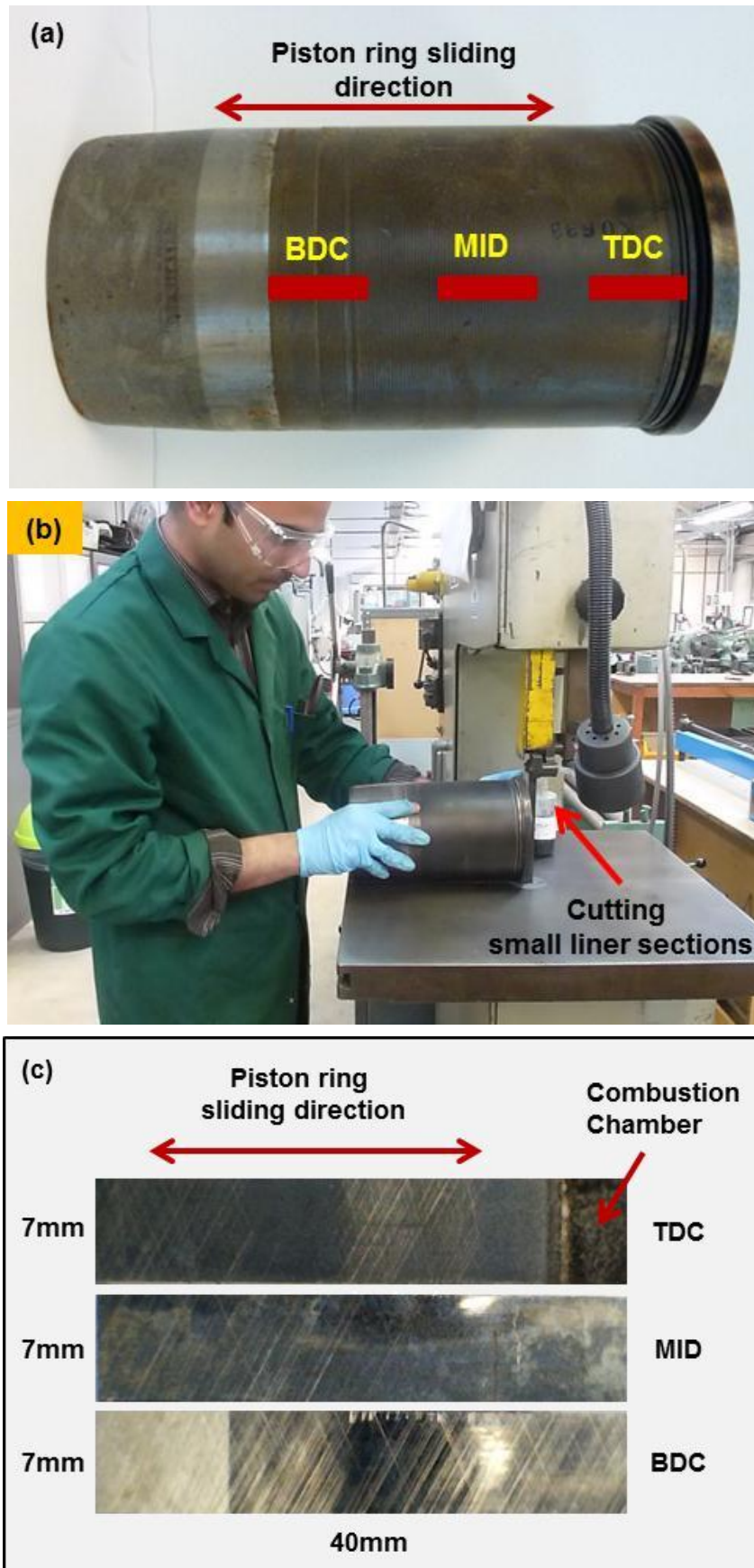


Figure 34: Actual cylinder liner used for wear analysis of bore surface in (a); sample preparation in (b); samples used for surface analysis in (c)

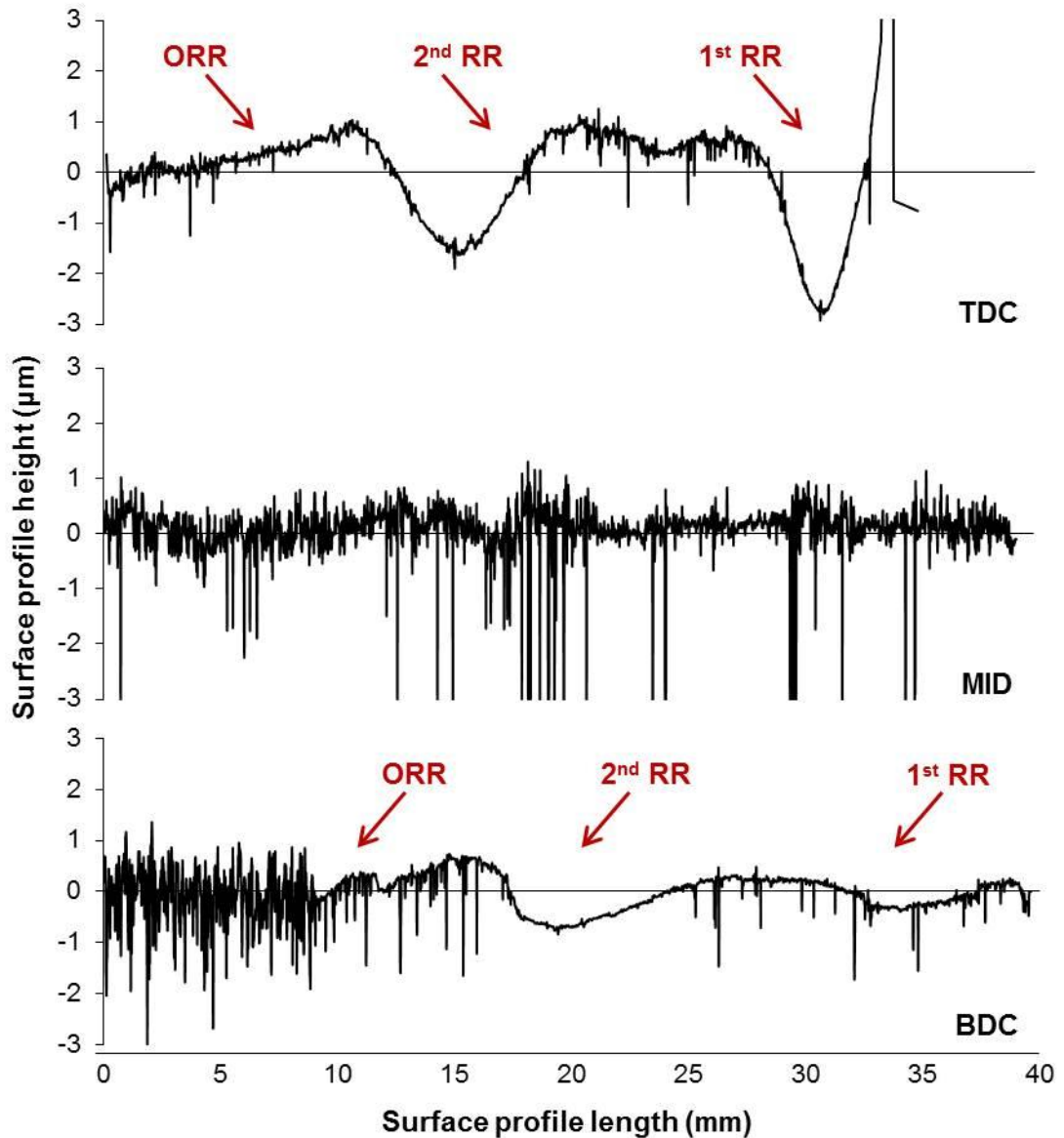


Figure 35: Surface profile of three sections cut from an actual cylinder at TDC, MID stroke and BDC locations

The abbreviations used in Figure 35, i.e. 1st RR, 2nd RR and ORR refer to first ring reversal, second ring reversal and oil ring reversal points, respectively. Clearly it can be seen in Figure 35 that higher wear takes place near the top ring reversal region on cylinder liner surface at TDC. The maximum depths of the surface profile of cylinder liner noted at TDC region is 3.03 μm at 1st RR and 2.01 μm at 2nd RR which is clearly higher than the depth of respective surface profiles in MID and BDC region. This observation could be attributed to the fact that the combustion gas pressure is at its maximum in TDC region for every alternative cycle for the 4-stroke engines (i.e. power

stroke). Indisputably, the combustion gas pressure acting behind the piston rings pushing them radially against the liner surface is a few orders higher than the pre-loaded elastic nature of piston rings, thus providing them with a tight fit with the liner surface ensuring minimal gas leakage into crankcase. The gas pressure varies with the amount of fuel injected during the power stroke. In case of RNLI lifeboats' operating conditions employed during the rescue operations, engines are run at their highest load, hence maximum loading of piston rings against liner surface at TDC region.

In addition, the temperature is high due to combustion and speed is low, which further limits the availability of lubricant in top ring reversal region at TDC. Hence the enhanced asperity to asperity interaction prevails resulting in higher wear of comparatively softer grey cast iron made cylinder liner surface in contrast to hard chromium coated top compression piston ring. The boundary lubrication regime exists under such tribological conditions and boundary film forming anti-wear additives present in fully-formulated engine lubricating oil are responsible to reduce asperity interaction and control wear rates.

Due to extensive tribological shearing of lubricants the degradation of such lubricants results in anti-wear additive depletion and thence the increased wear of cylinder liner surfaces, as observed in the case discussed above.

4.8. Stability of lubricant and ionic liquid mixtures

The stability of the mixtures containing non-polar lubricants (such as mineral based engine oil 15W40) and polar ILs (such as phosphonium based ILs) is very important for the overall performance of newly developed formulation both during testing stage and real applications. Using IL as additive in fully-formulated lubricant can be a challenge since it can produce an unstable emulsion. This concern has also been raised by other researchers in past, when proposing ILs to use as additive in either base oil or fully-formulated oil. Bo Yu et al. [28] has demonstrated the verification of oil stability (or single phase fluid and not emulsion) by using the comparison of experimentally measured viscosity of the oil-IL mixture with that of theoretical value obtained by the Refutas equation. In addition to this, the visual inspection to detect

phase separation (or cloud formation) in mixture was used. Both methods showed that the two phosphonium ILs, Trihexyltetradecyl phosphonium bis(2,4,4-tri-methylpentyl) phosphinate and Trihexyltetradecyl phosphonium bis(2-ethylhexyl) phosphate, are fully miscible in the non-polar hydrocarbon oils of both base oil and fully-formulated types.

In the current research, the above mentioned phosphonium ILs have been used since it is expected that these would also be fully mixed in used oils and thence the improvement in tribological performance of the lubricant and IL mixtures can be evaluated.

The visual inspection of the mixtures of used oil (315h) and ILs was not possible due to their opaque appearance, The same problem was encountered in case of the in-service oils (135h and 196h) but the mixtures of ILs with new and base oils were clearly inspected with no phase separation (or cloud formation) even after a month of storage in tightly sealed bottle. Although the visual inspection is quicker among the other analytical methods for oil stability analysis but it is rather subjective due to dependence upon the inspector's observation, and may possess some error.

A more accurate approach for oil stability analysis which redundant the verification requirement with theoretical results is the optical scanning technique using Turbiscan Lab instrument. This technique has been employed in past by many other researchers analysing the dispersion or suspension state of different oils [46, 86-89]. J. A. Ostlund et al. [86] demonstrated the higher accuracy of Turbiscan Lab and its tendency to detect even very small differences in the stability of different oil mixtures over traditional methods such as spot-test (visual inspection), hot-filtration and p-value methods.

In current research, Turbiscan Lab instrument has been employed to analyse stability of the mixtures fully-formulated engine oil with phosphonium ILs mentioned above. Four different mixtures including New Oil with IL1, New Oil with IL2, Used Oil with IL1 and Used Oil with IL2 were analysed for 11 days (test performed once each day) at 30°C using the procedure mentioned in section 3.3.2.6. The graphical results obtained from the analysis are discussed below.

Figure 36, Figure 37, Figure 38 and Figure 39 show the stability analysis spectra for the four different oil and IL mixtures. Each vertical scan of the sample produced a light transmission and backscattering profile. Starting from left to right of the profile (or horizontal axis in each figure) corresponds to the bottom then middle followed by top part of the oil sample bottle subjected to scanning. Since oil used in the experiments is of considerable viscosity, therefore its mixture with ILs produces a meniscus with the sample bottle walls at the top. This meniscus formation results in different light transmission/backscattering profile in comparison to rest of the sample. This effect was evident in all the four mixtures and can be seen at right side of the profiles between around 40 and 50 mm of samples' height.

The de-stability is measured by looking for the variation in profile as function of time since the testing was repeated 11 times over the period of 11 days (once each day). A reference profile is generated at the beginning of the test and all subsequent profiles obtained are subtracted from the reference profile to observe any variation occurred over time.

The first expected variation could be in terms of phase separation (or cloud formation) since lubricating oil is slightly less dense (0.884 gm/ml) than both the ILs (~0.91gm/ml). This density difference can results in sedimentation process leading to settling down of heavier dispersed phase (IL) in less dense continuous phase (lubricating oil) under the action of gravity. Such phenomenon may results in change in transmission and/or backscattering of light through sample where the concentration of dispersed phase changes.

The second expected variation could be due to sedimentation of wear and contaminant debris more likely to present in used oil and IL mixtures. Debris possesses much higher density than continuous phase (lubricating oil), hence may result a shift in light transmission and/or backscattering as the sedimentation process progresses over time.

After the stability analysis was completed for all the four oil mixture the transmission and backscattering profiles were analysed. Figure 36 and Figure 37 show stability analysis spectra for new oil with IL1 and IL2, respectively. In both the cases no

change in the transmission and backscattering of light can be seen. Hence these two mixtures can be considered to be stable and single phase homogeneous mixture.

Figure 38 and Figure 39 show stability analysis spectra for used oil with IL1 and IL2, respectively. Again, in both the cases no change in the transmission and backscattering of light can be seen. Hence these two mixtures can also be considered as stable and single phase homogeneous mixture. No sedimentation of debris was observed from the results obtained. This could be due to the presence of dispersant additives in the fully-formulated engine lubricant which are responsible to keep all contaminants dispersed in the oil during engine operation such that debris can get filtered out when the oil is passed through the oil filter instead of depositing over the surface of lubricated engine components.

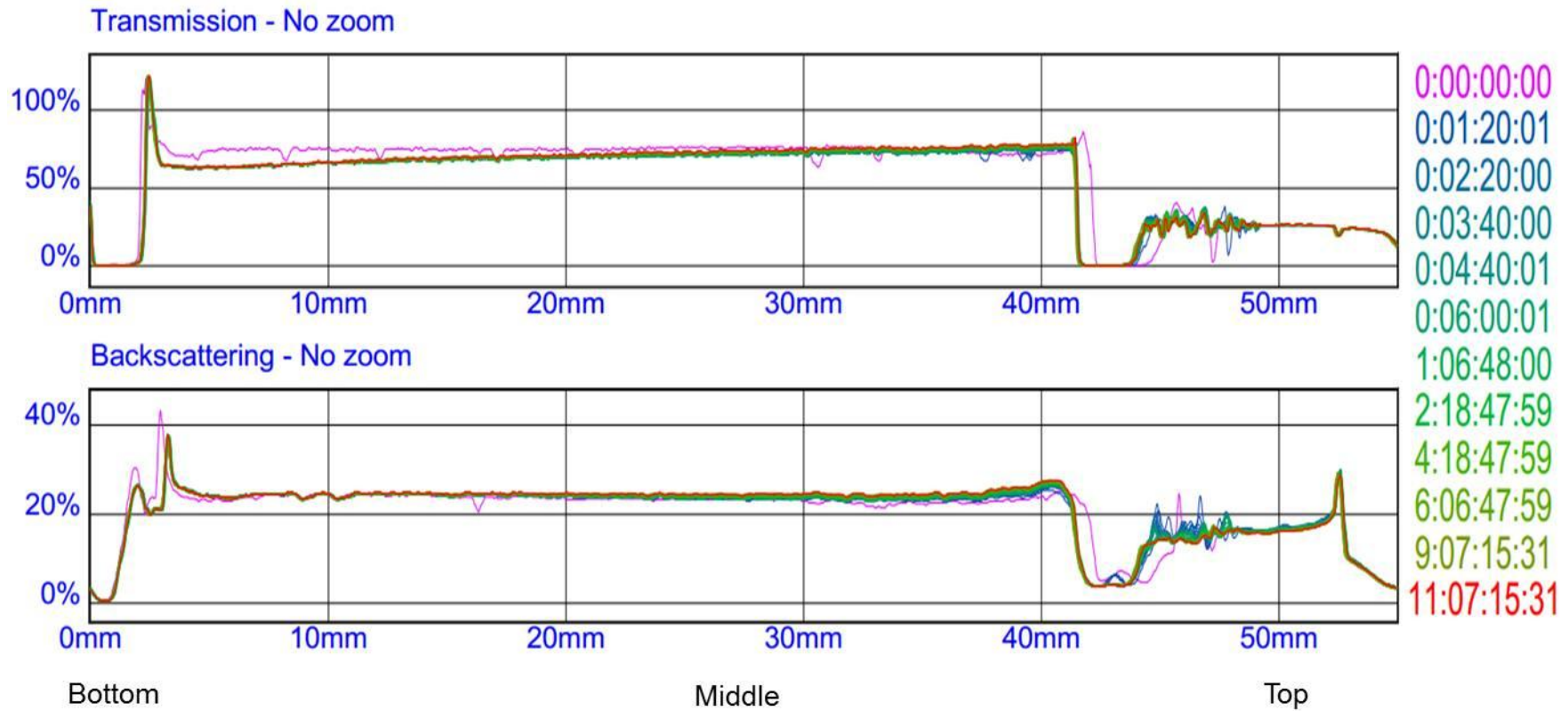


Figure 36: Stability analysis spectra for 6% volume IL1 in New 15W40 engine oil at 30°C using Turbiscan Lab Expert. The horizontal axis corresponds to height of oil sample bottle. The colour of different profiles corresponds to time scale on vertical axis on right.

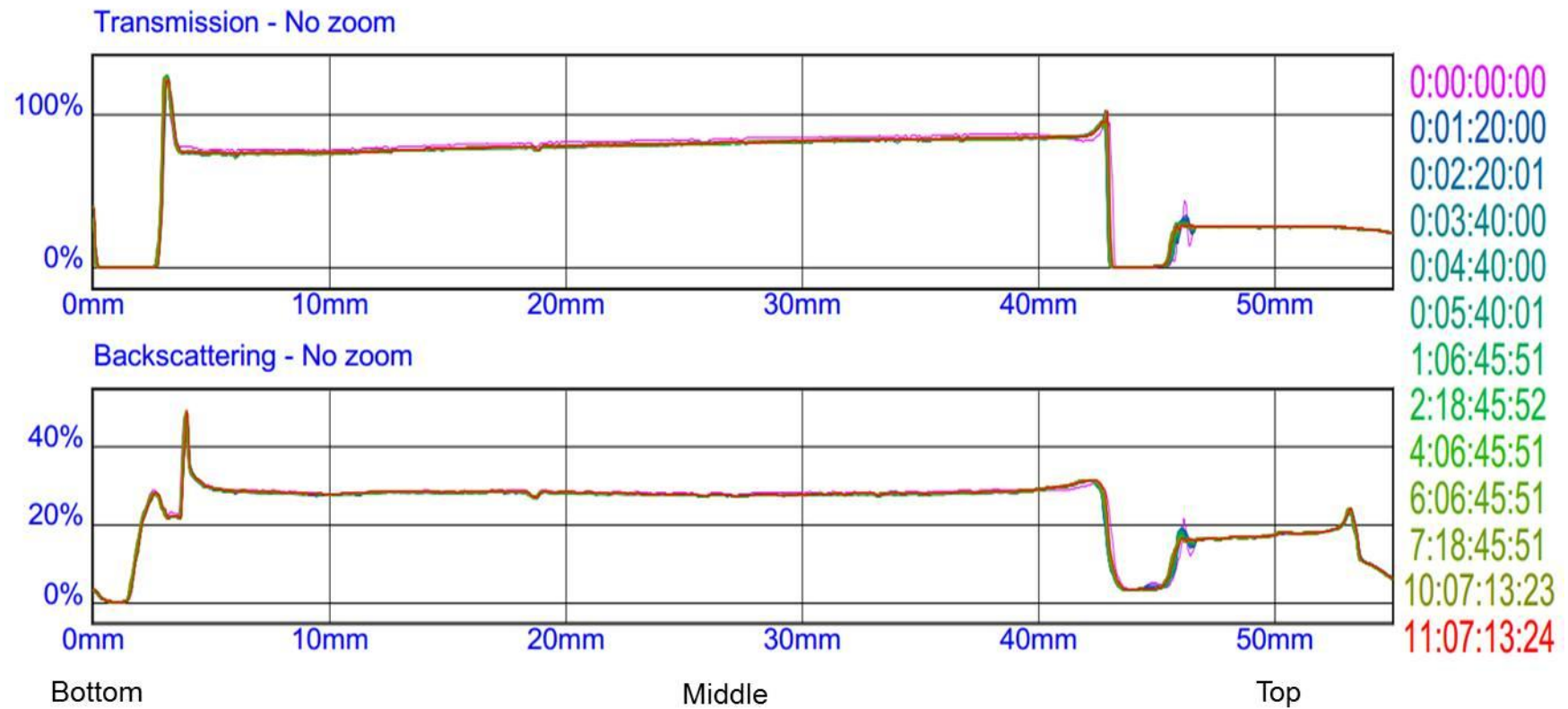


Figure 37: Stability analysis spectra for 6% volume IL2 in New 15W40 engine oil at 30°C using Turbiscan Lab Expert. The horizontal axis corresponds to height of oil sample bottle. The colour of different profiles corresponds to time scale on vertical axis on right

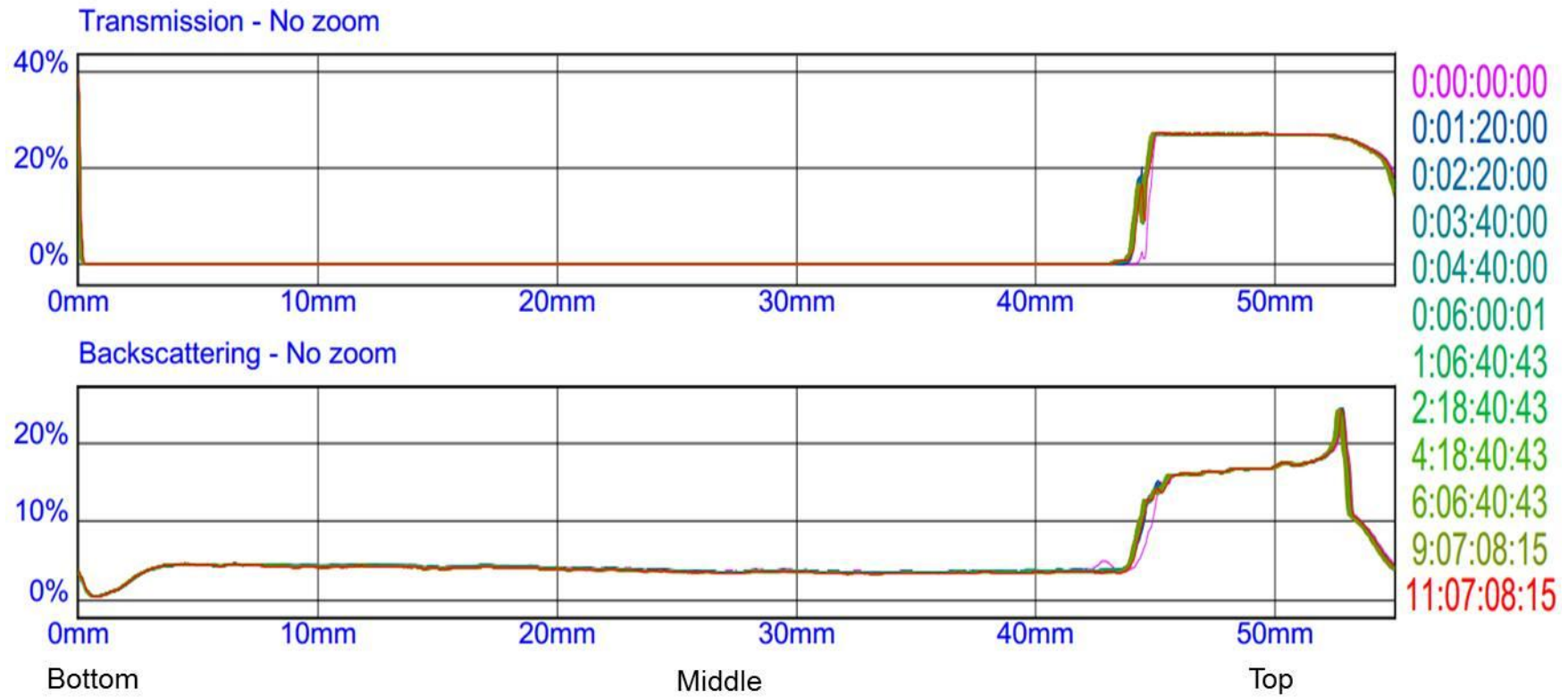


Figure 38: Stability analysis spectra for 6% volume IL1 in Used 15W40 engine oil at 30°C using Turbiscan Lab Expert. The horizontal axis corresponds to height of oil sample bottle. The colour of different profiles corresponds to time scale on vertical axis on right

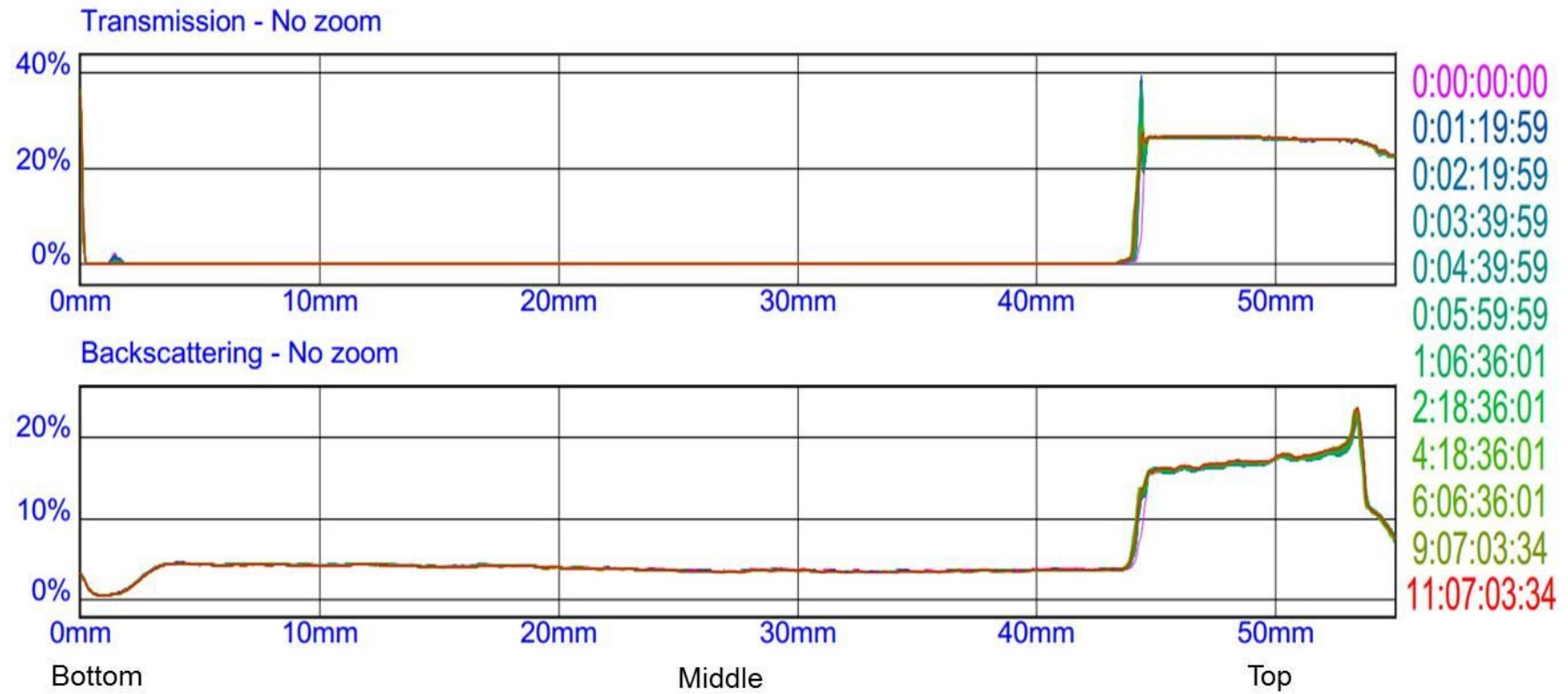


Figure 39: Stability analysis spectra for 6% volume IL2 in Used 15W40 engine oil at 30°C using Turbiscan Lab Expert. The horizontal axis corresponds to height of oil sample bottle. The colour of different profiles corresponds to time scale on vertical axis on right

Chapter 5 Results of Tribological Analysis

The boundary lubrication conditions that exist near the top dead centre of cylinder liner during the engine running were simulated at bench level using the high frequency micro-friction tribometer (Plint TE77). The experimental simulation involved the piston ring and cylinder liner contact in the reciprocating sliding motion under lubricated conditions such that boundary regime can be produced and effect of lubricant additives can be evaluated. This experimental approach is not new and has been adopted by several researchers in the past to study different aspects of tribological behaviour of different materials and contribute to the much needed scientific knowledge for further development in both automotive and lubricant industry.

The aim was to analyse the effect of lubricant degradation in lifeboat engines on its tribological performance. Also investigate the scope of improvement in the tribological performance of lubricants at the end of its service-life to further extend its service period. It was hypothesised that the addition of 6 volume% of phosphonium IL could improve the tribological performance of used engine lubricant. Since the similar amount of IL is also employed in past by other researchers for slightly different and new engine lubricants, it was expected that the comparison could be made to add to the existing scientific knowledge with performing tests with used engine lubricants. For comparison purpose the different lubricants such as mineral base oil, new and in-service engine lubricants were also evaluated in the same manner as used lubricants. The comparison was expected to support better understanding of the lubricant degradation in lifeboat engines and also to validate the experimental results for new 15W40 engine oil with those of published literature since it is widely studied.

The following parameters were analysed during and post-testing.

- Coefficient of friction as function of sliding duration
- Electrical Contact Resistance (ECR) to analyse kinematics of tribo-film formation process during sliding
- Wear volume and Wear rate
- Wear mechanisms on worn surfaces
- Surface chemistry of boundary antiwear films

5.1. Friction and ECR results

Engine lubricants help controlling the friction between the ring and liner surfaces to an optimum level to maintain the engine fuel efficiency. Otherwise in case of dry sliding between chromium coated ring and cast iron liner surfaces, scuffing mode could eventually lead to seizure, since these materials have strong adhesion for each other, as reflected by the Compatibility Chart developed by Rabinowicz [90] in J.L. Basse [91].

The above mentioned action of lubricant in controlling (or reducing) the friction is performed by preventing the contact between the ring and liner surfaces. During major part of the piston stroke, the ring-liner contact experiences elasto-hydrodynamic lubrication regime such that friction is a function of lubricant internal resistance (viscous-shear). The chemical nature of lubricants (additives) is immaterial. Whereas, the top dead centre (TDC) and bottom dead centre (BDC) regions experience the boundary lubrication regime conditions, where bulk properties of lubricant like density and viscosity, are of little importance [62]. This is because at high load and small sliding speed, lubricant cannot form thick film to separate the surfaces. Therefore in these regions, surface properties and the chemical composition of lubricant play a significant role. Polar molecules of additives get adsorbed on the solid surfaces to form layers possessing lower shear strength than underlying solid surface, thus separating the surfaces and reducing the friction and wear.

The mean values of kinetic friction coefficient values obtained during the tribo-testing are plotted in Figure 40 (a, b, c, d and e) and Figure 41 (a, b) for tests conducted at 100°C and 25°C, respectively. These figures compare the frictional behaviour of different lubricants with and without phosphonium ILs (referred in graphs as IL1 and IL2). Figure 40 (e, f, g, h and i) and Figure 41 (c, d) show the typical measurement of Electrical Contact Resistance (ECR), for the same lubricants and lubricant-IL mixtures mentioned in Figure 40 (a, b, c, d and e) and Figure 41 (a, b), respectively. The x-coordinate in all cases represents the testing time in seconds. The effect of temperature on tribological performance of different engine lubricants and lubricant-IL mixtures was also studied. Experiments were conducted at 100°C which is an average engine oil temperature during engine operation and 25°C which is room temperature at which engine normally starts. Tribo-tests were run to achieve a steady-

state kinetic friction force, therefore, continuous measurements at every 1s of the complete bench test duration was made and divided by the normal applied force to derive the corresponding kinetic friction coefficient values. Each test was run 3 times so that average of kinetic friction coefficient results can be used for analysis purpose and also the repeatability of tests can be assessed. The repeatability (relative standard deviation) of friction coefficient results was calculated less than 10% in all tests carried out in laboratory.

Friction coefficient values obtained during the tribo-testing in all cases indicate the boundary lubrication regime (i.e. friction coefficient ~ 0.1) and are consistent with the literature [1, 20, 46, 85]. Also it is further verified (see Append B), that theoretical lubrication regime modelling using lambda ratio which involves minimum oil film thickness and combined roughness of mating surfaces, depicted boundary lubrication conditions inside the contact zone during tribological process. It is well known that friction coefficient of a system operating under boundary lubrication regime is a function of properties of both lubricant and mating surfaces due to partial contact between the surfaces [92]. Therefore, in the experiments performed, the properties of test specimens (cast iron flat and piston ring segment) were maintained constant in all cases so that the effectiveness of only lubricant present between the interfacing surfaces could be examined. Further, the presence of wear debris in the contact zone during sliding can also affect the friction force, this phenomenon is expected since the in-service and used lubricants contains wear debris generated during the engine operations before been sampled for laboratory testing.

ECR displays the process of boundary anti-wear film formation between the two contacting surfaces during the sliding process. In the current research, boundary lubrication conditions were simulated during the sliding process therefore the thin boundary film formed by the lubricant additives (or presence of metal oxides) at the contact interface was analysed using ECR method. This boundary film act as a resistance to the electrical current flow between the interfacing surfaces of metallic test samples such that the measure of resistance provides a qualitative indication of separation between surfaces during the tribological process. The micro-friction tribometer records these results in the form of contact potential (voltage) which means high contact voltage is due to high contact resistance. Zero volts means no lubricant film formed (hence complete metallic contact) whereas 50mV means complete

separation between the surfaces (hence no metallic contact occurring at all). E. S. Yamaguchi et al. [93] in their work demonstrated the use of ECR method for analysing the boundary film formation process for different additives and their mixtures with base oil. They explained the concept of Induction Time for interpreting the boundary film formation process. According to their theory, at the beginning of sliding, chemical change may be occurring resulting in surface species to form, and with continued sliding, the sufficient accumulation of such species results in rapid boundary film formation. The time gap between the start of sliding and start of resistive film formation is defined as induction time. They demonstrated that induction time can vary with different additives and additive mixtures. Also sudden abruptness in film formation reflected by drop in contact resistance (which quickly reverses again) can be attributed to metal-to-metal contacts, produced either by wear or by slight lateral oscillations of the slider; losses of anti-wear film; changes in the film composition in the contact, possibly reflecting the tenacity of the film or its shear strength or changes in its conductivity.

The attributes of friction-time curve that characterizes the running-in process are as follow [94]:

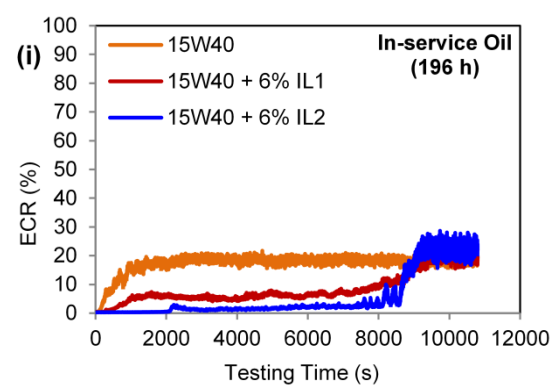
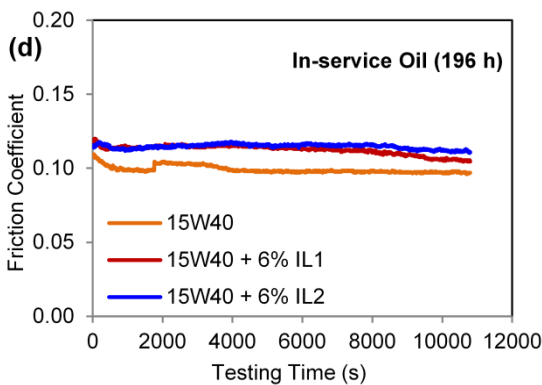
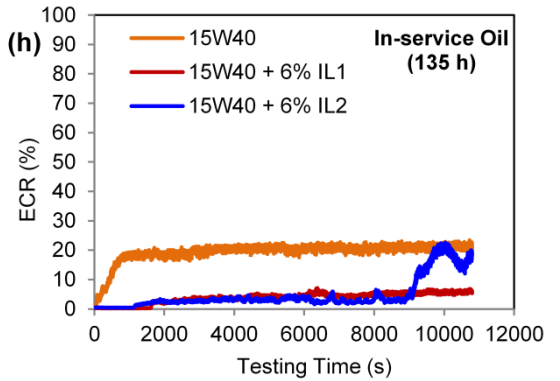
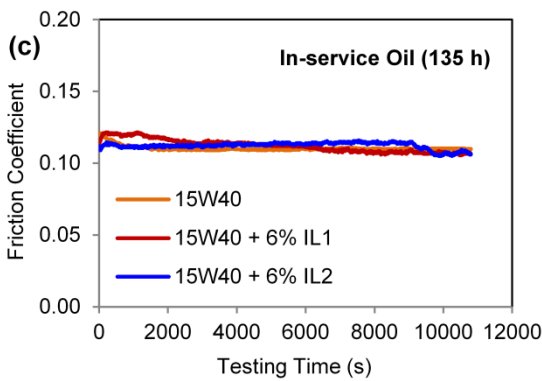
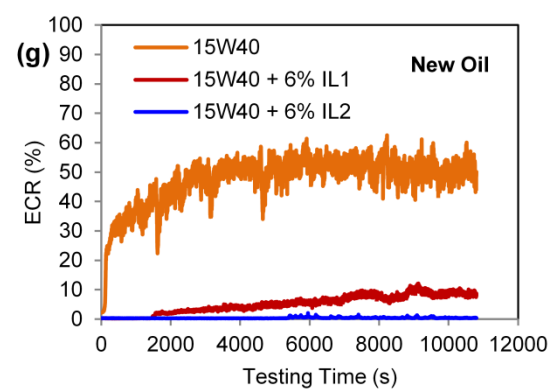
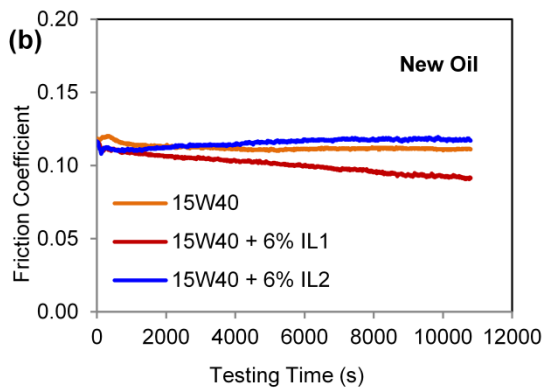
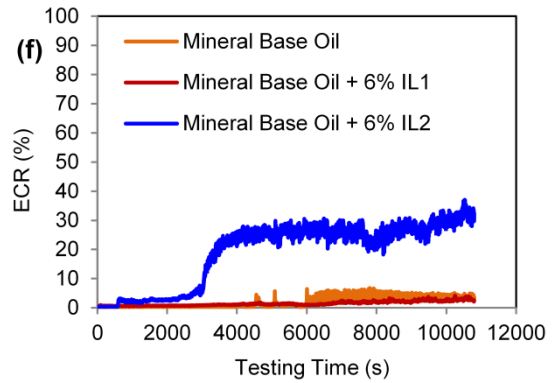
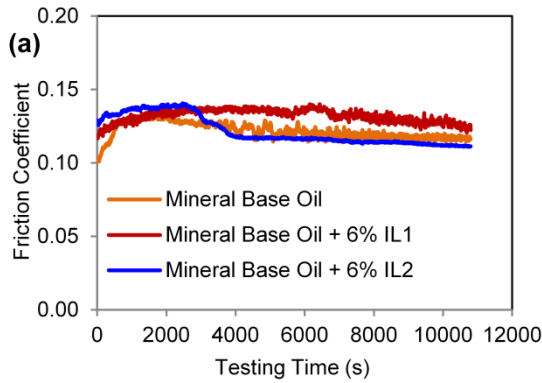
- Change in curve shape
- Duration of certain features of the curve
- Magnitude of fluctuations in the friction force at different time

Steady-state sliding could be characterised from the friction-time curve by constant average value of kinetic friction coefficient. Therefore, attention was given to these key features while interpreting obtained friction-time curves.

The attributes of ECR curves used to characterize the boundary film formation process, based on the work of E. S. Yamaguchi et al.[93] are as follow:

- Induction time for boundary film formation
- Time to reach stable film formation
- Abrupt reversals in contact resistance that quickly reverse back

At 100°C



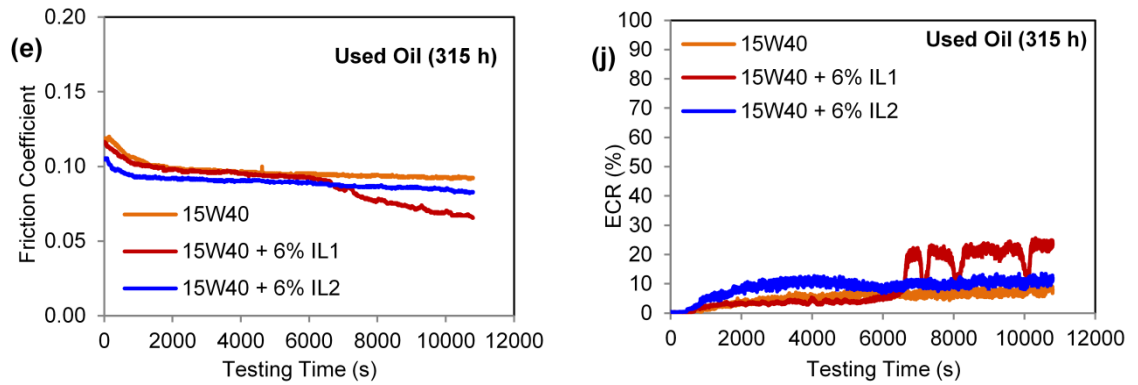


Figure 40: Mean Friction coefficient and Electrical Contact Resistance behaviour for different lubricants and lubricant-IL mixtures during 3h sliding testing at 100°C

For experiments conducted at 100°C, Friction-time curve in all cases, shown in Figure 40 (a, b, c, d and e), clearly depict 2 stages of tribological process: running-in and steady-state sliding. Fast-transition in friction coefficient (>0.2) which is a representative of increased adhesion between sliding surfaces leading to scuffing failure, was not evident in any case.

During running-in at 100°C, friction coefficient in all cases was unstable and time to reach steady-state friction varied for different lubricants and lubricant-IL mixtures. Mineral base oil took longer (~4000s) to reach steady-state than fully formulated lubricants (~2000s), both with and without ILs. Jun Qu et al. [95] demonstrated similar observation for the time required to reach steady-state sliding (or running-in period) for new 15W40 diesel engine oil in neat form lubricating ring-liner contact at 100°C. Also, it was noted that time to reach steady-state was reduced by addition of ILs to the individual lubricants. But the effect was different when IL1 was added to new oil and used oil. In case of new oil with IL1, steady-state period was never reached and friction coefficient continuously changed (dropped) along sliding duration, see Figure 40 (a). Whereas, in case of used oil with IL1, steady-state period only short-lived after initial running-in and then friction coefficient started to drop after 6000s, see Figure 40 (e). ECR results, shown in Figure 40 (f, g, h, I, j and k), further explains the contact situation between the piston ring segment and cast iron flat sample during lubricated sliding process.

Figure 40 (f) shows longer induction time (~6000s) for neat mineral base oil and mixture containing mineral base oil with IL1, than mixture of mineral base oil with IL2 which started to form film after 380s of initial sliding. Time to form a stable boundary film at the interface was > 4000s for mixture containing IL2. This phenomenon was absent in case of neat base oil which has no boundary film forming additives. Surprisingly, the addition of IL1 to neat mineral base oil could also not produce any difference to ECR results. These ECR results match closely with their corresponding friction-time curve shown in Figure 40 (a).

Figure 40 (g) shows 0s induction time and rapid film formation by neat new oil leading to a stable film in around 2000s from the test start time. ECR results for neat new oil also matches with its friction response (Figure 40 b) to the tribo-system which depicts running-in period up to 2000s of sliding after which both ECR and friction coefficient remained steady. This boundary film is likely to be formed by the ZDDP and Ca based detergent additives present in new oil. 0% ECR was noted for the mixture of new oil and IL2 which also matches with its slightly higher friction response. Induction time for the mixture of new oil and IL1 was noted to be 1200s depicting slow film formation process. After 1200s the film formation builds up in a quasi-linear manner for the remaining sliding duration and no stable film was formed. On comparison with friction-time curve, ECR results suggested that addition of IL1 to new oil could not produce the effective boundary anti-wear film at the interface as new oil; hence, there were some other factors that contributed to the reduction in friction. This observation could be attributed to low-shear strength layer of metal oxides produced due to oxidation of nascent sites of metal surface on reaction with oxygen from air dissolved in lubricant or IL, which can produce lower friction values due to low ductility [46]. The presence of metal oxides on the worn surface was later verified by the XPS analysis and is discussed later in this thesis.

Figure 40 (c) shows no difference in the friction response of in-service oil (135h) by addition of ILs. ECR results (Figure 40h), demonstrated 0s induction time for in-service oil. Also, it effectively formed a stable boundary film after 1000s of sliding process and this observation aligns with the running-in period of friction-time curve. Addition of ILs resulted in longer induction time for both mixture of in-service oil with IL1 (1400s) and with IL2 (1000s). ECR results further showed no stable film was formed by either of the oil-IL mixtures, and little spikes (noise) in case of IL2, which

could be attributed to the presence of wear and contaminant debris (dust particles) or metal-oxide layer. The wear debris can oxidise during the tribological process and act as insulating layer leading to unstable and high resistance between the metallic surfaces [46, 96]. After 9000s, rise in contact resistance of oil and IL2 mixture, indicates the sufficient accumulation of film forming species on sliding surfaces eventually leading to the formation of relatively thicker film, as discussed by E. S. Yamaguchi et al. [93].

Figure 40 (d) showed slightly higher friction coefficient after addition of IL1 and IL2 to the neat in-service oil (196h). Also friction-time curve for neat in-service oil showed a high friction event between 1500s and 4000s during which friction coefficient increased slightly and then dropped back to its previous nominal value. This short transition in friction behaviour of tribo-system could be due to the sudden entrance of wear debris in the sliding interface which was present in the in-service oil due to its service in lifeboat engine prior to tribo-testing. Figure 40(i) shows the effect of addition of ILs on the boundary film formation capability of in-service oil. Addition of ILs resulted in longer induction time for both mixture of in-service oil with IL1 (280s) and with IL2 (~2000s), in comparison to neat in-service oil (100s). In both cases, after ~8000s, a rise in contact resistance leading to stable film formation was noticed. However, in case of mixture containing in-service oil and IL2, the increase in resistance is highly unstable as reflected by the reversal spikes giving the appearance of much broader curve.

Figure 40 (e) showed reduction in the running-in time by the addition of ILs to the neat used oil (315h), i.e. from 2000s to 1000s. The shorter running-in period could be owing to rapid truncation of interacting asperities which experience high concentrated stresses on application of load during sliding. ECR results, Figure 40 (j), demonstrated that mixtures of used oil and ILs outperformed the boundary film formation capability of neat used oil. Since the induction time reduces from 900s for neat used oil to 670s after addition of IL1 and 460s after the addition of IL2. Also a formation of stable film was seen after addition of both ILs (separately) to used oil. In case of mixture of used oil and IL1, a further slow rise in contact resistance after 5500s with frequent reversals in resistance which are also evident from the corresponding friction-time curve.

It is worth mentioning that ECR curves are the net result of both film forming and film removal processes [93]. JL Viesca et al. [46] in their work demonstrated the use of ECR measurements to assess boundary film formation process. They found that at higher temperature like 100°C, the chemical reactivity of lubricant additives with sliding surfaces increases the film formation rate, while the film removal rate also increases owing to the decrease of durability of the boundary film material and the reduction of hydrodynamic fluid film thickness due to decreasing viscosity of the lubricant. Therefore, it can be seen that the equilibrium between film formation and removal rate is important, since it can also affect the ECR results.

At 25°C

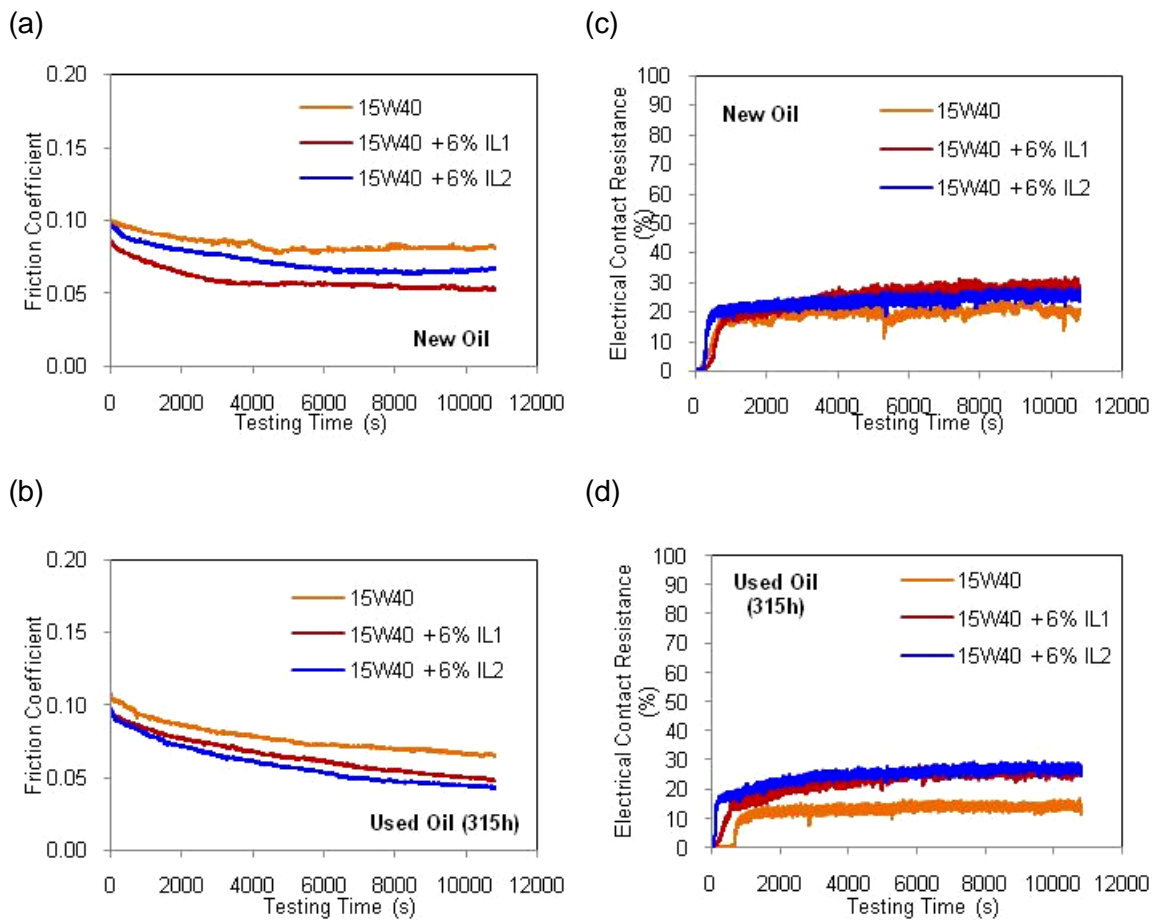


Figure 41: Mean Friction coefficient and Electrical Contact Resistance behaviour for different lubricants and lubricant-IL mixtures during 3 h sliding testing at 25°C

During the experiments conducted at 25°C, friction response of tribo-system with new and used engine lubricants (with and without ILs) was noted to be completely different than that observed during tests conducted at 100°C. At 25°C, running-in period lasted longer, but generally, the friction response in terms of average kinetic friction coefficient was lower.

Figure 41 (a), shows friction-time curve obtained for new oil with and without ILs. Clearly, the time to reach steady-state sliding (running-in process) varied in all three cases. Friction response of tribo-system to neat new lubricant was slightly unstable for a major portion of test duration and running-in lasted for approximately 5000s (nearly half-of-test duration). Whereas, after addition of IL1 to the new engine oil, running-in concluded more gradually with little variations but took little longer (~6000 s) than neat new oil. Similar phenomenon as IL1, was noted by addition of IL2 to the neat new engine oil, and steady-state was reached after 3000 s of initial sliding process. ECR

results (Figure 41 c) demonstrated 169 s induction time for new oil. Also, it effectively formed a stable boundary film after 608 s of sliding process with a few reversals in resistance which are also reflected by the friction-time curve. Addition of IL1 to new oil resulted in longer induction time (309 s) and also the time to reach stable film (1000 s). On the other hand, addition of IL2 in new oil, also showed no improvement in induction time (222 s) but the stable film formed a little quicker (422 s) than new oil. Furthermore, it was observed that the separation between the sliding surfaces was more due to the presence of ILs (IL1 and IL2) in fully-formulated new oil. ECR curve shape also matches with the friction-time curve in all cases of new oil with and without ILs. However, running-in period is not noticeable from ECR results. This is obvious since ECR results not always relate to the friction behaviour of tribo-system (which is a collective response of all process causing friction) rather they indicate the electrical insulation between the asperities of interfacing metal surfaces.

Figure 41 (b), shows friction-time curve obtained for used oil with and without ILs. In case of neat used oil, steady-state was reached at 6200 s but it was only short-lived until 9000 s after which friction coefficient dropped again. However, no distinct steady-state friction behaviour was noted in cases when IL1 and IL2 were added to neat used oil, separately. This phenomenon is clearly evident from the continuous drop in kinetic friction coefficient in a quasi-linear manner from the beginning of tests. Maybe near the end of test (~9000 s) some stability in friction coefficient can be seen. It could be ascribed to the fact that various processes begin to operate during running-in stage. The superposition of their influence leads to complex friction changes until a balance (or equilibrium) is achieved but sometimes these processes continue to evolve and steady-state is either not achieved or short-lived [94]. Figure 41 (d) showed 646 s induction time for used oil. Thereafter, a rapid rise in resistance takes place leading to relatively a stable boundary film after 755s of initial sliding. Unlike neat used oil sample, mixtures of used oil with ILs started to form boundary film in much less time, such that induction time by addition of IL1 and IL2 reduced to 100 s and 64 s, respectively, compared to 646 s for used oil. Also addition of ILs resulted in less time needed to form a stable film, in case of both mixture of used oil with IL1 (390 s) and with IL2 (150 s). Furthermore, a higher degree of separation between the sliding surfaces was noted due to addition of ILs. This phenomenon indicated the contribution of ILs in boundary film formation leading to reduced asperities contact between interfacing surfaces. The effect of increased ECR and reduced friction coefficient was also reflected on the wear volume observations which are discussed in the next section.

5.2. Wear results

After the completion of each tribo-test, both the piston ring segment and cast iron flat samples showed the smooth glossy worn areas depicting the polishing of rough surface due to boundary conditions.

Since the material removed from the test samples was significant enough for comparison therefore wear volume measurements were carried out. The surface mapping of worn surfaces was carried out using the 3D White Light Interferometer (ZYGO). The direct measurements of wear volume, i.e. the volume of material lost from the test sample, were carried out using the procedure and equipment as explained in section 3.4.1. The analysis was done at 1x magnification using the zoom reduction capabilities provided by the instrument (ZYGO). The low magnification helped in mapping the complete wear scar area without the need of additional editing of images, for instance stitching of multiple images captured at higher magnifications. Also the calibration of measurement software was done using a known volume of an indentation mark.

Wear volume measurements were only carried out on cast iron samples since no special sample preparation was needed, on contrary, due to compound curvatures of piston ring profile the direct wear volume measurement were not possible. Wear volume results for cast iron flat samples lubricated with different lubricants at two different operating temperatures 100°C and 25°C are shown in Figure 42 and Figure 43, respectively. Each case was evaluated by repeating tests 3 times and an average of measured wear volume was considered for analysis purpose such that the repeatability (relative standard deviation) of wear volume results was noted within 10%.

Obtained volume values were then used to calculate the specific wear rate using the following relation [15]:

$$V = K F s$$

Where V is the obtained wear volume, F is the applied load, s is the sliding distance, and K is the specific wear rate coefficient (mm^3/Nm). The calculated values of specific wear rate for different lubricants and IL mixtures are shown in Table 10 in the section 5.2.3.

Wear mechanisms taking place during the tribo-testing process on the cast iron samples were analysed by surface analysis of worn surface area using SEM technique. The details of the procedure and equipment employed for analysis are mentioned in section 3.4.2 and 3.4.3. The two different magnifications of 200x and 1500x were used for overall condition and much closer detailed inspection, respectively. Comparison between the wearing mechanisms of cast iron samples in presence of different lubricant and lubricant-IL mixtures has been carried out. Figure 44 to Figure 48 show the SEM images of worn surfaces for tests conducted at operating temperature of 100°C , whereas Figure 49 and Figure 50 show those conducted at 25°C .

It is worth mentioning that the amount of wear produced in the bench test was expected to be higher than that can be found in ring-liner sliding contact in actual running engine for the same duration of sliding process [31] but the wear mechanism must not be altered. This is due to the fact that constant static load was applied during the complete bench test duration which resulted in accelerated wear of the test samples, whereas in actual engine the radial load between piston ring and liner interface varies with the piston stroke length between top and bottom dead centres. Also the effect of reduction in applied contact pressure due to increasing contact area with wear was neglected as it was not possible to apply variable loads on the tribometer used.

5.2.1. Wear volume results at 100°C

The relative loss of material from cast iron samples in terms of wear volume, defines the effectiveness of different lubricants and lubricant-IL mixtures. Figure 42, shows the effect of lubricant degradation on its anti-wear performance and also change in its anti-wear capability after addition of phosphonium ILs. It was clearly evident that new 15W40 engine oil has produced the least wear and mineral base oil produced the maximum wear. New 15W40 oil contains the well-designed additive package that

provides maximum protection in boundary wear conditions. These additives are not present at all in mineral base oil hence the wear is highest. As the new lubricant was put into service in heavy duty diesel engine, its effectiveness has reduced which is reflected by the increasing trend of wear volume results obtained from bench testing of different in-service lubricants. The trend of increasing wear volume was expected since the lubricants has lost its effectiveness as a function of its duty cycles in actual engine represented by number of hours, i.e. 135h, 196h and 315h. Used engine oil which serviced around 315h in actual engine, produced significantly higher amount of wear among all the fully-formulated engine oils but lower than mineral base oil. This infers to the remaining effective additives content in the used lubricant in comparison to mineral base oil which has none. Since the standard oil analysis of used engine oil showed it as unfit for further service in engines therefore the wear produced can be considered as the critical limit to the effectiveness of the fully-formulated engine oil.

The effect of addition of IL1 and IL2 to the different engine-conditioned oils can be seen in Figure 42. Wear in case of used engine oil reduced by 58% and 34% by addition of IL1 and IL2, respectively. However increment in wear in all other cases of fully-formulated engine oils by addition of both the ILs was noted. Interestingly, ILs helped reducing wear when added as additive to mineral base oil but the anti-wear performance was not as good as new fully-formulated oil.

Many previous studies [36, 39, 95] have mentioned that owing to the unique dipolar structure, negatively charged moiety of ILs tend to get adsorbed on the positively charged metal surface, thus forming a protective film on the surface. The same is also true for ZDDP anti-wear additives typically present in engine lubricants. It has also been mentioned that such additives require optimum thermo-mechanical conditions to form boundary film on the surfaces [29, 30, 40, 97]. The aforementioned findings indicated the antagonistic interaction between the already present additives in fully-formulated engine oils and later added ILs. Such interaction could be attributed to the strong affinity of film forming additives towards the metal surfaces leading to competitive aggression with ILs which possess similar tendency. It has been mentioned that tribo-chemical reactions taking place at the surface could also be detrimental when the synergy of chemical (corrosion) and mechanical (e.g., abrasion and adhesion) stresses accelerates material removal [40]. Therefore such phenomenon could have happened by the competitive response of all additives to

form boundary film on surface eventually leading to generation of stresses causing higher film removal rate than film formation rate. Hence, it provided more local sites for contact between the mating surfaces which resulted in higher material removal rate from the softer cast iron surface. The wear volume results are also in line with ECR results as discussed in the previous section.

Another interesting observation is that the aforementioned wear results seem to have no symmetry with their friction counterpart. Due to similar steady-state friction behaviour of fully-formulated engine oils after addition of ILs, it was expected that wear rate response of tribo-system to the new formulated lubricant-IL mixtures would be same. However, comparing friction-time curves in Figure 40 with corresponding wear volume results in Figure 42, showed that addition of ILs to fully-formulated engine oils have no appreciable effect on their friction behaviour; on the contrary, it does affect their anti-wear performance significantly. This observation could be justified by the fact that friction and wear are not directly related. The processes that lead to friction and wear may arise from different material and systems properties and often do not reach steady-state at the same time. Therefore, the same friction behaviour of oil with and without ILs doesn't necessarily means no-effect on wear as well. This is because frictional energy input to the system is partitioned differently from one tribo-system to another. This energy may be used to form oxides, grow cracks, plough through the surface, heat the surface, or shear debris layers [46, 94].

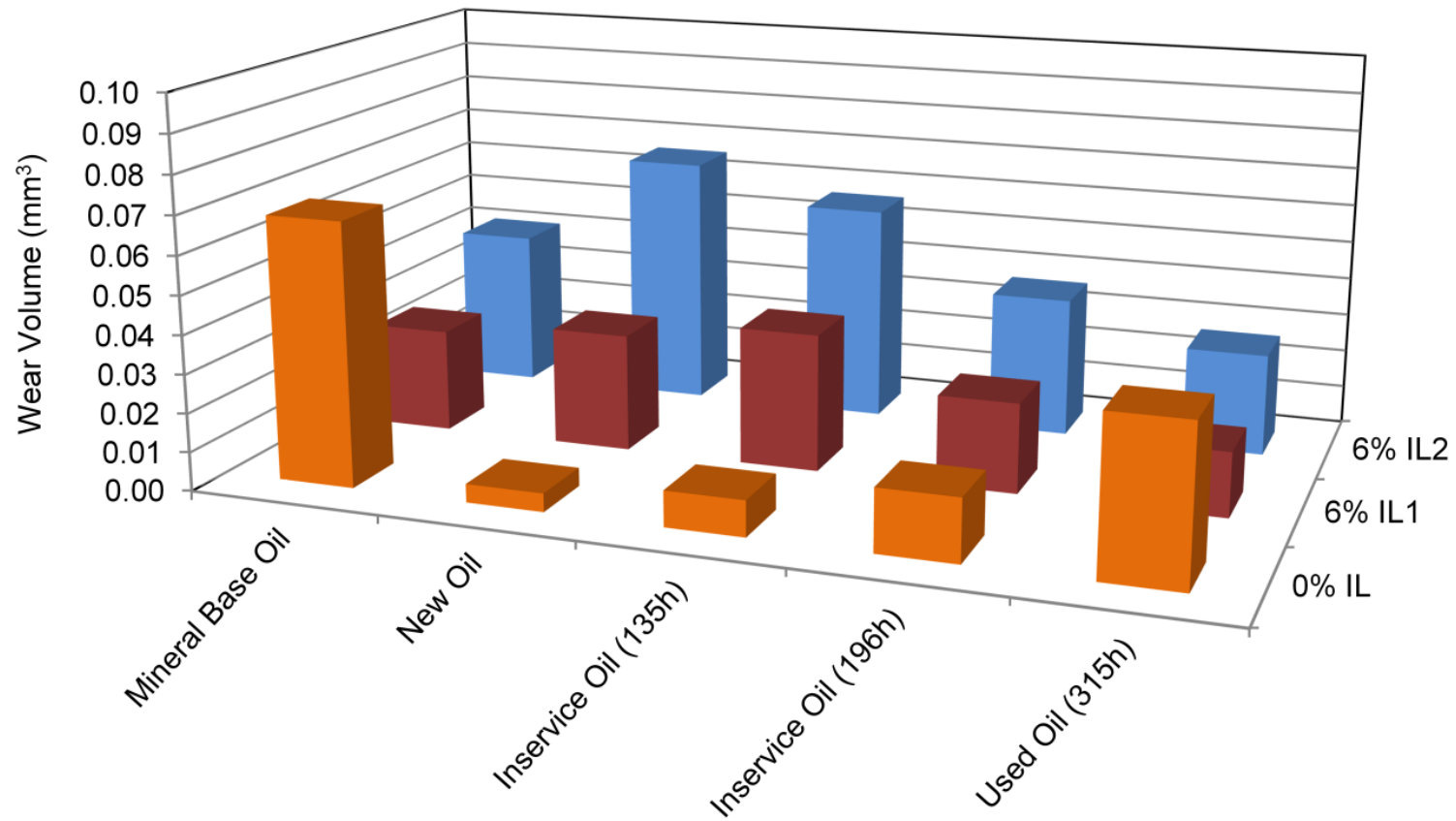


Figure 42: Wear Volume results of cast iron specimens after 3h sliding at 100°C. Repeatability (relative standard deviation) of results is within 15%

5.2.2. Wear volume results at 25°C

Strong effect of operating temperature on the anti-wear performance of new and used engine lubricants was observed. However effect of asperities contact temperature at the sliding interface was not considered. Figure 43 shows that wear produced by new oil at room temperature testing (25°C) is higher than that noted at 100°C. On the other hand, the used engine lubricant produced less wear at room temperature (25°C) than that noted at 100°C. Obtained wear volume results also matches closely with the friction behaviour at 25°C.

The effect of temperature on tribological performance of fully-formulated engine oil, especially in used form, has been mentioned by other researchers as well [1, 31]. It is well known de facto when simulated boundary lubrication regime that viscosity of lubricants has least effect on its tribological performance and additives are mainly responsible for reducing friction and wear. Therefore change in wear performance of engine lubricants owing to temperature dependence can be attributed to film forming additives present in lubricants.

Furthermore, the effect of addition of IL1 and IL2 to the both new and used oils can be seen in Figure 43. Wear in case of used engine oil reduced by 62% and 64% by addition of IL1 and IL2, respectively. However, interestingly no appreciable change in the anti-wear performance of new fully-formulated engine oil by addition of both the ILs was noted. Hence, depicting the positive response of ring-liner tribo-system to the lubricant-IL mixtures at 25°C which is normally the engine start temperature.

Clearly a better synergistic interaction is seen between the ILs and already present additives in fully-formulated engine oil in used form at room temperature than 100°C. Interestingly, the new oil-IL mixtures also demonstrated much lower wear than that noted at 100°C depicting synergistic interaction between the ILs and other additives. Jun Qu et al. [29] and Bo Yu et al. [28] also demonstrated similar improvement in anti-wear performance of oil-IL mixtures at room temperature due to synergistic interaction between phosphonium ILs and existing oil additives. Used fully-formulated oil and its oil-IL mixtures produced higher wear at 100°C than 25°C but stronger temperature dependence of oil-ILs mixture was seen than neat oil. That means better synergy

existed between ILs and other additives at room temperature than 100°C. Mixtures of used oil with IL1 and IL2 even outperformed the new oil, both in terms of friction and wear reduction capabilities. Hence demonstrating great potential of using the phosphonium ILs as additive in used fully-formulated engine oils.

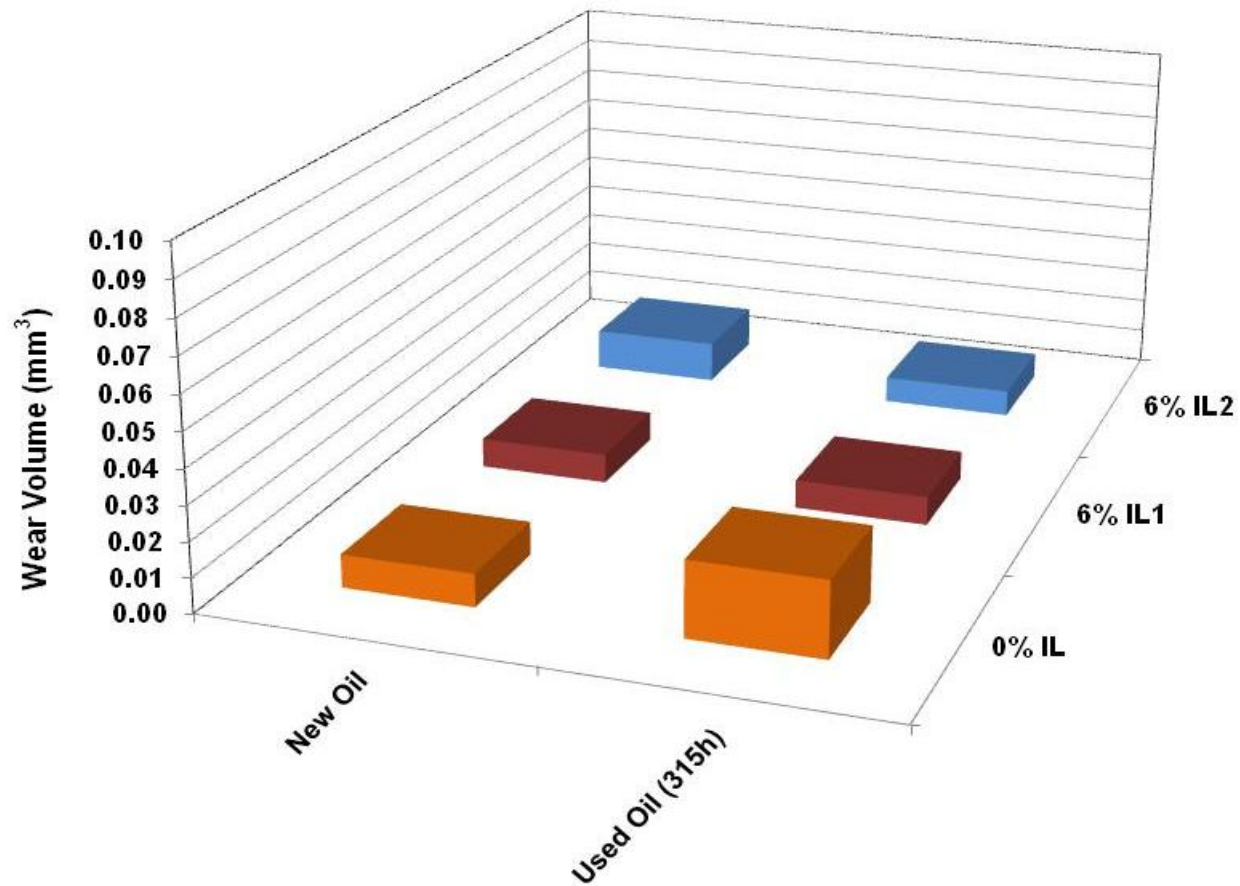


Figure 43: Wear Volume results of cast iron specimens after 3h sliding at 25°C. Repeatability (relative standard deviation) of results is within 15%

5.2.3. Wear rate results

Specific wear rate (mm/Nm) allows further a comparison of wear behaviour of any candidate material tested using different load and sliding distance [18]. In current research effect of load and sliding distance was not evaluated, however, wear rate results could allow comparison of wear behaviour with the work carried out by other researchers using this phosphonium IL as additive in mineral base oil and new fully-formulated engine oil.

The wear volume results for different engine lubricants and their mixtures with phosphonium ILs were used to calculate specific wear rate using the following relation [15]:

$$V = K F s$$

Where V is the obtained wear volume, F is the applied load, s is the sliding distance, and K is the specific wear rate (mm^3/Nm). The calculated values of specific wear rate for different lubricants and IL mixtures are shown in Table 10.

Table 10: Comparison of specific wear rate

Testing Temperature	Lubricant	15W40	15W40 + 6% IL1	15W40 + 6% IL2
100°C	Mineral base oil	28.66	11.31	17.26
	New oil	2.01	12.88	27.65
	In-service oil (135h)	3.90	15.05	23.78
	In-service oil(196h)	6.82	9.83	15.38
	Used oil (315h)	16.90	7.05	11.20
25°C	New oil	3.98	3.56	5.07
	Used oil (315h)	9.11	3.45	3.22

Specific wear rate results for cast iron samples lubricated with different combinations of oils and ILs are shown in Table 10. The values are considered severe for test conducted at 100°C using mineral base oil and used fully-formulated oil. While both new and used oil produced mild wear at room temperature (25°C). Effect of adding ILs to fully-formulated oils in some cases, such as new oil and in-service oils (135h and 196h) was detrimental leading to increase in wearing rate of cast iron samples. But the same is not true for used fully-formulated oil and ILs mixture in which wear rate found to be considerably reduced. Similar effect of ILs addition to fully-formulated oils was noted at room temperature testing, however, much more reduction in wear rates was noted in used oil case and no appreciable change in new oil case was observed.

Wear rate in engine applications for cylinder liner material should be less than 10^{-7} mm/Nm [18]. This suggestion was seen to be in line with wear rate noted in case of new fully-formulated oil both at 100°C (average engine oil operating temperature) and also at 25°C (cold engine start condition). In addition to above, the wear results observed for new oil with and without phosphonium ILs at room temperature testing are similar to those reported by other authors [28]. The increase in wear rate for fully-formulated oils as a function of duty cycle (number of servicing hours) in actual engine before tribo-testing is obvious due to degradation of anti-wear additives as discussed in Chapter 4.

5.3. Wear mechanisms

The investigation of wear mechanisms taking place during the sliding process between the rubbing surfaces under different lubricated conditions was carried out after the completion of tribo-testing. The centre of worn surface area of the cast iron samples was analysed using Scanning Electron Microscopy (SEM). The SEM micrographs taken for different cases of lubricants with and without ILs are shown in Figure 44 to Figure 50.

Sliding wear has been mentioned to be almost caused by a number of surface damaging processes, (in case of metals) such as [81]

- Plastic deformation
- Adhesion and material transfer

- Melting (seizing)
- Cutting wear
- Fatigue fracture (pitting)
- Surface reactions, etc.

Surface analysis results shown in Figure 44 to Figure 48, for tribo-testing carried out at 100°C, depict similar trend in surface damage as noted previously from wear volume results (Figure 42).

In all cases, smoothing of asperities of cast iron surface covering the shallow valleys and forming smooth plateaus with glossy finish depicted plastic deformation mechanism is observed under boundary wear regime. Scuffing damage was not seen and also not reflected by the mean friction coefficient values (i.e. < 0.2), in any case. The cast iron surface lubricated with New Oil is covered by dark lubricant film, Figure 45, unlike the Used Oil case in which material inherited porosities are clearly exposed, Figure 48. In the latter case, severe wear lines were also seen due to debris present at the sliding interface either as free particles within oil leading to 3-body abrasion and/or embossed onto counterpart piston ring running surface leading to 2-body abrasion.

Addition of ILs to the Used Oil, shown in Figure 48 resulted in wear reduction evident by fewer mild abrasive wear lines and less exposed porosities. Although the plastic deformation of asperities (peaks) has taken place even after the addition of ILs the effect of abrasion wear mode is reduced due to boundary film formation by ILs. Addition of ILs to the New Oil, shown in Figure 45, resulted in increased wear clearly evident from material inherited porosities been clearly exposed. Also abrasive wear liners are clearly visible after the addition of ILs, possibly due to debris generated during the sliding process causing two and/or three body abrasion at the sliding interface. In other cases, including In-service Oils (135h and 196h), addition of ILs has caused comparatively less damaged to the surface than the case of new oil with ILs. However the effect of addition of ILs is not positive and mild abrasive lines are visible after ILs addition, which are otherwise not evident in both cases of neat In-service Oils (135h and 196h). Also like New Oil without ILs, the worn surface is seem to be covered with a dark lubricant film, most likely boundary lubricant film, which gets disappeared after the addition of ILs to the In-service Oils (135h and 196h).

In Figure 49 and Figure 50, the worn surface of cast iron lubricated with New and Used oil with and without ILs is presented, for tribo-testing carried out at room temperature (25⁰C). All the testing parameters were kept same except the operating temperature was changed to 25⁰C than the previous tests conducted at higher temperature (100⁰C).

Clearly New Oil showed no evidence of abrasive wear in comparison to the cast iron surface lubricated with the Used Oil. Also due to the possible depletion of the anti-wear additives in Used Oil, severe plastic deformation of asperities can be seen leaving no evidence of initial polishing marks of unworn surface before testing. Whereas presence of such anti-wear additives in New Oil resisted the boundary lubrication conditions onto the deformation of asperities. Such that some of the valleys of the ploughing grooves originated during the surface polishing (manufacturing stage of samples) can be seen in New Oil. No significant change in the wearing mechanism is noted after the addition of ILs to the New Oil. However, the effect of ILs addition to the Used Oil is significantly beneficial as surface topography seem to be similar to that of New Oil case. This positive effect of ILs addition to Used Oil relates closely to its wear volume results (Figure 43) noted previously.

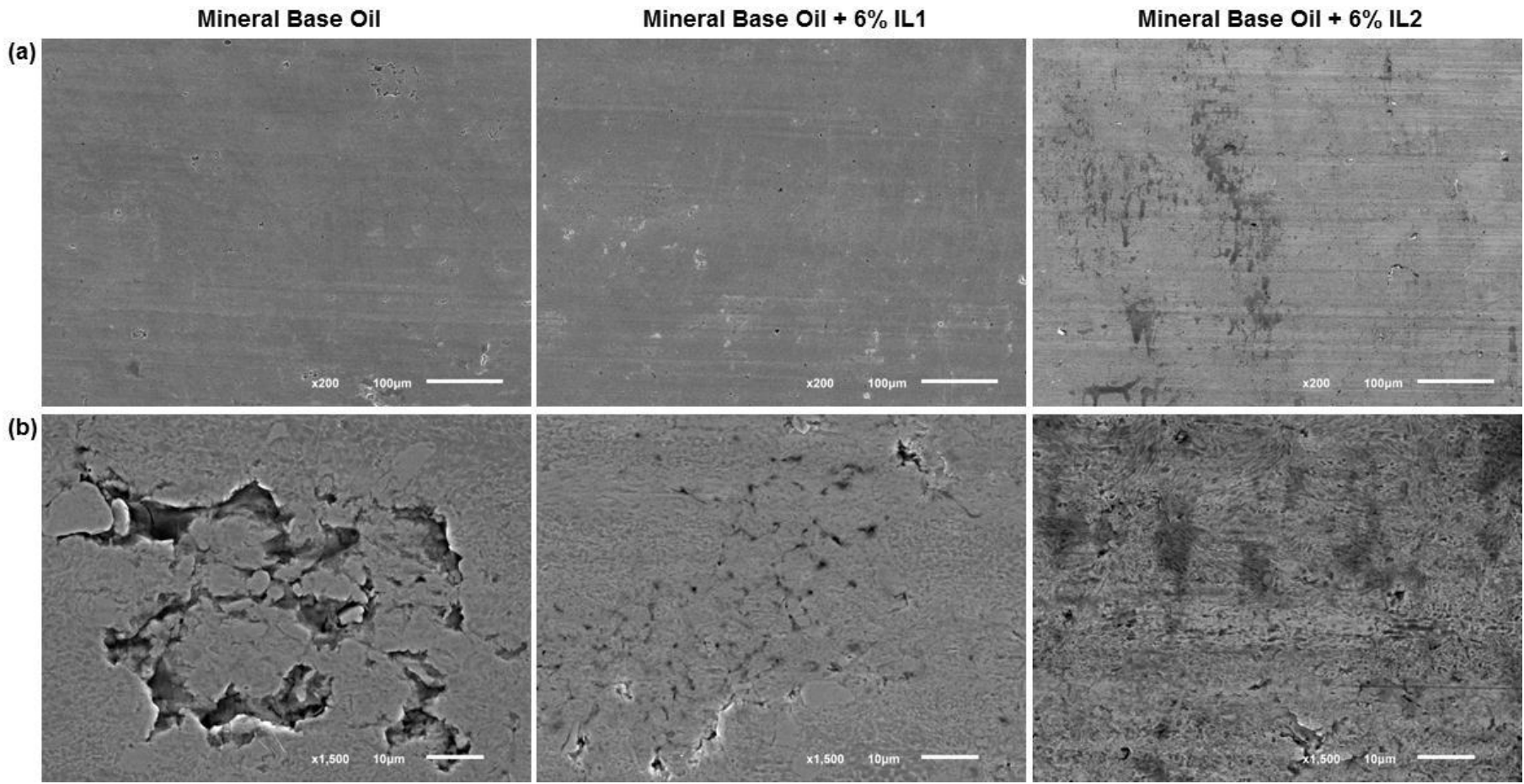


Figure 44: SEM images of worn flat specimen in Mineral Base Oil w/o 6% ILs after 3h sliding at 100°C; (a) Magnification of images is 200x; (b) Magnification of images is 1500x

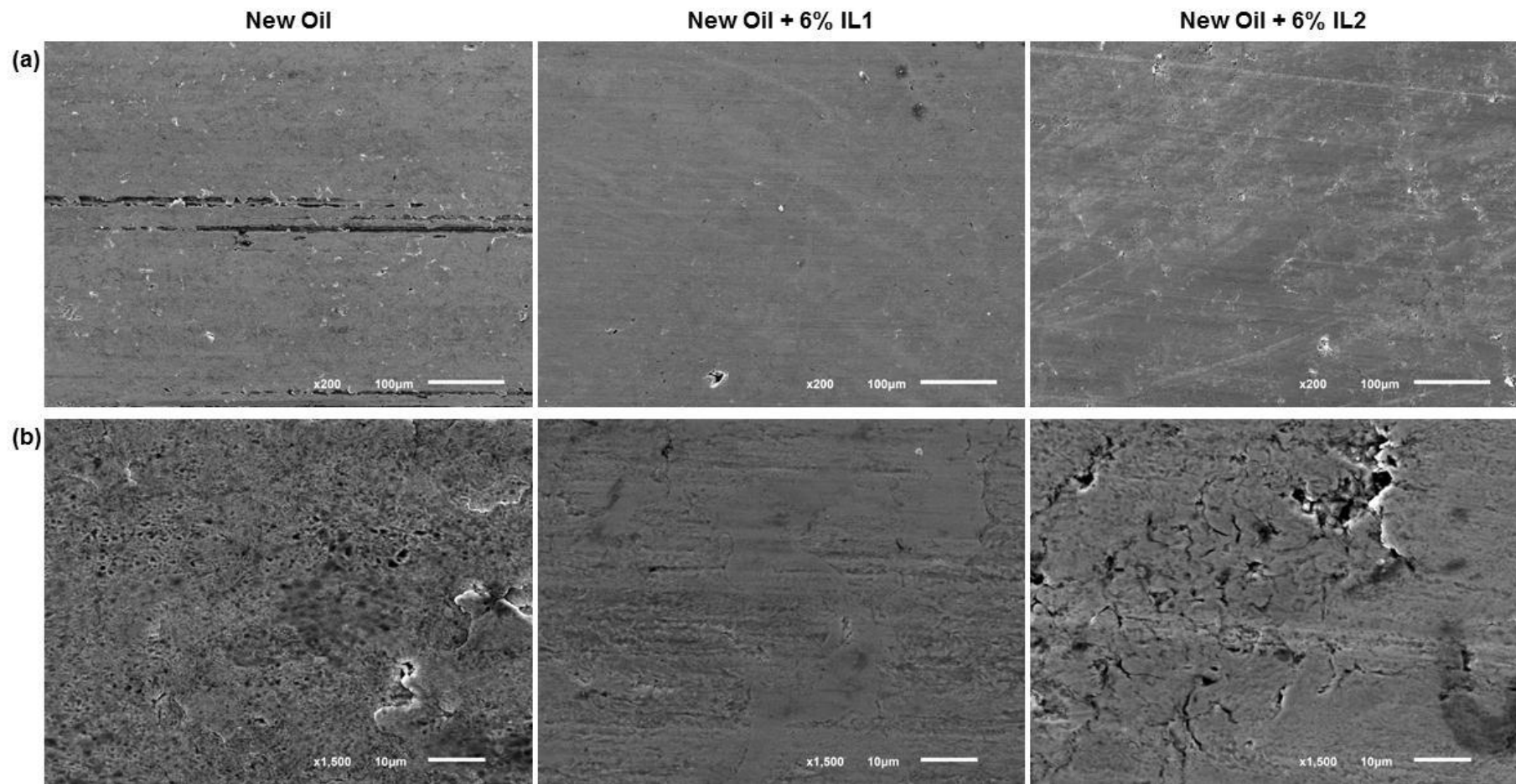


Figure 45: SEM images of worn flat specimen in New 15W40 Oil w/o 6% ILs after 3h sliding at 100°C; (a) Magnification of images is 200x; (b) Magnification of images is 1500x

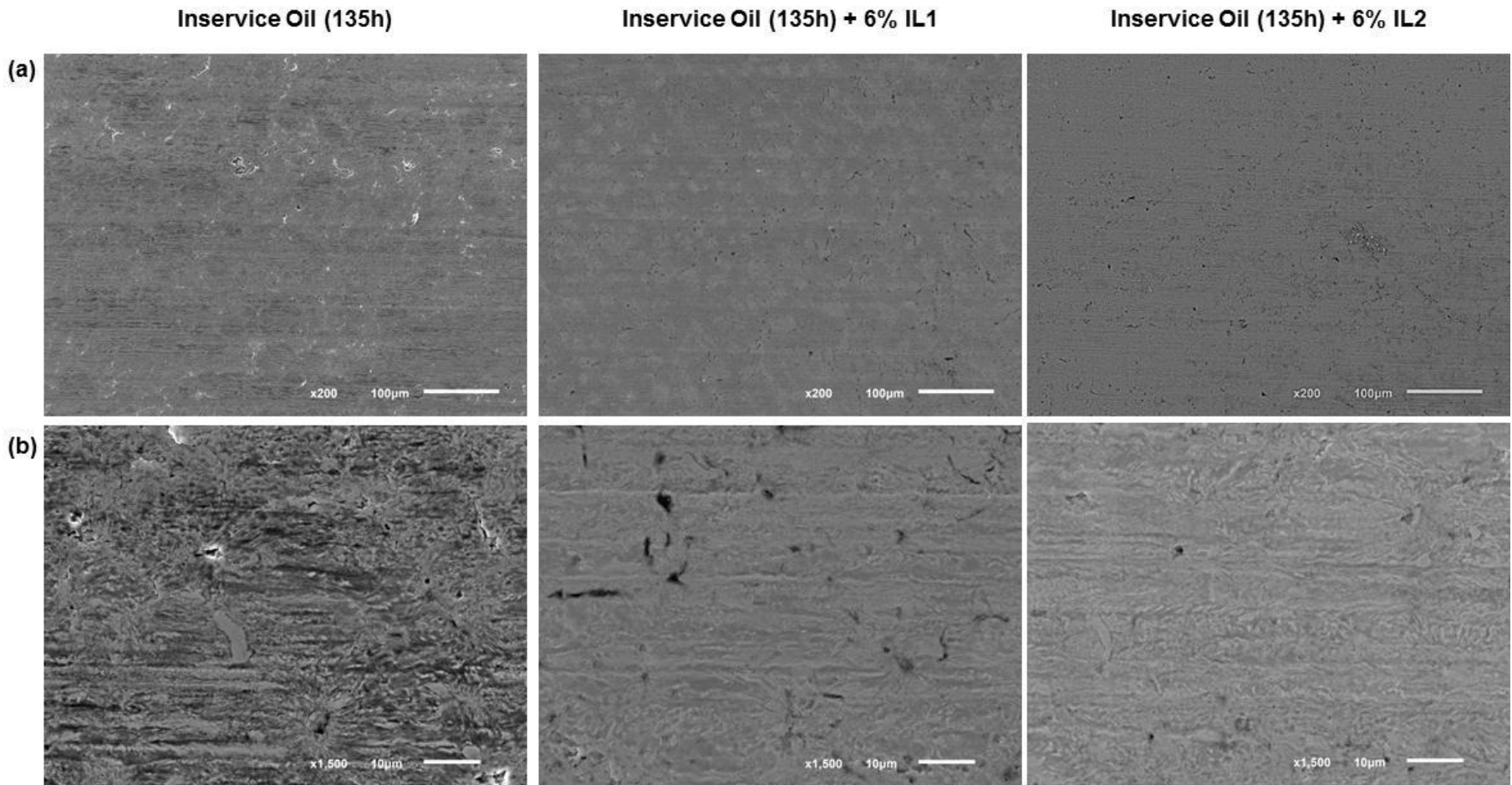


Figure 46: SEM images of worn flat specimen in Inservice 15W40 Oil (135h) w/o 6% ILs after 3h sliding at 100⁰C; (a) Magnification of images is 200x; (b) Magnification of images is 1500x

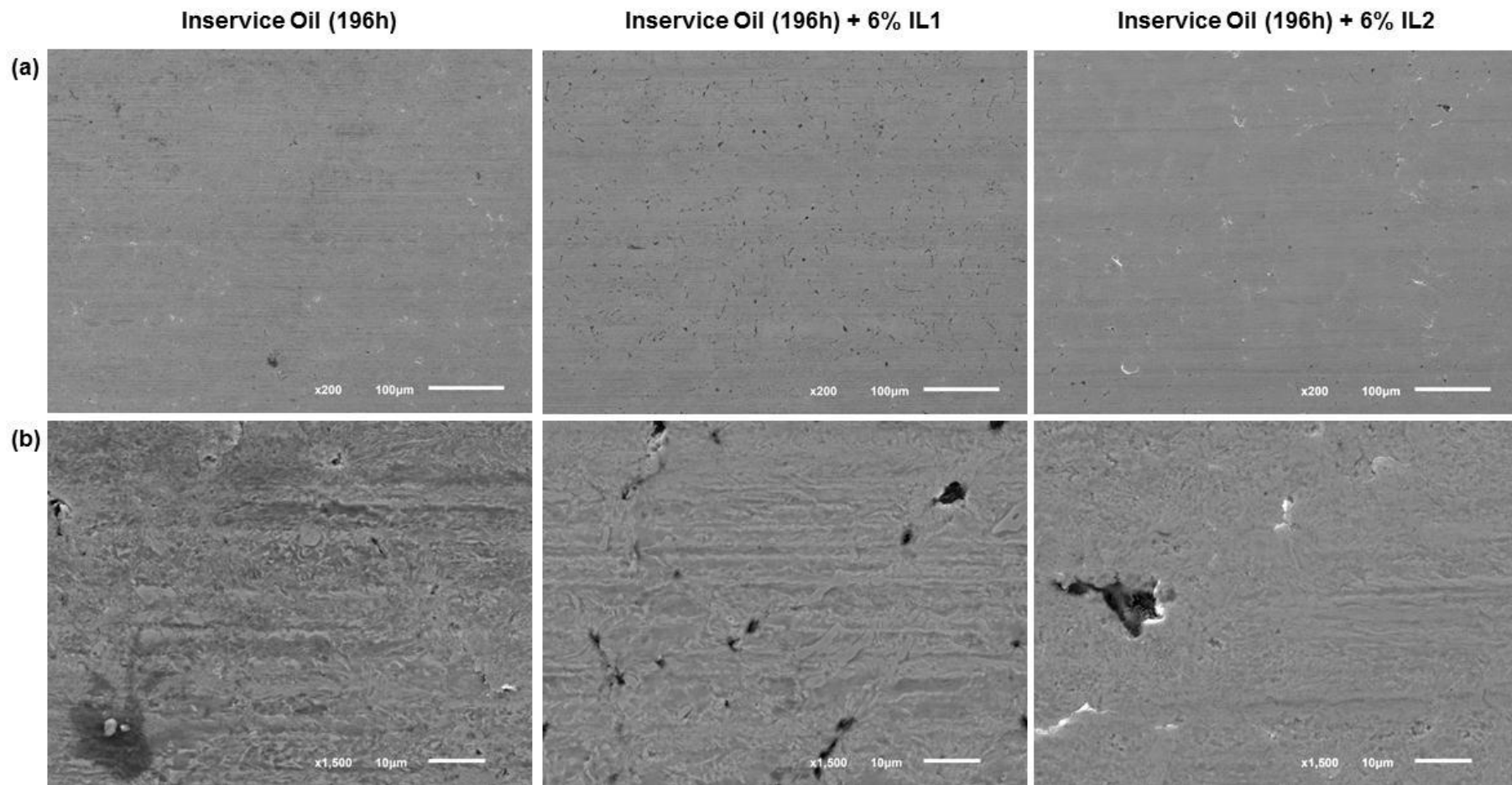


Figure 47: SEM images of worn flat specimen in Inservice 15W40 Oil (196h) w/o 6% ILs after 3h sliding at 100⁰C; (a) Magnification of images is 200x; (b) Magnification of images is 1500x

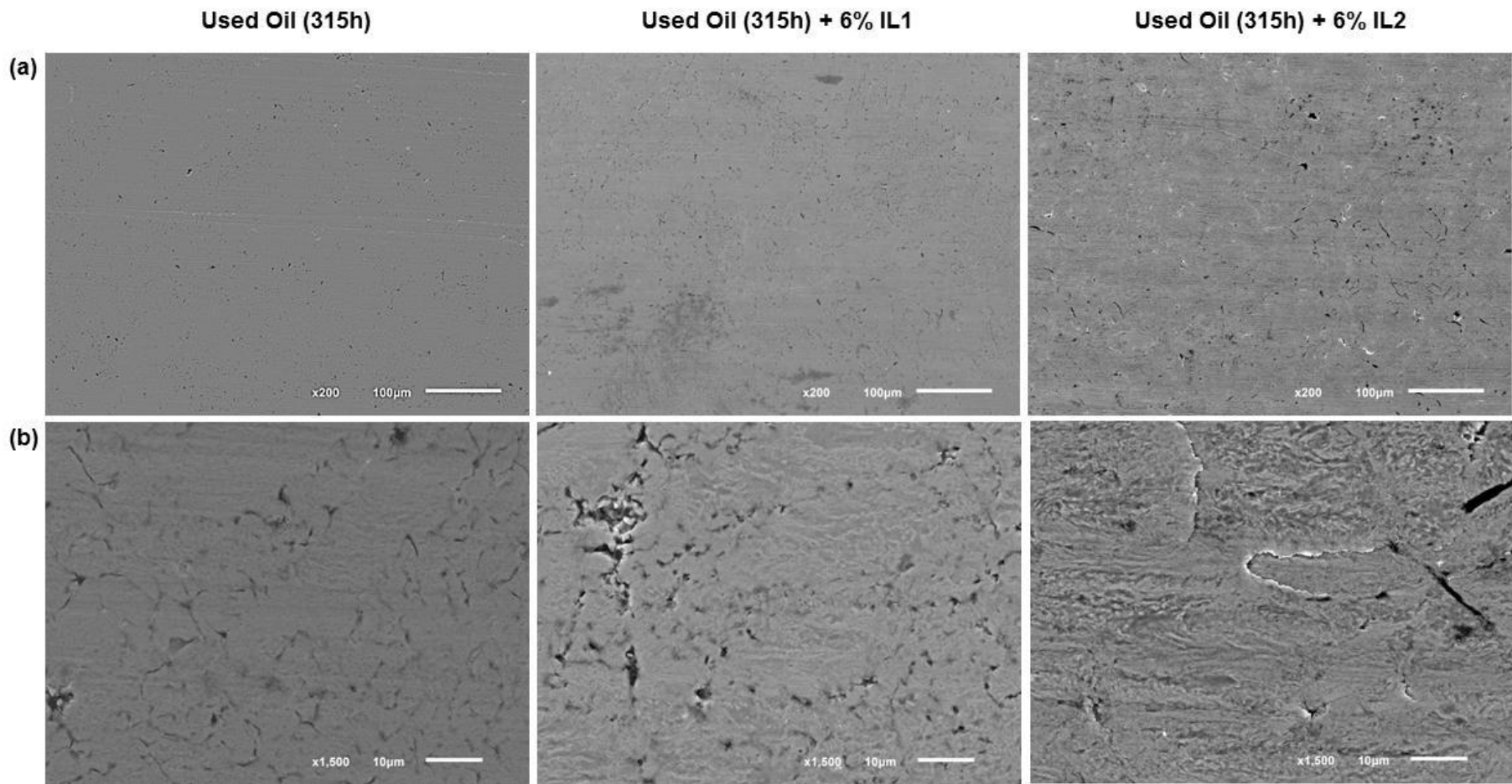


Figure 48: SEM images of worn flat specimen in Used 15W40 Oil (315h) w/o 6% ILs after 3h sliding at 100⁰C; (a) Magnification of images is 200x; (b) Magnification of images is 1500x

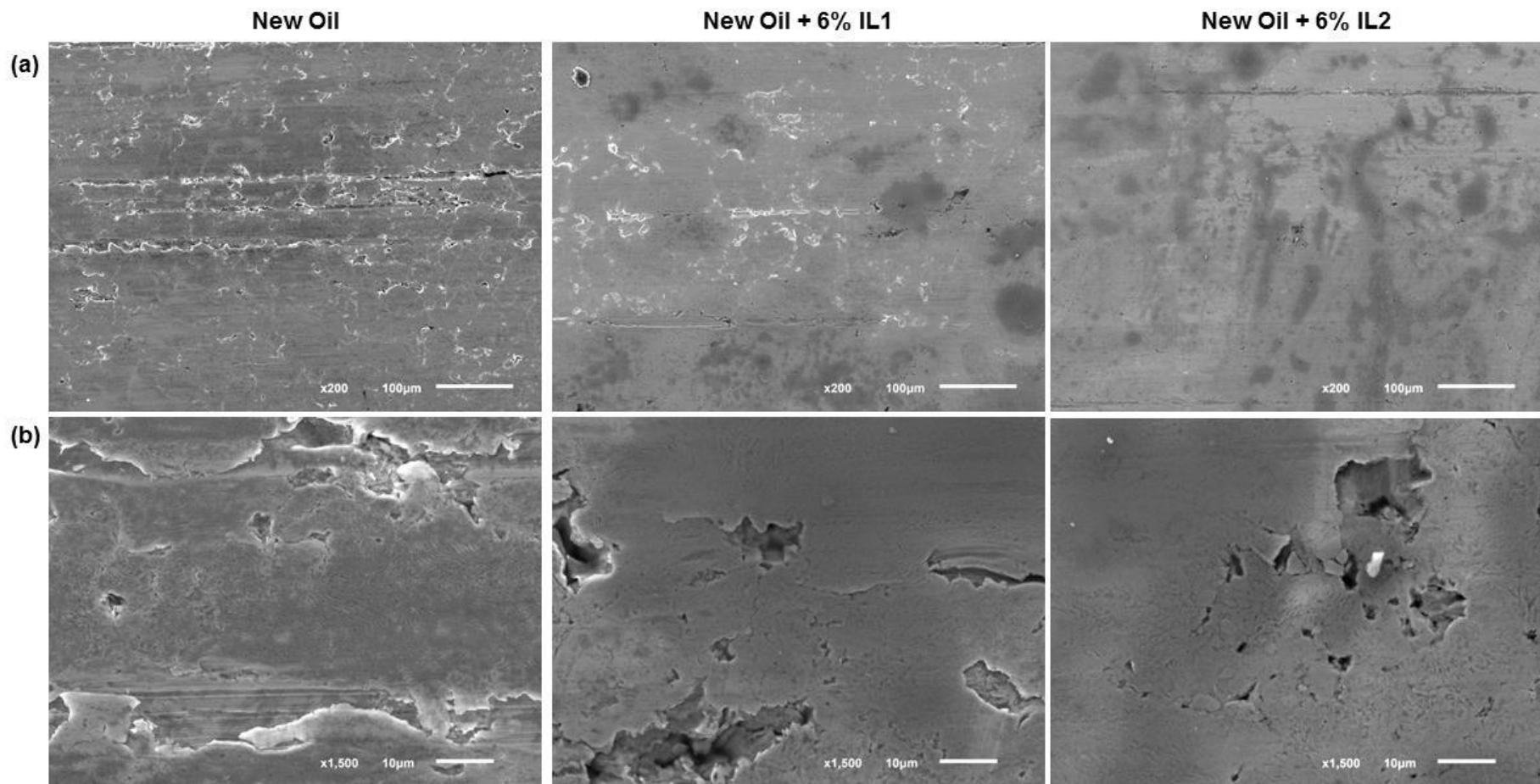


Figure 49: SEM images of worn flat specimen in New 15W40 Oil w/o 6% ILs after 3h sliding at 25⁰C; (a) Magnification of images is 200x; (b) Magnification of images is 1500x

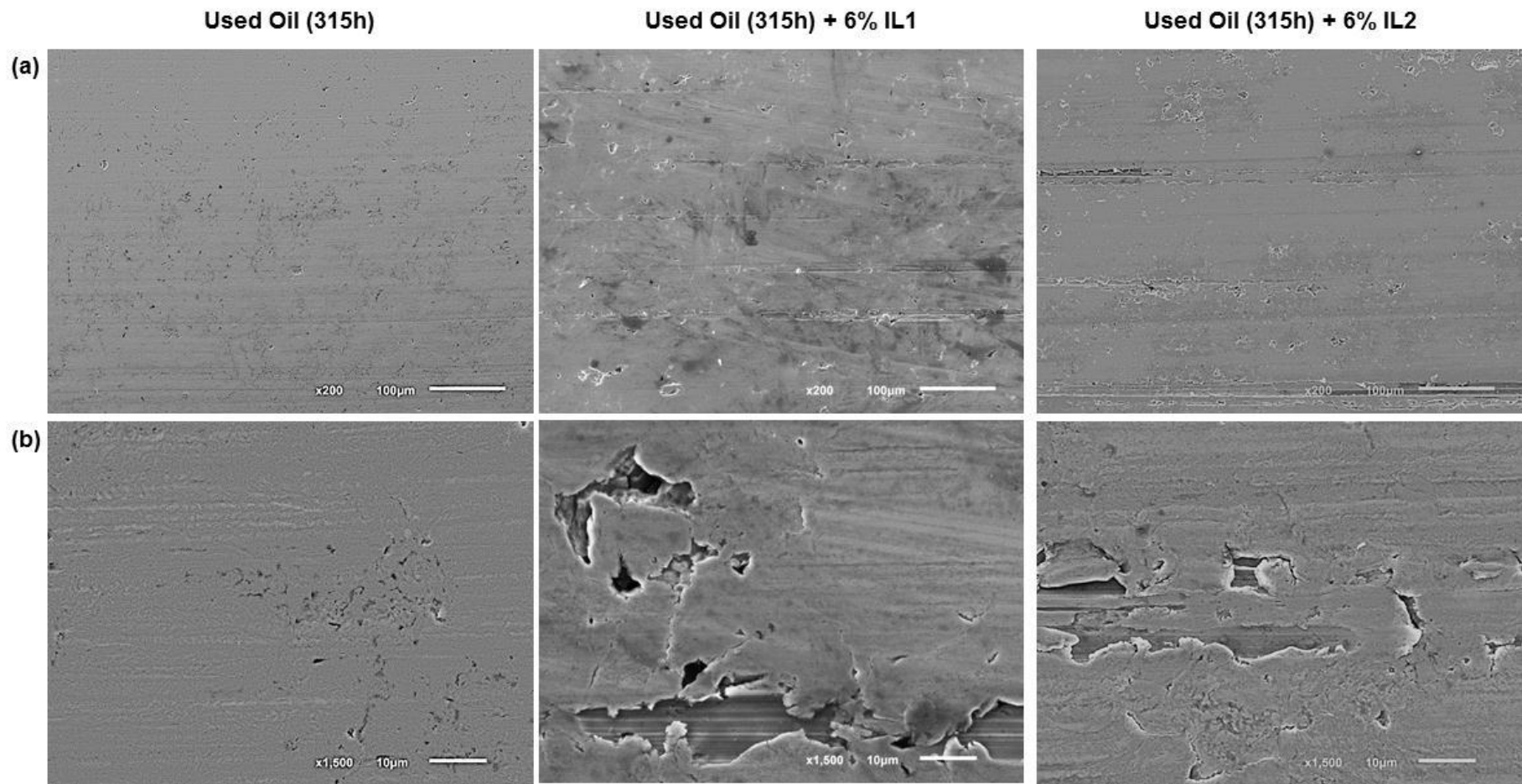


Figure 50: SEM images of worn flat specimen in Used 15W40 Oil (315h) w/o 6% ILs after 3h sliding at 25⁰C; (a) Magnification of images is 200x; (b) Magnification of images is 1500x

5.4. Surface Chemistry (EDX and XPS analysis)

The analysis of chemical composition of surface films formed by lubricant between two sliding surfaces can help understand the factors affecting the anti-wear performance of lubricant used [e]. Also the analysis can provide much needed information about the interaction of lubricant's antiwear additives with the rubbed (or sliding) surfaces. Therefore, surface analysis techniques such as XPS and EDX were employed to perform aforementioned chemical analysis of worn surfaces of cast iron flat samples employed in the current research. It is worth mentioning the difference between the detection capabilities of XPS and EDX techniques. XPS can provide information about the chemical composition of the first few nanometric layers (i.e. 1-5nm) whereas EDX can detect up to the depth of a few microns. Hence both techniques provide a wealth of information about the surface layer that is formed by the lubricants.

There is also some limitations to the use of EDX analysis as if the surface layer is considerably thinner than the penetration depth of scanning source (electron beam) then the analysis results only provide information about the substrate material and the surface layer constitutes get much diluted to be detected. Another difficulty with EDX when analysing thin layers is the results produced could be ambiguous due to multiple sources of the same elemental species, exemplifying carbon (C) which could be a constituent of lubricant or metal substrate. XPS does eliminate this problem owing to its lesser depth penetration capability up to 5nm and provide information about the chemical state of elemental species present in films in a compound form. XPS cannot provide information about the bulk of the surface films. Despite their limitations these surface analysis techniques act as a powerful tool when a collective interpretation of obtained results is performed. In past, researchers have studied antiwear films produced by different types of lubricants and additives using XPS[30, 36, 53, 54, 97, 98] and EDX [28-30, 99] techniques.

In current research, analysis was performed on the worn surfaces of cast iron flat samples lubricated with mineral base oil, new fully formulated 15W40 oil and in-service fully formulated 15W40 oils sampled after 135h and 196h from engine and also used oil sampled after 315h from the engine. Analysis was also performed on the worn surfaces of cast iron flat samples lubricated with the mixtures of above oils with

two different phosphonium ILs referred as IL1 and IL2 in 6% volume proportions. The comparison was made to the chemical composition of the surface films formed by neat lubricants and their corresponding Oil-IL blends.

5.4.1. Mineral base oil with/without IL1 and IL2 (at 100°C)

The low resolution survey spectra were performed in order to detect all the elements present on the surface with binding energies ranging between 1 and 1200 eV. Energy step of 1eV each with a dwell time of 0.3sec was considered to identify the key elements present in the scanned area. The high intensity peak elements were later analysed at higher resolution for detailed study of their binding energy values and corresponding chemical compounds.

The low resolution survey scans were taken at the centre of worn surface of cast iron flat samples as shown in Figure 44 (a, b, c) respectively. It can be seen that Fe, Mn, O, C and Si elements were detected in each case but P was only noted on worn surfaces lubricated with oil and IL blends. In addition, EDX analysis results shown in Table 11 also confirm the presence of element P only in case of oil and IL blends.

It can be deduced from the results that phosphonium based ILs (IL1 and IL2) have reacted with the metal surface during the tribo-testing process and produced a phosphorus containing boundary antiwear film on the rubbed surface. Interestingly, Cr was noted only in the case of neat mineral base oil as depicted by XPS analysis. In contrast the addition of ILs reduced the chromium level below the detectable limits. This suggested that material transfer (adhesive wear) from the surface of chromium coated piston ring has taken place during the sliding process when neat mineral base oil was used. But EDX results provided no evidence of Cr on the worn surfaces in all the three cases suggesting it was below the detectable limits of this technique.

Table 12 shows the binding energy shifts for Fe, O and P elements, each of which have been discussed above. These elements are the main constituents of the cast iron flat sample and lubricant or IL employed. Therefore change in their binding energy values reflect the change in their chemical state and indicate the thermo-chemical reactions taking place during the sliding process inside of worn surface. The higher resolution scan of main elements such as Fe, O and P has been taken using XPS to evaluate the change in chemical state of these elements by measuring their

binding energies. The measurement was also taken outside the worn surface (wear scar) in neat mineral base oil case for comparison purpose.

Table 11: Elemental concentration inside worn surface obtained by EDX analysis

Cast iron flat surface lubricated with	Element concentration (in weight %)					
	C	O	Si	Mn	Fe	P
Mineral Base Oil	7.32	11.77	2.01	0.64	78.27	<i>nd</i>
Mineral Base Oil + 6% IL1	6.96	15.14	1.67	<i>nd</i>	75.66	0.57
Mineral Base Oil + 6% IL2	6.44	10.46	2.26	0.61	77.98	1.18

nd – not detectable

Table 12: XPS results – binding energy shifts – worn surface on cast iron flat samples

Element	Binding Energy (eV)		Assignable Chemical Compounds					
	Mineral Base Oil		Mineral Base Oil + 6% IL1			Mineral Base Oil + 6% IL2		
	Outside wear scar	Inside wear scar	Inside wear scar		Inside wear scar			
Fe	711.0	Fe ₂ O ₃	710.9	Fe ₂ O ₃	710.9	Fe ₂ O ₃	710.9	Fe ₂ O ₃
			713.1	Fe metallic				
O	530.4	Fe ₂ O ₃	530.3	Fe ₂ O ₃	530.2	Fe ₂ O ₃	530.5	Fe ₂ O ₃
	532.4	<i>na</i>	532.3	<i>na</i>	531.7	FePO ₄	531.9	FePO ₄
P	<i>nd</i>		<i>nd</i>		133.2	FePO ₄	133.5	FePO ₄

na – not assignable; nd – not detectable

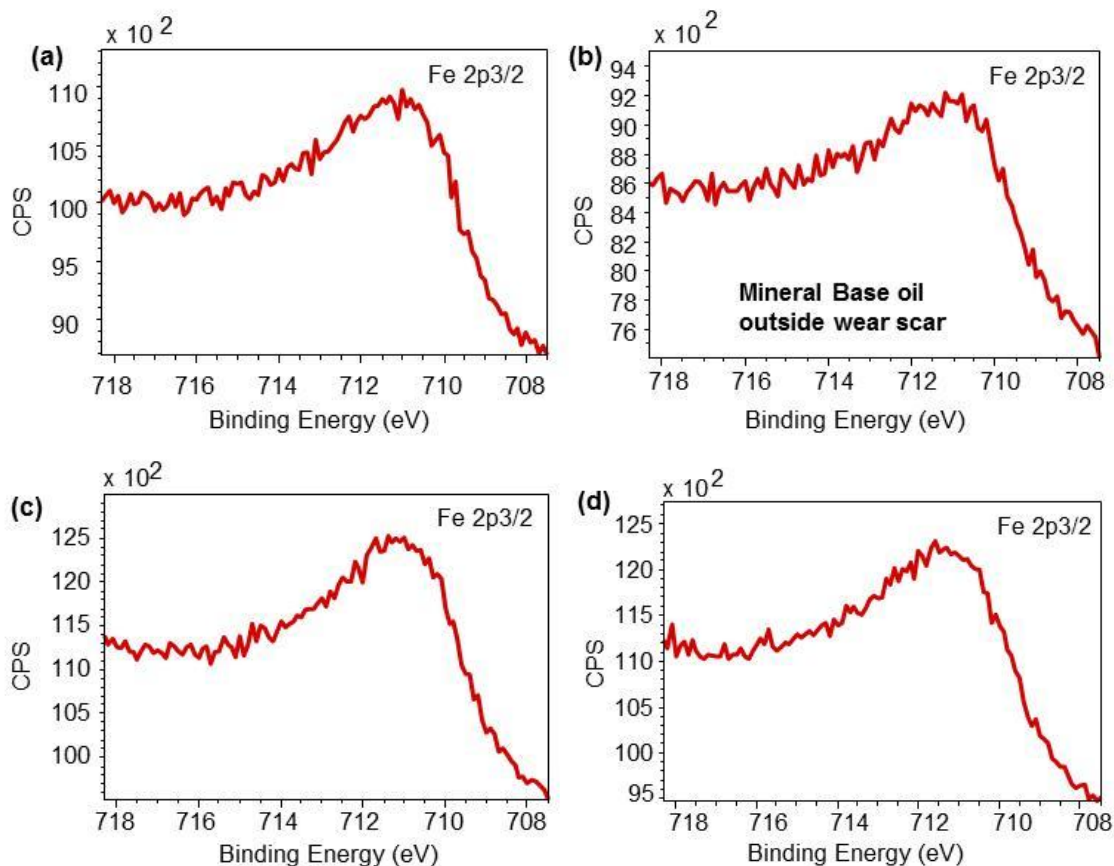


Figure 51: High resolution Fe 2p_{3/2} XPS spectra of the worn surface on cast iron flat samples lubricated with (a) Mineral Base Oil (b) Outside wear scar – Mineral Base Oil (c) Mineral Base Oil + 6% IL1 (d) Mineral Base Oil + 6% IL2

Figure 51 (a) and (b) show the high resolution spectra of Fe_{2p_{3/2}} taken inside and outside the worn surface, respectively, on the cast iron flat samples lubricated with neat mineral base oil. Two peaks were detected inside the worn surface located at 710.9 eV ($fwhm^1 = 2.68$ eV) and 713.1 eV ($fwhm = 2.68$ eV). The first peak could be assigned to Fe oxides (Fe₂O₃) and second peak to the Fe metallic surface structure which possess different binding energies compared to the bulk of the substrate material. Only one peak at 711 eV ($fwhm = 2.62$ eV) was noted outside the worn surface and was assigned to Fe-oxides. Samples lubricated by the mineral base oil + 6% IL1 and mineral base oil + 6% IL2, demonstrated only one peak at 710.9 eV ($fwhm = 2.68$ eV) assigned to Fe₂O₃, as shown in Figure 51 (c) and (d), respectively.

¹*fwhm* – full width half maximum

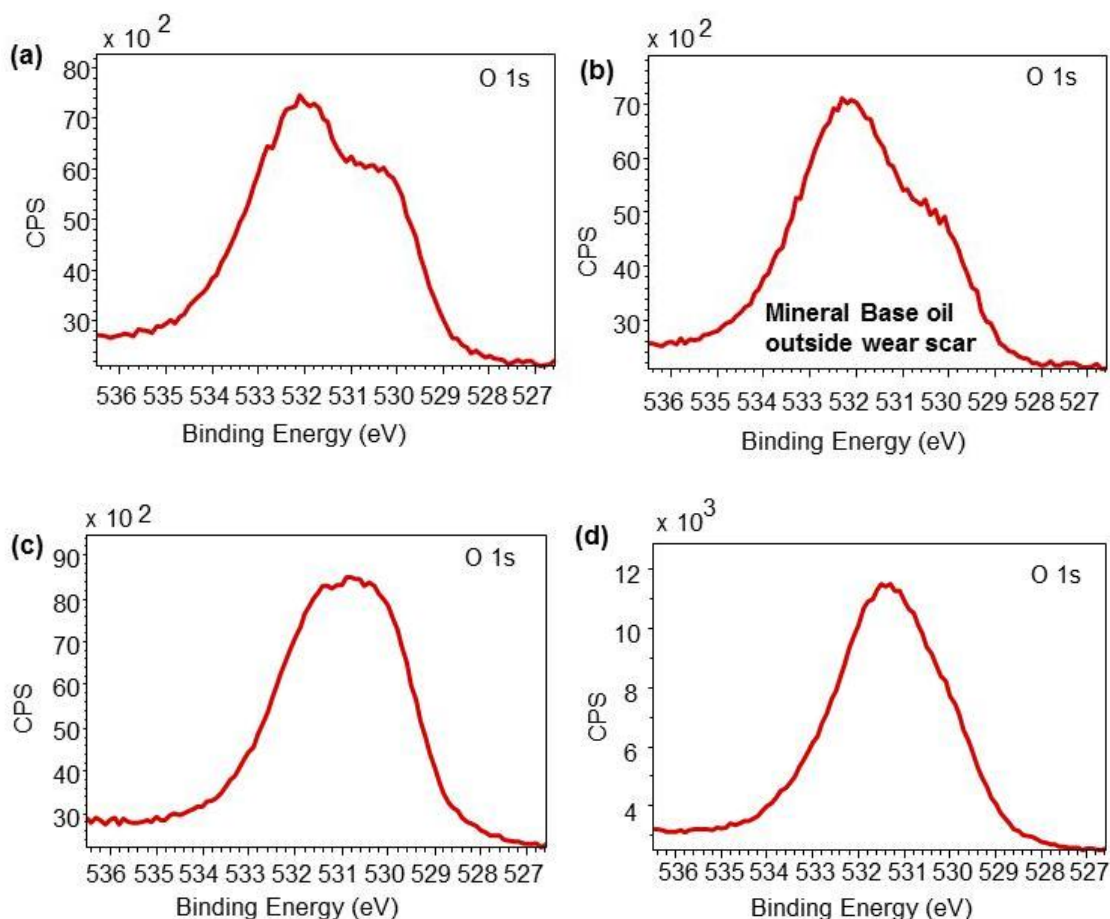


Figure 52: High resolution O1s XPS spectra of the worn surface on cast iron flat samples lubricated with (a) Mineral Base Oil (b) Outside wear scar – Mineral Base Oil (c) Mineral Base Oil + 6% IL1 (d) Mineral Base Oil + 6% IL2

Figure 52 (a) and (b) show the high resolution spectra of O1s taken inside and outside the worn surface, respectively, on the cast iron flat samples lubricated with neat mineral base oil. Inside the worn surface two peaks were detected at 530.3 eV (fwhm = 1.96 eV) and 532.3 eV (fwhm = 1.96 eV). The first peak could be assigned to Fe_2O_3 whereas the second peak was difficult to assign to any specific compound of oxygen but more likely it is associated with the mineral base oil. A very similar phenomenon was noted outside the worn surface with two peaks at 530.4 eV (fwhm = 1.98 eV) and 532.4 eV (fwhm = 1.98 eV) belonging to the same sources. When phosphonium ILs were added to the mineral base oil, a shift in the binding energy of O1s was noted. In case of sample lubricated with mineral base oil + 6% IL1 a new peak at 531.7 eV (fwhm = 2.1 eV) indicative of iron phosphate (FePO_4) was noted along with another peak at 530.2 eV (fwhm = 1.9 eV) corresponding to Fe_2O_3 , as shown in Figure 52 (c). Similarly in case of sample lubricated with mineral base oil +

6% IL2 a new peak at 531.9 eV (fwhm = 2.0 eV) indicative of iron phosphate (FePO_4) was noted along with another peak at 530.5 eV (fwhm = 2.0 eV) corresponding to Fe_2O_3 , as shown in Figure 52 (d). Therefore it is clearly found that the concentration of O element is higher inside the worn surface than outside, in all the cases. Hence it can be deduced that the tribo-chemical reactions between the different constituents of lubricant and metal surfaces have taken place during sliding process.

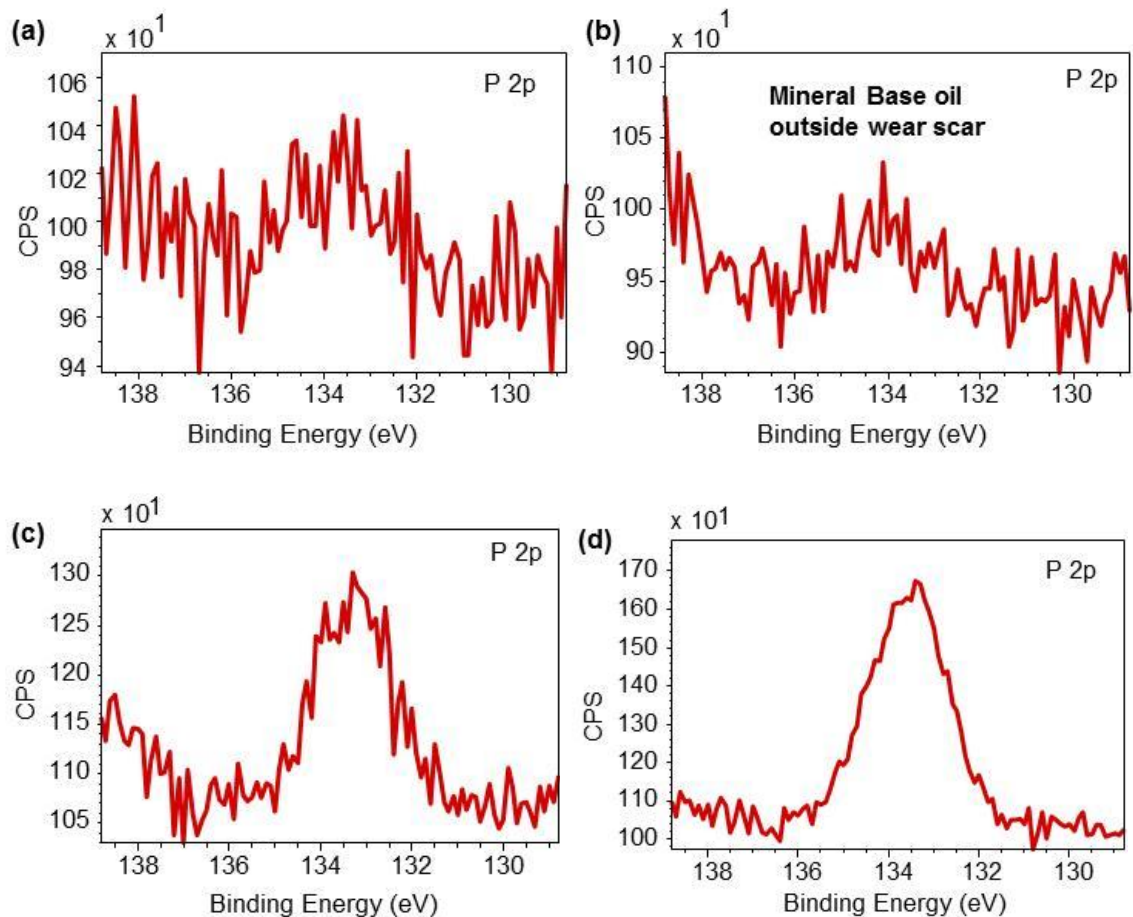


Figure 53: High resolution P2p XPS spectra of the worn surface on cast iron flat samples lubricated with (a) Mineral Base Oil (b) Outside wear scar – Mineral Base Oil (c) Mineral Base Oil + 6% IL1 (d) Mineral Base Oil + 6% IL2

Figure 53 (a) and (b) show the high resolution spectra of P2p taken inside and outside the worn surface, respectively, on the cast iron flat samples lubricated with neat mineral base oil. Clearly low intensity peaks were noted in both the cases which infers that concentration of phosphorus is too low to be appreciated which is obvious since the only source of phosphorus in these cases is cast iron substrate material which contains as low as 0.4 to 1.1 % of elemental P. But since XPS detects upto the depth of first few nanometers therefore surface outside the worn area could be covered with the adsorbed layer of mineral base oil which does not contain P. Samples lubricated by the mineral base oil + 6% IL1 and mineral base oil + 6% IL2, demonstrated considerable concentration of P with a peak at 133.2 eV (fwhm = 2.0 eV) and a peak at 133.5 eV (fwhm = 2.0 eV), both of which could be assigned to iron phosphate (FePO_4), as shown in Figure 53(c) and (d), respectively. It is worth mentioning here that the low amount of P in these two cases resulted in a low ratio of $\text{Fe}_2\text{O}_3/\text{FePO}_4$.

thus hardening the detection of iron phosphate in the Fe2p3/2 spectra which are discussed earlier in this section.

5.4.2. New Oil with/without IL1 and IL2 (at 100°C)

The low resolution survey scans were taken at the centre of worn surface of cast iron flat samples as shown earlier in Figure 45(a, b, c) respectively. It can be seen that Fe, Mn, O, Ca, C, P and Si elements were detected in each case. In addition, EDX analysis results in Table 13 also show same elements in addition to S and Zn which are otherwise not evident from XPS analysis. This could be due to depth penetration limit of XPS analysis up to 1-5 nm whereas EDX can detect elemental concentration up to the depth of a few microns.

P, Zn and S are the main constituent elements of ZDDP additives which are added to the engine lubricants for antiwear protection [30, 97]. Ca is main constituent of calcium sulphonate which is a typical detergent additive in engine lubricants [30]. The function of detergent additive is to neutralize the in-organic acidic combustion by-products and the organic acidic products formed by oil degradation processes. In addition it prevents the formation and build-up of varnishes on engine component surfaces. Fe, C and Si are the major constituents of cast iron flat sample, as mentioned earlier in the section 3.3.2. The key elemental constituents of ILs (IL1 and IL2) are C, O and P. Also, C and O can come from hydrocarbon chain of mineral base oil and surface contaminants, and also O could be contributed by air resolved in lubricant [100].

From the results it can be seen that the concentration of Ca, P, Zn and S has reduced inside worn surface by addition of ILs to the New fully formulated 15W40 oil. The effect is more severe in the case of New 15W40 Oil + 6% IL2. On the contrary, the concentration of O has increased by addition of ILs to the New fully formulated 15W40 oil. Therefore it can be deduced from these observations that addition of ILs to fully formulated oil resulted in reduced reactivity of ZDDP (antiwear) and Calcium Sulphonate (detergent) additives with the Fe containing cast iron surface. Increased reactivity of O element was studied in detail using XPS analysis and explained later in this section. Interestingly, no Cr, if any exists, was noted, therefore suggesting no

material transfer (adhesive wear) from the surface of chromium coated piston ring had taken place during the sliding process in all the three cases.

Table 13: Elemental concentration inside worn surface obtained by EDX analysis

Cast iron flat surface lubricated with	Element concentration (in weight %)								
	C	O	Si	S	Ca	Zn	Mn	Fe	P
New 15W40 Oil	6.69	5.24	1.99	1.25	0.66	1.63	0.77	80.85	0.92
New 15W40 Oil + 6% IL1	6.17	8.92	1.77	0.07	0.52	0.47	<i>nd</i>	81.29	0.78
New 15W40 Oil + 6% IL2	7.38	7.31	2.10	0.23	<i>nd</i>	<i>nd</i>	0.54	82.02	0.42

nd – not detectable

Table 14: XPS results – binding energy shifts – inside worn surface on cast iron flat samples

Element	Binding Energy (eV)		Assignable Chemical Compounds			
	New Oil		New Oil + 6% IL1		New Oil + 6% IL2	
Fe	710.2	Fe ₃ O ₄	710.7	Fe ₂ O ₃	710.8	Fe ₂ O ₃
	712.2	FePO ₄				
O	530.2	Fe ₂ O ₃	528.5	Fe ₃ O ₄	528.5	Fe ₃ O ₄
	531.8	FePO ₄	530.0	Fe ₂ O ₃	529.9	Fe ₂ O ₃
			531.8	FePO ₄	531.7	FePO ₄
Ca	347.5	Ca ₃ (PO ₄) ₂	347.9	Ca ₃ (PO ₄) ₂	347.9	Ca ₃ (PO ₄) ₂
			344.7	Ca-metal	344.7	Ca-metal
P	133.4	FePO ₄	129.9	Fe ₂ P	130.8	<i>na</i>
					133.8	FePO ₄

na – not assignable

Table 14 shows the binding energy shifts for Fe, O, Ca and P elements, each of which have been discussed above. These elements are the main constituents of the cast iron flat sample and lubricant or IL employed. Therefore change in their binding energy values reflect the change in their chemical state and indicate the thermo-chemical reactions taking place during the sliding process inside of worn surface. The higher resolution scan of main elements such as Fe, O, Ca and P has been taken using XPS to evaluate the change in chemical state of these elements by measuring their binding energies.

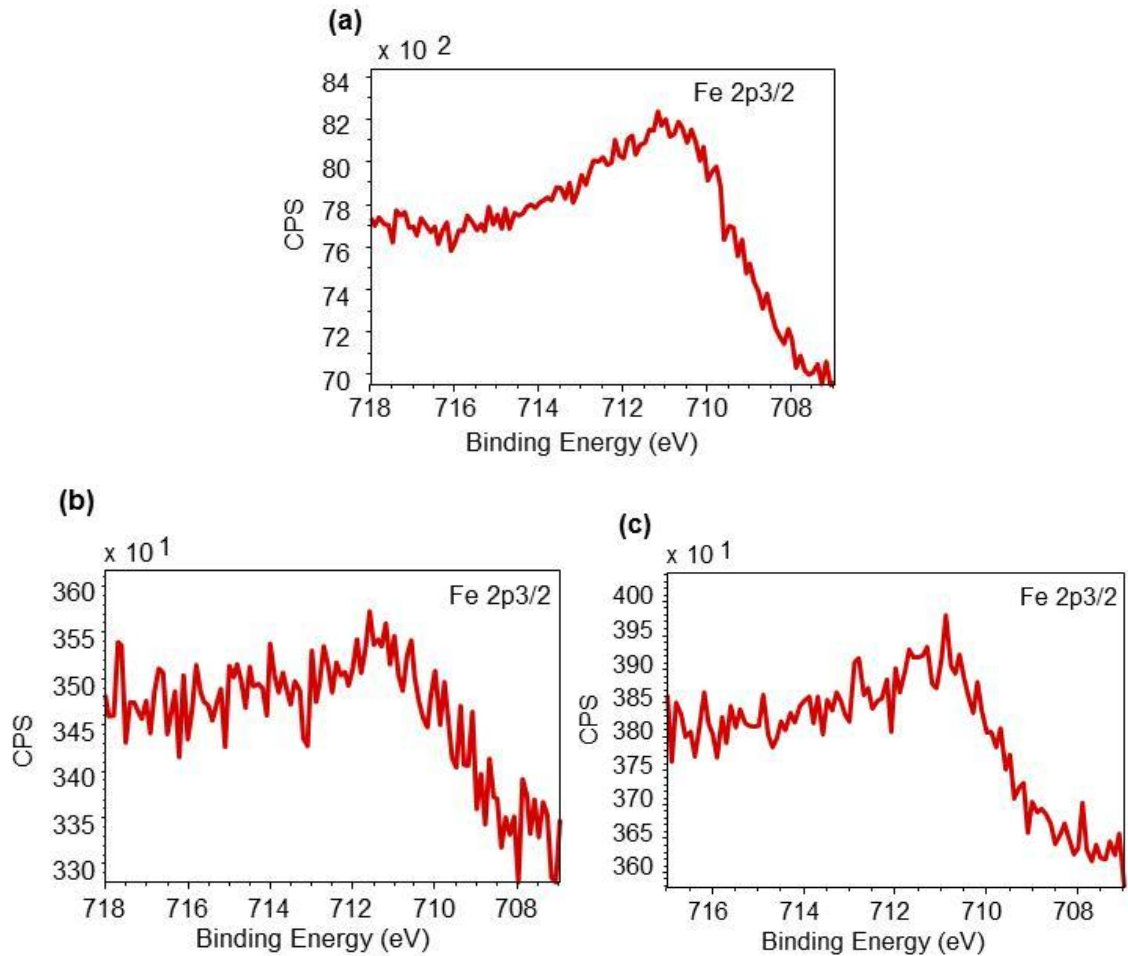


Figure 54: High resolution Fe 2p_{3/2} XPS spectra of the worn surface on cast iron flat samples lubricated with (a) New Oil (b) New Oil + 6% IL1 (c) New Oil + 6% IL2

Figure 54 (a, b, c) show the high resolution spectra of Fe_{2p_{3/2}} taken inside the worn surface on the cast iron flat samples lubricated with New fully formulated 15W40 oil with and without ILs. Figure 54 depicts (a) two peaks located at 710.2 eV (fwhm = 2.6 eV) and 712.2 eV (fwhm = 2.6 eV) detected inside the worn surface on the cast iron flat sample lubricated with New fully formulated 15W40 oil. The first peak could be assigned to Fe oxides (Fe₃O₄) [101] and second peak to the Iron Phosphate (FePO₄) [102]. In Figure 54 (b), a single peak at 710.7 eV (fwhm = 2.6 eV) was noted for the worn surfaces lubricated with blends containing 6 volume% of IL1. A similar peak at 710.8 eV (fwhm = 2.6 eV) was noted for New Oil + 6% IL2. Both peaks were assigned to Fe oxides (Fe₂O₃) [103-105].

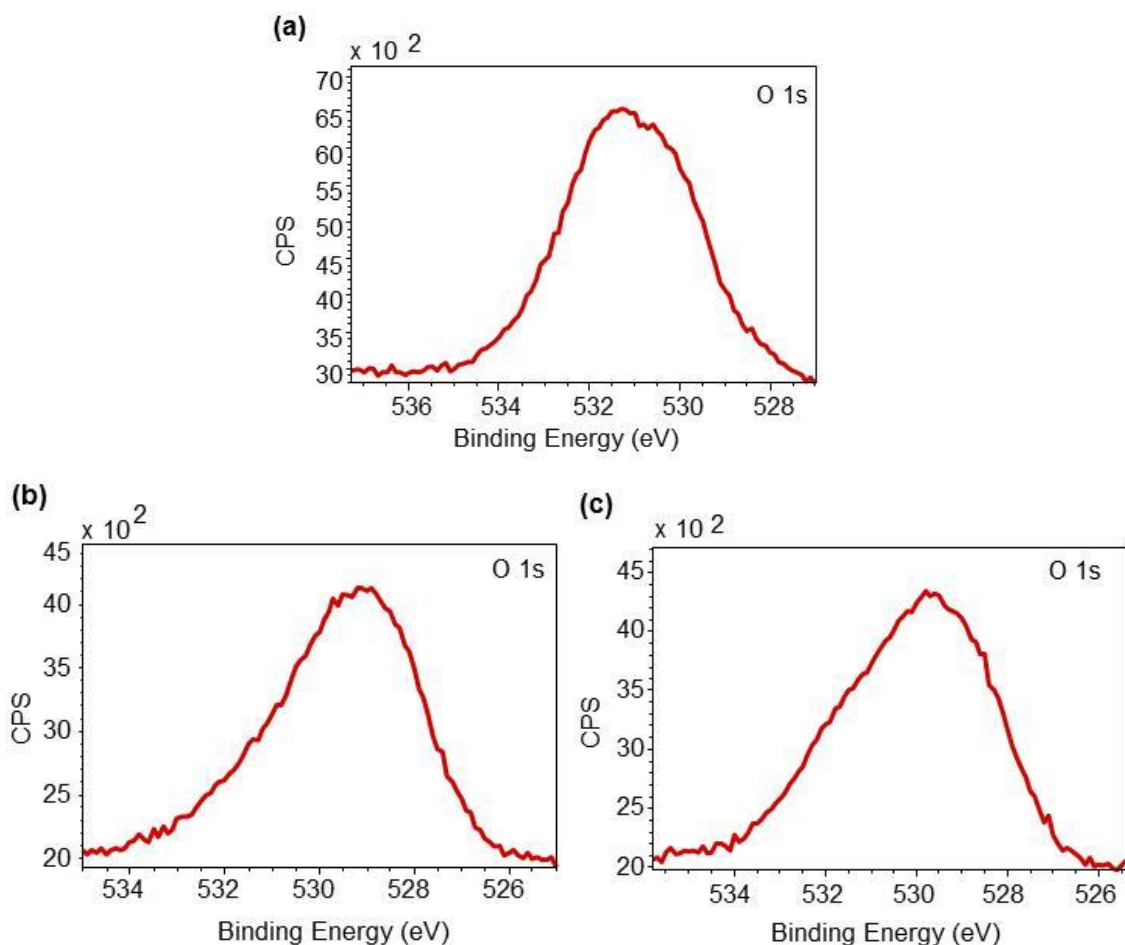


Figure 55: High resolution O1s XPS spectra of the worn surface on cast iron flat samples lubricated with (a) New Oil (b) New Oil + 6% IL1 (c) New Oil + 6% IL2

Figure 55 (a, b, c) show the high resolution spectra of O1s taken inside the worn surface on the cast iron flat samples lubricated with New fully formulated 15W40 oil with and without ILs. In the sample lubricated with New fully formulated 15W40 oil without IL, two peaks located at 530.2 eV (fwhm = 2.2 eV) and 531.8 eV (fwhm = 2.2 eV) were measured in the O1s high resolution spectrum. These peaks were assigned to Fe_2O_3 and FePO_4 , respectively [106, 107]. In the case of New Oil + 6% IL1 (see Figure 55 b), the peak from Fe_2O_3 (B.E.= 530.0 eV; fwhm = 2.2 eV) and FePO_4 (B.E. = 531.8 eV; fwhm = 2.2 eV) remained and a third peak was detected at 528.5 eV (fwhm = 2.0 eV) which was assigned to Fe_3O_4 , according to NIST database [106]. Similar observations were made on cast iron sample lubricated with New Oil + 6% IL2 (Figure 55c), such that peaks were detected at 528.5 eV, 529.9 eV and 531.7 eV.

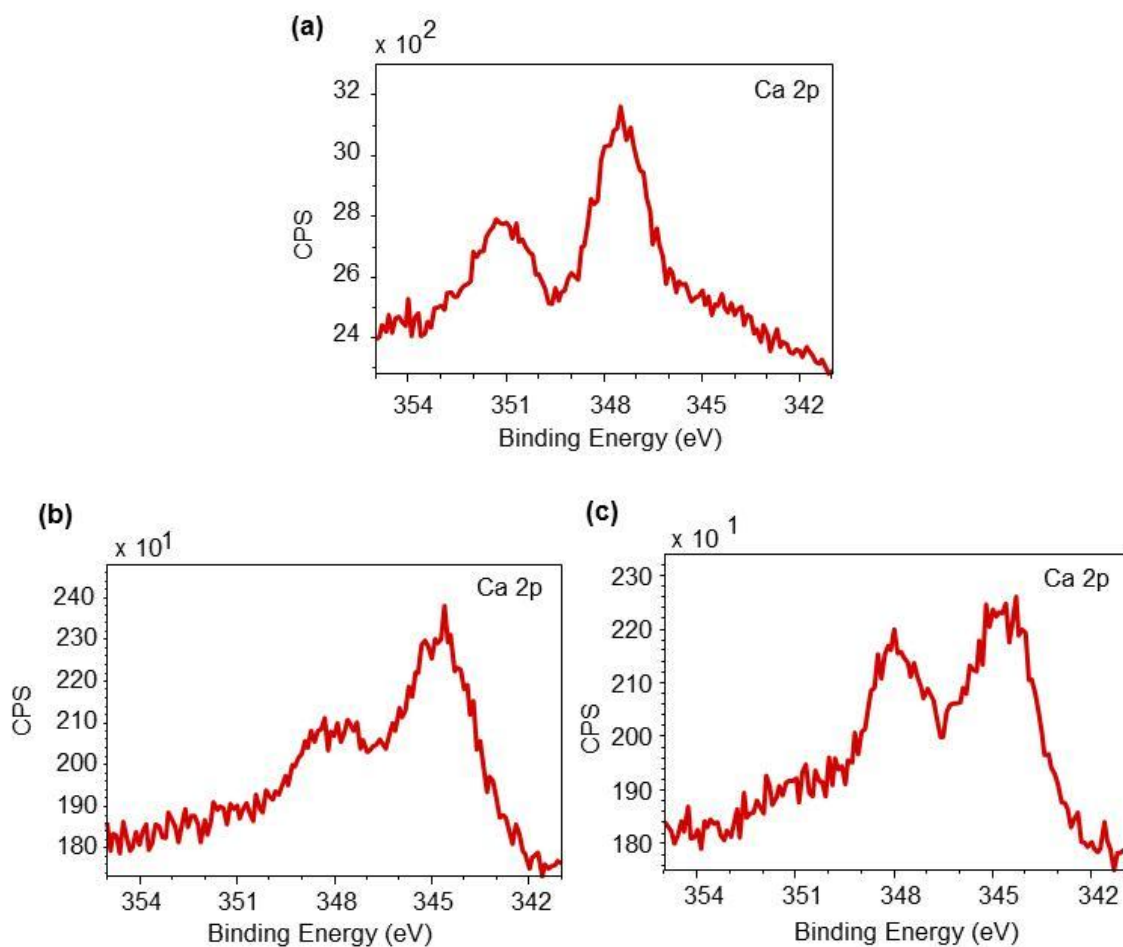


Figure 56: High resolution Ca 2p XPS spectra of the worn surface on cast iron flat samples lubricated with (a) New Oil (b) New Oil + 6% IL1 (c) New Oil + 6% IL2

Figure 56 (a, b, c) show the high resolution spectra of Ca2p taken inside the worn surface on the cast iron flat samples lubricated with New fully formulated 15W40 oil with and without ILs. In the sample lubricated with New fully formulated 15W40 oil without IL, as shown in Figure 56 (a), one doublet consisting of Ca 2p_{3/2} and Ca 2p_{1/2} was noted. For the analysis purpose, only 2p_{3/2} peak was considered which defines the chemical state of Ca element. This could be because of high intensity of his peak compared to 2p_{1/2} peak, and secondly the both peaks could be widely spread (with significant difference in their B.E. values) such that one peak can be considered for comparison with that of other samples. Therefore, the Ca 2p_{3/2} peak in (a) was detected at 347.5 eV (fwhm = 1.7 eV), which was assigned to Ca₃(PO₄)₂. Addition of both ILs to the new oil resulted in a new doublet of Ca2p in addition to the previously noted without ILs. Such that as shown in Figure 56 (b) and (c), the 2p_{3/2} peaks were noted at 344.7 eV (fwhm = 2.4 eV) and 347.9 eV (fwhm = 2.3 eV). These new peaks were assigned to Ca-metal [108, 109] and Ca₃(PO₄)₂ [106], respectively.

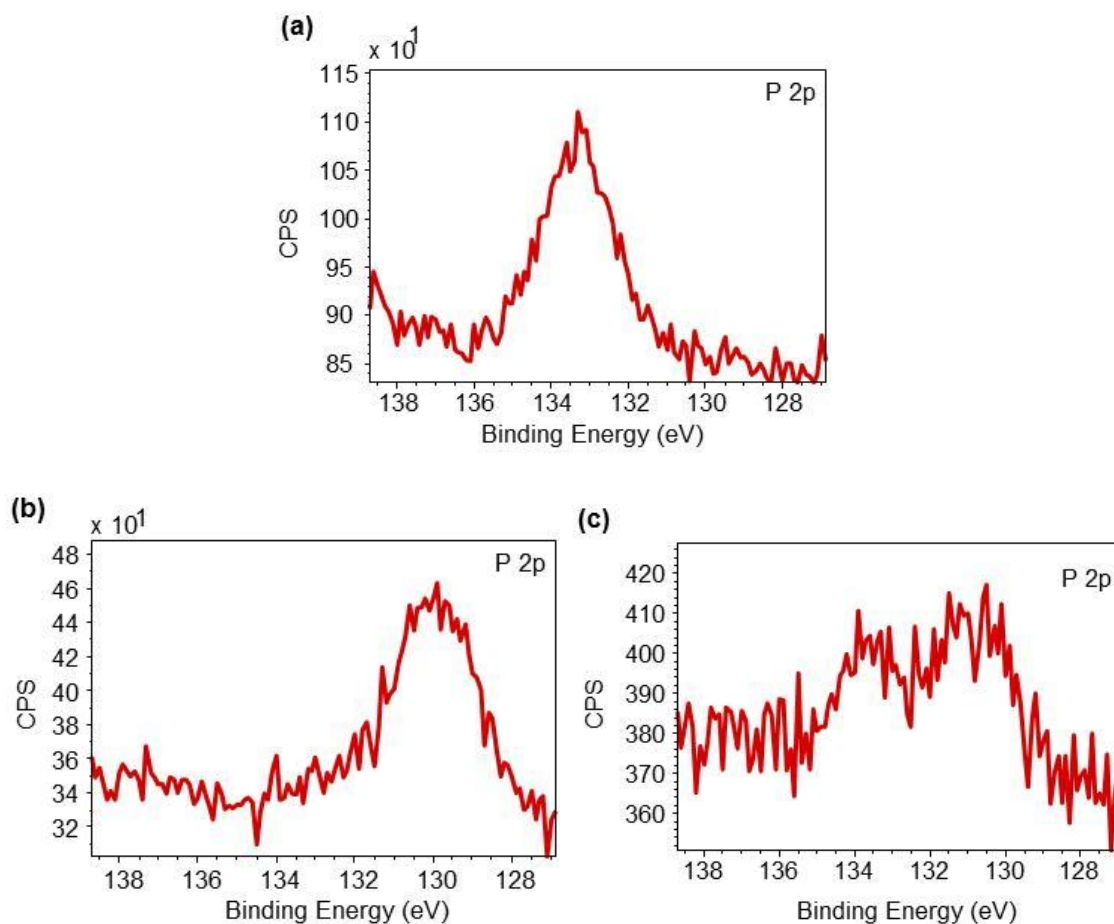


Figure 57: High resolution P 2p XPS spectra of the worn surface on cast iron flat samples lubricated with (a) New Oil (b) New Oil + 6% IL1 (c) New Oil + 6% IL2

Figure 57 (a, b, c) show the high resolution spectra of P2p taken inside the worn surface on the cast iron flat samples lubricated with New fully formulated 15W40 oil with and without ILs. In the sample lubricated with New fully formulated 15W40 oil without ILs, one peak located at 133.4 eV (fwhm = 2.3 eV) was measured in the P2p high resolution spectrum. This peak was assigned to FePO_4 [106, 107]. In the case of New Oil + 6% IL1 (see Figure 57 b), the one peak from the compound Fe_2P (B.E. = 129.9 eV; fwhm = 2.2 eV) was detected, according to NIST database [106]. Similar observations were made on cast iron sample lubricated with New Oil + 6% IL2 (Figure 57 c), such that two peaks were detected at 130.8 eV (fwhm = 2.7 eV) and 133.8 eV (fwhm = 2.2 eV). First peak was difficult to be assigned and second was assigned to FePO_4 . Boundary film seems to be a combination of both iron phosphate and calcium phosphate in new oil; however the addition of ILs caused change in the reactivity of element P with both Fe substrate and Ca detergent additive to form boundary film on the surface.

5.4.3. In-service oil (135h) with/without IL1 and IL2 (at 100°C)

The low resolution survey scans were taken at the centre of worn surface of cast iron flat samples as shown earlier in Figure 46(a, b, c) respectively. It can be seen that Fe, Mn, Cr, O, Ca, C, P and Si elements were detected in each case. In addition, EDX analysis results in Table 15 also show almost all of the same elements in addition to S and Zn which are otherwise not evident from XPS analysis. This could be due to depth penetration limit of XPS analysis up to 1-5 nm whereas EDX can detect elemental concentration up to the depth of a few microns. Some elements mentioned as not detectable that means they were below the detection capabilities of the EDX instruments employed.

From the results it can be seen that the concentration of Ca, Zn and S has reduced inside worn surface by addition of ILs to the In-service Oil (135h). On the contrary, the concentration of O and P has increased by addition of ILs to the oils. Therefore it can be deduced from these observations that addition of ILs to fully formulated oil resulted in reduced reactivity of ZDDP (antiwear) and Calcium Sulphonate (detergent) additives with the Fe containing cast iron surface. Increased reactivity of O element was studied in detail using XPS analysis and explained later in this section. Interestingly, no Cr was noted by EDX analysis, which is otherwise reflected by XPS, therefore suggesting a very mild material transfer (adhesive wear) from the surface of chromium coated piston ring had taken place during the sliding process in all the three cases.

Table 16 shows the binding energy shifts for Fe, O, Ca and P elements, each of which have been discussed above. These elements are the main constituents of the cast iron flat sample and lubricant or IL employed. Therefore change in their binding energy values reflect the change in their chemical state and indicate the thermo-chemical reactions taking place during the sliding process inside of worn surface. The higher resolution scan of main elements such as Fe, O, Ca and P has been taken using XPS to evaluate the change in chemical state of these elements by measuring their binding energies.

Table 15: Elemental concentration inside worn surface obtained by EDX analysis

Cast iron flat surface lubricated with	Element concentration (in weight %)								
	C	O	Si	S	Ca	Zn	Mn	Fe	P
In-service Oil	7.44	9.57	2.07	0.57	0.48	0.82	nd	78.11	0.93
In-service Oil + 6% IL1	6.02	15.70	1.86	0.42	0.42	nd	0.66	74.21	0.72
In-service Oil + 6% IL2	nd	11.79	2.18	0.07	0.40	0.36	nd	84.13	1.07

nd – not detectable

Table 16: XPS results – binding energy shifts – inside worn surface on cast iron flat samples

Element	Binding Energy (eV)		Assignable Chemical Compounds			
	Inservice Oil (135h)		Inservice Oil (135h) + 6% IL1		Inservice Oil (135h) + 6% IL2	
Fe	710.4	Fe ₃ O ₄	710.3	Fe ₃ O ₄	710.6	Fe ₃ O ₄
	712.1	FePO ₄	711.6	Fe ₂ O ₃	712.7	FePO ₄
O	530.2	Fe ₂ O ₃	530.1	Fe ₂ O ₃	530.1	Fe ₂ O ₃
	531.9	FePO ₄	531.7	FePO ₄	531.6	FePO ₄
	533.3	<i>na</i>				
Ca	347.8	Ca ₃ (PO ₄) ₂	347.5	Ca ₃ (PO ₄) ₂	347.5	Ca ₃ (PO ₄) ₂
P	133.8	FePO ₄	133.4	FePO ₄	133.5	FePO ₄

na – not assignable

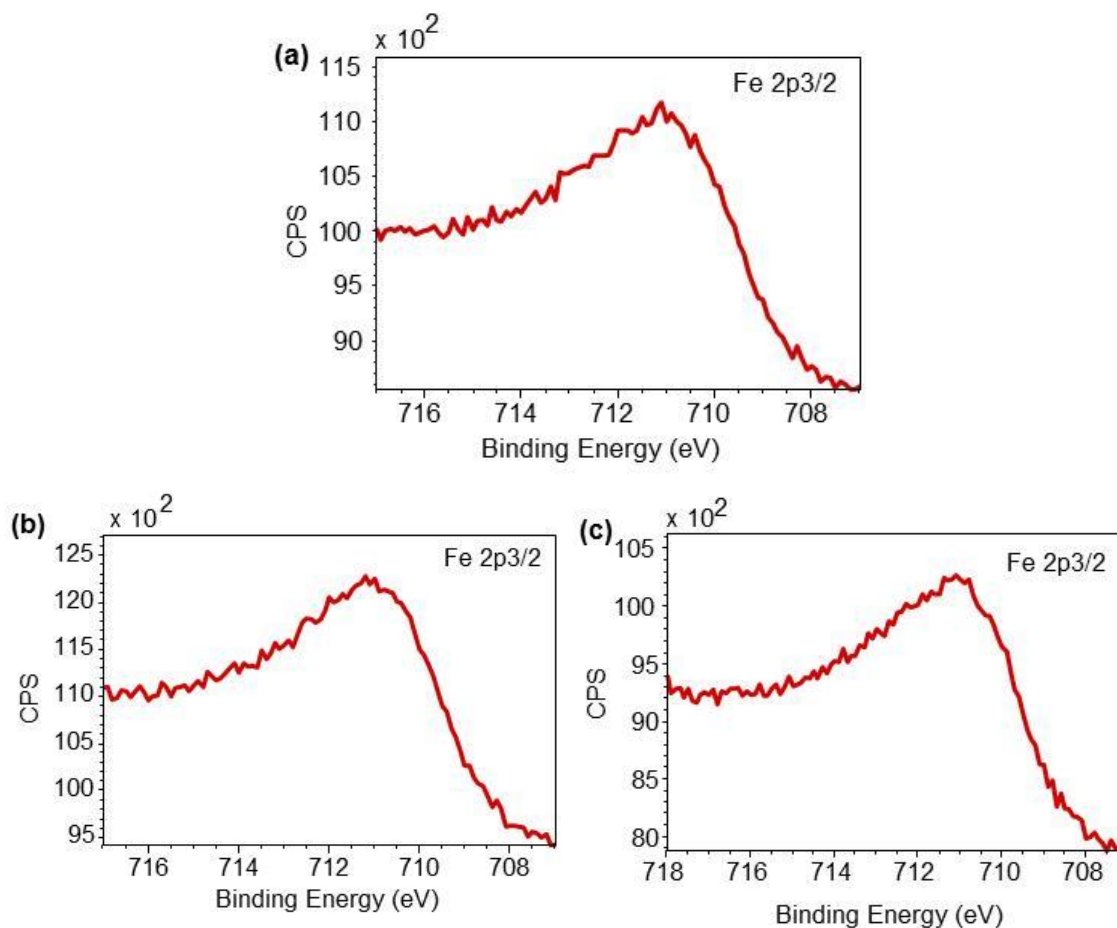


Figure 58: High resolution Fe 2p_{3/2} XPS spectra of the worn surface on cast iron flat samples lubricated with (a) Inservice Oil (135h); (b) Inservice Oil (135h) + 6% IL1; (c) Inservice Oil (135h) + 6% IL2

Figure 58 (a, b, c) show the high resolution spectra of Fe2p_{3/2} taken inside the worn surface on the cast iron flat samples lubricated with In-service Oil (135h) with and without ILs. Figure 58 (a) depicts two peaks located at 710.4eV (fwhm = 2.4 eV) and 712.1 eV (fwhm = 2.5 eV) detected inside the worn surface on the cast iron flat sample lubricated with neat In-service Oil. The first peak could be assigned to Fe₃O₄ [101] and second peak to FePO₄ [102]. Addition of IL1 in the in-service Oil (135h) resulted in two peaks, as shown in Figure 58 (b), located at 710.3eV (fwhm = 2.3 eV) and second peak at 711.6eV (fwhm = 2.8 eV) assignable to Fe₃O₄ and Fe₂O₃ [103], respectively. Similarly, addition of IL2 in in-service Oil (135h) resulted in two peaks, as shown in Figure 58 (c). First one appeared at 710.6eV (fwhm = 2.7 eV) and second peak at 712.7eV (fwhm = 2.5 eV) assignable to Fe₃O₄ and FePO₄, respectively.

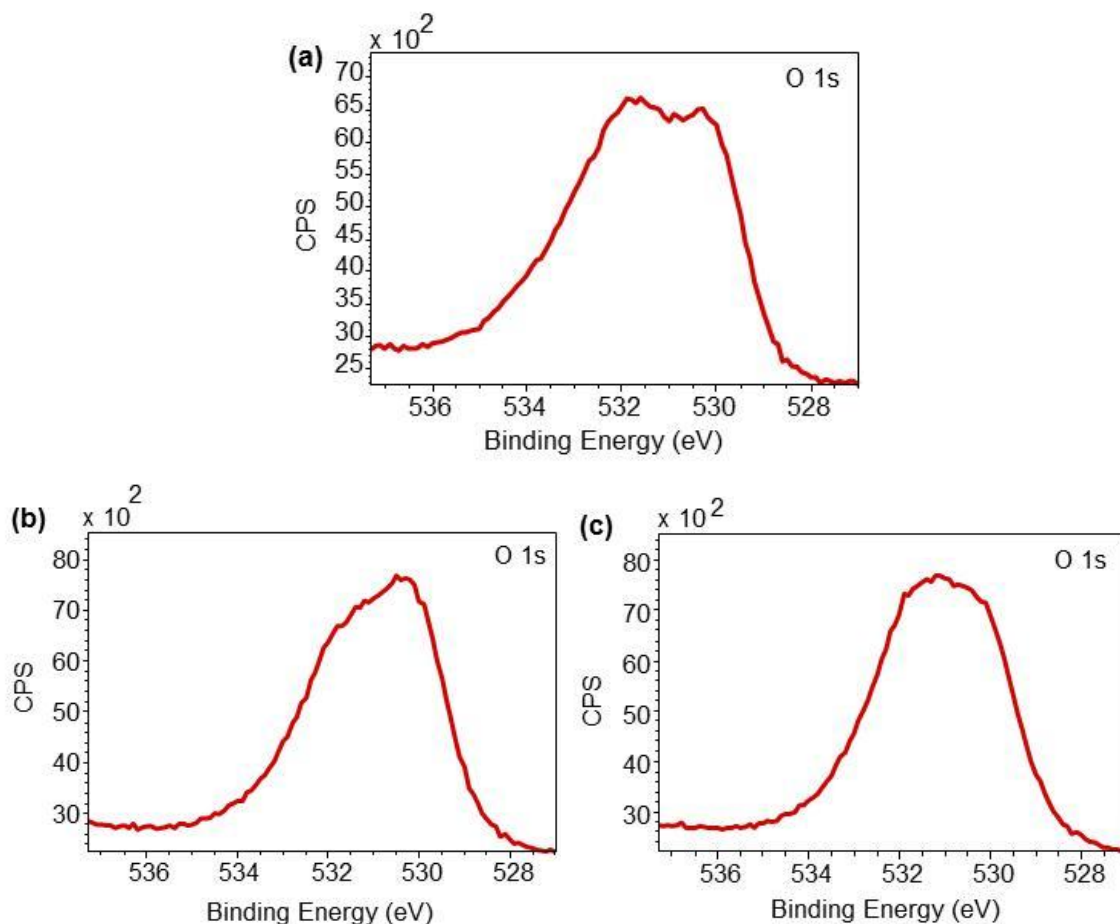


Figure 59: High resolution O1s XPS spectra of the worn surface on cast iron flat samples lubricated with (a) In-service Oil (135h); (b) In-service Oil (135h) + 6% IL1; (c) In-service Oil (135h) + 6% IL2

Figure 59(a, b, c) show the high resolution spectra of O1s taken inside the worn surface on the cast iron flat samples lubricated with In-service Oil (135h) with and without ILs. The surface analysis showed results very similar to that noted for New Oil case (with/without ILs). Figure 59 (a) depicts three peaks located at 530.2 eV (fwhm = 1.8 eV), 531.9 eV (fwhm = 1.8 eV) and 533.3 eV (fwhm = 2.2 eV) measured for sample lubricated with In-service Oil (135h) oil without ILs. First two peaks were assigned to Fe_2O_3 and FePO_4 , respectively, [106, 107]. In the case of In-service Oil (135h) + 6% IL1 (see Figure 59b), the peak from Fe_2O_3 (B.E. = 530.1 eV; fwhm = 1.8 eV) and FePO_4 (B.E. = 531.7 eV; fwhm = 2.5 eV) remained. Similar observations were made on cast iron sample lubricated with In-service Oil (135h) + 6% IL2 (Figure 59c), such that peaks were detected at 530.1 eV, and 531.6 eV. Interestingly the third peak which was detected at 533.3 eV (fwhm = 2.2 eV) and difficult to be assigned has disappeared after the addition of both ILs.

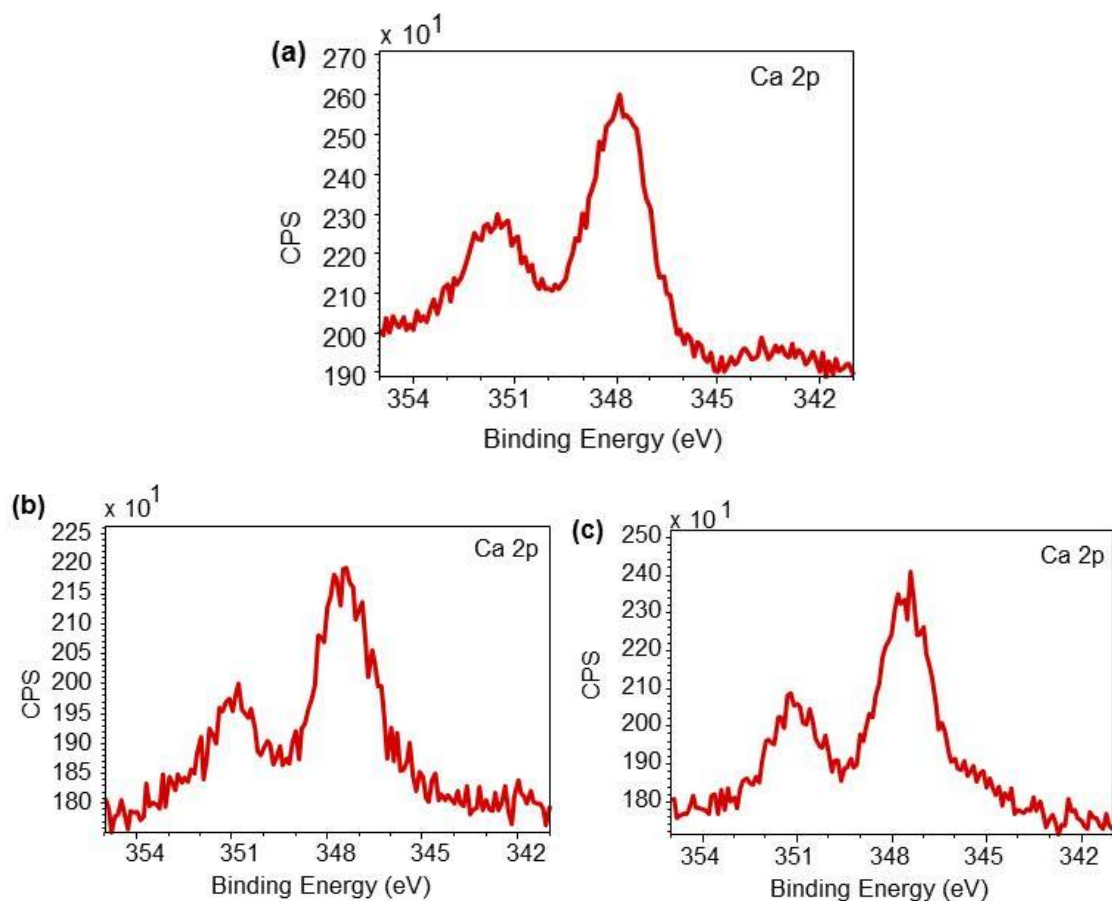


Figure 60: High resolution Ca2p XPS spectra of the worn surface on cast iron flat samples lubricated with (a) In-service Oil (135h); (b) In-service Oil (135h) + 6% IL1; (c) In-service Oil (135h) + 6% IL2

Figure 60 (a, b, c) show the high resolution spectra of Ca2p taken inside the worn surface on the cast iron flat samples lubricated with In-service Oil (135h) with and without ILs. In the sample lubricated with In-service Oil (135h) oil without IL, as shown in Figure 60 (a), one doublet consisting of Ca 2p_{3/2} and Ca 2p_{1/2} was noted. Same as the previous case of New Oil only 2p_{3/2} peak was considered for the analysis purpose, which defines the chemical state of Ca element. Therefore, the Ca 2p_{3/2} peak in (a) was detected at 347.8 eV (fwhm = 2.0 eV) which can be assigned to Ca₃(PO₄)₂. Unlike New Oil, addition of both ILs to the In-service Oil (135h) does not result in the formation of a new doublet of Ca2p in addition to the previously noted without ILs. Therefore, as shown in Figure 60 (b) and (c), Ca 2p_{3/2} peak was noted at 344.5 eV (fwhm = 2.0 eV) in both cases. These new peaks were assigned to Ca₃(PO₄)₂[106]. Clearly a shift of previous peak by 0.3 - 0.4eV can be seen after the addition of ILs.

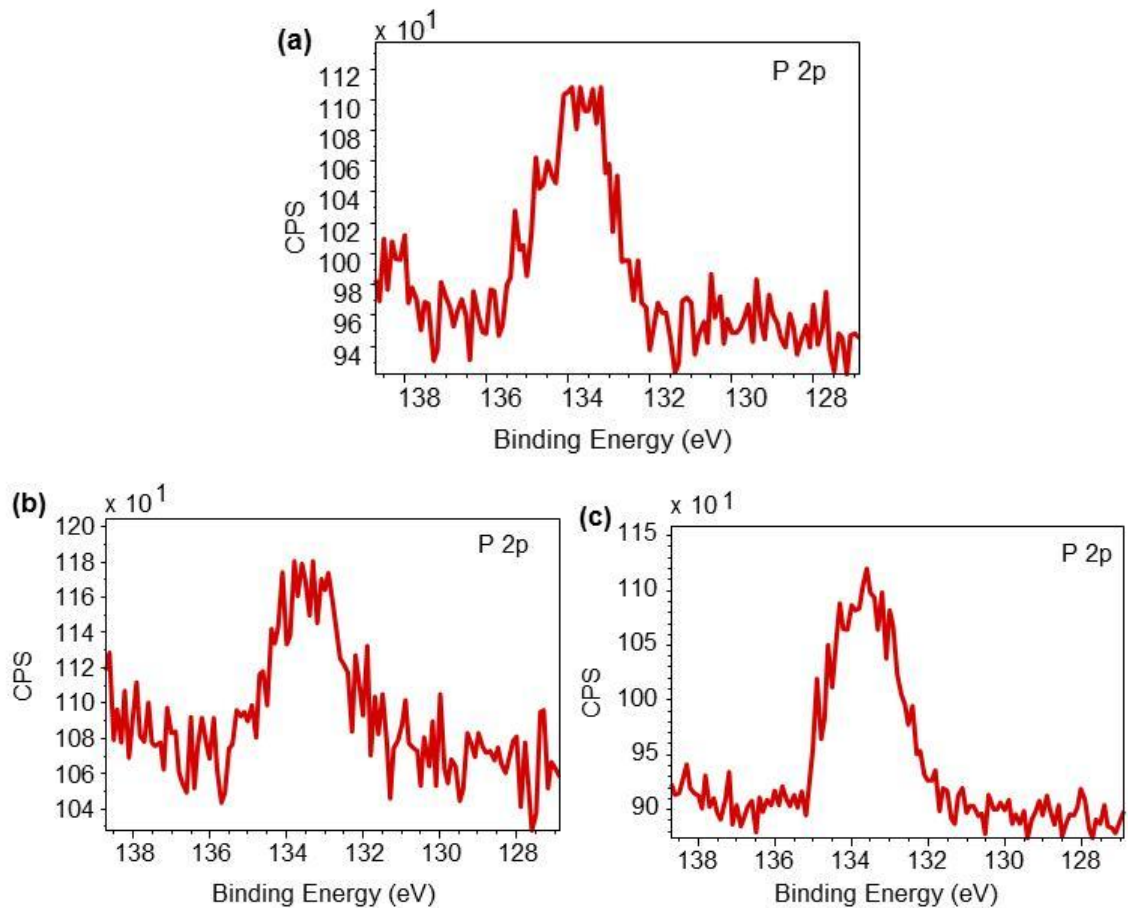


Figure 61: High resolution P2p XPS spectra of the worn surface on cast iron flat samples lubricated with (a) In-service Oil (135h); (b) In-service Oil (135h) + 6% IL1; (c) In-service Oil (135h) + 6% IL2

Figure 61(a, b, c) show the high resolution spectra of P2p taken inside the worn surface on the cast iron flat samples lubricated with In-service Oil with and without ILs. In the sample lubricated with In-service Oil without ILs, one peak located at 133.8 eV (fwhm = 2.1 eV) was measured in the P2p high resolution spectrum. This peak was assigned to FePO_4 [106, 107]. In the case of In-service Oil + 6% IL1 (see Figure 61b), the one peak from the compound FePO_4 (B.E. = 133.4 eV; fwhm = 2.6 eV) was detected, according to NIST database [106]. Similar observations were made on cast iron sample lubricated with In-service Oil+ 6% IL2 (Figure 61c), such that one peak was detected at 133.5 eV (fwhm = 2.0 eV) and assigned to FePO_4 . Like New Oil case, boundary film seems to be a combination of both iron phosphate and calcium phosphate; and the addition of ILs caused no change in the reactivity of element P with both Fe substrate and Ca detergent additive to form boundary film on the cast iron surface during the sliding process.

5.4.4. Used Oil (315h) with/without IL1 and IL2 (at 100°C)

The low resolution survey scans were taken at the centre of worn surface of cast iron flat samples as shown earlier in Figure 48 (a, b, c) respectively. It can be seen that Fe, Mn, Cr, O, Ca, C, P and Si elements were detected in each case. In addition, EDX analysis results in Table 17 also show almost all of the same elements in addition to S and Zn which are otherwise not evident from XPS analysis. This could be due to depth penetration limit of XPS analysis up to 1-5 nm whereas EDX can detect elemental concentration up to the depth of a few microns.

From the results it can be seen that, unlike the case of New Oil and In-service Oil (135h) discussed earlier in this section, the concentration of Ca and Zn has increased by the addition of ILs to the Used Oil (315h). However no significant change in concentration of S can be seen inside worn surface by addition of ILs. On the contrary, the concentration of O and P has increased same as in the case of In-service Oil (135h). Therefore it can be deduced from these observations that addition of ILs to fully formulated oil resulted in increased the reactivity of ZDDP (antiwear) and Calcium Sulphonate (detergent) additives with the Fe containing cast iron surface. Increased reactivity of O element was studied in detail using XPS analysis and explained later in this section. Interestingly, Cr was noted by EDX analysis, only in case of Used Oil suggesting material transfer (adhesive wear) from the surface of chromium coated piston ring had taken place during the sliding process in all the three cases. Addition of ILs resulted in reduced adhesive wear since Cr was only detected in XPS analysis and not in EDX analysis.

Table 18 shows the binding energy shifts for Fe, O, Ca and P elements, each of which have been discussed above. These elements are the main constituents of the cast iron flat sample and lubricant or IL employed. Therefore change in their binding energy values reflect the change in their chemical state and indicate the thermo-chemical reactions taking place during the sliding process inside of worn surface. The higher resolution scan of main elements such as Fe, O, Ca and P has been taken using XPS to evaluate the change in chemical state of these elements by measuring their binding energies.

Table 17: Elemental concentration inside worn surface obtained by EDX analysis

Cast iron flat surface lubricated with	Element concentration (in weight %)									
	C	O	Si	S	Ca	Zn	Mn	Fe	P	Cr
Used Oil	7.86	8.75	2.24	0.36	nd	nd	0.75	79.55	0.26	0.22
Used Oil +6% IL1	7.56	11.40	2.14	0.28	0.45	0.40	0.51	76.77	0.48	nd
Used Oil + 6% IL2	6.82	12.88	1.80	0.34	0.36	0.20	nd	77.01	0.58	nd

nd – not detectable

Table 18: XPS results – binding energy shifts – inside worn surface on cast iron flat samples

Element	Binding Energy (eV)		Assignable Chemical Compounds			
	Used Oil (315h)		Used Oil (315h) + 6% IL1		Used Oil (315h) + 6% IL2	
Fe	710.2	Fe ₃ O ₄	710.5	Fe ₃ O ₄	710.3	Fe ₃ O ₄
	711.4	Fe ₂ O ₃	712.4	FePO ₄	711.8	Fe ₂ O ₃
	712.9	FePO ₄				
O	530.2	Fe ₂ O ₃	530.1	Fe ₂ O ₃	530.0	Fe ₂ O ₃
	531.7	FePO ₄	531.8	FePO ₄	531.7	FePO ₄
	532.5	na				
Ca	347.8	Ca ₃ (PO ₄) ₂	347.7	Ca ₃ (PO ₄) ₂	347.8	Ca ₃ (PO ₄) ₂
P	133.7	FePO ₄	133.4	FePO ₄	133.8	FePO ₄

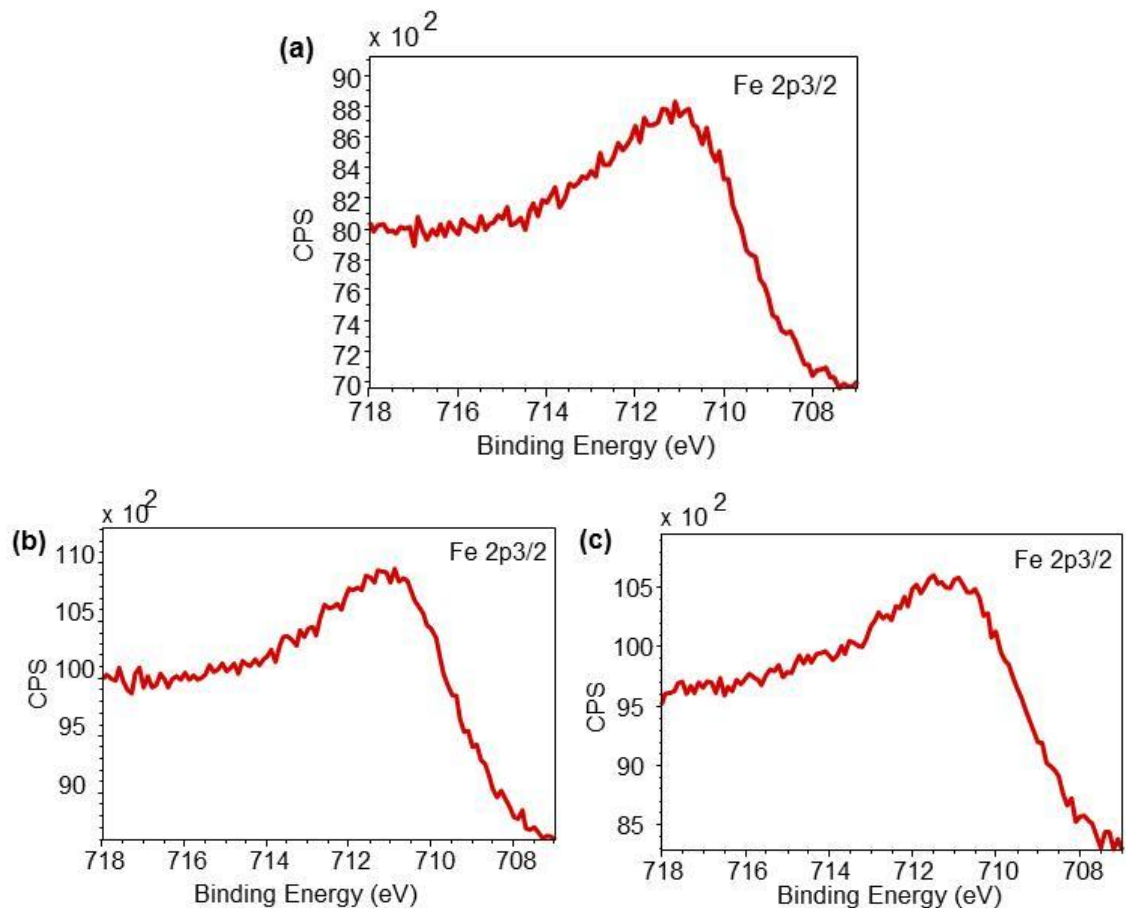


Figure 62: High resolution Fe 2p_{3/2} XPS spectra of the worn surface on cast iron flat samples lubricated with (a) Used Oil (135h); (b) Used Oil (135h) + 6% IL1; (c) Used Oil (135h) + 6% IL2

Figure 62 (a, b, c) show the high resolution spectra of Fe_{2p_{3/2}} taken inside the worn surface on the cast iron flat samples lubricated with Used Oil (315h) with and without ILs. Figure 62 (a) showed that Fe_{2p_{3/2}} band could be fitted with three different peaks at 710.2eV (fwhm = 2.2 eV), 711.4eV (fwhm = 2.1 eV) and 712.9 eV (fwhm = 2.2 eV). Peaks observed could be assigned to Fe₃O₄[101], Fe₂O₃[103-105]and FePO₄[102], respectively. Addition of IL1 in the Used Oil (315h) resulted in two peaks, as shown in Figure 62 (b), located at 710.5 eV (fwhm = 2.7 eV) and 712.4 eV (fwhm = 2.0 eV) assignable to Fe₃O₄ [101]and FePO₄ [102], respectively. Similarly, addition of IL2 in Used Oil (315h) resulted in two peaks, as shown in Figure 62 (c). First one appeared at 710.3eV (fwhm = 2.9 eV) and second peak at 711.8eV (fwhm = 3.6 eV) assignable to Fe₃O₄ [101]and Fe₂O₃ [103-105] respectively.

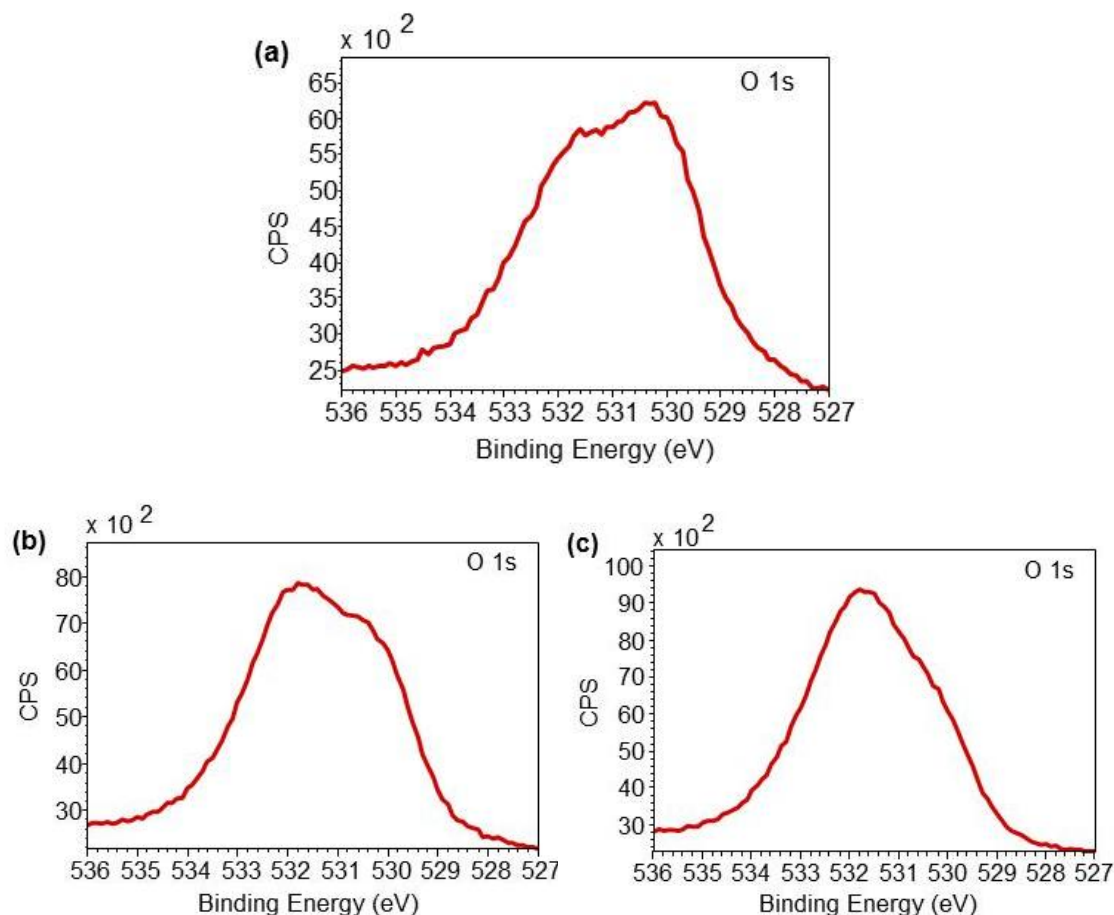


Figure 63: High resolution O1s XPS spectra of the worn surface on cast iron flat samples lubricated with (a) Used Oil (135h); (b) Used Oil (135h) + 6% IL1; (c) Used Oil (135h) + 6% IL2

Figure 63(a, b, c) show the high resolution spectra of O1s taken inside the worn surface on the cast iron flat samples lubricated with Used Oil (315h) with and without ILs. Figure 63(a) depicts three peaks located at 530.2 eV (fwhm = 2.0 eV), 531.7 eV (fwhm = 1.4 eV) and 532.5 eV (fwhm = 2.1 eV) measured for sample lubricated with Used Oil (135h) without ILs. First two peaks were assigned to Fe_2O_3 and FePO_4 , respectively, [106, 107]. In the case of Used Oil (315h) + 6% IL1 (see Figure 63b), the peak from Fe_2O_3 (B.E. = 530.1 eV; fwhm = 1.7 eV) and FePO_4 (B.E. = 531.8 eV; fwhm = 2.4 eV) remained. Similar observations were made on cast iron sample lubricated with Used Oil (315h) + 6% IL2 (see Figure 63c), such that peaks were detected at 530.0 eV (fwhm = 1.4 eV) and 531.7 eV (fwhm = 2.7 eV). Interestingly the third peak which was detected at 532.5 eV (fwhm = 2.1 eV) and difficult to be assigned has disappeared after the addition of both ILs.

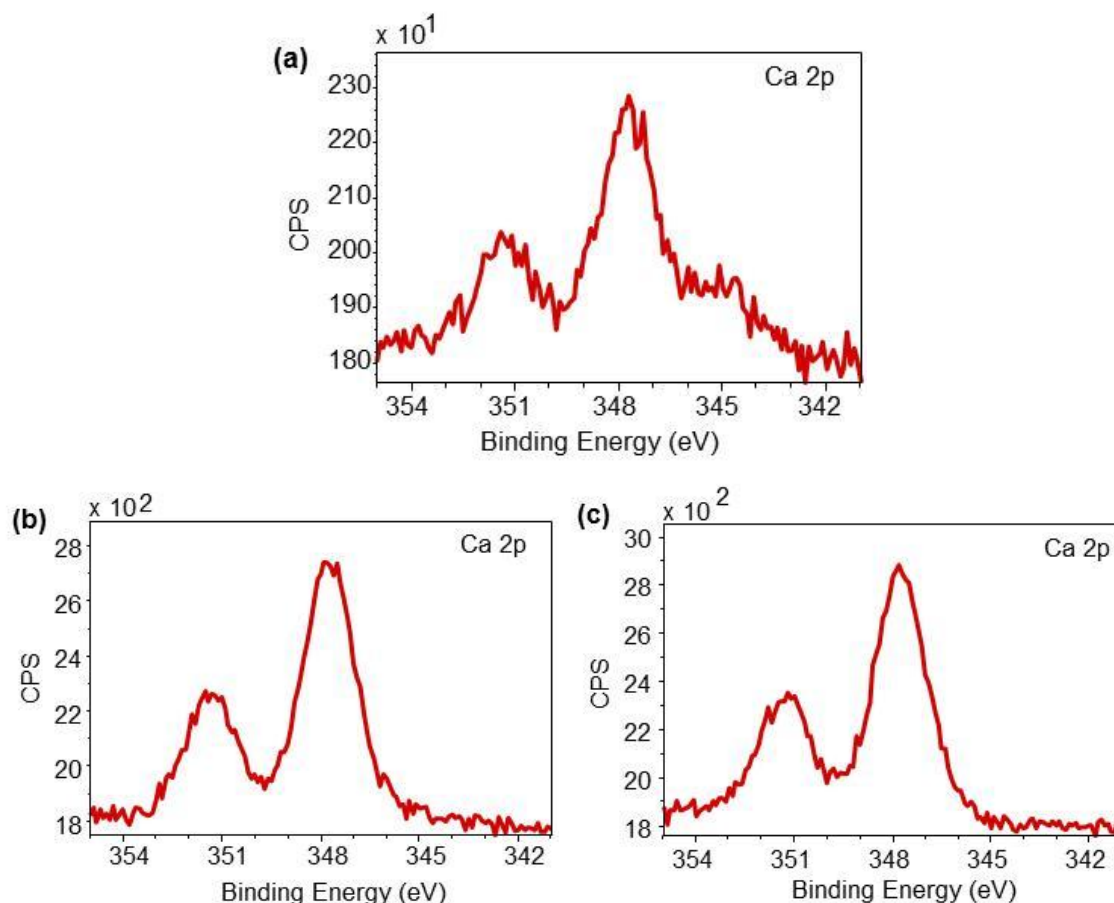


Figure 64: High resolution Ca 2p XPS spectra of the worn surface on cast iron flat samples lubricated with (a) Used Oil (135h); (b) Used Oil (135h) + 6% IL1; (c) Used Oil (135h) + 6% IL2

Figure 64 (a, b, c) show the high resolution spectra of Ca2p taken inside the worn surface on the cast iron flat samples lubricated with Used Oil (135h) with and without ILs. In the sample lubricated with Used Oil (135h) without IL, as shown in Figure 64 (a), one doublet consisting of Ca 2p_{3/2} and Ca 2p_{1/2} was noted. Same as the previous cases of New Oil and In-service Oil (135h), only 2p_{3/2} peak was considered for the analysis purpose, which defines the chemical state of Ca element. Therefore, the Ca 2p_{3/2} peak in (a) was detected at 347.8 eV (fwhm = 1.7 eV) which can be assigned to Ca₃(PO₄)₂. Again the addition of both ILs to the Used Oil (315h) does not result in the formation of a new doublet of Ca2p in addition to the previously noted without ILs. Therefore, as shown in Figure 64(b) and (c), Ca 2p_{3/2} peak was noted at 344.7 eV (fwhm = 1.8 eV) for IL1, and 347.8 eV (fwhm = 1.9 eV) for IL2, respectively. These new peaks were also assigned to Ca₃(PO₄)₂ [106].

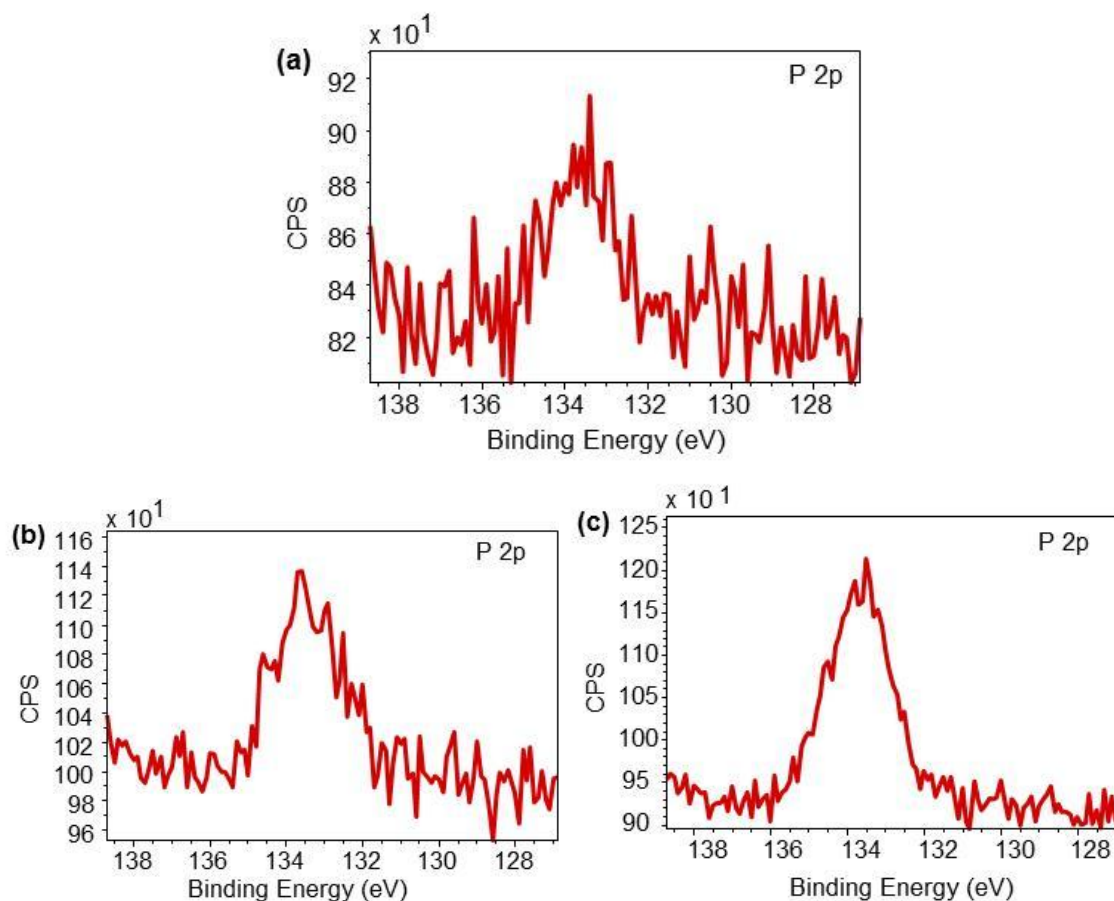


Figure 65: High resolution P 2p XPS spectra of the worn surface on cast iron flat samples lubricated with (a) Used Oil (315h); (b) Used Oil (315h) + 6% IL1; (c) Used Oil (315h) + 6% IL2

Figure 65(a, b, c) show the high resolution spectra of P2p taken inside the worn surface on the cast iron flat samples lubricated with Used Oil (315h) with and without ILs. In the sample lubricated with Used Oil (315h) without ILs, one peak located at 133.7 eV (fwhm = 1.9 eV) was measured in the P2p high resolution spectrum. This peak was assigned to FePO_4 [106, 107]. In the case of Used Oil (315h) + 6% IL1 (see Figure 65b), the one peak from the compound FePO_4 (B.E. = 133.4 eV; fwhm = 2.0 eV) was detected, according to NIST database [106]. Similar observations were made on cast iron sample lubricated with Used Oil (315h) + 6% IL2 (Figure 65c), such that one peak was detected at 133.8 eV (fwhm = 2.0 eV) and assigned to FePO_4 . Hence, addition of ILs to Used Oil, increased the intensity of P2p band, making it comparable to that noted in case of New Oil without ILs.

5.4.5. New Oil with/without IL1 and IL2 (at 25°C)

The low resolution survey scans were taken at the centre of worn surface of cast iron flat samples as shown earlier in Figure 49(a, b, c) respectively. It can be seen that Fe, Zn, O, Ca, C, P and S elements were detected in each case. In addition, EDX analysis results in Table 19 also show almost all of these elements.

From the above results it can be seen that no change in the concentration of Ca, Zn and P was noted by the addition of ILs to the New Oil. However the concentration of S has reduced slightly by addition of ILs. On the contrary, the concentration of element O has increased appreciably. Therefore it can be deduced from these observations that addition of ILs to fully formulated oil has no significant effect on the reactivity of ZDDP (antiwear) and Calcium Sulphonate (detergent) additives with the Fe containing cast iron surface. Increased reactivity of O element was studied in detail using XPS analysis and explained later in this section. Interestingly, Cr was noted by EDX analysis unlike XPS, suggesting mild material transfer (adhesive wear) has taken place in all cases from the surface of chromium coated piston ring during the sliding process. Increase in C and O elements in EDX results could be attributed to the reactivity of ILs with iron (Fe) metal surface, since both elements are present in the long hydrocarbon chain structure of ILs.

Table 20 shows the binding energy shifts for Fe, Ca, P, Zn and S elements, each of which have been discussed above. These elements are the main constituents of the cast iron flat sample and lubricant or IL employed. Therefore change in their binding energy values reflect the change in their chemical state and indicate the thermo-chemical reactions taking place during the sliding process inside of worn surface. The higher resolution scan of main elements such as Fe, Ca, P, Zn and S has been taken using XPS to evaluate the change in chemical state of these elements by measuring their binding energies.

Table 19: Elemental concentration inside worn surface obtained by EDX analysis

Cast iron flat surface lubricated with	Element concentration (in weight %)									
	C	O	Si	S	Ca	Zn	Mn	Fe	P	Cr
New Oil	8.41	3.88	2.37	0.30	0.36	0.34	0.71	83.27	0.26	0.10
New Oil +6% IL1	19.44	5.17	2.01	0.11	0.34	0.31	nd	72.27	0.22	0.12
New Oil + 6% IL2	18.49	6.24	1.53	0.05	0.42	0.29	0.50	72.08	0.27	0.13

nd – not detectable

Table 20: XPS results – binding energy shifts – inside worn surface on cast iron flat samples

Element	Binding Energy (eV)		Assignable Chemical Compounds			
	New Oil		New Oil + 6% IL1		New Oil + 6% IL2	
Fe	708.8	Fe ₃ O ₄	nd	nd	708.4	Fe ₃ O ₄
	710.6	Fe ₂ O ₃			710.2	
Ca	347.1	CaO	347.6	Ca ₃ (PO ₄) ₂	347.2	CaO
P	nd	nd	132.6	Ca ₃ (PO ₄) ₂	133.2	FePO ₄
Zn	1020.8	Zn ⁰ or ZnS	1022.8	ZnO	1021.6	ZnO
S	162.0	ZnS	162.8	FeS ₂	nd	nd

na – not assignable; nd – not detectable

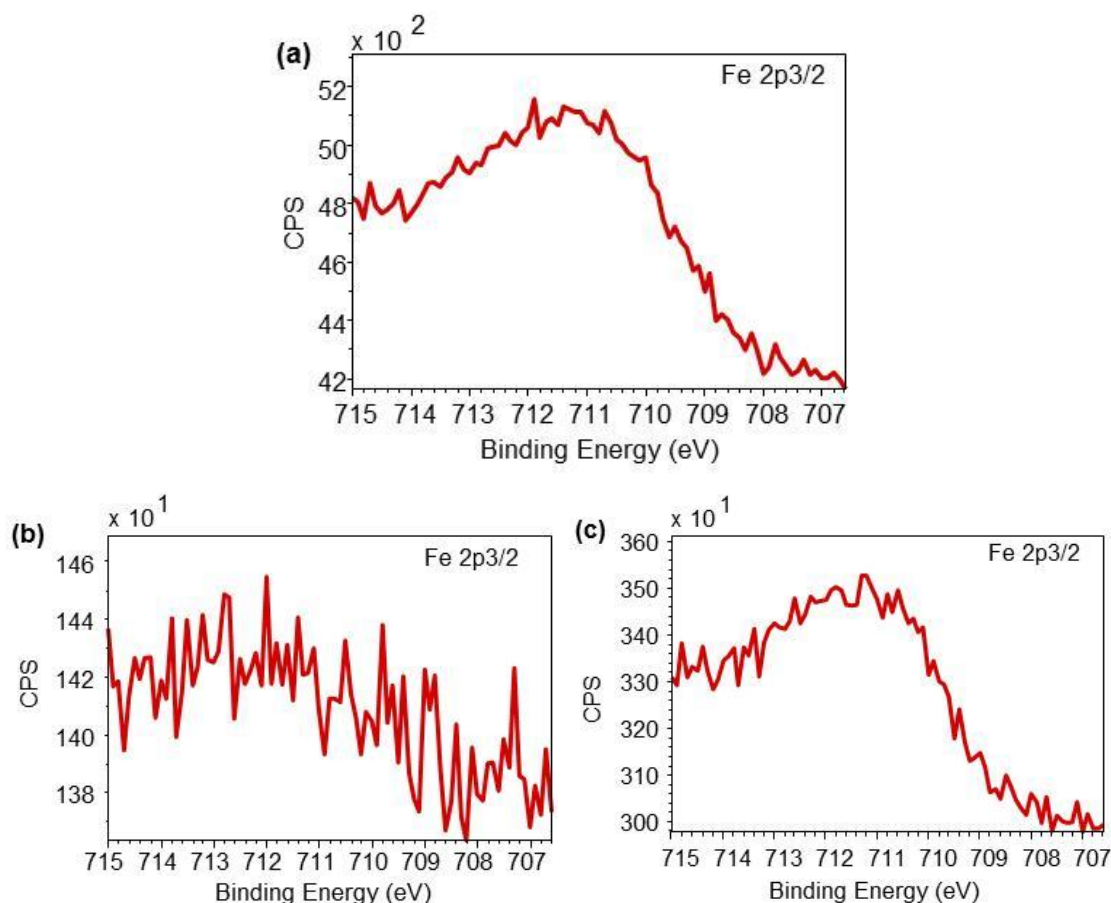


Figure 66: High resolution Fe 2p_{3/2} XPS spectra of the worn surface on cast iron flat samples lubricated with (a) New Oil (b) New Oil + 6% IL1 (c) New Oil + 6% IL2

Figure 66 (a, b, c) show the high resolution spectra of Fe_{2p_{3/2}} taken inside the worn surface on the cast iron flat samples lubricated with New Oil, with and without ILs. Figure 66 (a) showed that Fe_{2p_{3/2}} band could be fitted with two different peaks at 708.8eV and 710.6eV assigned to Fe₃O₄ and Fe₂O₃ respectively[110, 111]. It was difficult to conclude Fe 2p_{3/2} spectra for sample lubricated with the mixture of IL1 and New Oil, due to high level of noise, as shown in Figure 66 (b). A number of different bands belonging to iron oxides and iron disulphide could be possible such that making it difficult to conclude. However, addition of IL2 in New Oil resulted in two peaks, as shown in Figure 66(c). First peak appeared at 708.4eV and second one at 710.2eV assignable to Fe₃O₄ [101].

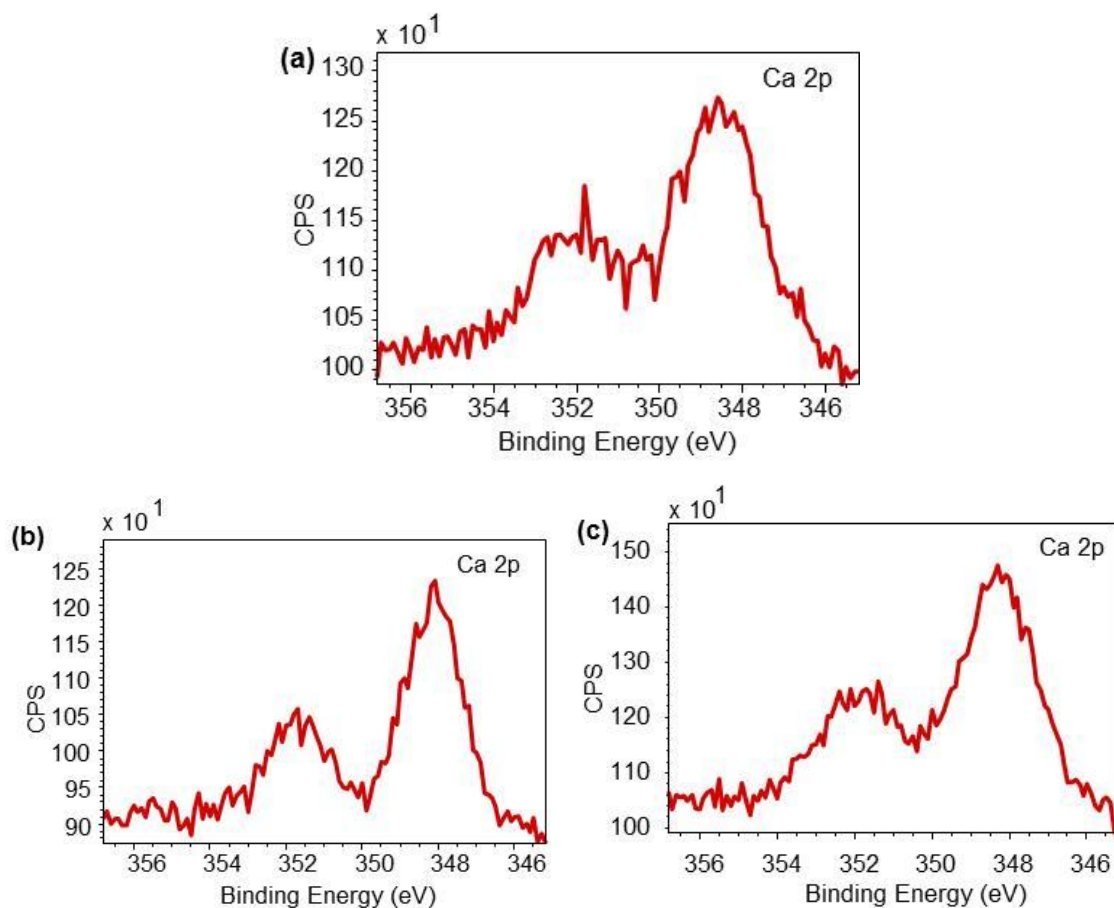


Figure 67: High resolution Ca 2p XPS spectra of the worn surface on cast iron flat samples lubricated with (a) New Oil (b) New Oil + 6% IL1 (c) New Oil + 6% IL2

Figure 67(a, b, c) show the high resolution spectra of Ca2p taken inside the worn surface on the cast iron flat samples lubricated with New Oil with and without ILs. In the sample lubricated with New Oil without IL, as shown in Figure 67(a), one doublet consisting of Ca 2p_{3/2} and Ca 2p_{1/2} was noted. Same as the previous cases of New Oil at 100°C, however, only 2p_{3/2} peak was considered for the analysis purpose, which defines the chemical state of Ca element. Therefore, the Ca 2p_{3/2} peak in (a) was detected at 347.1 eV which was assigned to CaO [112]. By the addition of IL1 to the New Oil the binding energy of Ca 2p_{3/2} peak shifted to 347.6 eV, assignable to Ca₃(PO₄)₂[107], see Figure 67 (b). On the other hand no significant change in binding energy was noted for Ca 2p_{3/2} peak after addition of IL2. Therefore, the 2p_{3/2} peak was noted at 347.2 eV assignable to CaO [112], see Figure 67 (c).

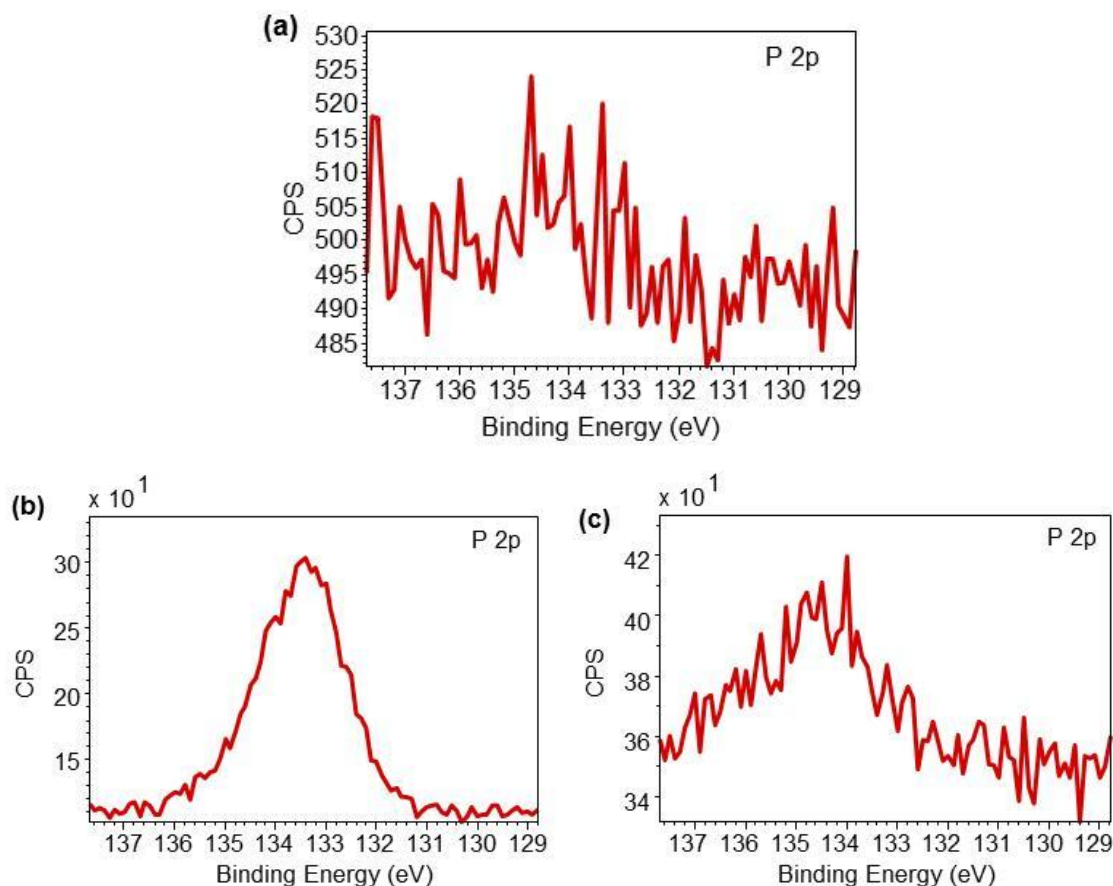


Figure 68: High resolution P2p XPS spectra of the worn surface on cast iron flat samples lubricated with (a) New Oil (b) New Oil + 6% IL1 (c) New Oil + 6% IL2

Figure 68(a, b, c) show the high resolution spectra of P2p taken inside the worn surface on the cast iron flat samples lubricated with New Oil with and without ILs. In the sample lubricated with New Oil without ILs, the concentration of phosphorus was noted to be very low on the worn surface, as shown in Figure 68 (a), and therefore no peak could be assigned. In the case of New Oil + 6% IL1 (see Figure 68 b), the one peak from the compound $\text{Ca}_3(\text{PO}_4)_2$ (B.E. = 132.6 eV) was detected, according to [113]. A slightly different observations were made on cast iron sample lubricated with New Oil + 6% IL2 (Figure 68 c), such that a peak was detected at 133.2 eV assigned to FePO_4 [102]. Although addition of ILs to New Oil resulted in clear P2p peaks but change in the intensity of P2p band was not observed. Different compounds by addition of IL1 and IL2 indicates difference in their reactivity to form boundary film.

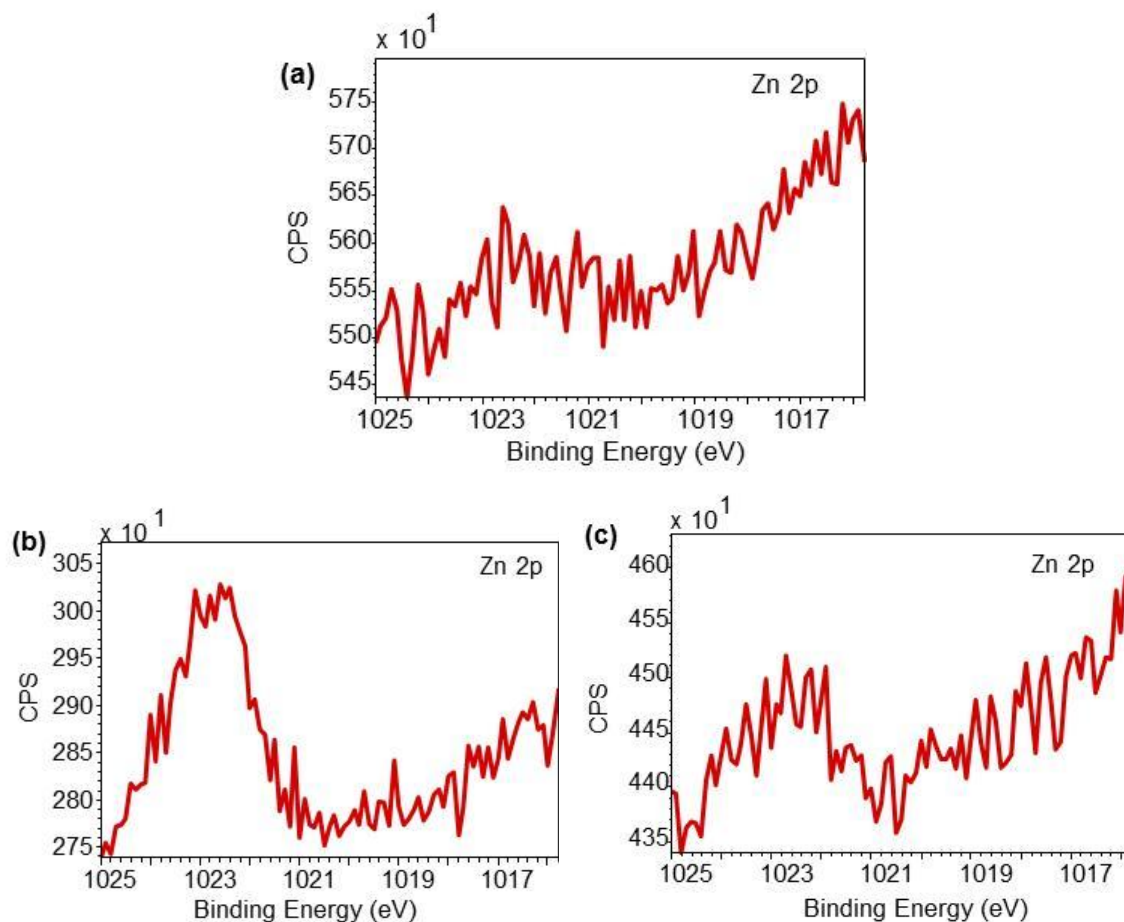


Figure 69: High resolution Zn 2p XPS spectra of the worn surface on cast iron flat samples lubricated with (a) New Oil (b) New Oil + 6% IL1 (c) New Oil + 6% IL2

High level of noise in the spectrum made the curve fitting difficult. However following observation were made. Figure 69 (a, b, c) show the high resolution spectra of Zn 2p taken inside the worn surface on the cast iron flat samples lubricated with New Oil, with and without ILs. New Oil without ILs (Figure 69 a) showed that Zn 2p band could be fitted with one peak at 1020.8 eV which is assignable to either ZnS [114]. After addition of IL1 and IL2 to the New Oil, the shift in the binding energy of Zn 2p band was noted. As shown in Figure 69 (b) and (c), a peak in each case was appeared at 1022.8 eV (for IL1[115]) and 1021.6 eV (for IL2[116]), both assignable to ZnO. Thus it is clearly evident that a change in the reactivity of ZDDP additive has taken place which resulted in formation of ZnO instead of ZnS after the addition of ILs.

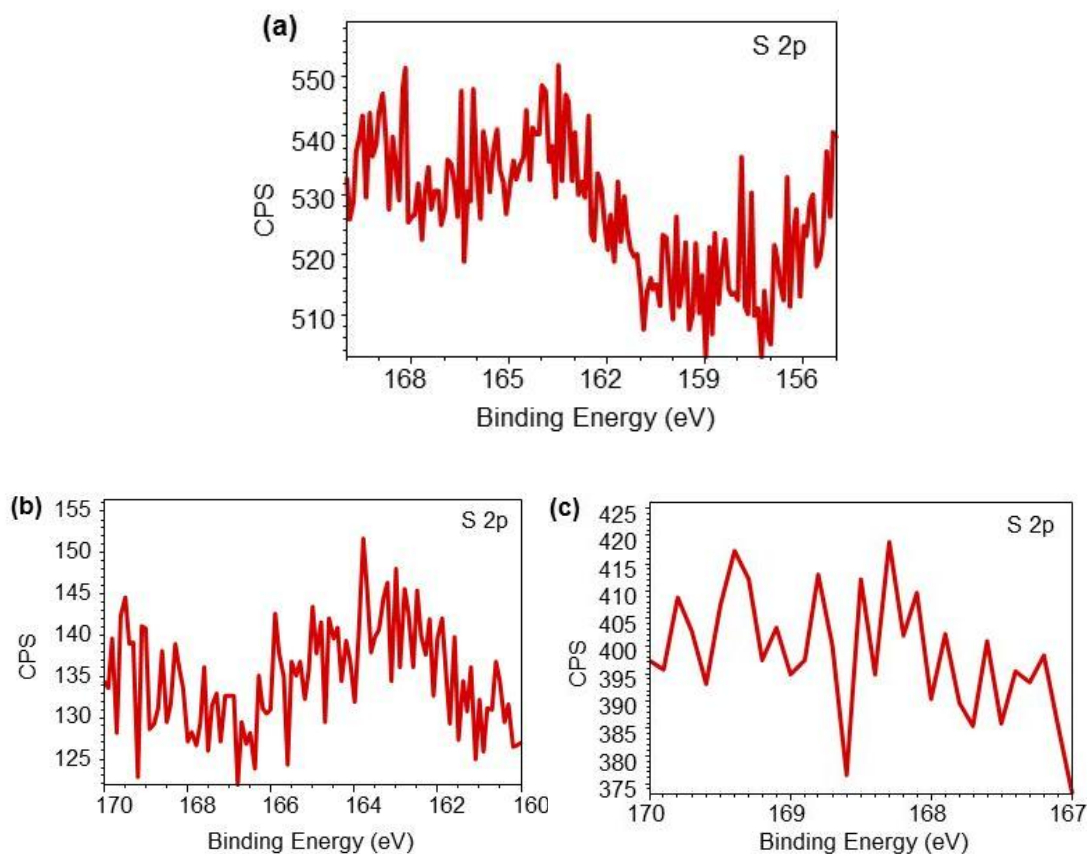


Figure 70: High resolution S 2p XPS spectra of the worn surface on cast iron flat samples lubricated with (a) New Oil (b) New Oil + 6% IL1 (c) New Oil + 6% IL2

Figure 70 (a, b, c) show the high resolution spectra of S 2p taken inside the worn surface on the cast iron flat samples lubricated with New Oil with and without ILs. In the sample lubricated with New Oil without ILs, one peak located at the binding energy of 162.0 eV as shown in Figure 70 (a), was assigned to ZnS [117, 118]. In the case of New Oil + 6% IL1 (see Figure 70b), a peak from the compound FeS₂ (B.E. = 162.8 eV) was detected, according to NIST database [106, 119]. The content of sulphur was low to be appreciated by the XPS analysis after addition of IL2, as evident from the Figure 70 c. Therefore it can be inferred that the addition of ILs reduces the involvement of sulphur containing ZDDP additive in boundary film formation. This argument is also well supported by the corresponding EDX results (Table 19).

5.4.6. Used Oil with/without IL1 and IL2 (at 25°C)

The low resolution survey scans were taken at the centre of worn surface of cast iron flat samples as shown earlier in Figure 50 (a, b, c) respectively. It can be seen that Fe, Zn, O, Ca, C, P and S elements were detected in each case. In addition, EDX analysis results in Table 21 also show almost all of these elements in addition to Cr in case of Used Oil only.

From the above results it can be seen that the concentration of Ca, S and P has increased slightly by the addition of ILs to the Used Oil (315h). However the concentration of Zn and C has reduced significantly by addition of ILs. On the contrary, the concentration of element O has not changed much. Therefore it can be deduced from these observations that addition of ILs to fully formulated oil has increased the reactivity of Calcium Sulphonate (detergent) additive with the Fe containing cast iron surface; but has reduced the same for ZDDP (antiwear). Increase in element P could be attributed to the phosphorus containing ILs (IL1 and IL2). However decrease in element C is difficult to describe. XPS analysis performed on these elements for change in their chemical state could provide some explanation about the chemical reactions taking place on the surface. Interestingly, Cr was noted by EDX analysis unlike XPS, only in the case of Used Oil suggesting mild material transfer (adhesive wear) has taken place from the surface of chromium coated piston ring on the cast iron sample during the sliding process. Addition of ILs seems to be effective in reducing the adhesive wear, since only XPS could detect the Cr in low resolution spectra and not much appreciably in high resolution spectra of Used Oil case.

Table 22 shows the binding energy shifts for Fe, Ca, P, Zn and S elements, each of which have been discussed above. These elements are the main constituents of the cast iron flat sample and lubricant or IL employed. Therefore change in their binding energy values reflect the change in their chemical state and indicate the thermo-chemical reactions taking place during the sliding process inside of worn surface. The higher resolution scan of main elements such as Fe, O, Ca, P, Zn and S has been taken using XPS to evaluate the change in chemical state of these elements by measuring their binding energies.

Table 21: Elemental concentration inside worn surface obtained by EDX analysis

Cast iron flat surface lubricated with	Element concentration (in weight %)									
	C	O	Si	S	Ca	Zn	Mn	Fe	P	Cr
Used Oil	13.16	5.7	2.09	0.04	0.06	0.49	0.58	77.69	0.17	0.04
Used Oil +6% IL1	10.22	4.3	2.28	0.12	0.19	nd	0.64	81.97	0.29	nd
Used Oil + 6% IL2	7.52	5.3	2.21	0.09	0.18	nd	0.65	83.78	0.30	nd

nd – not detectable

Table 22: XPS results – binding energy shifts – inside worn surface on cast iron flat samples

Element	Binding Energy (eV)		Assignable Chemical Compounds			
	Used Oil		Used Oil + 6% IL1		Used Oil + 6% IL2	
Fe	708.8	Fe ₃ O ₄	710.0	Fe ₃ O ₄	709.7	Fe ₃ O ₄
	710.1	Fe ₃ O ₄			711.3	Fe ₂ O ₃
Ca	347.3	Ca ₃ (PO ₄) ₂	347.7	Ca ₃ (PO ₄) ₂	347.3	Ca ₃ (PO ₄) ₂
P	132.9	Ca ₃ (PO ₄) ₂	132.8	Ca ₃ (PO ₄) ₂	132.9	Ca ₃ (PO ₄) ₂
Zn	nd	nd	1022.2	ZnO	1021.9	ZnO
S	162.9	FeS ₂	nd	nd	nd	nd

na – not assignable; nd – not detectable

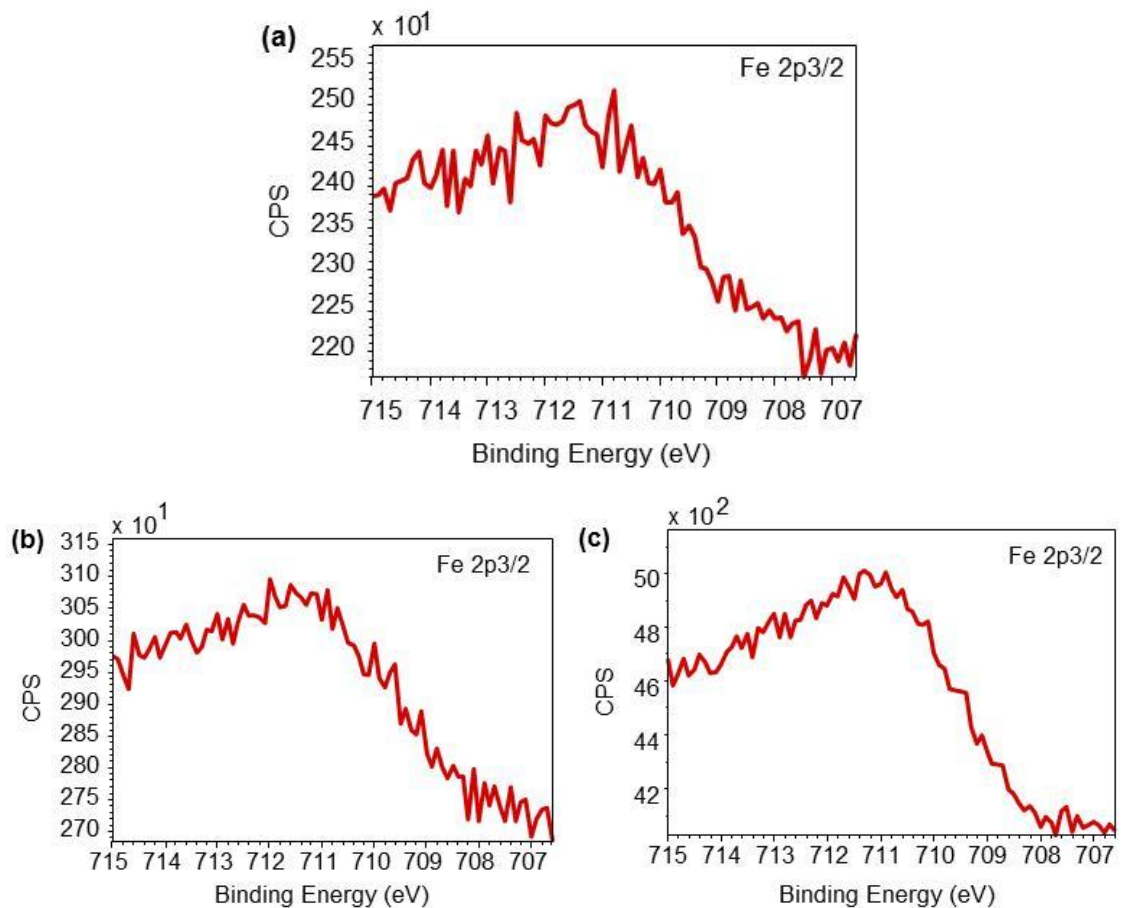


Figure 71: High resolution Fe 2p_{3/2} XPS spectra of the worn surface on cast iron flat samples lubricated with (a) Used Oil (315h); (b) Used Oil (315h) + 6% IL1; (c) Used Oil (315h) + 6% IL2

Figure 71(a, b, c) show the high resolution spectra of Fe2p_{3/2} taken inside the worn surface on the cast iron flat samples lubricated with Used Oil, with and without ILs. Figure 71(a) showed that Fe2p_{3/2} band could be fitted with two different peaks at 708.8eV [110] and 710.1eV [101] assigned to Fe₃O₄. Addition of IL2 in used oil showed one peak at 710.0eV, as shown in Figure 71 (b) also assigned to Fe₃O₄. However, addition of IL2 in Used Oil resulted in two peaks, as shown in Figure 71(c). First peak appeared at 709.7eV and second one at 711.3eV assignable to Fe₃O₄ [101] and Fe₂O₃ [103-105], respectively.

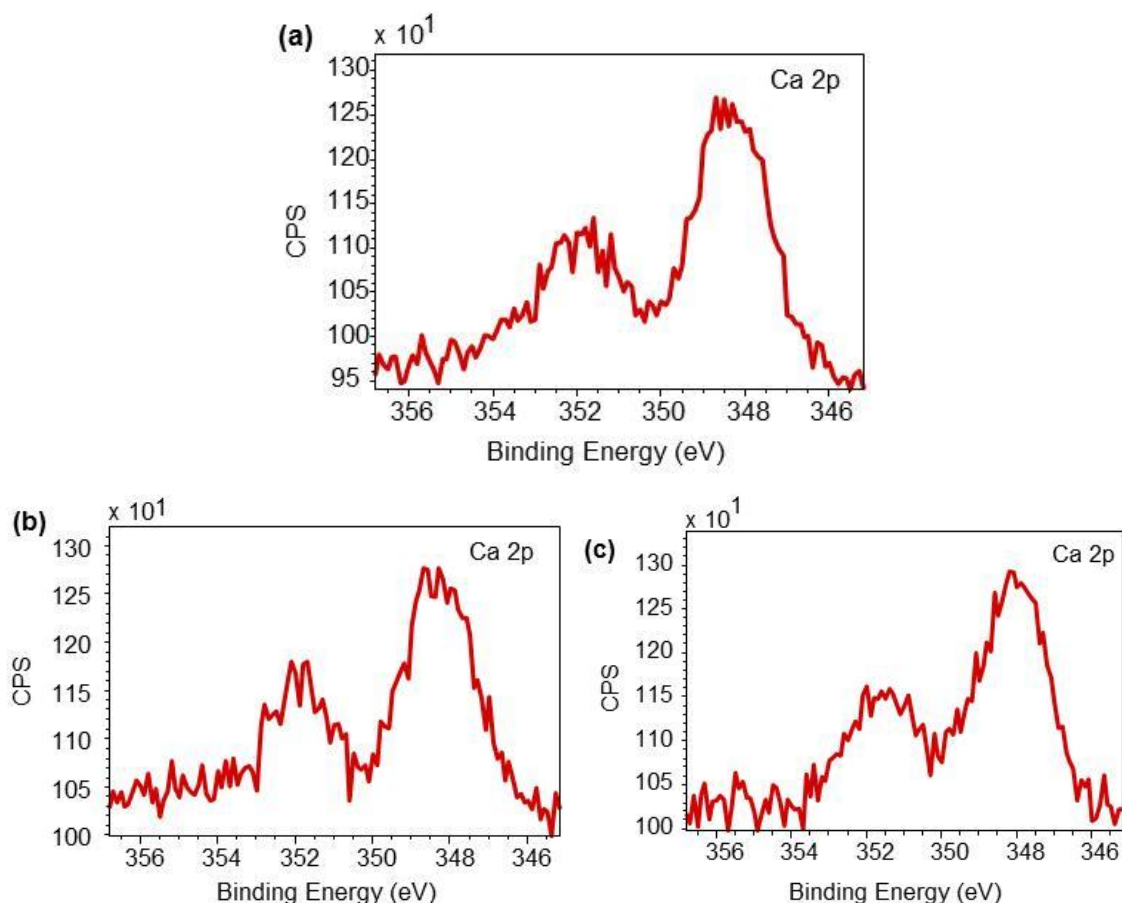


Figure 72: High resolution Ca 2p XPS spectra of the worn surface on cast iron flat samples lubricated with (a) Used Oil (315h); (b) Used Oil (315h) + 6% IL1; (c) Used Oil (315h) + 6% IL2

Figure 72 (a, b, c) show the high resolution spectra of Ca2p taken inside the worn surface on the cast iron flat samples lubricated with Used Oil (135h) with and without ILs. In the sample lubricated with Used Oil (315h) without IL, as shown in Figure 72 (a), one doublet consisting of Ca 2p_{3/2} and Ca 2p_{1/2} was noted. Same as the previous cases of New Oil at 25⁰C, only 2p_{3/2} peak was considered for the analysis purpose, which defines the chemical state of Ca element. Therefore, the Ca 2p_{3/2} peak in (a) was detected at 347.3 eV which was assigned to Ca₃(PO₄)₂ [120]. By the addition of IL1 to the Used Oil (315h) the binding energy of Ca 2p_{3/2} peak shifted slightly to 347.7 eV, assignable to Ca₃(PO₄)₂, see Figure 72 (b), same binding energy assigned in [107]. On the other hand no change in binding energy was noted for Ca 2p_{3/2} peak after addition of IL2. Therefore, the 2p_{3/2} peak was noted at 347.3 eV assignable to Ca₃(PO₄)₂, [120], see Figure 72 (c).

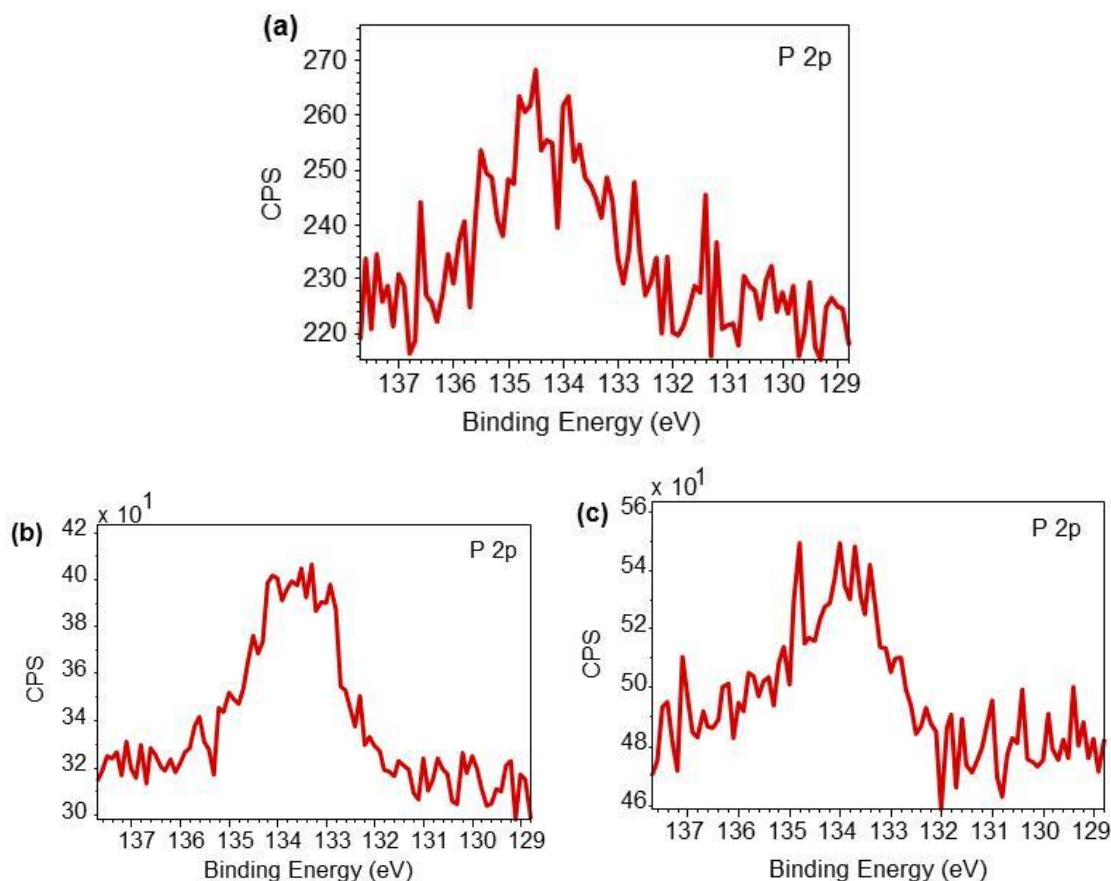


Figure 73: High resolution P2p XPS spectra of the worn surface on cast iron flat samples lubricated with (a) Used Oil (315h); (b) Used Oil (315h) + 6% IL1; (c) Used Oil (315h) + 6% IL2

Figure 73 (a, b, c) show the high resolution spectra of P2p taken inside the worn surface on the cast iron flat samples lubricated with Used Oil (315h) with and without ILs. In the sample lubricated with Used Oil (315h) without ILs, one peak located at the binding energy of 132.9 eV as shown in Figure 73(a), was assigned to $\text{Ca}_3(\text{PO}_4)_2$ [113]. In the case of Used Oil (315h) + 6% IL1 (see Figure 73b), a peak from the compound $\text{Ca}_3(\text{PO}_4)_2$ (B.E. = 132.8 eV) was detected, according to NIST database [106, 113]. Again, no change in binding energy was noted after the addition of IL2, and a peak was noted at 132.9 eV assigned to $\text{Ca}_3(\text{PO}_4)_2$, as shown in Figure 73c. Hence, although no change in the chemical state of element P was noted after addition of ILs to Used Oil, but increase in the intensity of P2p band made Used Oil comparable to that noted in case of New Oil without ILs.

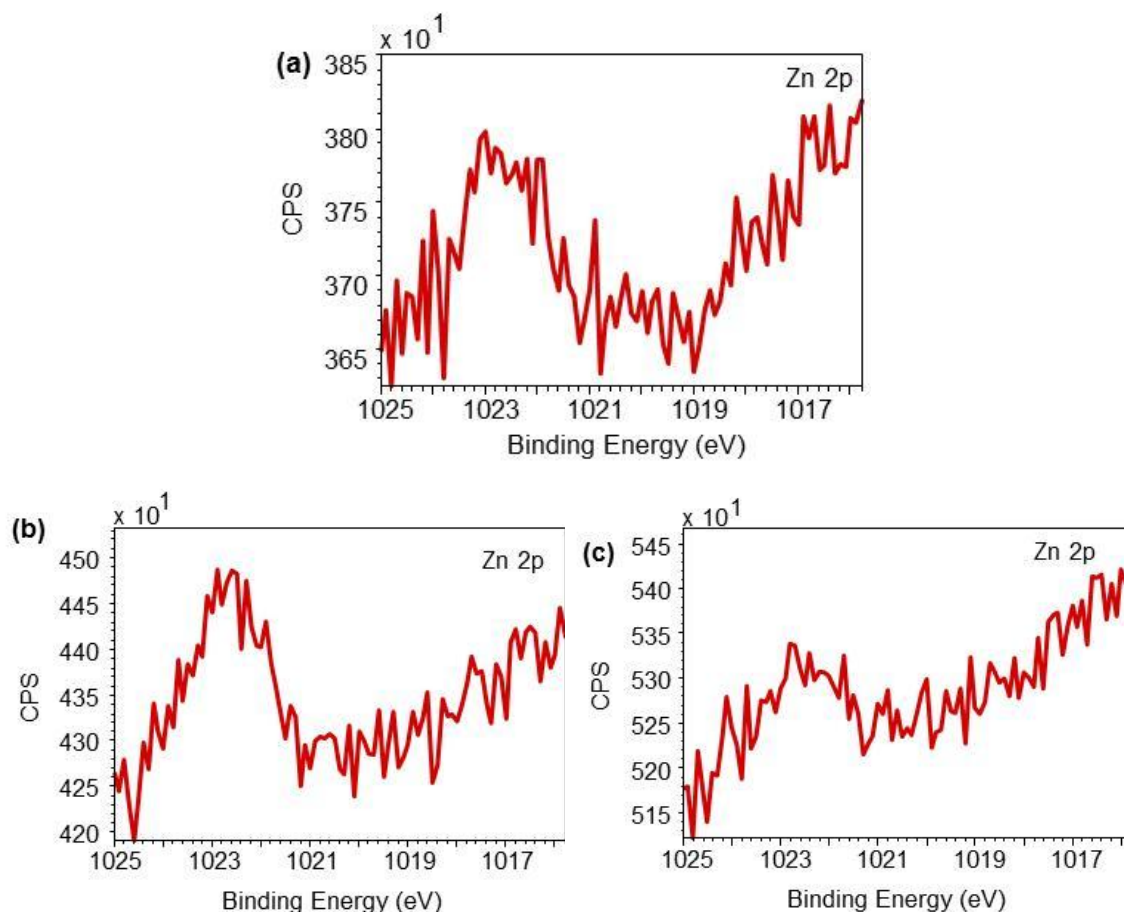


Figure 74: High resolution Zn 2p XPS spectra of the worn surface on cast iron flat samples lubricated with (a) Used Oil (315h); (b) Used Oil (315h) + 6% IL1; (c) Used Oil (315h) + 6% IL2

Low content of Zinc made in the Used Oil possibly due depleted ZDDP additive made its detection difficult in high resolution spectra of Zn 2p. However following observation were made. No detectable Zn content was noted in case of Used Oil without ILs as shown in Figure 74(a). Although it was not expected that addition of ILs would increase Zn in boundary film since ILs do not contain Zn at all. However, after addition of IL1 and IL2 to the Used Oil (315h), a single peak of Zn 2p band was noted. As shown in Figure 74 (b) and (c), a peak in each case appeared at 1022.2 eV [115] (for IL1) and 1021.9 eV [116] (for IL2), both assignable to ZnO. The reason for this appearance of Zn after addition of ILs is not clear since corresponding EDX results showed no Zn in these cases. May be Zn is only present near the surface within the first few layers and its concentration reduces along the thickness of boundary film thus making it hard to be detected from the top of the film by XPS.

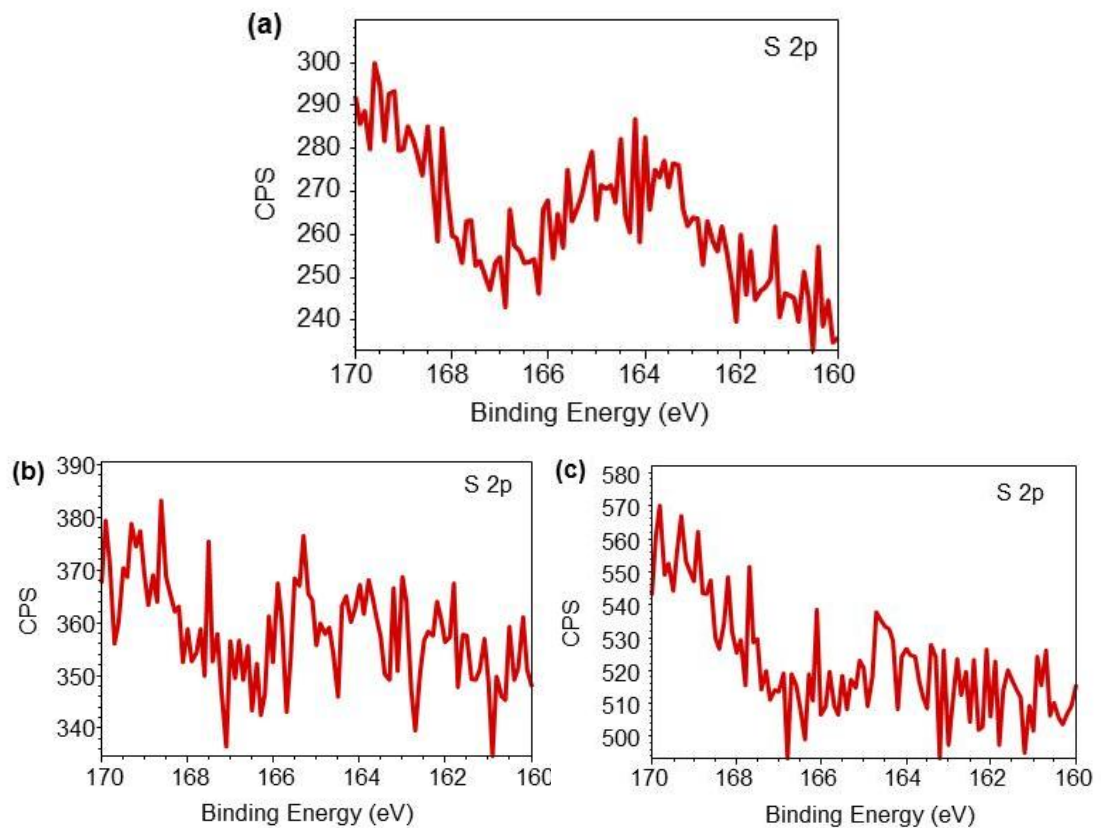


Figure 75: High resolution S 2p XPS spectra of the worn surface on cast iron flat samples lubricated with (a) Used Oil (315h); (b) Used Oil (315h) + 6% IL1; (c) Used Oil (315h) + 6% IL2

Figure 75 (a, b, c) show the high resolution spectra of S 2p taken inside the worn surface on the cast iron flat samples lubricated with Used Oil (315h) with and without ILs. In the sample lubricated with Used Oil (315h) without ILs, one peak located at the binding energy of 162.9 eV as shown in Figure 75 (a), was assigned to FeS_2 [119]. The content of sulphur was low to be appreciated by the XPS analysis after addition of both the ILs, such that no clear peak of S2p could be noted, as shown in Figure 75 (b) and (c). Therefore like New Oil case, the addition of ILs to the Used Oil reduces the involvement of sulphur containing ZDDP additive in boundary film formation.

5.5. Validation of tribological experimental results

The theoretical lubrication regime modelling (Appendix B) depicted that boundary lubrication conditions exist within the contact zone during sliding tests. In addition, friction coefficient values obtained are also projected towards the boundary lubrication regime (friction coefficient ~ 0.1) and are consistent with the published literature [1, 20, 28, 46, 85].

The wear rate results (see Table 10) observed for new fully-formulated engine oil with and without phosphonium IL1 at room temperature testing are similar to those reported by B. Yu et al. [28].

This agreement in friction coefficient and wear rate results indicates that the testing method employed in this research is capable of simulating boundary lubrication conditions that exist between the top piston ring and cylinder liner near top dead centre.

Furthermore, regarding the transferability of tribo-testing results - M. Woydt and N. Kelling [18], had mentioned that a qualitative wear ranking of tribo-couples as worst or best candidates can be done using tribo-testing, however there is no quantitative comparison possible with the engine testing. Also, it has been mentioned that the worn surface morphology of bench test specimens must be compared to that of actual running engine components to look for same basic wear mechanism taking place [16, 18, 19]. Therefore, the same approach has been adopted in current research.

The cylinder liner was obtained at the end of its service life from the actual engine during the overhaul which is part of planned maintenance programme for the RNLI lifeboat's marine engines at LH (Part of the Wabtec Group, UK). Also a new cylinder liner of the same engine was kindly supplied by Pilkington Marine Engineering Ltd (UK). Both cylinder liners were cut at the top dead centre region to prepare small samples for analysis under SEM. The material specification of the cylinder liner was identical to that of the cast iron flat specimens employed in the current research during tribo-testing.

The comparison of worn surface morphology was made between the actual cylinder liner (new and used form) and cast iron flat specimen (unworn and worn surfaces) tested with the used 15W40 engine oil (without ILs) at 100°C and 25°C.

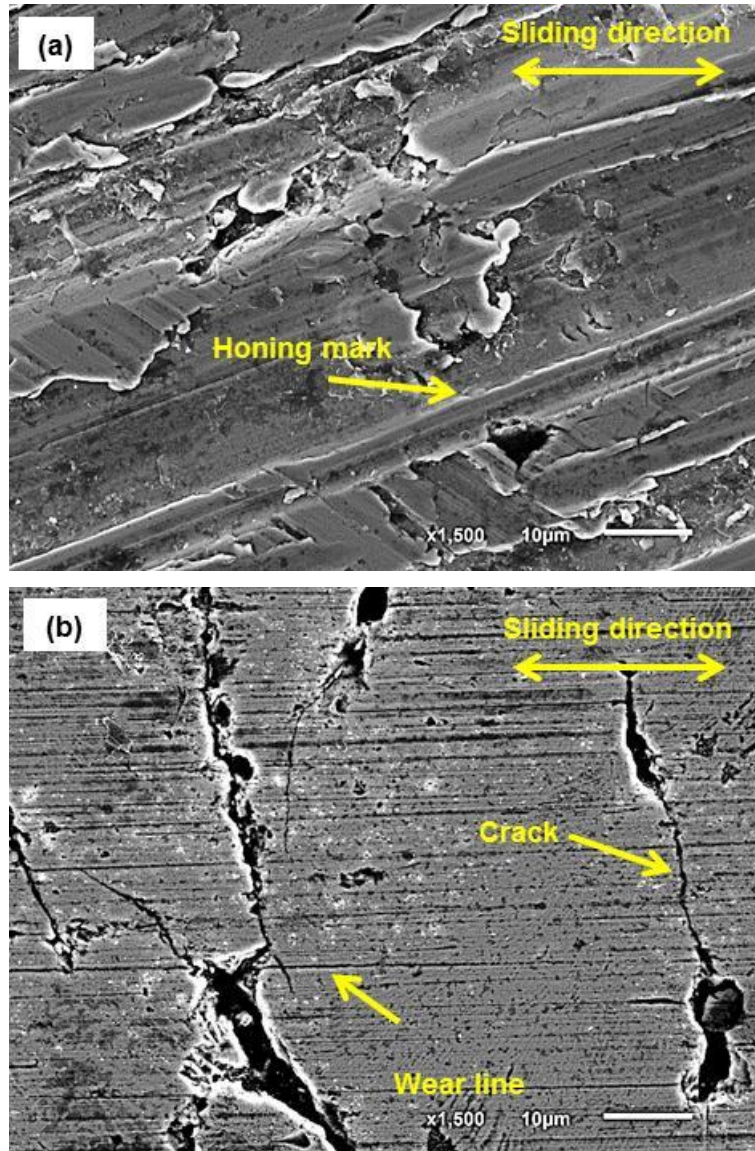


Figure 76: SEM images of actual cylinder liners near top dead centre; (a) unworn surface of new liner; (b) worn surface of used liner at end of its service life

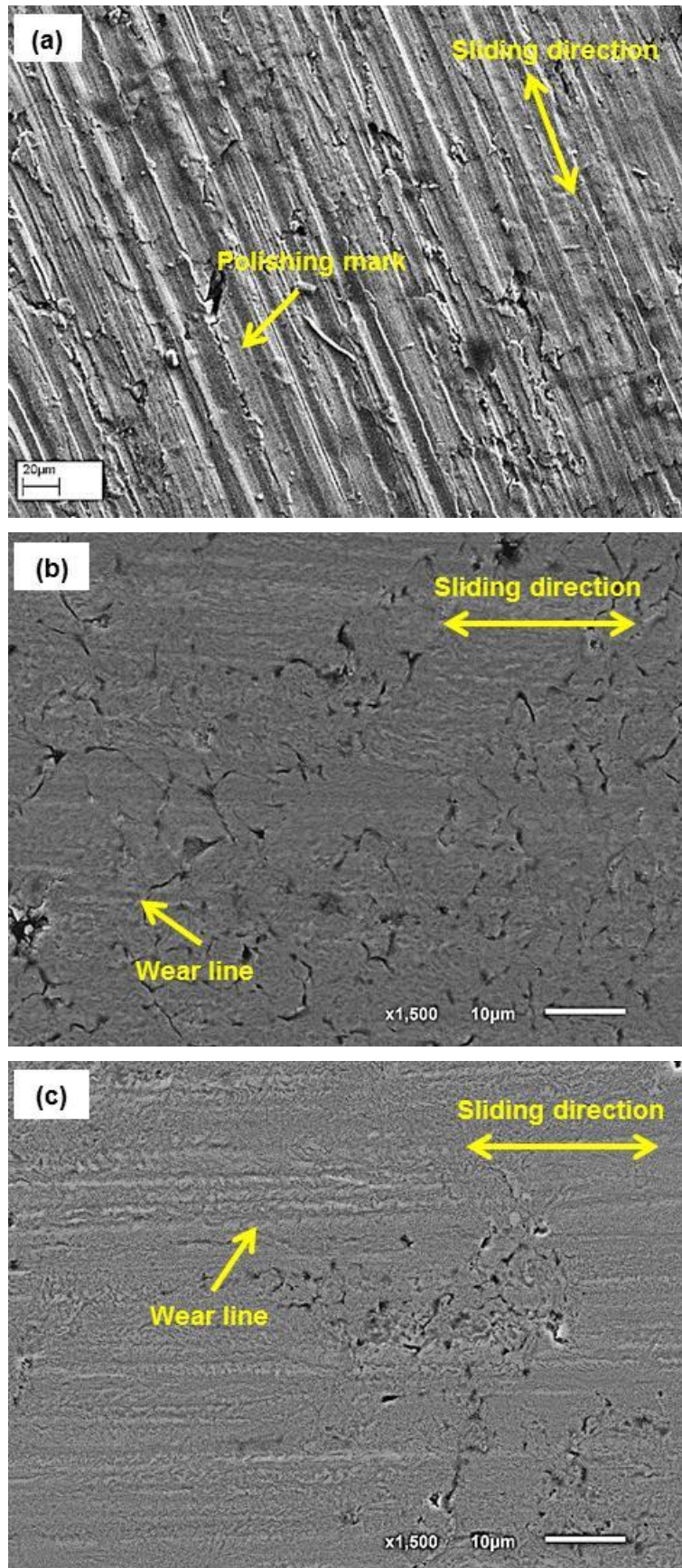


Figure 77: SEM images of cast iron test specimens; (a) unworn surface before test; (b) worn surface after test at 100°C; (c) worn surface after test at 25°C

The wear mechanism on cylinder liner in real engine condition has been studied by other researchers in past. With reference to their findings, the following comparison between surface morphology of the actual cylinder liner (Figure 76) and the cast iron test specimens (Figure 77) have been made as below.

- Honing marks which are present on the new liner surface (shown in Figure 76 a) have completely disappeared on the used liner surface (shown in Figure 76 b) which was at the end of its service life leading to the very smooth surface. Similar wear behaviour was found on comparison of surface morphology of the unworn surface of cast iron flat specimens (shown in Figure 77 a) with the worn surfaces tested at 100⁰C (shown in Figure 35 b) and 25⁰C (shown in Figure 35 c). Here the polishing marks which are present on unworn surface have almost completely disappeared on worn surface tested at 100⁰C but are slightly evident on worn surface tested at 25⁰C. The above wear observation is explained by M.F. Jensen et al. [85] for a similar case, mentioning about the reason behind smoothing of surfaces. The progression of smearing of asperities (peaks) material lead to the covering of shallow regions (valleys) such that initial rough surface now appears very smooth with large plateaus. This smearing of material results from the plastic deformation due to collisions of asperities during the sliding process. It has also been mentioned that although smoothing of surfaces reduces the chances of asperity-asperity collisions but smoothing beyond the critical limit may eventually results in scuffing. Such conditions often prevail near top dead centre region of liner where starved lubrication is predominant and increased contact between surfaces leads to scuffing wear.
- The wear lines present on the liner surface (Figure 76 b) and test specimens (Figure 77 b and c) indicates mild abrasive wear in the direction of sliding motion. This is a typical wear caused by wear and contaminant debris present at the sliding interface either as free particle with in oil leading to 3-body abrasion and/or embossed onto counterpart piston ring running surface (also piston in actual engine case) leading to 2-body abrasion of relatively softer liner surface. Additionally, these wear lines could also be due to the polishing wear that has been mentioned to take place near top-ring-reversal region if carbon formation is occurring around the ring and in the ring groove [1].
- The porosities can also be seen on the surface of liner and test specimens which are inherent for the cast iron material [28]. However, these porosities are

dimensionally less evident on worn surfaces of test specimens (Figure 77 b and c) than liner (Figure 76 b).

- Surface cracks are only visible on the used liner surface (Figure 76 b). Plausible explanation for its wear mechanism could be the dynamic loading experienced by the liner surface leading to fatigue cracking of the surface [121]. This phenomenon is absent in test specimens since these were subjected to constant loading applied during the complete tribo-testing duration.

The above similarities in the worn surface morphologies suggested that the wear phenomena observed in the bench tribo-testing correspond closely to the conditions encountered in actual service life of cylinder liner.

Chapter 6 Conclusions and recommendations for future work

- In RNLI lifeboat operations, lubricant degradation in marine engines of different classes of RNLI lifeboats revealed that average serviceable life of lubricants is 300 hrs.
- The primary reason for the lubricant change in the marine engines of all classes of RNLI lifeboats (except Mersey Class) was noted as the high concentration of iron in lubricant in the form of wear debris. Mersey Class lifeboats suffer lubricant change due to combined effects of high iron concentration and high lubricant viscosity.
- The lubricant degradation mechanism includes the depletion of anti-wear additives (ZDDP) present in the fully-formulated engine lubricants. These additives become less effective around 300 hrs of engine service as found by the Nuclear Magnetic Resonance (NMR) spectroscopy.
- Cylinder liners are the main engine components affected by the depletion of ZDDP additives resulting in small ferrous debris of size range 5 to 15 μm . Wear occurring mainly near the top dead centre (TDC) region of cylinder liner where boundary lubrication regime is present and anti-wear additives are responsible to form the protective boundary film.
- Real-time lubricant condition monitoring results obtained using a commercially available oil sensor at bench level for different lubricant samples demonstrated the dielectric constant as a good indicator of lubricant degradation.
- Future work should focus on taking dielectric constant measurements for lubricants at engine level tests in RNLI lifeboat to monitor lubricant degradation in real-time.
- After discussion with RNLI engineering department, the installation of oil sensor in the oil gallery just after the oil filter in the marine diesel engines could be an ideal location to have least disturbance from the wear debris on the oil sensing results.

- Obtained friction coefficient and wear rate results for ring-liner configuration lubricated with the mixture of new 15W40 engine oil and Phosphonium Ionic Liquids (ILs) are in good agreement with published literature. In addition, the worn surface morphology of cast iron made flat test samples was found similar to that of the actual engine cylinder liner's bore surface near TDC region. These similarities in results show that the operating conditions experienced near the TDC region at the ring-liner interface were adequately simulated at bench level using a reciprocating high frequency friction tribometer.
- The addition of Phosphonium ILs as additive in the used engine oil improved its friction and wear behaviour.
- The addition of Phosphonium ILs to relatively less degraded engine oils e.g. half intended service life (than fully used oil) worsens the wear and produces no significant change in friction performance.
- Interference between Phosphonium ILs and existing additives in engine oils was noted.
- ILs effectively contributed to the boundary film formation when existing additives (such as ZDDP) are substantially depleted as seen in the case of used engine oil.
- The extension of service life of used engine oils can be achieved and has potential of significant savings in terms of fuel economy, engine reliability and also by reduced oil consumption and drainage into the environment.
- Further work should focus on lower concentrations of Phosphonium ILs as additives in used engine lubricants to meet limits on overall phosphorus content as per ILSAC GF-5.

References

- [1] J. J. Truhan, J. Qu, and P. J. Blau, "The effect of lubricating oil condition on the friction and wear of piston ring and cylinder liner materials in a reciprocating bench test," *Wear*, vol. 259, pp. 1048-1055, 2005.
- [2] J. B. Heywood, *Internal Combustion Engine Fundamentals*: McGraw-Hill Inc. USA, 1988.
- [3] H. T. Hiroshi Moritani, Mamoru Tohyama, Hiroyuki Mori, Toshihide Ohmori, Motoichi Murakami, "Challenge to the Diesel Engine Lubrication with Fuel," in *JSAE/SAE International Fuels and Lubricants Meeting*, Kyoto, Japan, 2007.
- [4] S. C. Tung and M. L. McMillan, "Automotive tribology overview of current advances and challenges for the future," *Tribology International*, vol. 37, pp. 517-536, 7// 2004.
- [5] M. Nakasa, "Engine friction overview," in *Proceedings of International Tribology Conference*, Yokohama, Japan, 1995.
- [6] J. Spearot, "Friction, wear, health, and environmental impacts—tribology in the new millennium," presented at the A keynote lecture at the STLE Annual Meeting, Nashville, Tennessee, May, 2000.
- [7] D. F. Li, S. M. Rohde, and H. A. Ezzat, "AN AUTOMOTIVE PISTON LUBRICATION MODEL," *Asle Transactions*, vol. 26, pp. 151-160, 1983 1983.
- [8] J. C. Walker, T. J. Kamps, and R. J. K. Wood, "The influence of start-stop transient velocity on the friction and wear behaviour of a hyper-eutectic Al-Si automotive alloy," *Wear*, // 2012.
- [9] D. V. Bhatt, M. A. Bulsara, and K. N. Mistry, "Prediction of Oil Film Thickness in Piston Ring - Cylinder Assembly in an I C Engine: A Review," *World Congress on Engineering 2009, Vols I and II*, pp. 1638-1641, 2009 2009.
- [10] S. Q. A. Rizvi, "Additives for Automotive Fuels and Lubricants," *Journal of the Society of Tribologists and Lubrication Engineers*, vol. 34, 1999.
- [11] S. Q. A. Rizvi, "Lubricant Testing," in *A Comprehensive Review of Lubricant Chemistry, Technology, Selection, and Design*, ed: ASTM International, 2009, pp. 531-578.

- [12] A. M. Barnes, K. D. Bartle, and V. R. A. Thibon, "A review of zinc dialkyldithiophosphates (ZDDPS): characterisation and role in the lubricating oil," *Tribology International*, vol. 34, pp. 389-395, Jun 2001.
- [13] E. A. Bardasz and G. D. Lamb, *Lubricant additives: chemistry and applications*, 2nd ed.: CRC Press, 2010.
- [14] A. L. G. Pereira, M. Kasrai, G. M. Bancroft, P. R. Norton*, M. Abrecht, P. U. P. A. Gilbert, T. Regier, R. I. R. Blyth and J. Thompson, "Chemical and mechanical analysis of tribofilms from fully formulated oils Part 1 – Films on 52100 steel," *Tribology*, vol. 1, 2007.
- [15] A. Greenall, A. Neville, A. Morina, and M. Sutton, "Investigation of the interactions between a novel, organic anti-wear additive, ZDDP and overbased calcium sulphonate," *Tribology International*, vol. 46, pp. 52-61, Feb 2012.
- [16] P. Blau and S. C. Tung, "Bench Performance Test Methods for Lubricated Engine Materials," in *Automotive Lubricants and Testing*, ed: ASTM International, Nov 2012, pp. 215-230.
- [17] A. Morina and A. Neville, "Understanding the composition and low friction tribofilm formation/removal in boundary lubrication," *Tribology International*, vol. 40, pp. 1696-1704, 10// 2007.
- [18] M. Woydt and N. Kelling, "Testing the tribological properties of lubricants and materials for the system "piston ring/cylinder liner" outside of engines," *Industrial Lubrication and Tribology*, vol. 55, pp. 213-222, 2003.
- [19] A. Morina, P. Lee, M. Priest, and A. Neville, "Challenges of simulating 'fired engine' ring-liner oil additive/surface interactions in ring-liner bench tribometer," *Tribology-Materials, Surfaces & Interfaces*, vol. 5, pp. 25-33, 2011.
- [20] J. Galligan, A. Torrance, and G. Liraut, "A scuffing test for piston ring/bore combinations: Part I. Stearic acid lubrication," *Wear*, vol. 236, pp. 199-209, 1999.
- [21] P. M. Lee and R. J. Chittenden, "Consideration of test parameters in reciprocating tribometers used to replicate ring-on-liner contact," *Tribology Letters*, vol. 39, pp. 81-89, 2010.
- [22] L. Galda, A. Dzierwa, J. Sep, and P. Pawlus, "The effect of oil pockets shape and distribution on seizure resistance in lubricated sliding," *Tribology Letters*, vol. 37, pp. 301-311, 2010.

- [23] E. George, G. E. Kurien, U. Vishal, and P. M. Anil, "A study on the effect of oil pocket density on the effectiveness of boundary lubrication in the liner-ring interface," 2013, pp. 1062-1068.
- [24] S. Johansson, P. H. Nilsson, R. Ohlsson, and B.-G. Rosén, "Experimental friction evaluation of cylinder liner/piston ring contact," *Wear*, vol. 271, pp. 625-633, 6/3/ 2011.
- [25] P. De Silva, M. Priest, P. Lee, R. Coy, and R. Taylor, "Tribometer investigation of the frictional response of piston rings with lubricant contaminated with the gasoline engine biofuel ethanol and water," *Proceedings of the Institution of Mechanical Engineers, Part J: Journal of Engineering Tribology*, vol. 225, pp. 347-358, 2011.
- [26] S. Johansson, P. H. Nilsson, R. Ohlsson, C. Anderberg, and B.-G. Rosén, "New cylinder liner surfaces for low oil consumption," *Tribology International*, vol. 41, pp. 854-859, 2008.
- [27] S. C. Tung and H. Gao, "Tribological characteristics and surface interaction between piston ring coatings and a blend of energy-conserving oils and ethanol fuels," *Wear*, vol. 255, pp. 1276-1285, 2003.
- [28] B. Yu, D. G. Bansal, J. Qu, X. Sun, H. Luo, S. Dai, et al., "Oil-miscible and non-corrosive phosphonium-based ILs as candidate lubricant additives," *Wear*, vol. 289, pp. 58-64, // 2012.
- [29] J. Qu, D. G. Bansal, B. Yu, J. Y. Howe, H. Luo, S. Dai, et al., "Antiwear performance and mechanism of an oil-miscible IL as a lubricant additive," *ACS Applied Materials & Interfaces*, vol. 4, pp. 997-1002, 2012.
- [30] J. Qu, P. J. Blau, S. Dai, H. M. Luo, and H. M. Meyer, "ILs as Novel Lubricants and Additives for Diesel Engine Applications," *Tribology Letters*, vol. 35, pp. 181-189, Sep 2009.
- [31] J. J. Truhan, J. Qu, and P. J. Blau, "A rig test to measure friction and wear of heavy duty diesel engine piston rings and cylinder liners using realistic lubricants," *Tribology International*, vol. 38, pp. 211-218, 3// 2005.
- [32] C. M. C. Forest, M.I. De Barros Bouchet, M. Mazarin and J.M. Martin, "New Biofuel for low friction in Piston Ring Cylinder Liner Contact," presented at the 5th World Tribology Congress 2013, Italy, 2013.

- [33] S. C. Tung, K. Brogan, and Y. C. Wang, "Tribological evaluation of oil pump relief valve coatings compatible with an aluminum oil pump body," *Wear*, vol. 250, pp. 690-705, Oct 2001.
- [34] M. T. Noorman, D. N. Assanis, D. J. Patterson, S. C. Tung, and S. I. Tseregounis, "Overview of techniques for measuring friction using bench tests and fired engines," SAE International, pp. 1-11, 2000.
- [35] P. Olander, P. Hollman, and S. Jacobson, "Piston ring and cylinder liner wear aggravation caused by transition to greener ship transports—Comparison of samples from test rig and field," *Wear*, vol. 302, pp. 1345-1350, 4// 2013.
- [36] X. Q. Liu, F. Zhou, Y. M. Liang, and W. M. Liu, "Tribological performance of phosphonium based ILs for an aluminum-on-steel system and opinions on lubrication mechanism," *Wear*, vol. 261, pp. 1174-1179, Nov 30 2006.
- [37] C. F. Ye, W. M. Liu, Y. X. Chen, and L. G. Yu, "Room-temperature ILs: a novel versatile lubricant," *Chemical Communications*, pp. 2244-2245, 2001.
- [38] W. M. Liu, C. F. Ye, Q. Y. Gong, H. Z. Wang, and P. Wang, "Tribological performance of room-temperature ILs as lubricant," *Tribology Letters*, vol. 13, pp. 81-85, Aug 2002.
- [39] G. Mordukhovich, J. Qu, J. Y. Howe, S. Bair, B. Yu, H. M. Luo, et al., "A low-viscosity IL demonstrating superior lubricating performance from mixed to boundary lubrication," *Wear*, vol. 301, pp. 740-746, Apr-May 2013.
- [40] J. Qu, M. F. Chi, H. M. Meyer, P. J. Blau, S. Dai, and H. M. Luo, "Nanostructure and Composition of Tribo-Boundary Films Formed in IL Lubrication," *Tribology Letters*, vol. 43, pp. 205-211, Aug 2011.
- [41] M. D. Bermúdez, A. E. Jiménez, J. Sanes, and F. J. Carrión, "ILs as advanced lubricant fluids," *Molecules*, vol. 14, pp. 2888-2908, // 2009.
- [42] I. Minami, "ILs in Tribology," *Molecules*, vol. 14, pp. 2286-2305, 2009.
- [43] J. Qu, J. J. Truhan, S. Dai, H. Luo, and P. J. Blau, "ILs with ammonium cations as lubricants or additives," *Tribology Letters*, vol. 22, pp. 207-214, // 2006.
- [44] A. H. Battez, R. González, J. L. Viesca, D. Blanco, E. Asedegbega, and A. Osorio, "Tribological behaviour of two imidazolium ILs as lubricant additives for steel/steel contacts," *Wear*, vol. 266, pp. 1224-1228, // 2009.

- [45] A. E. Jiménez, M. D. Bermúdez, P. Iglesias, F. J. Carrión, and G. Martínez-Nicolás, "1-N-alkyl -3-methylimidazolium ILs as neat lubricants and lubricant additives in steel-aluminium contacts," *Wear*, vol. 260, pp. 766-782, // 2006.
- [46] J. L. Viesca, A. H. Battez, R. González, T. Reddyhoff, A. T. Pérez, and H. A. Spikes, "Assessing boundary film formation of lubricant additivised with 1-hexyl-3-methylimidazolium tetrafluoroborate using ECR as qualitative indicator," *Wear*, vol. 269, pp. 112-117, // 2010.
- [47] K. Mistry, M. F. Fox, and M. Priest, "Lubrication of an electroplated nickel matrix silicon carbide coated eutectic aluminium-silicon alloy automotive cylinder bore with an IL as a lubricant additive," *Proceedings of the Institution of Mechanical Engineers, Part J: Journal of Engineering Tribology*, vol. 223, pp. 563-569, // 2009.
- [48] J. Qu, P. J. Blau, S. Dai, H. Luo, H. M. Meyer Iii, and J. J. Truhan, "Tribological characteristics of aluminum alloys sliding against steel lubricated by ammonium and imidazolium ILs," *Wear*, vol. 267, pp. 1226-1231, // 2009.
- [49] Z. Mu, W. Liu, S. Zhang, and F. Zhou, "Functional room-temperature ILs as lubricants for an aluminum-on-steel system," *Chemistry Letters*, vol. 33, pp. 524-525, // 2004.
- [50] R. G. Rodriguez, J. L. V. Rodriguez, A. H. Battez, E. Asedegbega, A. H. Garrido, and A. T. Perez, "1-hexyl-3-methylimidazolium hexafluorophosphate as oil additive for the lubrication of steel-steel contacts and its influence on the running-in and wear-in periods," 2011, pp. 87-89.
- [51] H. Kamimura, T. Kubo, I. Minami, and S. Mori, "Effect and mechanism of additives for ILs as new lubricants," *Tribology International*, vol. 40, pp. 620-625, Apr 2007.
- [52] I. Minami, M. Kita, T. Kubo, H. Nanao, and S. Mori, "The tribological properties of ILs composed of trifluorotris(pentafluoroethyl) phosphate as a hydrophobic anion," *Tribology Letters*, vol. 30, pp. 215-223, Jun 2008.
- [53] I. Minami, T. Inada, R. Sasaki, and H. Nanao, "Tribo-Chemistry of Phosphonium-Derived ILs," *Tribology Letters*, vol. 40, pp. 225-235, Nov 2010.
- [54] L. J. Weng, X. Q. Liu, Y. M. Liang, and Q. J. Xue, "Effect of tetraalkylphosphonium based ILs as lubricants on the tribological performance of a steel-on-steel system," *Tribology Letters*, vol. 26, pp. 11-17, Apr 2007.

- [55] B. S. Phillips, G. John, and J. S. Zabinski, "Surface chemistry of fluorine containing ILs on steel substrates at elevated temperature using Mossbauer spectroscopy," *Tribology Letters*, vol. 26, pp. 85-91, May 2007.
- [56] R. P. Swatloski, J. D. Holbrey, and R. D. Rogers, "ILs are not always green: hydrolysis of 1-butyl-3-methylimidazolium hexafluorophosphate," *Green Chemistry*, vol. 5, pp. 361-363, 2003.
- [57] G. A. Baker and S. N. Baker, "A simple colorimetric assay of IL hydrolytic stability," *Australian journal of chemistry*, vol. 58, pp. 174-177, 2005.
- [58] N. V. Plechkova and K. R. Seddon, "Applications of ILs in the chemical industry," *Chemical Society Reviews*, vol. 37, pp. 123-150, 2008.
- [59] C. Kajdas, "Importance of anionic reactive intermediates for lubricant component reactions with friction surfaces," *Lubrication Science*, vol. 6, pp. 203-228, 1994.
- [60] I. M. Hutchings, *Tribology: friction and wear of engineering materials: ELSEVIER SCIENCE TECHNOLOGY*, UK, 1992.
- [61] H. S. Cheng, "Introduction to Lubrication," in *ASM Handbook - Friction, Lubrication, and Wear Technology*. vol. 18, ed: ASM International, 1992, pp. 79-80.
- [62] J. A. Williams, "Boundary Lubrication and Friction," in *Engineering Tribology*, ed New York: Oxford University Press Inc., 1994, pp. 348-380.
- [63] S. Q. A. Rizvi, in *A Comprehensive Review of Lubricant Chemistry, Technology, Selection and Design*, ed: ASTM International, West Conshohocken, PA, 2009, pp. 1-22.
- [64] S. Hogmark, S. Jacobson, and O. Vingsbo, "Surface Damage." vol. 18, ed: *ASM Handbook - Friction, Lubrication, and Wear Technology*, 1992, pp. 176-183.
- [65] K. C. Ludema, "Introduction to Wear," 18, *ASM Handbook - Friction, Lubrication, and Wear Technology*, ASM International, 1992.
- [66] K. C. Ludema, "Sliding and Adhesive Wear," in *ASM Handbook - Friction, Lubrication, and Wear Technology*. vol. 18, ed: ASM International, 1992, pp. 236-241.
- [67] J. H. Tylczak, "Abrasive Wear," in *ASM Handbook - Friction, Lubrication, and Wear Technology*. vol. 18, ed: ASM International, 1992, pp. 184-190.

- [68] B. W. Madsen, "Corrosive Wear," in ASM Handbook - Friction, Lubrication, and Wear Technology. vol. 18, ed: ASM International, 1992, pp. 271-279.
- [69] P. J. Blau, "Rolling Contact Wear," in ASM Handbook - Friction, Lubrication, and Wear Technology. vol. 18, ed: ASM International, 1992, pp. 257-262.
- [70] A. W. Ruff, "Wear Measurement," in ASM Handbook - Friction, Lubrication, and Wear Technology. vol. 18, ed: ASM International, 1992, pp. 362-369.
- [71] N. Corporation. (2002) Oil Viscosity - How It's Measured and Reported. Machinery Lubrication.
- [72] "Standard Test Method for Kinematic Viscosity of Transparent and Opaque Liquids (and Calculation of Dynamic Viscosity)," in ASTM D445 - 12, ed: ASTM International.
- [73] G. Hall. (2008) Determining Fuel Diluents in Lubrication Oils. Machinery Lubrication.
- [74] "Standard Test Method for Determination of Additive Elements, Wear Metals, and Contaminants in Used Lubricating Oils and Determination of Selected Elements in Base Oils by Inductively Coupled Plasma Atomic Emission Spectrometry (ICP-AES)," in ASTM D5185 - 09, ed: ASTM International.
- [75] D. Wooton. (2005) Using Nuclear Magnetic Resonance to Track Additive Depletion. Machinery Lubrication.
- [76] M. Barrett. (2000) Analytical Ferrography - Make It Work For You. Machinery Lubrication.
- [77] A. International, "Standard Practice for Microscopic Characterization of Particles from In-Service Lubricants by Analytical Ferrography," in ASTM D7690 - 11, ed, 2011.
- [78] M. Specialities, FPS28X0B12C4 Installation Guide vol. 01: Measurement Specialities, 2012.
- [79] P. T. Limited, "Operating Instructions TE 57 Pressurized Lubricity Tester," ed, 2002.
- [80] "Standard Test Method for Conducting Friction Tests of Piston Ring and Cylinder Liner Materials under Lubricated Conditions," in ASTM G181-11, ed: ASTM International.
- [81] L. E. a. H. Klingele, An Atlas of Metal Damage. Munich, Germany: Wolfe Science Books, 1981.

- [82] A. I. G. a. S. I. Rice, "Surface Chemical Analysis," in ASM Handbook - Friction, Lubrication, and Wear Technology. vol. 18, ed: ASM International, 1992.
- [83] N. Morris, R. Rahmani, H. Rahnejat, P. King, and B. Fitzsimons, "Tribology of piston compression ring conjunction under transient thermal mixed regime of lubrication," Tribology International, 2012.
- [84] P. Mishra, S. Balakrishnan, and H. Rahnejat, "Tribology of compression ring-to-cylinder contact at reversal," Proceedings of the Institution of Mechanical Engineers, Part J: Journal of Engineering Tribology, vol. 222, pp. 815-826, 2008.
- [85] M. F. Jensen, J. Bøttiger, H. H. Reitz, and M. E. Benzon, "Simulation of wear characteristics of engine cylinders," Wear, vol. 253, pp. 1044-1056, 2002.
- [86] J. ÖSTLUND, T. Russel, S. Walker, Å. Håkansson, L. Greek, and G. Richards, "Evaluation of a Novel Method to Study Oil Stability," ed, 2007.
- [87] A. Cambiella, J. Benito, C. Pazos, J. Coca, M. Ratoi, and H. Spikes, "The effect of emulsifier concentration on the lubricating properties of oil-in-water emulsions," Tribology Letters, vol. 22, pp. 53-65, 2006.
- [88] D. Blanco, A. H. Battez, J. Viesca, R. González, and A. Fernández-González, "Lubrication of CrN coating with ethyl-dimethyl-2-methoxyethylammonium tris (pentafluoroethyl) trifluorophosphate IL as additive to PAO 6," Tribology letters, vol. 41, pp. 295-302, 2011.
- [89] D. Blanco, R. González, A. Hernández Battez, J. Viesca, and A. Fernández-González, "Use of ethyl-dimethyl-2-methoxyethylammonium tris (pentafluoroethyl) trifluorophosphate as base oil additive in the lubrication of TiN PVD coating," Tribology International, vol. 44, pp. 645-650, 2011.
- [90] E. Rabinowicz, "The Determination of the Compatibility of Metals through Static Friction Tests," A S L E Transactions, vol. 14, pp. 198-205, 1971/01/01 1971.
- [91] J. Larsen-Basse, "Basic Theory of Solid Friction." vol. 18, S. D. Henry, Ed., ed: American Society of Metal Handbook, Friction, Lubrication and Wear Technology, ASM International, 1992, pp. 27-38.
- [92] K. Budinski, "Laboratory testing methods for solid friction," Materials Park, OH: ASM International, 1992., pp. 45-58, 1992.

- [93] E. Yamaguchi, P. Ryason, S. Yeh, and T. Hansen, "Boundary film formation by ZnDTPs and detergents using ECR," *Tribology transactions*, vol. 41, pp. 262-272, 1998.
- [94] P. J. Blau, *Friction science and technology: from concepts to applications*: CRC press, 2012.
- [95] J. Qu, P. J. Blau, S. Dai, H. Luo, and H. M. Meyer III, "ILs as novel lubricants and additives for diesel engine applications," *Tribology Letters*, vol. 35, pp. 181-189, 2009.
- [96] T. Narayanan, Y. W. Park, and K. Y. Lee, "Fretting corrosion of lubricated tin plated copper alloy contacts: Effect of temperature," *Tribology International*, vol. 41, pp. 87-102, 2008.
- [97] M. A. Nicholls, T. Do, P. R. Norton, M. Kasrai, and G. M. Bancroft, "Review of the lubrication of metallic surfaces by zinc dialkyl-dithiophosphates," *Tribology International*, vol. 38, pp. 15-39, 2005.
- [98] Y. Kondo, S. Yagi, T. Koyama, R. Tsuboi, and S. Sasaki, "Lubricity and corrosiveness of ILs for steel-on-steel sliding contacts," *Proceedings of the Institution of Mechanical Engineers, Part J: Journal of Engineering Tribology*, vol. 226, pp. 991-1006, 2012.
- [99] J. Qu, H. Luo, M. Chi, C. Ma, P. J. Blau, S. Dai, et al., "Comparison of an oil-miscible IL and ZDDP as a lubricant anti-wear additive," *Tribology International*, vol. 71, pp. 88-97, 2014.
- [100] J. Qu, P. J. Blau, J. Y. Howe, and H. M. Meyer III, "Oxygen diffusion enables anti-wear boundary film formation on titanium surfaces in zinc-dialkyl-dithiophosphate (ZDDP)-containing lubricants," *Scripta Materialia*, vol. 60, pp. 886-889, 2009.
- [101] B. J. Tan, K. J. Klabunde, and P. M. Sherwood, "X-ray photoelectron spectroscopy studies of solvated metal atom dispersed catalysts. Monometallic iron and bimetallic iron-cobalt particles on alumina," *Chemistry of Materials*, vol. 2, pp. 186-191, 1990.
- [102] I. Otero, E. R. López, M. Reichelt, and J. Fernández, "Friction and anti-wear properties of two tris (pentafluoroethyl) trifluorophosphate ILs as neat lubricants," *Tribology International*, vol. 70, pp. 104-111, 2014.

- [103] C. Wagner, W. Riggs, L. Davis, J. Moulder, and G. Muilenberg, "Handbook of X-ray photoelectron spectroscopy, 1979," Perkin-Elmer, Eden Prairie, MN, 1977.
- [104] E. Paparazzo, "X-ray photo-emission and Auger spectra of damage induced by Ar⁺-ion etching at SiO₂ surfaces," *Journal of Physics D: Applied Physics*, vol. 20, p. 1091, 1987.
- [105] H. Seyama and M. Soma, "Fe 2*p* spectra of silicate minerals," *Journal of electron spectroscopy and related phenomena*, vol. 42, pp. 97-101, 1987.
- [106] (February 03, 2014). NIST X-ray Photoelectron Spectroscopy Database. Available: <http://srdata.nist.gov/xps/Default.aspx>
- [107] Y. Barbaux, M. Dekioux, D. Le Maguer, L. Gengembre, D. Huchette, and J. Grimblot, "Bulk and surface analysis of a Fe-PO oxydehydrogenation catalyst," *Applied Catalysis A: General*, vol. 90, pp. 51-60, 1992.
- [108] Y. A. Teterin, K. Ivanov, I. Utkin, D. Bek-Uzarov, A. Y. Teterin, K. Maslakov, et al., "XPS study of ceramics (Ca 0.5 GdU 0.5)(ZrTi) O 7 and (Ca 0.5 GdU 0.5) Zr 2 O 7 with pyrochlore and fluorite structures," 2005.
- [109] A. Y. Teterin, K. I. Maslakov, Y. A. Teterin, K. E. Ivanov, S. V. Yuditsev, S. V. Stefanovsky, et al., "The XPS study of pyrochlore matrixes for the radioactive waste disposal," *Nuclear Technology and Radiation Protection*, vol. 25, pp. 157-163, 2010.
- [110] W. A. Brainard and D. R. Wheeler, "AN XPS STUDY OF THE ADHERENCE OF REFRACTORY CARBIDE SILICIDE AND BORIDE RF-SPUTTERED WEAR-RESISTANT COATINGS," *J Vac Sci Technol*, vol. 15, pp. 1800-1805, 1978.
- [111] H. J. Mathieu and D. Landolt, "An investigation of thin oxide films thermally grown in situ on Fe₂₄Cr and Fe₂₄Cr₁₁Mo by auger electron spectroscopy and X-ray photoelectron spectroscopy," *Corrosion Science*, vol. 26, pp. 547-559, 1986.
- [112] T. Hanawa and M. Ota, "Calcium phosphate naturally formed on titanium in electrolyte solution," *Biomaterials*, vol. 12, pp. 767-774, 1991.
- [113] R. Franke, T. Chassé, P. Streubel, and A. Meisel, "Auger parameters and relaxation energies of phosphorus in solid compounds," *Journal of Electron Spectroscopy and Related Phenomena*, vol. 56, pp. 381-388, 1991.

- [114] D. Chadwick and T. Hashemi, "Adsorbed corrosion inhibitors studied by electron spectroscopy: Benzotriazole on copper and copper alloys," *Corrosion Science*, vol. 18, pp. 39-51, 1978.
- [115] T. L. Barr, M. Yin, and S. Varma, "Detailed x-ray photoelectron spectroscopy valence band and core level studies of select metals oxidations," *Journal of Vacuum Science & Technology A*, vol. 10, pp. 2383-2390, 1992.
- [116] G. Schön, "Auger and direct electron spectra in X-ray photoelectron studies of zinc, zinc oxide, gallium and gallium oxide," *Journal of Electron Spectroscopy and Related Phenomena*, vol. 2, pp. 75-86, // 1973.
- [117] B. R. Strohmeier and D. M. Hercules, "Surface spectroscopic characterization of the interaction between zinc ions and γ -alumina," *Journal of Catalysis*, vol. 86, pp. 266-279, 1984.
- [118] S. Karthe, R. Szargan, and E. Suoninen, "Oxidation of pyrite surfaces: a photoelectron spectroscopic study," *Applied Surface Science*, vol. 72, pp. 157-170, 1993.
- [119] H. Peisert, T. Chassé, P. Streubel, A. Meisel, and R. Szargan, "Relaxation energies in XPS and XAES of solid sulfur compounds," *Journal of Electron Spectroscopy and Related Phenomena*, vol. 68, pp. 321-328, 1994.
- [120] B. Demri and D. Muster, "XPS study of some calcium compounds," *Journal of Materials Processing Tech.*, vol. 55, pp. 311-314, 1995.
- [121] K. C. Radil, "Test Method to Evaluate Cylinder Liner-Piston Ring Coatings for Advanced Heat Engines," DTIC Document1997.
- [122] J. Qu, M. Chi, H. M. Meyer III, P. J. Blau, S. Dai, and H. Luo, "Nanostructure and composition of tribo-boundary films formed in IL lubrication," *Tribology Letters*, vol. 43, pp. 205-211, 2011.
- [123] W. C. Young and R. G. Budynas, in *Roark's Formulas For Stress and Strain*, Seventh ed: McGraw-Hill Companies, Inc., 2002, pp. 689-707.
- [124] K. L. Johnson, *Contact Mechanics*: Cambridge University Press, 1985.

Appendix A: Contact Pressure Calculation

Since non-conformal contact geometries were used in the bench tests, therefore the maximum compressive pressure on the contact surface were calculated using the Hertz theory. The maximum contact pressure can be calculated using the following equation [123]

$$\sigma_{\max} = 0.918 \sqrt[3]{\frac{F}{K_D^2 C_E^2}}$$

Equation 1

Table 23: Known parameters of piston ring segment-on-flat contact

Known Parameters	Values	SI Units
v_1 = Poisson ratio of piston ring	0.3	
v_2 = Poisson ratio of flat sample	0.26	
E_1 = Modulus of Elasticity of piston ring	2.9E+11	N/m ²
E_2 = Modulus of Elasticity of flat sample	1.3E+11	N/m ²
C_E =	1E-11	m ² /N
D_1 = Diameter of piston ring	0.128	m
D_2 = Diameter of flat	∞	m
$K_D = D_1$	0.128	m
F = Total load applied	50	N

For the parameters given in Table 23, the maximum contact pressure can be calculated using the Equation 1.

$$\sigma_{\max} = 284.9 \text{ MPa}$$

This is the maximum contact pressure which is expected to be present at the centre of interfacing contact zone.

Appendix B: Theoretical Lubrication Regime

The piston ring running face and counter-facing flat specimen are separated by a thin lubricating film which is responsible for carrying the applied load and also maintaining lower friction and wear during the reciprocating sliding motion. The thickness of such a lubricating film can be calculated theoretically and thence compared with the combined roughness of mating surfaces to model the existing lubrication regime. Minimum lubricant film thickness can be obtained by using the Hamrock and Dowson (1977a) elliptical contact equation for the case of piston ring segment-on-flat.

$$\frac{h_{min}}{R} = 3.63 \{2\alpha E^*\}^{0.49} \left\{ \frac{U\eta_o}{2E^*R} \right\}^{0.68} \left\{ \frac{W}{2E^*RL} \right\}^{-0.073} (1 - e^{-0.068K})$$

Equation 2

The above dimensionless equation relates the dependence of minimum lubricant film thickness on Load Parameter, Speed Parameter and Material Parameter.

Dimensionless Material Parameter = $2\alpha E^*$

Dimensionless Speed Parameter = $\frac{U \eta_o}{2E^*R}$

Dimensionless Load Parameter = $\frac{W}{2E^*RL}$

For the known data in Table 24, the values for the above dimensionless parameters can be calculated

Table 24: Known data for minimum lubricant film thickness

Known Parameters		SI Units
α = pressure-viscosity constant	1.149E-08	m ² /N
E^* = Reduced Young's Modulus for the materials of contacting surfaces	1.98E+11	N/m ²
η_0 = Dynamic viscosity of lubricant	0.0056	s-N/m ²
R = Reduced Radius of Curvature	0.01195	m
W = Applied Load	50	N
L = length of contact	0.0035	m
U = Sliding speed	0.022	m/s
ν_1 = Poisson ratio for piston ring	0.3	
ν_2 = Poisson ratio for Flat Plate	0.26	
E_1 = Modulus of Elasticity for Piston ring	2.89E+11	N/m ²
E_2 = Modulus of Elasticity for Flat Plate	1.34E+11	N/m ²

Dimensionless Material Parameter = $2\alpha E^* = 2275.02$

Dimensionless Speed Parameter = $\frac{U \eta_0}{2E^*R} = 9.72 \text{ E} - 15$

Dimensionless Load Parameter = $\frac{W}{2E^*RL} = 6.165 \text{ E} - 08$

Therefore the dimensionless minimum lubricant film thickness can now be calculated using Equation 2 as follows.

$$\frac{h_{\min}}{R} = 8.027\text{E} - 08$$

Equation 3

Using the value of 'R' from the Table 24 the minimum film thickness will be,

$$h_{\min} = 5.14 \text{ E} - 09 \text{ m}$$

The lambda ratio can be calculated using the combined RMS surface roughness values of piston ring running face and flat plate using the Equation 4.

$$\lambda = \frac{h_{min}}{\sqrt{R_a^2 + R_b^2}}$$

Equation 4

R_a = RMS roughness of piston ring running face = 3.72E-07 m

R_b = RMS roughness of flat plate = 6.47E-07 m

Hence, $\lambda = 0.01$

The lambda value depicts that tribo-tests were conducted under the boundary lubrication regime.

Appendix C:

MAN Engine Test Report

MAN		Motorenmeßblatt für Prüffeld (Engine testing data)												Prüfsand-Nr. (Test bed no.) 11																	
WPM-N		Motor-Nr. (Engine model) D2840LE 401		Motornummer (Engine number) 473 8673 150 H 301		Kraftstoffdichte (fuel density) 0.828		Typ (date) 3.11.1987		Bremsen (Test eng.-W. side)		Lade/lufttemp. °C																			
Barometerstand (barometer reading) 985 mbar		Spez. Kraftstoffverbrauch (Spec. fuel consumption) g/kWh		Einspritzmenge (Hub u. Stempel) mm ³		Rauchwert SZ		Fuel oil temp. °C		Anzugtemp. (Inlet air temp. °C)		Lube oil temp. °C		Lube oil pressure bar		Rohwassertemp. (Raw water temp. °C)		Abgas-temperatur (Exhaust temp. °C)		Kühlwassereintrittstemp. (Cool. water inlet temp. °C)		Kühlwasseraus-trittstemp. (Cool. water outlet temp. °C)		Boost pressure 1-5 mbar		Boost pressure 6-10 mbar		Crankcase Blow-by 1/min		Entlüftung mbar	
Messung of	Speed rpm	Drehmoment Nm	Leistung kW	Zeit für Durchlauf von 2000 cm ³	Spez. Kraftstoffverbrauch g/kWh	Einspritzmenge (Hub u. Stempel) mm ³	Rauchwert SZ	Fuel oil temp. °C	Intake air temp. °C	Lube oil temp. °C	Lube oil pressure bar	Rohwassertemp. (Raw water temp. °C)	Abgas-temperatur (Exhaust temp. °C)	Kühlwassereintrittstemp. (Cool. water inlet temp. °C)	Kühlwasseraus-trittstemp. (Cool. water outlet temp. °C)	Boost pressure 1-5 mbar	Boost pressure 6-10 mbar	Crankcase Blow-by 1/min	Entlüftung mbar	Lade/lufttemp. °C											
	2300	2449	632	40.8	231.2	255.8	1.0	34	24	107	4.5	22	393	67	81	763	769	182	182	49											
	2083	2264	444	58.5	215.0	196.0	0.3	34	24	100	4.6	22	292	65	76	7562	7579	762	762	42											
	1449	10805	158	171.5	220.0	96.6	1.0	34	24	86	4.9	22	285	63	70	316	278	81	81	18											
	2300	2449	632	40.9	230.6	255.1	0.9	34	24	105	4.6	22	390	67	78	760	764	183	183	47											
	2300	2449	632	41.0	230.1	254.5	0.8	34	24	102	4.6	22	392	67	80	762	765	180	180	49											
	2300	2449	632	40.9	230.6	255.1	0.8	34	24	107	4.5	22	395	67	81	764	769	179	179	49											
	2300	2449	632	41.0	230.1	254.5	0.9	34	24	107	4.5	22	394	67	81	764	769	181	181	49											
	2350	2668	627	41.8	227.5	244.3	0.8	34	24	106	4.5	22	386	67	80	738	744	185	185	48											
	2380	2417	573	45.3	228.8	222.6	0.6	34	24	105	4.5	22	355	66	78	769	769	198	198	48											
	2400	2287	589	47.5	228.7	210.5	0.5	34	24	104	4.5	22	340	66	78	764	769	199	199	48											
	2450	1819	445.7	57.2	233.9	171.3	0.4	34	24	102	4.6	22	295	65	75	1556	1553	202	202	48											
	2500	1202	300.5	78.3	253.4	122.6	0.4	34	24	98	4.6	22	244	64	72	1304	1299	192	192	42											
	2550	252	64.3	182.5	508.3	51.6	0.0	34	24	90	4.8	22	259	63	67	549	502	120	120	27											
	2585	Speed	Drop	(p-Grad: 12.4%)							5.0																				
	689										1.9																				

541 857



7.11.87